THE UNIVERSITY OF HULL
DEPARTMENT OF CHEMISTRY

Antiferroelectric and Ferroelectric Liquid Crystals in Terphenyl Systems

Being a Thesis submitted for the Degree of Doctor of Philosophy

In the University of Hull

by

Seung-Eun Lee, BSc, MSc (Ewha Womans University)

April 1998

Acknowledgements

I would like to express my sincerest gratitude to Professor J. W. Goodby for his inspired supervision during my time at the University of Hull. I also wish to thank to Dr K. J. Toyne for his kind advice and discussions.

My thanks go to Drs M. Hird, R. A. Lewis, C. J. Booth and other members of the staff in Liquid Crystal Group for numerous advice and help in the early synthetic work. Special thanks also go to Julie, Aileen and Judy (from the British Council) for their collaboration, consideration and friendship.

Thanks are also due to Mrs B. Worthington, Mr R. Knight, Mr A. D. Roberts and Mr A. Rendell for providing spectral analyses for the compounds and Mr. G. Palin for constructing electric equipment used in switching studies.

The time spent toiling in the Lab 210 & 307 was never boring due to the presence of Alex, Paul, Steve, Guirec, Mark, Peter and Gary and many others who I hope will forgive me for not mentioning them by name.

I wish to express my appreciation to the British Council, Merck UK, DERA(Malvern) and the University of Hull for their financial support.

Last, but by no means least, I thank my family for their continuous encouragement and supports in all kinds of ways during the long gestation of this thesis.

To my Mother and Father

Contents

1 Introduction

Liquid crystals stand between the isotropic liquid phase and strongly organized solid state. Life stands between complete disorder, which is death and completely rigidity, which is death again.

D. G. Dervichian (1977)

1. Introduction

1.1 A Brief History of Liquid Crystals

Over 100 years ago, the phenomenon of liquid crystallinity was discovered in two derivatives of cholesterol, cholesteryl benzoate and cholesteryl acetate (Fig. 1.1.1) by F. Reinitzer and O. Lehmann[1-2]. In the case of cholesteryl benzoate, the crystal melted sharply to a liquid at 145.5 °C, but the appearance of the liquid was opaque. Not until the temperature was increased to 178.5 °C did the opacity disappear suddenly, giving a clear isotropic liquid. Lehmann found that the opaque melt, which had characteristic flow properties like a liquid, was birefringent by means of polarized light microscopy. He described this phase as '*fliessende Kristalle*' (liquid crystal).

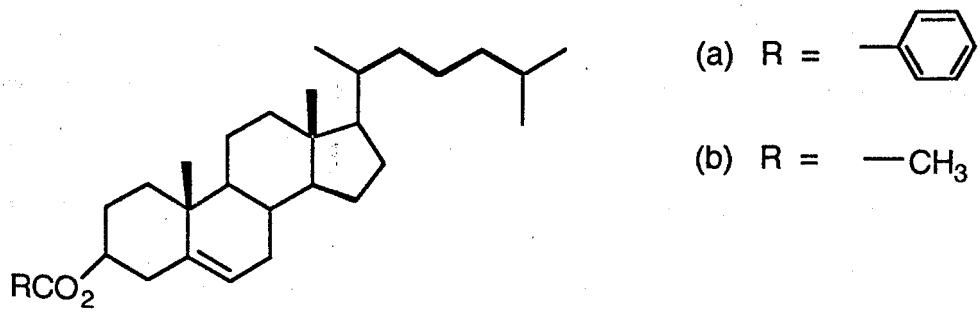

Fig. 1.1.1 Cholesterol derivatives (a) cholesteryl benzoate (b) cholesteryl acetate

In the 1920s, D. Vorlander[3] pointed out that the compounds exhibiting liquid crystal phase behaviour had rod-like molecular shapes and more than 300 liquid crystal compounds were synthesized at that time.

In 1922, G. Friedel[4] published the results of detailed optical studies whereby he could distinguish three different liquid crystal types; the nematic phase (N, Greek, *nematos*,

meaning 'thread-like'), the smectic phase (Sm, Greek, *smectos*, meaning 'soap-like'), and the cholesteric phase (Ch, this nomenclature derived from cholesterol). He also introduced the term mesophase (Greek, *mesos*, meaning intermediate) and the associated terms, mesogen, mesomorphism and mesogenic.

In nematic liquid crystals, formation of striped domains under an applied electric field and light scattering effects were found by R. Williams[5] and A. Kapustin[6]. In 1968, the first application of liquid crystals in display devices was reported by G. Heilmeir[7]. He found that a clear thin layer of a nematic liquid crystal showed a scattering texture under an applied voltage. Subsequently he developed a new type of dynamic scattering display device using this phenomenon.

In the 1970s, M. Schadt and W. Helfrich[8] and J. Ferguson[9] independently invented a new display configuration called the 'twisted nematic (TN)' mode which has been adopted for low information content devices such as watches or pocket calculators. The invention of this optical device demanded the availability of materials which exhibited stable room temperature mesophases. This problem was only fully resolved by the synthesis of cyanobiphenyls by G. Gray[10-11] in the early 1970s. The invention of super twisted nematic displays (STN) by T. Scheffer and J. Nehring[12] features higher levels of multiplexicability and allows high information content displays. A later generation is the thin-film transistor TN display (TFT-TN) which combines high speed and relatively good viewing angle characteristics. One of the latest display device developments is the ferroelectric liquid crystal display (FLC) which uses chiral smectic C materials and was invented by N. Clark and S. Lagerwall[13].

Today, research in the area of novel liquid crystal materials is still being pursued in order to meet the stringent requirements of new device technologies.

1.2. Classification of Liquid Crystals

Liquid crystals can be roughly divided into two areas, *lyotropic* and *thermotropic* liquid crystals.

Lyotropic liquid crystals are formed by mixing compounds possessing amphiphilic properties with solvents such as water. The molecular structure of a typical amphiphile is one where a hydrophilic polar head group is appended to a hydrophobic aliphatic moiety. Between the pure amphiphile and the dilute isotropic system exist mesogens which consist of ordered arrangements of micelles composed of molecules of the amphiphile and of the solvent. Such aggregates can self assemble and exhibit anisotropic properties and characteristics of liquid crystal phases. Lamellar, hexagonal and cubic phases have been identified. The appearance of these phases depends on the size of the hydrophilic head group, the number of hydrophobic aliphatic chains in the amphiphile, and nature and concentration of solvent. As the study of lyotropic phenomena is outside this current investigation, no further mention will be made of lyotropic liquid crystal systems.

Thermotropic liquid crystals are formed either by heating the crystal or by cooling the isotropic liquid. In a classical melting of a solid to liquid, the organized molecular array of the solid collapses to give the disorganized liquid where the molecules tumble and rotate freely. At the melt point the molecules undergo large and rapid simultaneous changes in rotational, positional and orientational order. However, in the melting process for a liquid crystal there is a stepwise breakdown in this order. The incremental steps of this break-down occur with increasing temperature, thus producing a variety of thermodynamically stable liquid-crystalline mesomorphic states. The transitions from liquid crystal to liquid crystal and from liquid crystal to isotropic liquid are essentially

reversible and occur with little hysteresis in temperature. The melting point of a material is usually a constant, but the recrystallization process can be subject to super-cooling. Mesophases which are formed on the heating cycle are called *enantiotropic* phases whereas phases that are formed below the melting point on the cooling cycle are called *monotropic* phases. Thermotropic liquid crystals may be subdivided into calamitic and columnar forms. In addition calamitic liquid crystals for example may exhibit a variety of phases derived from the nematic, smectic phases or disordered crystal phases (see Fig. 1.2.1). Some features of the sub-classes of the systems are discussed later.

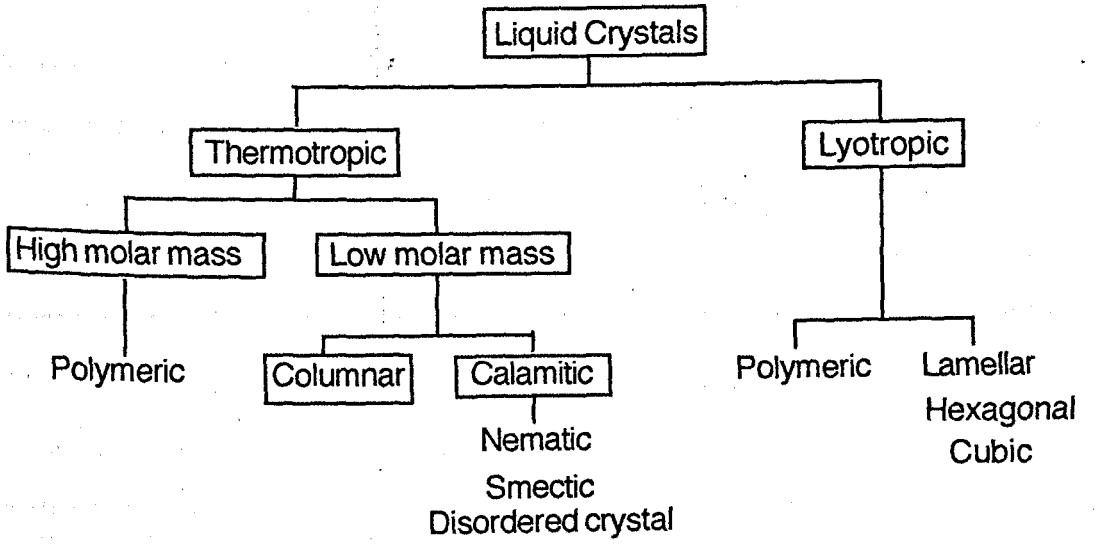

Fig. 1.2.1 The classification of liquid crystals

1.2.1 General Structure for Calamitic Liquid Crystals[14-15]

Fig. 1.2.2 shows a general template for the structure of calamitic liquid crystals where A and B are core units, Y is a linking group, the terminal chains R and R' can be linked to the core through groups X and Z respectively, and M and N could be lateral substituents.

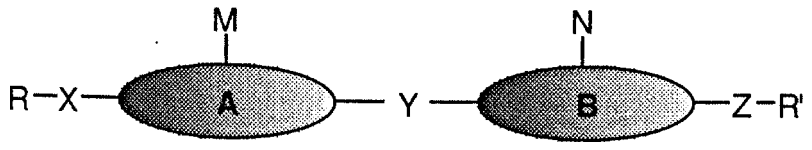

Fig. 1.2.2 General structural templates for calamitic liquid crystals

The structure of the core is often aromatic or alicyclic and the rings can be directly linked or may be joined by a linking group (Y) which maintains the linearity and the anisotropy of the molecular polarizability ($\Delta\alpha$) of the core (*e.g.* $-CO_2-$, $-C\equiv C-$, $-CH_2CH_2-$). Terminal chains (R and R') which extend the overall length of the molecules along their molecular axes without increasing the molecular breadth too much, increase the thermal range of the liquid crystal state. It is also true that the flexibility provided by the terminal chains lowers melting points and stabilise molecular alignment. The terminal chains employed are typically straight alkyl or alkoxy chains, and occasionally they can be branched. Lateral substituents (M and N) attached to the core can lower the clearing point by increasing the polarizability across the molecular axis and by increasing the intermolecular separation. The effects of the dipoles of the lateral substituents are insignificant in relation to decreasing the transition temperature of the nematic to isotropic liquid transition. Generally, the nematic phase is stabilised by using relatively short terminal chains in conjunction with a core of high longitudinal polarisability. The core is usually short and may possess a conjugative linking group. In contrast, for strongly dipolar lateral substituents there is a smaller decrease in transition temperature between the smectic and nematic or the smectic and isotropic liquid compared to systems with less dipolar substituents of approximately the same size. This suggests that dipolar interactions are more important in the stabilization of smectics in comparison to nematics.

1.2.2 The Nematic Phase

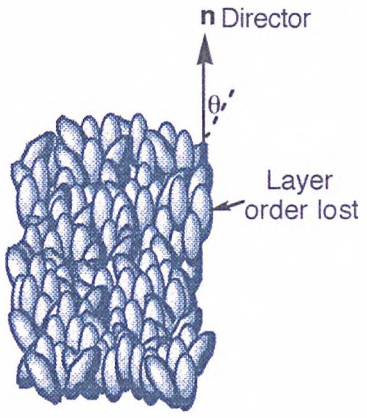

Fig. 1.2.3 Nematic phase

The positional order of the molecules in the nematic phase is only short-range in all directions, but the molecules do possess quasi-long-range orientational order of their long axes which tends to be parallel to a common axis labelled as the director **n** in Fig. 1.2.3.

The nematic phase has an opaque liquid-like appearance, the opacity being due to the birefringent nature of its optical properties. Accordingly, nematic liquid crystals are found to exhibit two principal refractive indices, the ordinary refractive index n_o and the extraordinary refractive index n_e. The ordinary refractive index n_o is observed with a light wave where the electric vector oscillates perpendicular to the optic axis. The extraordinary refractive index n_e is observed for a linearly polarized light wave where the electric vector is vibrating parallel to the optic axis. The optical anisotropy, or birefringence, Δn, is given by

$$\Delta n = n_e - n_o$$

The value for the birefringence for rod-like nematics is usually positive with values of Δn ranging between 0 to +0.4.

The degree to which the molecules are aligned along the director is termed the order parameter (S) of the phase which is defined by the equation below:

$$S = 1/2 \langle 3\cos^2\theta - 1 \rangle$$

where θ is the angle between the long axis and the director (see Fig. 1.2.3) and the brackets denotes a space/time average. For a typical nematic phase S has a value in the region of 0.4 to 0.7 indicating that the molecules are considerably disordered. The rod-like molecules in the nematic phase are free to rotate about their short axes and to some degree about their long axes, however, the relaxation times for rotations about the short axes are much longer ($\sim 10^{-6}$ s^{-1}) than those about their long axes ($\sim 10^{-11}$ s^{-1}). Thus the phase appears very mobile in the polarising microscope, and the molecular fluctuations give rise to extensive Brownian motion.

In the polarising microscope, the nematic phase shows *schlieren*[16-18] textures which are formed by a continuous change in the orientation of the molecules. The characteristic dark brushes appear when the molecules are in alignment with one or other of the two polarisers. The points of optic extinction from which the *schlieren* extend may have two or four brushes depending on the strength of the disclination. The defect is denoted by S where

$$S = \text{the number of brushes} / 4$$

and may have a value of ±1 and ±1/2. (see Fig. 1.2.4). If the brushes rotate in the same direction as the rotation of the polarisers the singularity is classified as positive and in the opposite fashion the value is negative.

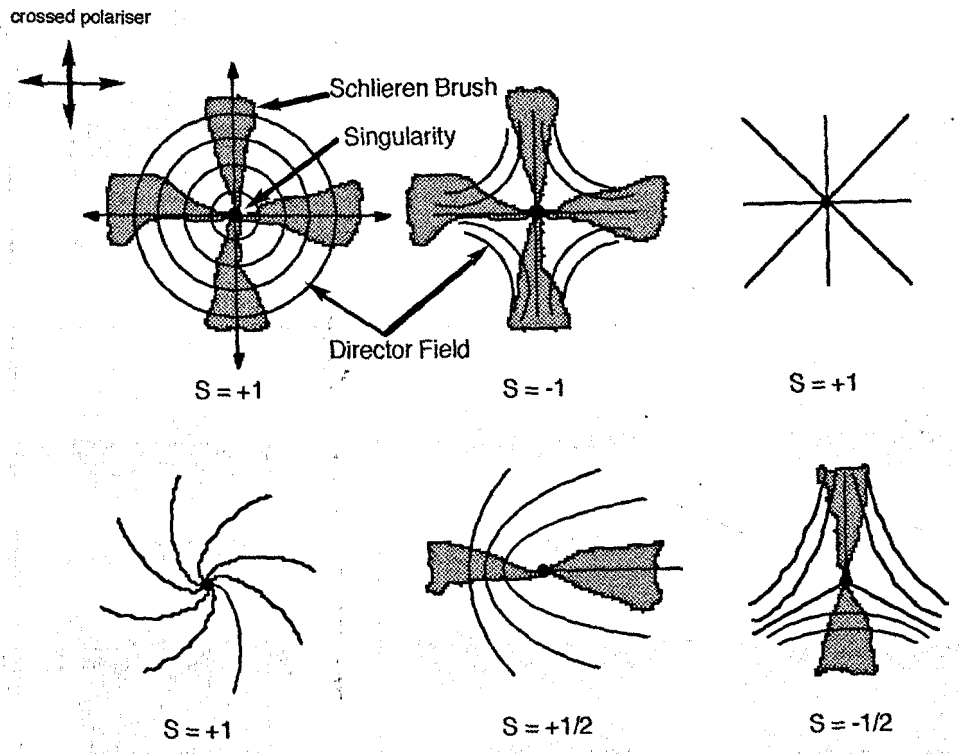

Fig. 1.2.4 4-Brush and 2-brush singularities in the nematic phases

1.2.3 Smectic Phases [19-20]

A number of smectic phases exist as shown schematically in Fig. 1.2.5. The structures of these phases depend on the local packing of the rod-like molecules. The molecules pack in diffuse layers in which the long axes are either orthogonal or tilted with respect to the layer planes. Locally the rod-like molecules are hexagonally close-packed on average, but the extent of this ordering is dependent on the mesophase type.

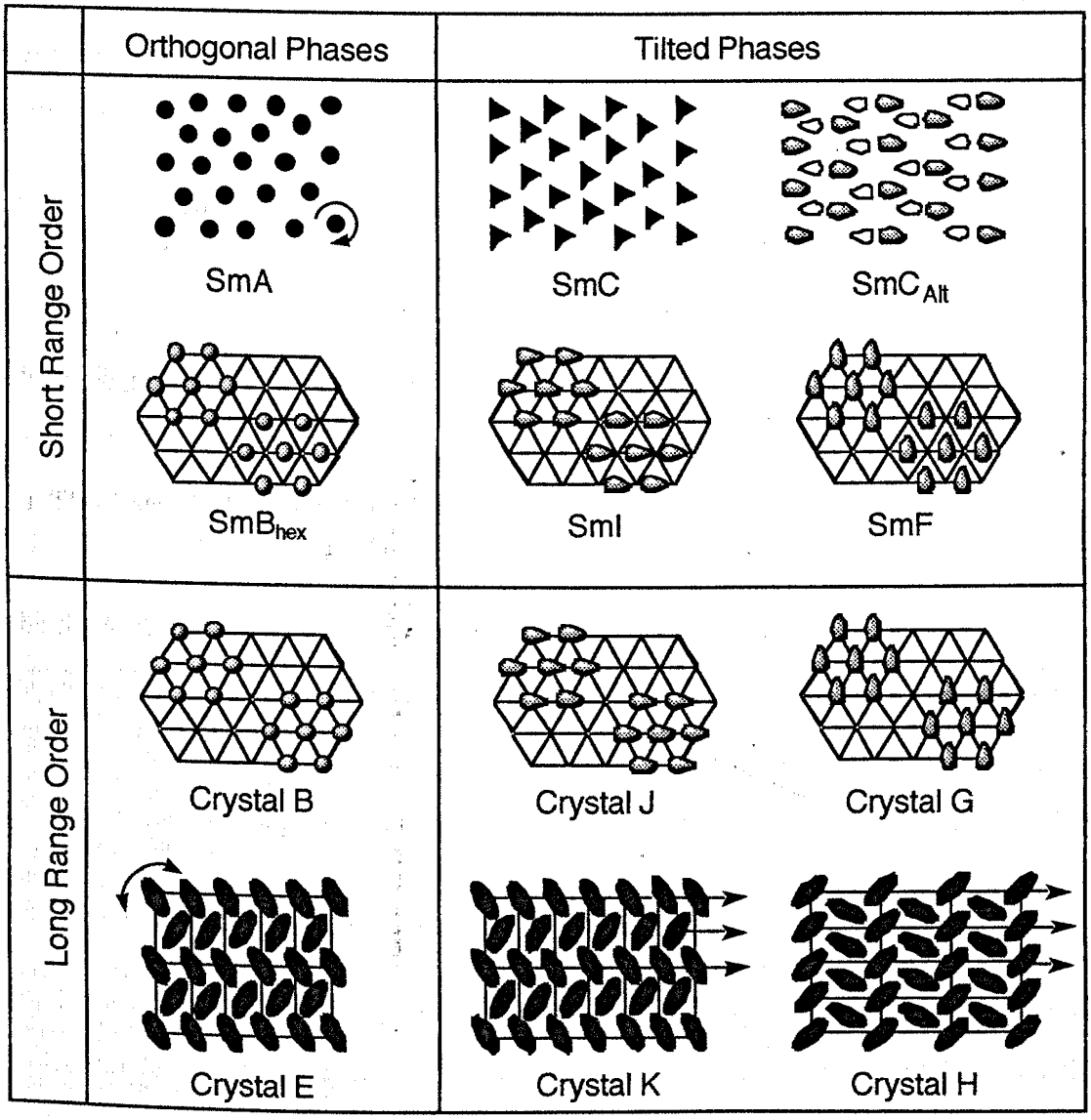

Fig. 1.2.5 Plan and side views of the structural representations for various polymesomorphic smectic phases

For example, in smectic A (SmA) and smectic C (SmC) phases the positional ordering of the molecules is short range (10-25 Å), whereas in hexatic B (SmB$_{hex}$), smectic I (SmI) and smectic F (SmF) it extends over a few hundred Å. In the plastic crystal phases of B, E, G, H, J, and K, the positional ordering is long range in, and between, the layers.

These mesophases have a defined thermodynamic order, *i.e.* if a hypothetical liquid-crystalline compound, which shows all of the phases exhibited by calamitic materials, is heated the mesophases will occur in a certain sequence as shown below;

Crystal, H, K, E, G, J, SmF, B, SmB_{hex}, SmI, SmC_{Alt}, SmC, SmA, N, Isotropic

-------> decreasing order -------->

Alternating smectic C (SmC_{Alt}) will be discussed separately in section 1.4.6.

(1) The Smectic A Phase (SmA)

The SmA phase consists of molecular layers with a random orthogonal arrangement of the molecules. The molecules have short range positional order within the layers and there is no translational periodicity in the planes of the layers or between the layers. Therefore, the molecules have only short range hexagonal ordering extending over a few molecular centres at most.

The layer spacing, d, in SmA phases is normally close to, but somewhat shorter than the molecular length. Losche *et al.*[21-22] suggested that the molecules gyrate about the centres for mass to give a time-dependent tilt angle of 10-20°, and this gives rise to a layer spacing, d, on average, slightly shorter than the molecular length. However, as this tilting occurs randomly across the bulk phase, the average direction of the long axes of the molecules is perpendicular to the layer planes.

In the polarising microscope, the most characteristic texture for the SmA phase is the focal conic defect. The focal conic texture is often formed when a smectic layer is supported between two surfaces or other nucleation points with which it can form strong attachments. Around each defect, the phase structure adopts a focal conic fan-like

arrangement within which both the layer thickness and lamellar structure are preserved; thus the layers curve. However, rather than forming spherically curved surfaces and a straight disclination line, the layers are found to form elliptical surfaces and hyperbolar disclination lines (Fig. 1.2.6 (a)). Sections through the layers in the plane of the ellipse give concentric circles and in the plane of the hyperbola give two sets of concentric circles, such that individual circles are paired-off in two sets. The sets of circles are known as 'Dupin cyclides' (Fig 1.2.6. (b)).

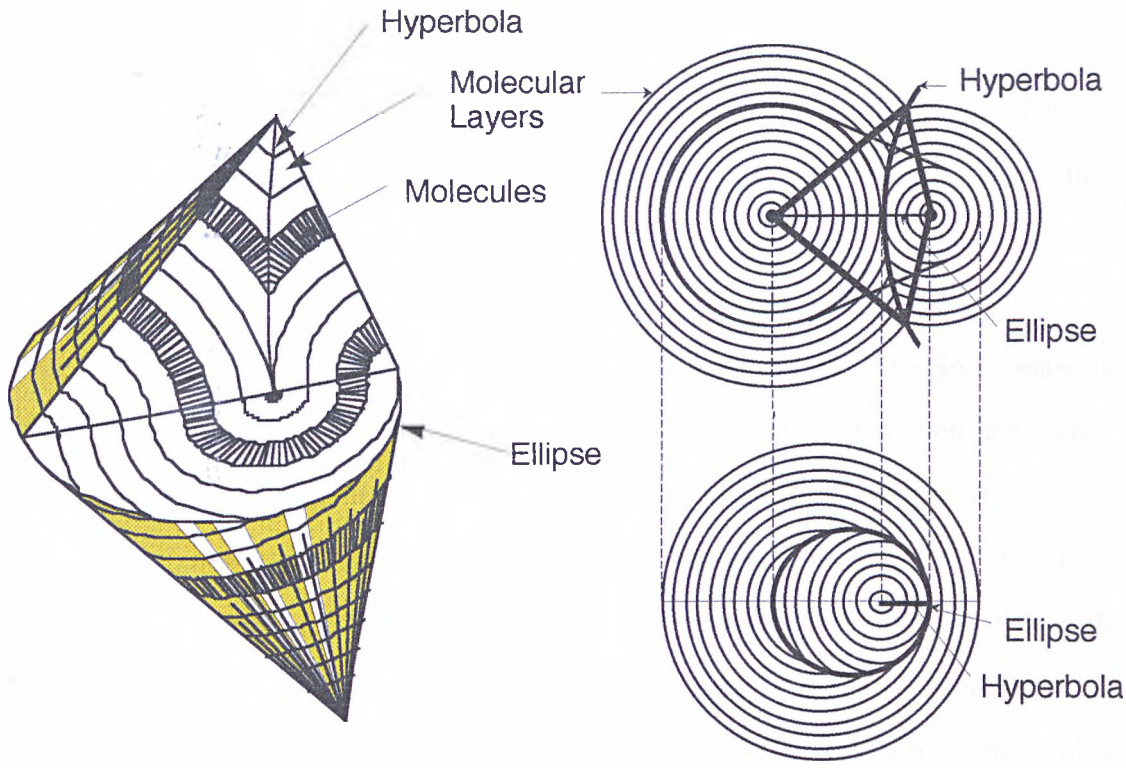

Fig. 1.2.6 (a) Focal conic domain (b) side elevation and plan of a focal conic domain

(2) The Smectic C Phase (SmC)

In the SmC phase, the molecules are randomly packed in diffuse layers with short range positional order where the long axes of the molecules are tilted at a temperature-dependent angle θ, with respect to the layer normal. The property of the temperature dependence of the tilt angle is described below;

$$\theta (T) = \theta_0 (T_C - T)^{\alpha}$$

where θ (T) is the tilt angle at temperature T °C, θ_0 is a constant, T_C is the temperature of the transition from SmA to SmC phase, T is the temperature being considered and α is an exponent theoretically predicted to equal 0.5. This power law equation shows that the value of the tilt angle becomes saturated as the temperature falls.

There are two classes of SmC materials[23]. In the majority of cases the SmC phase is formed from the SmA by cooling through a second-order phase transition and shows modest tilt angles which increases from 0° at the SmA-SmC phase transition when lowering the temperature. However, when the SmC phase is formed *via* a first-order transition, *i.e.* N-SmC or I-SmC phase transition, there is a jump in the value of the tilt angle, which may approach 45° at the transition. Additionally when the SmC phase is created directly from the nematic or from the isotropic liquid, layers of tilted molecules have to appear directly at the transition, and thus the transition is first order. The cyabotic layering[24] fluctuations at the nematic to SmC transition must have a preferred orientation inclined to the director, whereas the isotropic to SmC transition also includes the basic parallel ordering of the molecules which makes the transition even more strongly first order. After the initial jump in the value of the tilt angle, the angle remains fairly temperature independent.

Several theories have been developed which take into account specific features of the SmC phases. McMillan's[25] model shows SmC materials having two oppositely oriented outboard dipoles which are away from the geometric centre of the molecules. The molecules align by freezing out of the rotation of the molecules about their long axes. Thus the aligned anti-parallel outboard dipole moments couple to create a torque which tilts the molecules with respect to the layer normal.

A steric model proposed by Wulf[26] assumes that zig-zag shaped molecules, which may arise from obliquely directed end chains, coupled with freezing of free rotation around the long axes produces the tilted structure. But neutron scattering measurements and other experiments clearly indicate that the molecules in the SmC phase are freely rotating about their long axes, and consequently disagree with the models of both McMillan and Wulf. Van der Meer and Vertogen[27] argued that many compounds have only one outboard dipole moment and they proposed, in such cases, a permanent dipole in one molecule induces a dipole in a neighbouring molecule. There is an optimal location for this dipole in the molecule, and the alignment of the induced and the permanent dipoles can create the force for tilting which will be effective even when the molecules rotate freely. A model for the nematic, SmA and SmC developed by Priest[28] is based on the general coupling between second rank tensor quantities which are supposed to produce the orientational order of molecules. The theory does not discuss the relationship between the coupling constants and molecular structure. As Goosens[29] pointed out, none of the theories are satisfactory.

(3) Hexatic B, Smectic I and Smectic F Phases (SmB_{hex}, SmI and SmF)

These phases have short-range positional order with a correlation length of 100 Å or more which is about an order of magnitude longer than in the SmA or SmC phases.

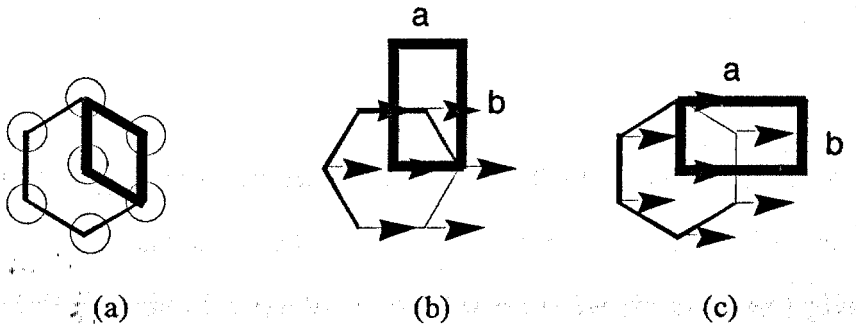

Fig. 1.2.7 Schematic drawing of the local structure of (a) SmB_{hex}, (b) SmI and (C) SmF phases. The arrows denote the tilt direction of the molecules

The SmB_{hex} phase has molecules arranged in layers with the molecular centres positioned in a hexagonally close-packed array (see Fig. 1.2.7 (a)). The molecular long axes were shown to be orthogonal to the layer planes, and an indication of this can be drawn from the fact that the phase exhibits a homeotropic texture and is positive uniaxial.

SmI and SmF are tilted with C_{2h} symmetry (see Fig. 1.2.7 (b), (c)). SmI phases are tilted towards an apex of the hexagon, where $a < b$, and SmF phases are tilted towards the side of the hexagon, where $a > b$.

1.2.4 The Cholesteric Phase

If a chiral molecule forms a nematic or tilted smectic liquid crystalline phase, the structure also becomes chiral and contains a helical twist. The helical N structure, denoted N* is called a cholesteric (Ch) phase. As the molecules in the nematic phase have no longer range positional order, no longer range ordering exists in the cholesteric phase.

The pitch of the helix can vary from about 0.1 x 10^{-6} m to almost infinity. When the pitch of the phase is comparable to the wave length of light, the cholesteric phase will selectively reflect light of a relatively narrow wave length band and give rise to a characteristic colour effect. The pitch of the phase is temperature dependent, and therefore the property of selective reflectance is also temperature dependent. If an extra pitch or half-pitch is inserted into the system an edge-dislocation is formed and a Grandjean planar texture which contains oily streaks is often found when viewed by polarising microscopy.

The helical rotary senses for a number of non-sterol cholesteric liquid crystals have been determined and a simple rule relating molecular structure, absolute configuration and twist sense was proposed by G. Gray and D. McDonnell[30]. They examined the contact region present between pairs of cholesteric compounds using optical microscopy. They observed that when the helical twist senses were opposite, a narrow band of nematic texture was observed, separating two cholesteric regions. (Fig. 1.2.8 (a)). However, when the interface of two cholesteric phases with the same helical senses was examined, no discontinuity in the texture was visible, *i.e.* a continuous cholesteric texture was observed from left to right across the field of view (Fig. 1.2.8 (b)).

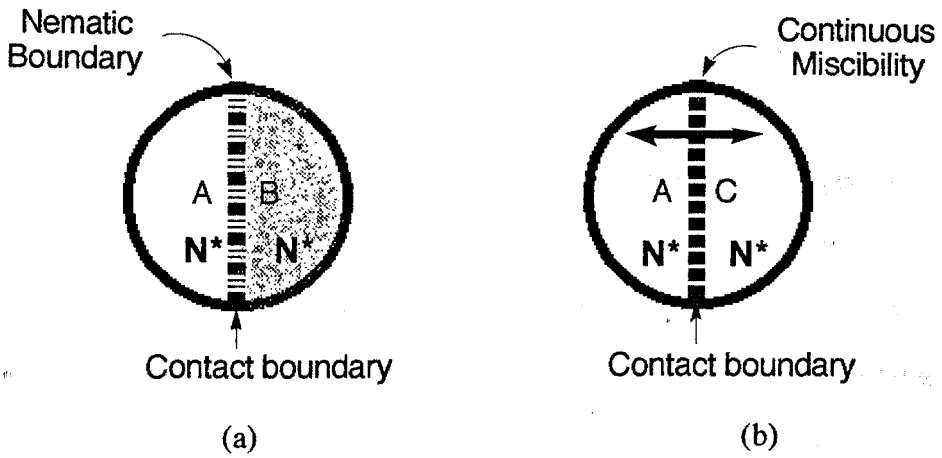

Fig. 1.2.8 Field of views from the contact method in the neighbourhood of the interface between (a) two cholesteric phases (A and B) of opposite helical senses (b) two cholesteric phases (A and C) of identical helical senses.

They proposed the following rule expressed as permissible combinations of three letters defined below;

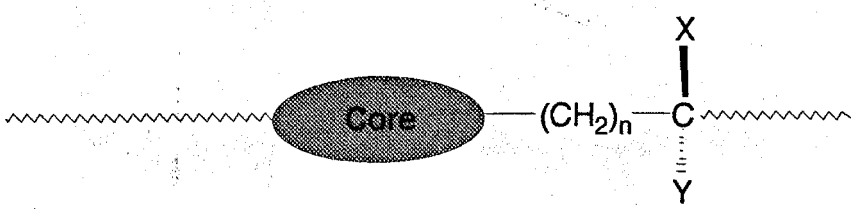

For a given spatial configuration R or S about the chiral centre

Right-handed cholesteric helices	Left-handed cholesteric helices
Sed	Sol
Rod	Rel

where, S and R refer to the absolute configuration at the chiral centre.

d and l refer to the senses of helical rotation, d (dextro), l (levo) respectively.

e and o refer to the parity of n in the spacer chain being an even or odd number of atoms.

1.2.5 Blue Phases (BPI, BPII and BPIII)

These phases often appear in a narrow range of the temperature (typically less than 0.5 °C) between the N* and isotropic liquid phases for N* phases of relatively short pitch (< 5000 Å). In blue phases, helices show in more than one preferred direction forming a double-twist structure. They were named for their visual appearance which was originally blue[31] but subsequently they have also been seen to be green or orange. Three forms of blue phase[32], two of which have cubic structures, have been classified to date, and in decreasing order of thermodynamic stability they are BPI, BPII (Fig. 1.2.9 (a) and (b)) and BPIII. BPI is a body-centred cubic lattice, BPII is a primitive cubic lattice with the only lattice parameters being the pitch length. Finally, BPIII, also known as 'blue fog' has had little if any structural information revealed so far.

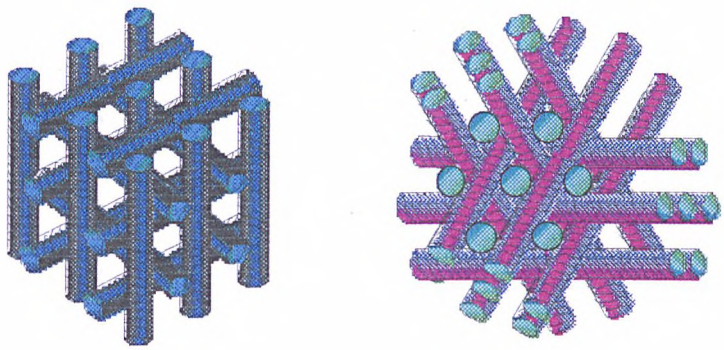

(a) (b)

Fig. 1.2.9 (a) Blue phase I (b) Blue phase II

1.3 Ferroelectricity

1.3.1 A Brief History of Ferroelectricity

The main characteristic property of a ferroelectric material is the spontaneous polarization (Ps), which is responsible for the coupling of the director with an applied dc field. In 1921 Valasek[33] first discovered ferroelectricity in a C_2-symmetric crystal modification of Rochell salt (potassium sodium tartrate, $KNaC_4H_4O_6$) which shows a dielectric hysteresis, indicating the presence of a Ps.

Ferroelectricity in liquid crystals was first demonstrated in 1975 by R. Meyer *et al.*[34]. They found the presence of a Ps in 2-methylbutyl 4-n-decyloxybenzylidene aminocinnamate (DOBAMBC) in its chiral SmC* phase which belongs to the monoclinic point group C_2 (Fig. 1.3.1).

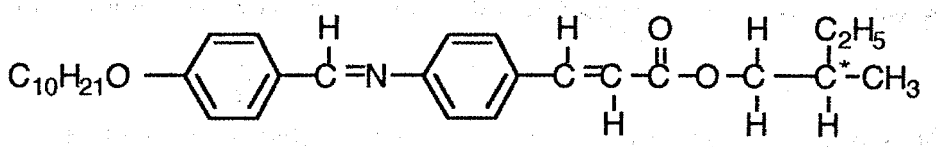

DOBAMBC

K 76 °C SmI* 63 SmC* 95 SmA* 117 I

Fig. 1.3.1 Structure and phase transition of DOBAMBC

1.3.2 Symmetry Arguments

(1) Space Symmetry

If a SmC phase is composed of nonchiral molecules arranged in layers with their long axes tilted with respect to the layer planes, the space symmetry elements for the molecules in this phase are: a mirror plane normal to the layers, a twofold axis of rotation parallel to the layers and normal to the tilt direction and a centre of symmetry. Thus the symmetry is described as C_{2h} (Fig. 1.3.2). When the molecules in this phase are optically active, *i.e.* they possess asymmetric atoms, these symmetry elements are reduced to C_2, which means that there is no longer a mirror plane or centre of symmetry and the only symmetry element left is the twofold rotation axis (C_2 axis) being perpendicular to the molecular tilt direction and to the layer normal (see also Fig. 1.3.2)[35]. Thus the low local symmetry causes the transverse dopole moments of the molecules to align in a time dependent fashion along the C_2 axis, leading to a macroscopic spontaneous polarization within the smectic layer so that the phase is ferroelectric. The arguments used so far only apply to individual layers. However in a bulk sample, there is a helical precession of the tilt axis along the direction perpendicular to the layers so that the phase can be described as helielectric[36]. Consequently the layer polarizations are averaged out to zero.

The polarization is a vector quantity and two directions are possible to act along as shown in Fig. 1.3.3 for an object molecule that is tilted back in the plane normal to the page. If the spontaneous polarization acts in the right hand direction then it is denoted as being positive, $Ps > 0$, and described as Ps (+); the reverse situation has negative $Ps < 0$ and described as Ps (-)[37].

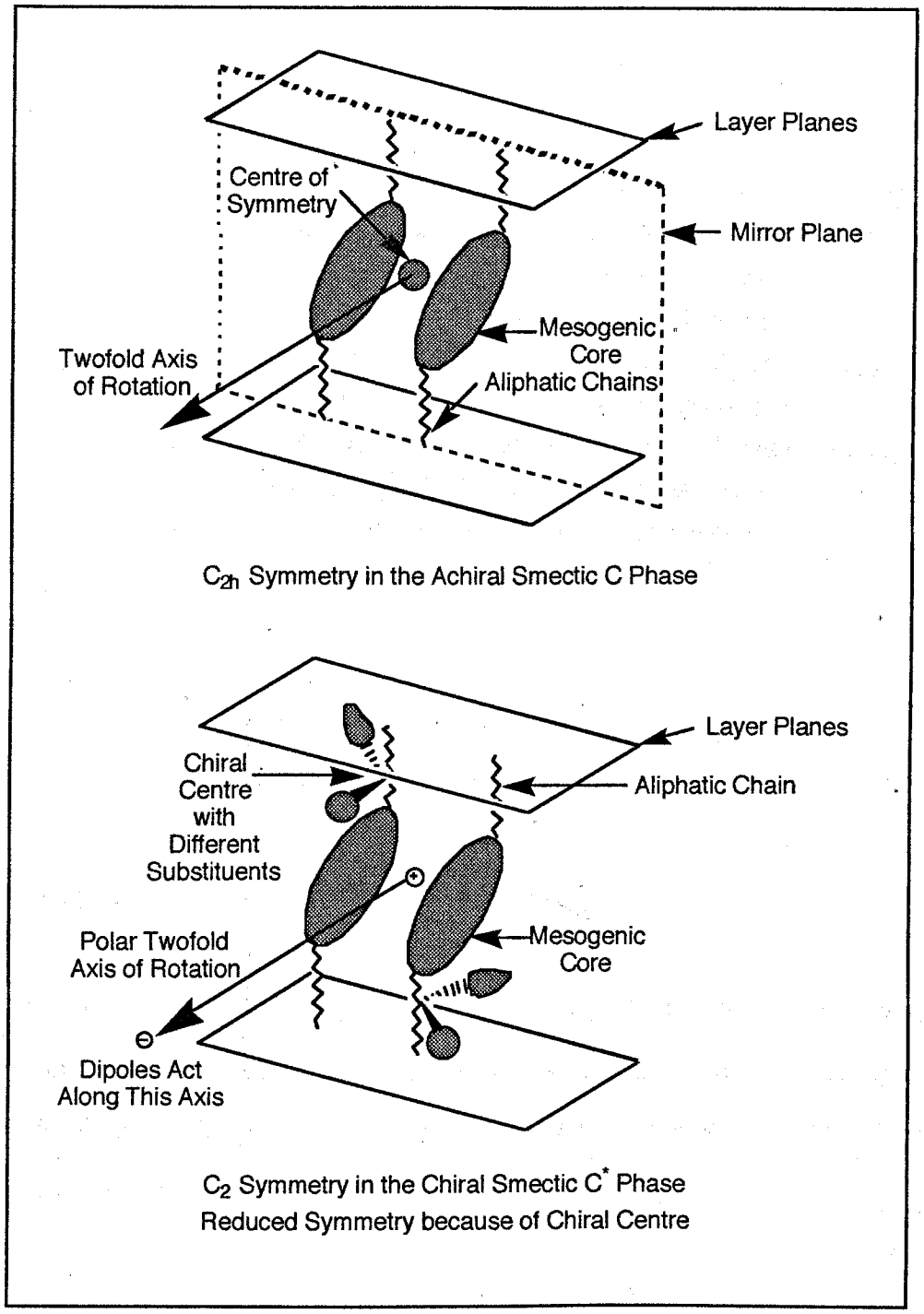

Fig. 1.3.2 Space symmetry in achiral and chiral SmC liquid crystal phases.

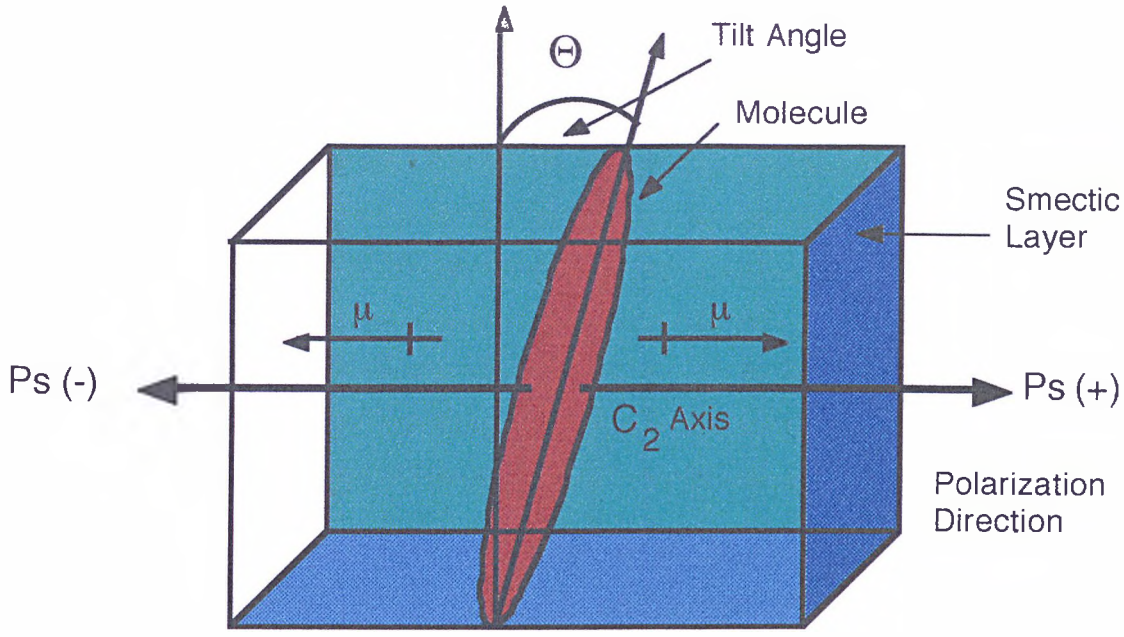

Fig. 1.3.3 The spatial orientation of the spontaneous polarization (Ps) in SmC* phases. The arrow indicating the direction of the Ps also indicates the local dipole direction.

(2) Phase Symmetry

In the SmC* phase, the long axes of the molecules are tilted with respect to the layer planes and the tilt of the molecules can precess about an axis normal to the layers on passing from layer to layer as shown in Fig. 1.3.4. The rotation of the tilt is in the same direction and hence a macroscopic helix is formed.

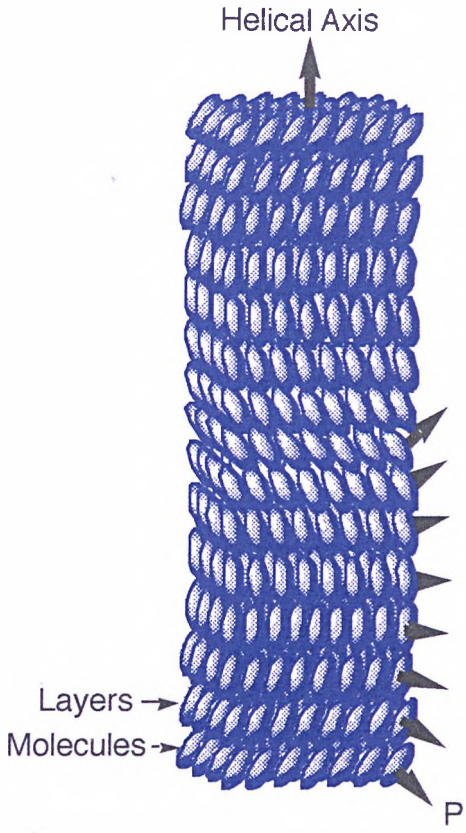

Fig. 1.3.4 Structure of chiral SmC* phases

A beam of plane polarized light traversing the SmC* phase will therefore be rotated by the helical ordering. The specific rotation [α] is usually much greater for these phases than for the specific rotations of individual molecules. The helical ordering can be defined as a left-hand or a right-hand helix by the direction of the rotation on moving away from an observation point along the helical axis. Plane polarized light traversing this structure will have its plane of polarization rotated in the same direction as the helix.

Usually, the pitch in the SmC* phase is longer than in the cholesteric phase and shorter than in SmI* or SmF* if the phases are exhibited by the same compound. For the SmC* phase, where the pitch length of the helix is of a similar magnitude to the wavelength of

the light, the light will be selectively reflected which gives the iridescent colour change due to increasing the tilt angle on the cooling process.

The helicoidal pitch, l, is typically of the order of 10^3 d (d is the smectic layer spacing). The helix can be unwound along the C_2 axis by applying an electric field and a net spontaneous polarization will occur.

(3) Molecular Symmetry

The spatial configuration about each chiral atom is denoted by an absolute configuration label as either *R* (*rectus*, right) or *S* (*sinister*, left) introduced by Cahn *et al.*[38-39]. The *R* and *S* absolute configuration system is obtained by determining the relationship of the group priorities about the asymmetric atom based on atomic number.

Some attempts have been made to relate the direction of the polarization to the spatial configuration of the molecules in a similar way to that used by Gray and McDonnell[30] for the helical structure mentioned in Section 1.2.4. The absolute spatial configuration of the chiral centre determines the direction of the associated dipole, and hence the direction of any resulting spontaneous polarization. The following relationships were found to have some use in SmC* liquid crystals.

Sed **P** (-) $+I$	Sol **P** (+) $+I$	Sod **P** (-) $-I$	Sel **P** (+) $-I$
Red **P** (-) $-I$	Rol **P** (+) $-I$	Rod **P** (-) $+I$	Rel **P** (+) $+I$

where S or R is the absolute configuration, o or e is the parity, l or d is the screw direction of the helix, **P** (+) or **P** (-) is the polarization direction and $-I$ or $+I$ is the inductive effect of the off-axis substituent at the chiral centre. The inductive effect

essentially determines the direction of the dipole at the chiral centre. This relationship works very well for simple molecules, but for more complicated structures it is not reliable[40-41].

1.3.3 Surface-Stabilized Ferroelectric Liquid Crystal (SSFLC)

Bulk ferroelectric liquid crystal (FLC) compounds do not have uniform director orientation but exhibit helicity. However, N. Clark and S. Lagerwall[13] found a unique method for unwinding the helical structure which can show stable oriented states suitable for bistable switching. The suppression of the helix requires a very thin cell gap which is set to be smaller than the helical pitch. They demonstrated that in a homogeneously aligned cell, *i.e.* with the director parallel to the glass plates, the helical structure of the SmC* phase is unwound when the cell thickness is thin enough, i.e. about 2 μm. In a surface stabilized FLC cell the smectic layers are almost normal to the electrodes and the net spontaneous polarization (Ps) is thus perpendicular to the glass plates. An external field may therefore couple directly to the Ps and a DC pulse can switch the material from $+\theta$ to $-\theta$ or in the reverse direction as shown in Fig. 1.3.5. The situation in Fig. 1.3.5 (a) refers to the case where an external electric field had been applied previously. The polarization vector always tends to align parallel to an electric field. The subsequent application of a reverse electric field makes the polarization vector swing around by 180° thereby forcing the director to rotate on a cone until the situation in Fig. 1.3.5 (b) is obtained. When the field is removed, the molecules remain in that state until a field of opposite polarity is applied. This property is termed *orientational bistability*. This is the highly desired memory effect which distinguishes ferroelectric displays from conventional nematic ones. FLC displays have a viewing angle dependency that is superior to other liquid crystal devices because the directors of the molecules switch around an axis which is essentially perpendicular to the light entering

Polarization Reversal in Smectic C* Liquid Crystals

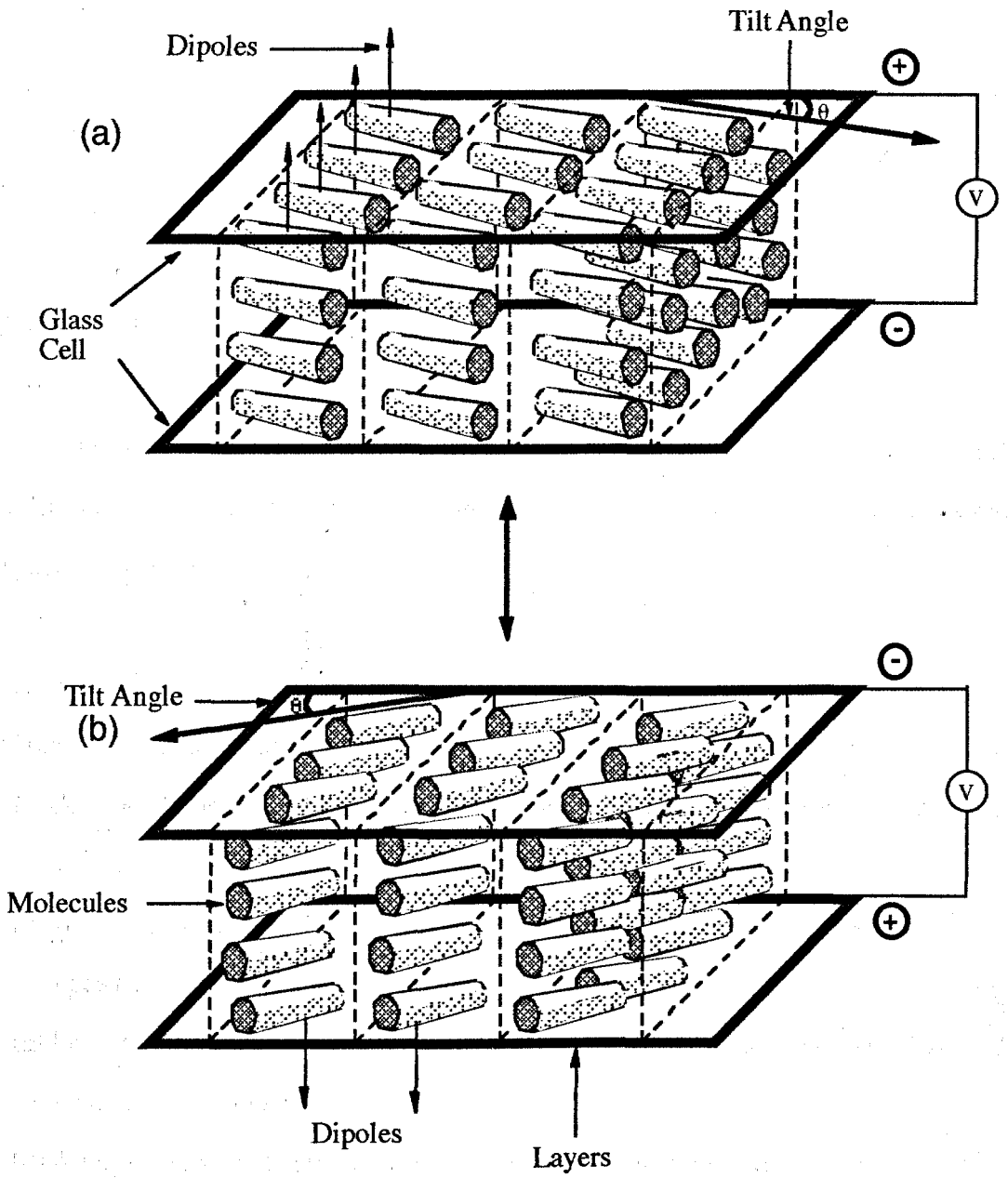

Polarity Reversal of the Applied DC Electric Field

Molecules Switch Through Twice the Tilt Angle

Fig. 1.3.5 (a) and (b) Schematic representation of a surface-stabilized FLC (SSFLC) cell in which the helix is unwound due to the strong surface interaction in thin cells.

the cell. This is an intrinsic property of the device geometry and the surface stabilized states.

In addition, due to the relatively strong coupling between the Ps and the externally applied field, the response time may be estimated as 10-50 ns; orders of magnitude faster than that for the twisted nematics.

1.3.4 Ferroelectric Liquid Crystals for Displays

Great interest has been shown in the properties of ferroelectric liquid crystals since the SSFLC device was proposed which can show the advantages over the conventional displays as mentioned previously.

There are several physical properties and requirements for their use in an FLC device, and these include the following[42-47]:

(a) A wide temperature range of the SmC* phase including room temperature is required.

(b) A low viscosity and a high polarization material is needed for fast switching speeds.

(c) Long helical pitches and a N*-SmA*-SmC* phase sequence are required to achieve good alignment.

(d) A large dielectric biaxiability is better in order to support a multiplex addressing device scheme.

(e) An appropriate tilt angle of 22.5° is needed for an optimum compromise between fast switching and good contrast ratio.

(1) SSFLC Cell Design Considerations

By means of a simple mechanical model, the response time τ[45] is approximately proportional to the rotational viscosity (γ) of the material but inversely proportional to the product of the polarization (Ps) and the electric field (E) as shown below:

$$\tau = \gamma \sin^2\theta / Ps\, E$$

The desired fast switching time is achieved by increasing the field strength. As E = U/d (U = applied voltage to the cell, d = cell gap), this can be aligned with either an increase voltage or a decreased cell gap. However, both are subject to electronic and mechanical limitations.

A more fundamental requirement for d is that the thickness should be smaller than the pitch of the helix. If d is much larger than the pitch, free macroscopic volumes exist where the helix is generated so the system is not ferroelectric. In order to avoid the formation of a helix in the bulk of the cell, d has to be made so small as to quench the helix. That is why this arrangement is called surface stabilized.

The optical path length difference ($d\Delta n$) is strongly related to the intensity (I) of light passing through the analyzer. I is given by the formula[13,48] below:

$$I = I_0 \sin^2 4\theta \sin^2 (\pi d\Delta n / \lambda)$$

where I_0 is the intensity of light passing through the cell in the configuration depicted in Fig. 1.3.5 but with the analyzer turned parallel to the polarizer and λ is the

corresponding wavelength. Maximum contrast is achieved for maximum I when $I = I_0$ and $\theta = 22.5°$.

When we can take $\lambda = 550$ nm as it is approximately the weighted centre of natural day light and $d\Delta n = (2k+1)\lambda / 2$, $k = 0, 1, 2, ...$, the optimum $d\Delta n$ is about 0.275 μm. The optical anisotropy for available SmC* materials is around 0.1 to 0.2, and this leads to a cell gap range from $1.3 \leq d \leq 2.8$ μm. Though the liquid crystal layer in an SSFLC cell is very thin[43], it is sufficiently birefringent to produce useful optical effects based on the different propagation characteristics of polarized light in the two states leading to affording a light valve with excellent contrast.

(2) Spontaneous Polarization and Rotational Viscosity

The most important properties of a material with regard to its switching time in an SSFLC cell are the rotational viscosity and the spontaneous polarization which makes demands on the chemists. Fast switching times can be achieved by a high polarization or a low viscosity of the materials.

There are at least two important molecular factors which influence the value of the polarization. The first factor is the size and direction of the molecular dipole, and the second the potential energy of a molecule for rotation around its long axis[49].

In relation to the dipole moment for a given molecular structure, the relationship between the polarization power δ_p, which describes the ability of a given chiral polar dopant to induce a polarization in a SmC host phase, and the molecular structure, was discussed by H. Stegemeyer[50] using the model shown in Fig. 1.3.6.

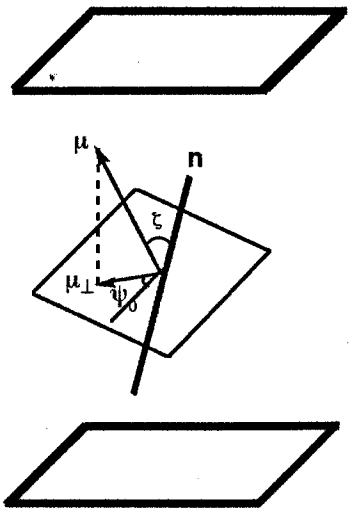

Fig. 1.3.6 Model of a molecule lying in a SmC layer. The molecule is in its minimal potential energy.

In order to obtain a large δ_p value, the following requirements were proposed: a large molecular dipole (μ), a large angle (ζ) between the dipole and molecular long axis and a small angle ψ_0, where U (ψ_0) is the minimal potential energy. The angle ζ scales the transverse dipole as $\mu_\perp = \mu \sin \zeta$ (see Fig. 1.3.6).

Some interesting correlations for Ps values[49] were reported as follows. For example, replacing the 2-methylbutyl chiral unit of (*S*)-DOBAMBC by a α-chloropropyl moiety, to give (*S*)-2-chloropropyl N-(4-hexyloxybenzylidene)-4'-aminocinnamate (HOBACPC), increases the Ps by a factor of 5. Replacement of the 2-methylbutyl chiral unit of DOBAMBC by the isomeric 1-metylbutyl unit (DOBA-1MBC) increases the Ps by more than a factor of 10 as shown in Fig.1.3.7.

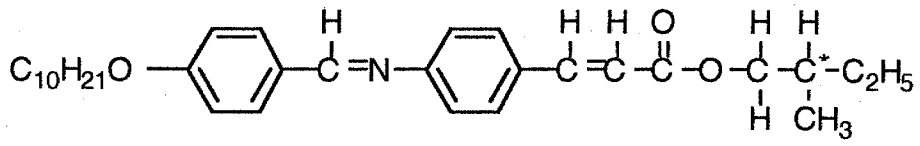

DOBAMBC Ps = 3 nC cm^{-2}

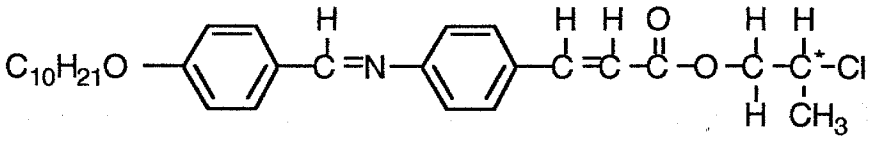

HOBACPC Ps = 15 nC cm^{-2}

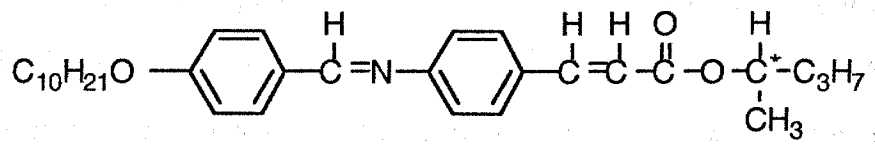

DOBA-1-MBC Ps = 40 nC cm^{-2}

Fig. 1.3.7 Comparisons of Ps

In addition, Goodby *et al.*[42] synthesised the homologous series of the (*R*)- or (*S*)-1-methylalkyl 4-n-alkanoyloxybiphenyl-4'-carboxylates and showed that the polarization decreases as the chiral centre of methylalkyl is moved further away from the core.

These observations suggest that (1) introducing a polar group attached to the chiral centre may increase Ps and (2) movement of the chiral centre close to the core may increase Ps. The further the dipole and the chiral centre are apart the more internal rotations are possible. Therefore the average dipole decreases very rapidly as the distance from the chiral centre is increased.

Concerning the potential energy for the rotation of a molecule around its long axis in a tilted SmC phase, a macroscopic model was introduced by Urbanc and Zeks[51]. They assumed the ordering of the transverse dipole $\mu_\perp$ is induced by the tilt only and a hindered rotation of the molecules around their long axes is taken account. If the angle

ψ describes the orientation of $\mu_\perp$ around the molecular long axis the potential U (ψ) for the hindered rotation is given by

$$U(\psi) = -a_1\theta \cos\psi - a_2\theta^2 \cos 2\psi$$

The first term is of a chiral nature, and the potential parameter a_1 is positive when the tilt tends to induce the polar ordering in the direction of $\psi = 0$. The second term is non-chiral in character and quadratic in θ. It leads to a quadrapolar ordering in the direction perpendicular to the tilt, *i.e.* $\psi = 0$ and 180° when the coefficient a_2 is positive. Some steric effects from a branch in the alkyl chain or a rigid molecular structure influence the values of a_1 and a_2. A large value of a_1 is needed for a high polarization. The influence of steric effects on a_1 is maximized by increasing the molecular chirality. On the other hand, molecular biaxiability can be one of the factors which influences the value of a_2.

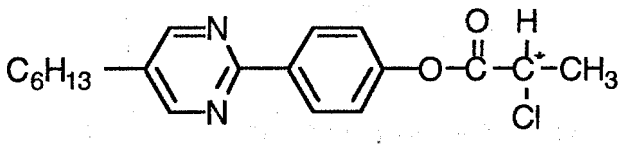

IS 1662 Ps = 50 nC cm^{-2}

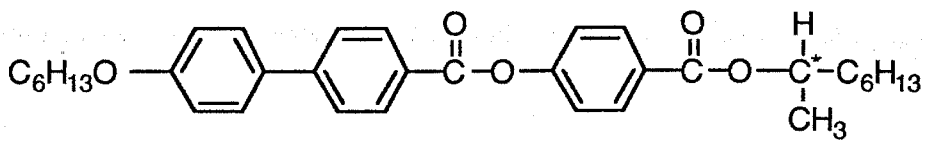

S811 Ps = 121 nC cm^{-2}

Fig. 1.3.8 Comparisons of Ps

In Fig. 1.3.8[50], the compound S811 shows a larger Ps value compared to the compound IS 1662. This may be attributed to the steric effects of the methyl branch plus there is no subtraction of two dipoles associated with the ester carbonyl and the chiral centre of compound S811, whereas the two dipoles in compound 1662 oppose one another.

Besides Ps, the only bulk property which determines the switching time is the rotational viscosity γ_φ which describes the friction experienced by the molecules as they jointly rotate about their lateral axes. The molecules move in three different ways[52] as shown in Fig. 1.3.9.

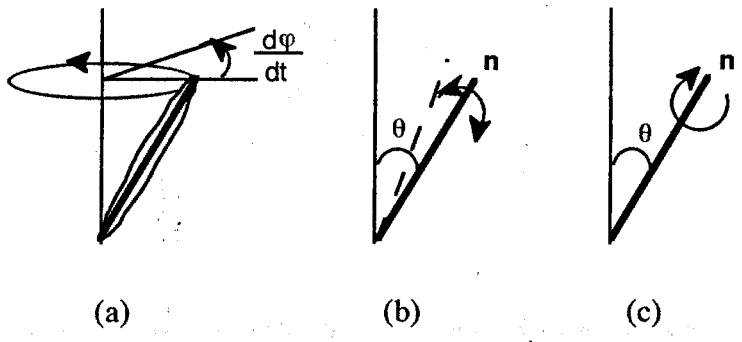

Fig. 1.3.9 The three different modes of rotation

(a) around the cone (Goldstone mode) with a rotational viscosity γ_φ, (b) around θ (soft mode) with a rotational viscosity γ_θ, (c) around the director n with a rotational viscosity γ_n.

Although viscosity is one of the most important parameters to measure, experimental results on the relationship between molecular structure and viscosity are poorly correlated at present. However several methods[13,53-57] for evaluating viscosities have been proposed. C. Escher *et al.*[58] suggested the simple dynamic model to relate the rotational viscosity to the spontaneous polarization, tilt angle and the electric field

strength. The derived relationship was used to determine the rotational viscosity. Its configuration in Fig. 1.3.10 is characterized by the normal to the smectic layers **N**, the **c** director which is a unit vector parallel to the projection of the long molecular axes on the smectic plane, the polarization vector **P**, the tilt angle is θ and the rotation angle α between the unit vector in the **z** direction $\mathbf{e_z}$ and the polarization vector **P**.

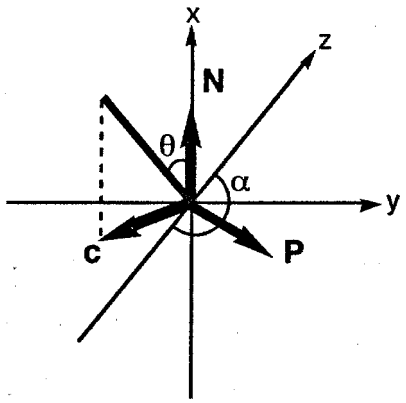

Fig. 1.3.10 A simple model shows the angle α (t) between **P** (t) and the space fixed z axis.

In an SSFLC cell, by applying an electric field **E** = **Eez** in the z direction, the polarization vector **P** tends to align parallel to the field due to the linear coupling of **P** and **E**. According the theory of S. A. Pikin[59], the director rotation around the SmC* layer normal **N** (parallel to the substrates) may be described as follows:

$$K\theta^2 (\partial^2\alpha/\partial N^2) + PsE\cdot\sin\alpha = \gamma_\alpha (\partial\alpha/\partial t) \qquad (1)$$

where K and γ_α are respectively the elastic and the viscosity constants in relation to the layer normal. The equation ignores the variations of the SmC* layer tilt angle θ under the influence of an electric field E because θ does not change during the application of the field. According to a qualitative theoretical description by M. I. Barnik *et al.*[56], the

elastic term $K\theta^2$ ($\partial^2\alpha/\partial N^2$) was not taken into account in equation (1) because the elastic constant does not play any role in switching if the electric field is high enough[60-62]. They obtained the following formula by solving equation (1) for a constant electric field.

$$\alpha = \arctan(A \cdot \exp(t/\tau)), \quad A = \tan(\alpha_0/2)$$

$$\text{where } \alpha_0 = \alpha(t_0) \text{ and } \tau = \gamma_\alpha/PsE$$

The rotational viscosity γ_α acts in the role of a kinetic coefficient, describing the dynamics of the azimuthal SmC* director angle for the fixed tilt angle θ. E. P. Pozhidayev *et at.*[63] showed the temperature dependence of another SmC* rotational viscosity γ_θ, related to the dynamic relaxation processes of the tilt angle θ at a constant value of α. The comparison of the γ_α and γ_θ leads to the conclusion that in general one deals with the tensor of the SmC* viscosity; γ_α and γ_θ being its principal components. However, if variations in θ are small, the electrooptic response dynamics may be described only with the help of the rotational viscosity γ_α. It is also known that γ_α compares in value with the typical rotational viscosity of nematic liquid crystals at room temperature or even less, while γ_θ remains by one or two orders of magnitude greater. The small value of the chiral SmC* liquid crystal viscosity γ_α may be explained by the symmetric peculiarities of SmC*; the dissipation of the C* free energy process of the director rotation around the layer normal remains reasonably low.

(3) Non-Chiral Smectic C Host Material and Dopants

There are two kinds of techniques employed to achieve usable FLC mixtures for display application as follows:

1) Method 1

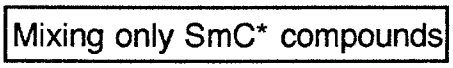

Initially, researchers focused on the development of fast switching chiral SmC* materials for displays by simply increasing the polarity associated with the asymmetric centre. However, this approach leads to the build up of a large internal fields in device switching[64-65], thereby making polarization reversal difficult because there is a latching effect that needs to take place before switching occurs.

2) Method 2

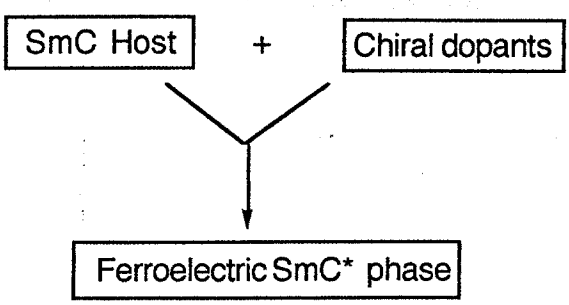

Mixtures created by adding a high polarization dopant to a non ferroelectric SmC host have been widely investigated in order to produce a low viscosity material. The use of doped SmC mixtures for devices also allows us to control phase type and transition temperatures. Thus, mixtures possessing a N*-SmA*-SmC* phase sequence can be produced with suitable temperature profiles where the helical phases could be engineered to have long helical pitches. Long helical pitches and a N*-SmA*-SmC*

phase sequence are required in order to generate, during cell fabrication, an aligned ferroelectric liquid crystal phase over a large area.

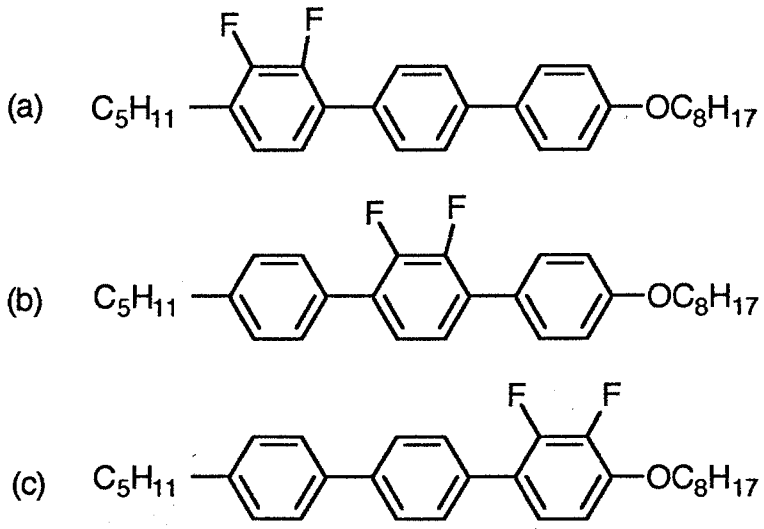

(a) I 166 °C N 165 SmA 155 SmC (mp 89)

(b) I 141.5 °C N 95 - SmC (mp 48.5)

(c) I 159 °C N 148 SmA 144 SmC (mp 93.5)

Fig. 1.3.11 Terphenyls used in host mixtures for ferroelectric displays

For example, three ring systems are found to have a high SmA-SmC transition temperatures, broad SmC temperature ranges and may have negative dielectric anisotropy. The use of lateral fluoro-substituents in the aromatic region of the core is particularly interesting and useful for the purposes of creating a negative dielectric anisotropy and a large dielectric biaxiality.

In this system, the transverse polarity and hence the dielectric biaxiality of smectic compounds can be increased. In addition, the incorporation of fluoro substituents has the effect of suppressing ordered smectic phases more than the SmC mesophase and lowering the melting point. Thus mixtures of difluoro-terphenyls can be created to form basic hosts to which chiral dopants can be added to give ferroelectric mixtures[66]. Fig. 1.3.11 shows a set of typical difluoro-terphenyls which when mixed together give SmC phases that exist over a wide temperature range of 70 to 80 °C.

1.4 Antiferroelectricity

1.4.1 Discovery of Antiferroelectric Liquid Crystals (AFLCs)

In 1983, Levelut *et al.*[67] reported the existence of a new smectic liquid crystal phase, called SmO* in 1-(methylheptyl)terephthalidene-bis-aminocinnamate (MHTAC, see Fig. 1.4.1). Later SmO* was proposed to have an herringbone packing structure by Galerne and Liebert[68]. In this structure the molecular tilt direction alternates on passing from one layer to the next.

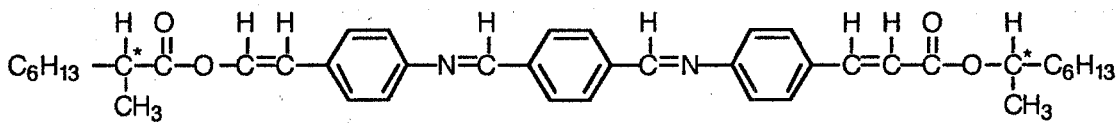

Fig. 1.4.1 Structure of MHTAC

In 1988, unusual switching behaviour was found in 4-(1-methylheptyloxycarbonyl)phenyl-4'-octyloxybiphenyl-4-carboxylate (MHPOBC, see Fig. 1.4.2).

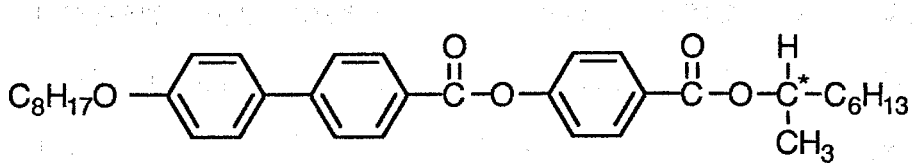

Fig. 1.4.2 Structure of MHPOBC

Hiji *et al.*[69] found the appearance of a third stable switched state in addition to the +/- θ tilted uniform states found in ferroelectric switching. Furukawa *et al.*[70] also noticed that the switching between the ferroelectric states exhibited a clear DC threshold. They considered the DC threshold to be a property of an as yet uncharacterised unknown

phase designated as SmY* which was not miscible with SmC*, SmI* and SmF*. Chandani *et al.*[71] later ascribed both of these observations as coming from the same origin, namely the emergence of an antiferroelectric SmC* mesophase, SmC_A*.

In 1988, Goodby *et al.*[72] found that the chiral compounds (*R*)- and (*S*)-1-methylpentyl 4-n-decyloxybenzoyloxybiphenyl 4'-carboxylate possess two extra smectic phases in comparison to the phase seen for the racemic form (see Fig. 1.4.3). They found that the SmC_{ferri}* and SmC_A* phase disappear when one of the enantiomers is mixed with the racemate. At percentages below 78% and 70% of the chiral isomer in the mixture the antiferroelectric and ferrielectric properties disappear. Therefore the optically active isomers appear to exhibit a different mesophase morphology to the racemate. They also reported that the transition to and from the SmC_{ferri}* and SmC_A* phases have extremely small enthalpies.

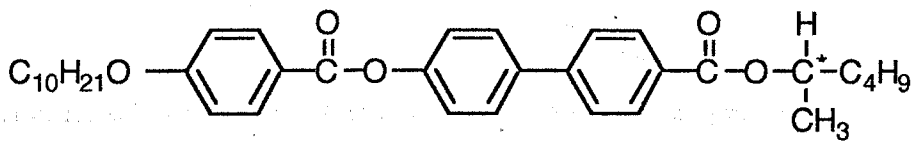

(*R*)	I	135.5 °C	SmA*	106.5	SmC*	86.6	SmC_{ferri}*	74.2	SmC_A*	48.1	SmJ*
(*S*)	I	133.9 °C	SmA*	106.7	SmC*	87.3	SmC_{ferri}*	85.0	SmC_A*	48.5	SmJ*
(*R/S*)	I	132.4 °C	SmA	105.4	SmC	86.6	-	-	-	46.1	SmJ

Fig. 1.4.3 Effect of optical purity on antiferroelectric phases

Since AFLCs exhibit unique characteristics for device applications such as a DC threshold and a double hysteresis loop related to a third stable switched state for a pulsed applied electric field, Nippon denso Co., and Showa Shell Sekiyu K. K. began to

construct displays based on tristable switching[73] and they developed several AFLCs compounds with a trifluoromethyl unit attached to the chiral centre[74] (see Fig. 1.4.4). In 1989, they demonstrated a prototype antiferroelectric liquid crystal display (AFLCD)[75] using a six component system containing (*R*)-(+)-4-(1-trifluoromethylheptyloxycarbonyl)phenyl 4'-n-octyloxybiphenyl-4-carboxylate (TFMHPOBC) , MHPOBC and their homologues.

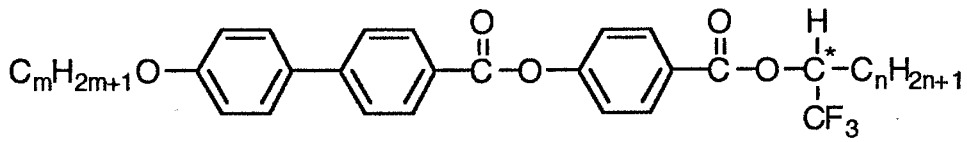

where m = 8, 9, 10 or 12 and n = 6 or 8

Fig. 1.4.4 Structure of chiral 4-(1-trifluoromethylalkoxy(n)carbonyl)phenyl 4'-alkoxy(m)biphenyl-4-carboxylate

1.4.2 Structure of Antiferroelectric Liquid Crystal and Subphases

The proposed structure of the chiral antiferroelectric mesophase SmC_A^* is depicted in Fig. 1.4.5 (a). As in the SmC* phase, chirality induces a precession of the tilt from layer to layer, leading to the formation of helicoidal structure with the axis parallel to the smectic layer normal. Molecules in neighbouring layers tilt in almost the same direction but with the opposite sense, and consequently the spontaneous polarizations associated with adjacent layers point in the opposite directions with respect to the tilt plane. Therefore there is no net spontaneous polarization. It was suggested that the structure of SmC_A^* phase was being stabilised by strong molecular chirality which causes the molecules in adjacent layers to tilt in opposite direction to one another. Thus in the

SmC_A* phase, the coupling in adjacent layers oppose one another and the spontaneous polarization falls to zero whereas the unwound state of the SmC* phase where the molecules tilt in the same direction can produce a macroscopic spontaneous polarization.

To date, the proposed structure of the SmC_A* phase (see Fig. 1.4.5 (a)) has not been directly confirmed by means of X-ray diffraction, because it is not easy to determine the in-plane structure due to the liquid-like ordering of the smectic layers.

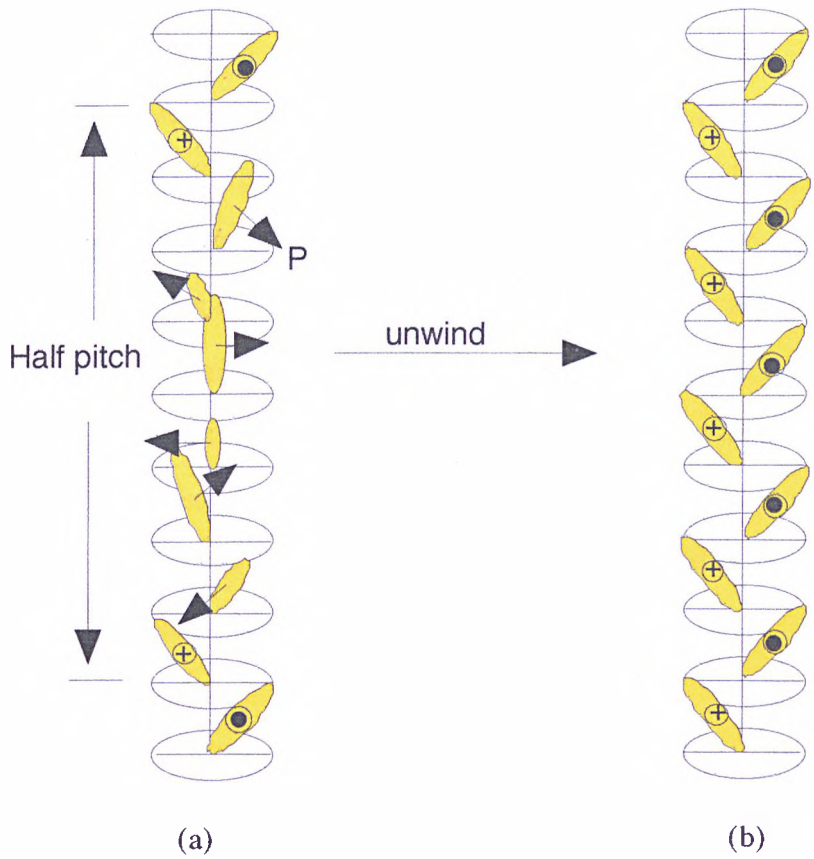

Fig. 1.4.5 (a) Proposed representation of the antiferroelectric helical structure of the SmC_A* phase (b) schematic representation of the unwound antiferroelectric phase

However the structure of an alternating tilt direction in neighbouring layers of SmC_A* phase depicted in Fig. 1.4.5 (b) was suggested by optical studies of a free standing film[76] of the compound MHPOBC. The thickness of these films ranges between several thousands and only two molecular smectic layers. Ellipsometric studies of very thin films consisting of four, three and two layers yielded direct evidence for the layer-by-layer alternating tilt in the SmC_A* phase. Galerne and Liebert[77-78] also confirmed the antiferroelectric herringbone structure in the so called SmO* phase of compound MHTAC (see Fig. 1.4.1) by studying thin SmO* films floating on the free surface of an isotropic MHTAC droplets. Thus, it was elucidated that the structures of SmC_A* phases differ from the conventional SmC* phases by their tilt direction structure.

The clarification of the subphase structures, *e.g.* SmC_γ* and SmC_α* in the SmC* region is essential for understanding antiferroelectricity in liquid crystals. A collection of intermediate states in the SmC* region can sometimes separate these two extremes of ferroelectric and antiferroelectric phases. These intermediate phases are known collectively as the ferrielectric phase, SmC_γ*. Hence for example, Fig. 1.4.6 shows a 1:1 relationship of zigzag bilayers to tilted monolayers, but other combinations can lead to 1:2 or 1:3 patterns. This unevenness in the layer distribution has led to a collection of structures that represent the so called ferrielectric phase. The structure of this phase was described as a 'Devil's staircase'[79-80].

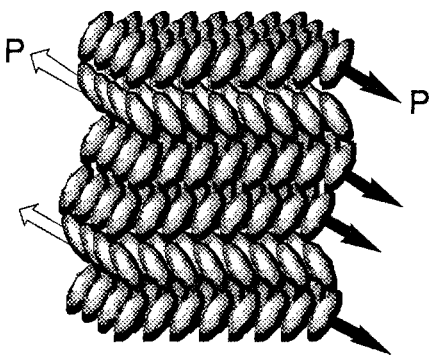

Fig. 1.4.6 Proposed structure of the ferrielectric phase

With respect to the SmC_α^* phase, thermal analysis[81-82] and XRD[83-84] have been found to be capable of detecting the SmA-SmC_α^* phase transition, and the results of these studies indicate that the molecules begin to tilt at the phase transition. It was suggested that the SmC_α^* phase has a tilted structure of the molecules with respect to the layer normal; antiferroelectric-like and ferrielectric-like ordering in the higher and lower temperature ranges of the phase respectively[83]. The competition between antiferroelectic and ferroelectric order may form another staircase structure. The possibility of randomness in the tilt direction can induce the complex structure of the SmC_α^* as follows;

(a) When the spontaneous polarization is zero, the SmC_α^* phase is an SmC-like phase with molecular tilting which is uncorrelated on the visible scale. When it is not zero, a novel type of Coulombic interaction between the smectic layers due to the presence of a collective polarization fluctuation causes the antiferroelectricity in the high temperature region of the SmC_α^* phase.

(b) SmC_α^* is a phase where the intra- and inter-layer correlations of the molecular tilting are greatly reduced whereas SmC_A^* and SmC_γ^* are phases with a long range correlation of the molecular tilt.

1.4.3 Antiferroelectric Switching Behaviour

(1) Tristable Switching and V-Shaped Switching

Ordinary antiferroelectricity in liquid crystals shows tristable switching. This is an electric field induced transition between the SmC_A^* and SmC* phases and has a characteristic DC threshold and double hysteresis loop[13, 80].

Fig. 1.4.7 (a) illustrates tristate switching of a homogeneously aligned cell placed between crossed polarizers, the axes of which are parallel and perpendicular to the smectic layer normal. By applying a positive or a negative bias field, switching between the third state and one of the bistable states occurs. For instance, under an applied voltage, Va, the directors are initially in the third state (Fig. 1.4.7 (a) point A). By superimposing a positive pulse of Vb, switching occurs from the third state to one of the bistable states occurs (Fig 1.4.7 (a) point B). The directors can be returned from point B to point A by superimposing a negative pulse of Vb. In tristable switching, when the electric field is applied, unwinding of the helicoidal structure of the SmC_A^* phase occurs and the direction of the tilt changes so a favourable polarization component grows in a direction perpendicular to the tilt plane, as illustrated in Fig. 1.4.7 (b). A long helicoidal pitch and a high threshold field for switching are assumed so that the unwinding process and the pretransitional effects can be considered as separate processes.

(a)

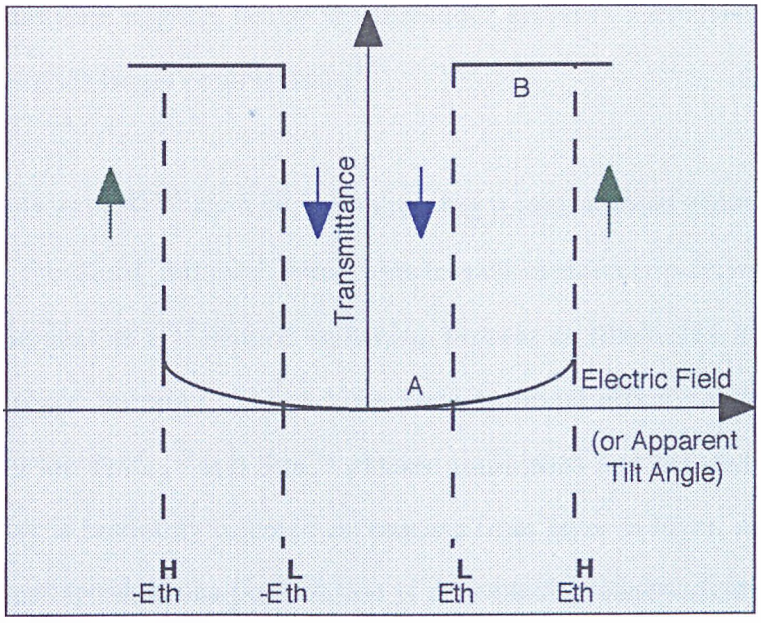

(b)

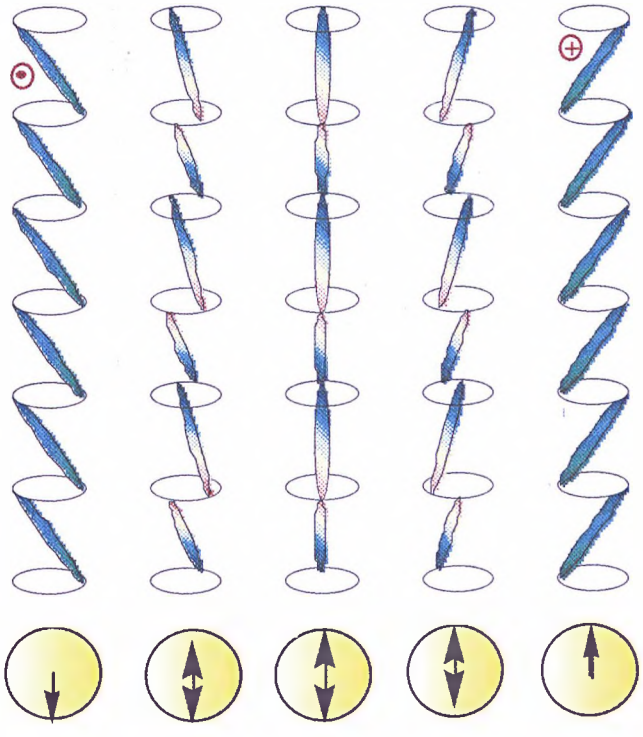

Fig. 1.4.7 (a) Tristable switching (b) molecular movements in the pretransitional effect

In the electric field induced antiferro-ferroelectric transition, pretransitonal effects which increase transmittance slightly below the threshold prevents antiferroelectric displays from achieving much larger contrast ratio.

However Fukuda *et al.*[85-86] showed, by enhancing pretransitional effects and reducing the threshold the field induced ferroelectric-antiferroelectric-ferroelectric phase transition can appear as a V-shaped switching process as illustrated in Fig. 1.4.8 (a). When the threshold becomes zero and the pretransitional effect prevails, the energy barrier between the SmC_A* and SmC* phases diminishes and the distribution of the polarizing vector is randomly oriented on passing from layer to layer, as shown in Fig. 1.4.8 (b). The net spontaneous polarization is cancelled by randomization, but not the antiparallel arrangement. Therefore the antiferro-ferroelectric phase transition occurs continuously. In the case of switching under a polarizing microscope, the visual field is varied uniformly and continuously without showing any irregularities, indicating that boundary movement characteristic of the tristable switching or the disclination lines caused by the helicoidcal unwinding of ferroelectric liquid crystals occurs. In V-shaped switching, the light transmission is almost linear to the applied field and free from the hysteresis which is good for analogue grey scale. Thus V-shaped switching is totally different from tristable switching and accompanying helicoidal unwinding.

(a)

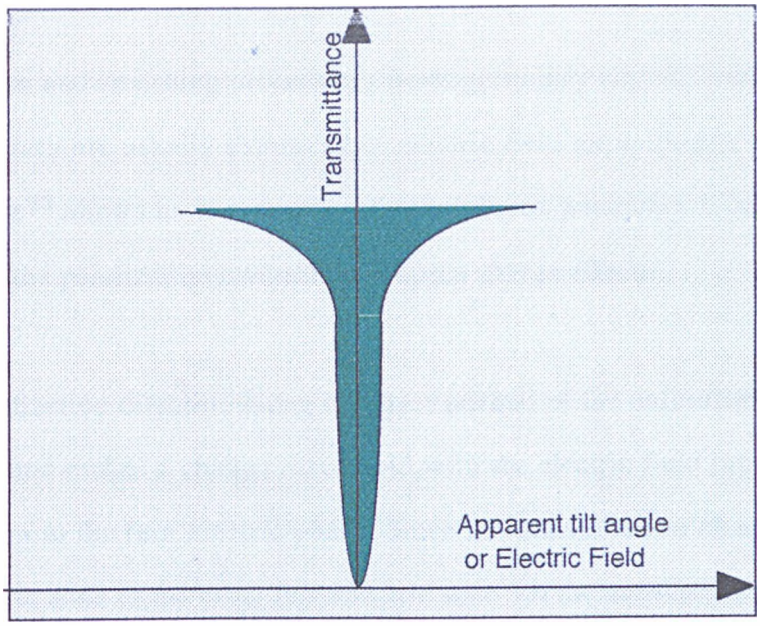

(b)

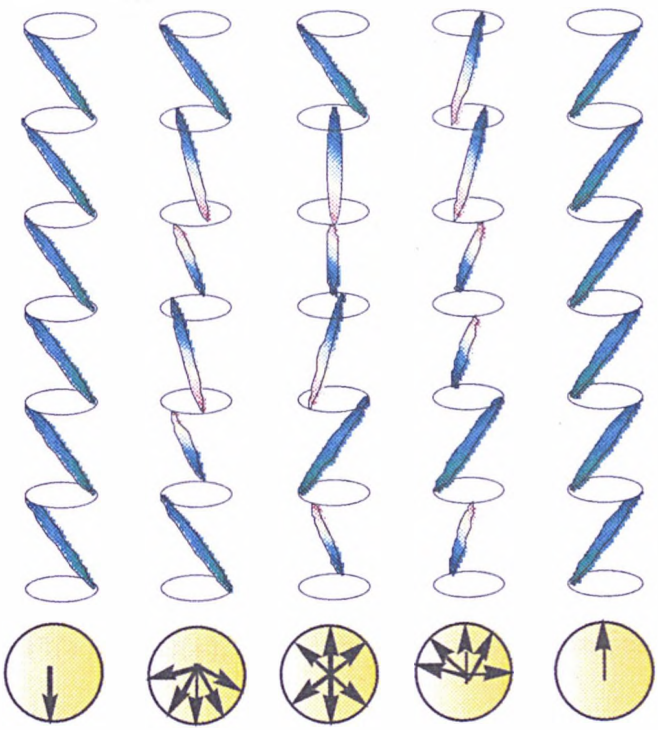

Fig. 1.4.8 (a) V-shaped switching (b) simplified model of the phase with thresholdless antiferroelectricity.

(2) Frequency-Dependent Spontaneous Polarization under Triangular Wave Studies

The polarization and switching process in a homogeneously aligned cell placed between crossed polarizers are usually examined in electric field experiments. Studies using a triangular wave[87] allows us to measure the spontaneous polarization independently, by separating out the polarization reversal from space charge effects.

The optical extinction direction along the layer normal of the antiferroelectric ordering is very stable and makes a change associated with the electric field induced first-order phase transition to the ferroelectric phase. Since the transmittance changes twice from one ferroelectric state to the other ferroelectric state *via* the antiferroelectric phase (see Fig. 1.4.7 (a)), under an AC field, dipole reversal takes place and two switching current peaks occur whereas a single peak appears in ferroelectric liquid crystal switching as shown in Fig. 1.4.9 (a) and (b).

In case of the switching in the SmC_γ^* phase, the four states, namely FO (ferroelectric state) (+), FI (ferrielectric state) (+), FI (-), and FO (-), are observed optically and show triple loops in the optical transmittance hysteresis loop where (+) and (-) specify the states stabilized by the positive and negative fields respectively. In the absence of a field, the stable molecular orientation is in one of the FI states, for instance, FI(-), which is chosen by the negative field, is stabilized when the positive field is turned off. Thus the change in θ with the respect to the electric field corresponds to the field induced changes of FI(-) -> FI(+) -> FO(+). Therefore the three switching peaks are observed as illustrated in Fig. 1.4.9 (c).

However, the switching behaviour in SmC_A^* and SmC_γ^* phases depends on the frequency of the triangular wave. At higher frequencies, direct switching occurs between the two FO states without passing through the AFO and FI states. The complicated frequency dependence is interpreted on the basis of the spatial ordering associated inhomogeneous domain switching[88]. If the relaxation time from field induced FO state to AFO state is slower compared with the inverse of the applied wave frequency, direct switching between two FO states occurs.

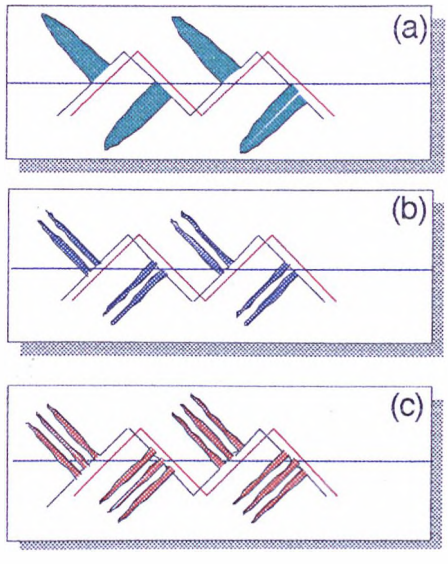

Fig. 1.4.9 Triangular wave studies for (a) ferroelectric (b) antiferroelectric (c) ferrielectric phases

1.4.4 Identification of Antiferroelectric Phases by Optical Microscopy

The *schlieren* texture observed in planar nematic cells is characterized by ±1/2 defects and ±1 defects (see Fig. 1.2.4), whereas homeotropic cells of tilted smectic phases such as the SmC phases exhibit singularities that only have four *schlieren* brushes. This is because of the existence of the c director in SmC phases, *i.e.* the projection of the director into the smectic plane and the sense of the c director, thus $c \neq -c$. The situation in nonchiral SmC_A may differ from that in the SmC because the c directors in adjacent

layers are oriented in the opposite sense, the director is c and -c in adjacent layers. Hence the discontinuous boundary, c ≠ -c disappears if a screw dislocation with a Burgers vector of the same magnitude as the layer spacing exists at the core of the defect. This kind of complex defect consisting of a screw dislocation and a wedge disclination is called a dispiration[89]. Therefore the defects of strength s = ±1/2 exist in the nonchiral SmC_A phase in addition to those observed in normal SmC phases (s = ± 1) (see Fig. 1.4.10).

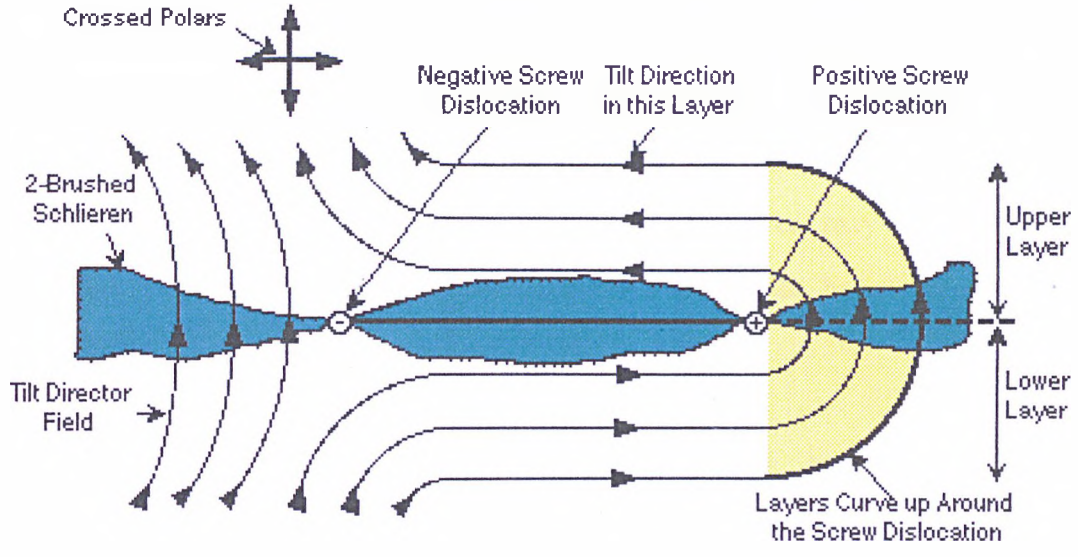

Fig. 1.4.10 S = ±1/2 dispirations

1.4.5 Antiferroelectric Liquid Crystalline Materials

Typically, molecules that exhibit antiferroelectric phases have structures that contain central rigid cores composed of at least three aromatic or heterocyclic rings. Attached to the core is a terminal chiral group that has its chiral centre positioned adjacent to the core, and on the peripheral side of the asymmetric atom there is a chain of at least six

carbon atoms in length. Thus, in effect, molecules with this form of structural architecture would be expected to exhibit strong molecular chirality, which may alter the liquid crystalline properties.

A number of homologous series have been found that exhibit antiferroelectric properties. To date, more than 300 compounds are known which possess an antiferroelectric phase[90]. Nearly all of these have either ester or carbonyl groups linking the chiral centre to the core; the core can have lateral substituents, and the chiral end group is either 1-methylheptyl, 1-ethylheptyl, 1-propylheptyl, or 1-trifluoromethylheptyl. All of the molecules have significantly large transverse permanent dipole moments on the terminal chiral group, therefore they possess relatively large spontaneous polarizations, *i.e.* of the order of 100 $nCcm^{-2}$. The magnitude of the spontaneous polarization value, however, may not have a direct relationship with the appearance of the antiferroelectric phase, because the phase was even observed in racemic modifications[91-93].

Some important results concerning the relationship between molecular structure and the appearance of the antiferroelectric phase have been reported as follows.

(1) Effect of the Chiral End-unit on the Antiferroelectric Properties

Antiferroelectric behaviour can occur when the chiral unit is linked to a benzoate or phenone core unit as shown in Fig. 1.4.11 (a) and (b), but thus far antiferroelectric phases have not been observed in compounds with an ether or a reverse ester linkage as shown in Fig. 1.4.11 (c) and (d)[94-95].

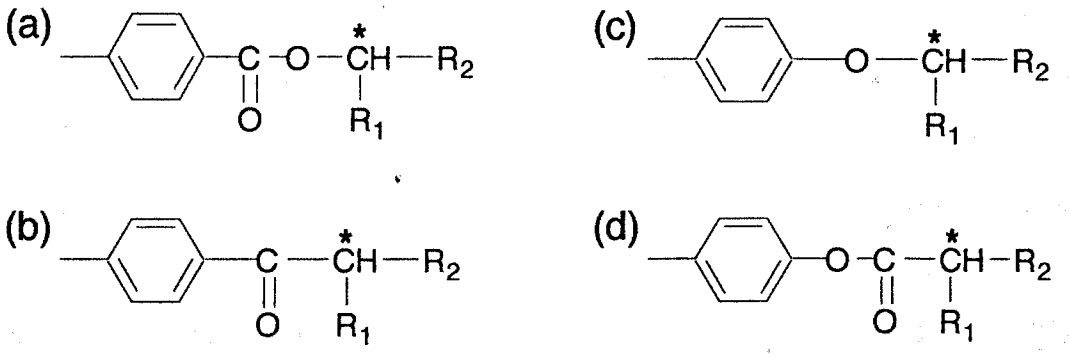

Fig. 1.4.11 Structures suitable for the appearance of SmC_A^* ((a), (b)) and unsuitable ((c), (d))

(2) Effect of the Length of the Lateral Branching Unit at the Chiral Centre

It was reported[96] that the introduction of a lateral ethyl group at the chiral centre instead of a methyl group (see Fig. 1.4.12) decreases overall the phase stability, but in opposing this trend, the SmC_A^* phases were enhanced by approximately 20 °C. Therefore, increasing the size of the chiral branching group increases the stability of the SmC_A^* phase.

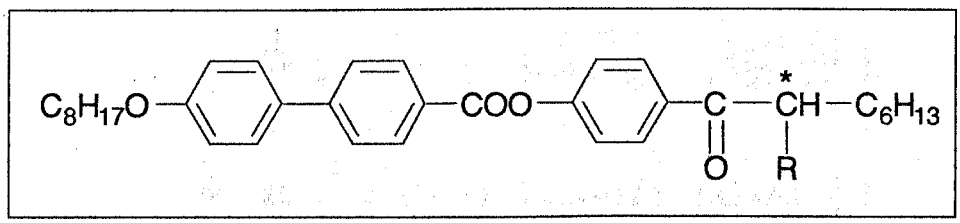

R = CH_3 I 150 °C SmA* 132 SmC* 65 SmC_A^*

R = C_2H_5 I 108 °C SmA* 100 SmC* 85 SmC_A^*

Fig. 1.4.12 Effect of the length of the lateral branching unit at the chiral centre

The results illustrated in Fig. 1.4.13 show that ferroelectric phases are depressed as the size of the lateral group at the chiral centre is increased. Conversely, the antiferroelectric phase is stabilized in the same process. The introduction of a propyl group, when r = 3, produces a layer steric effect which further stabilizes the antiferroelectric phase and suppresses ferroelectric phase formation totally. This effect has been coined the 'propyl effect'[97] hence, the ferroelectric phase becomes eclipsed and direct SmA to SmC_A^* transitions occur without the presence of a SmC* phase.

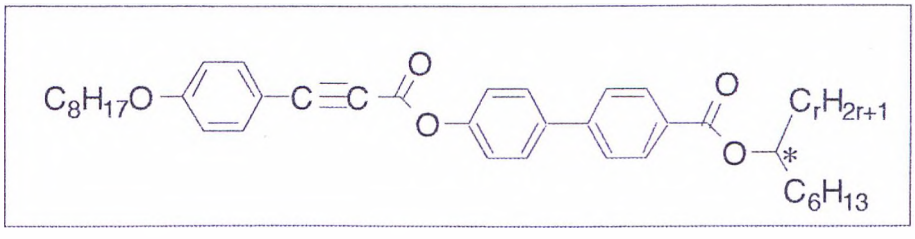

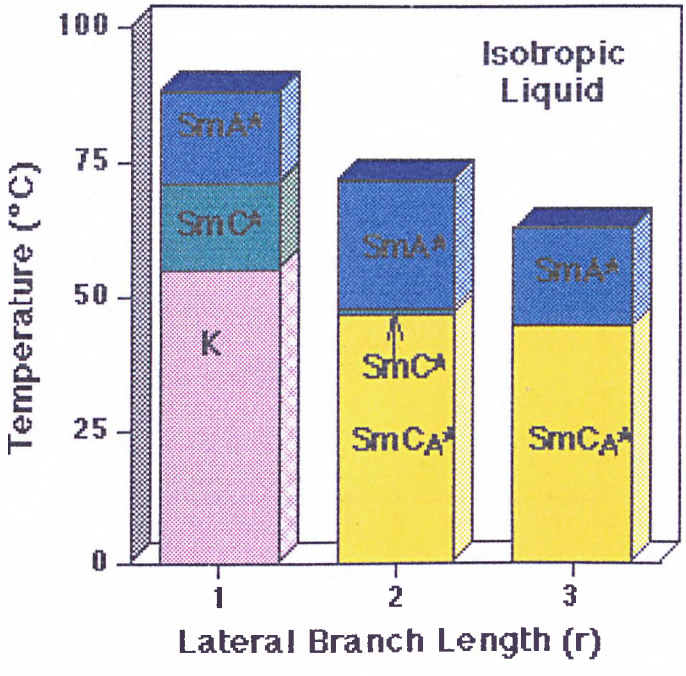

Fig. 1.4.13 Effect of terminal and lateral chain length on antiferroelectric phases

The apparent tilt angle as a function of the applied electric field measured at 2 °C below the upper transition temperature for the antiferroelectric phases (see Fig. 1.4.14) show that there is a remarkable increase in the value of threshold electric field, E_{th} for the larger branch compound (when p = 3) in comparison to the shorter chain length (when p = 2)[98]. These results demonstrate that the antiferroelectric phase in propyl branched system is considerably more stable than for the ethyl substituted system.

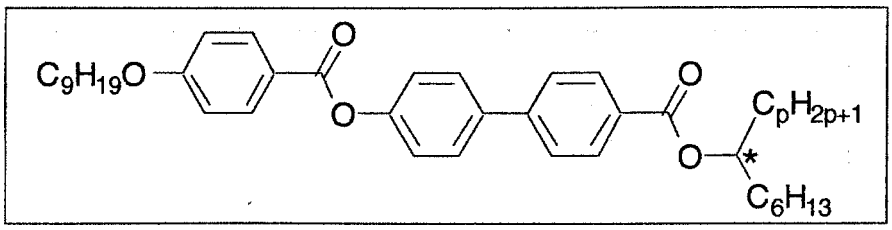

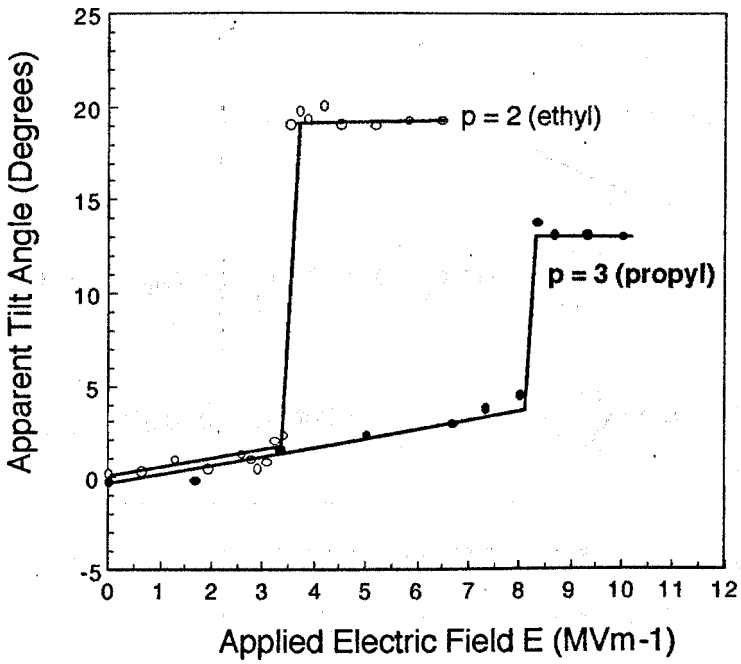

Fig. 1.4.14 The apparent tilt angle as a function of applied electric field measured for the antiferroelectric phase in (*R*)-1-ethylheptyl 4'-n-nonyloxybenzoyloxybiphenyl-4-carboxylate (p = 2) and (*R*)-1-propylheptyl 4'-n-nonyloxybenzoyloxybiphenyl-4-carboxylate (p = 3)

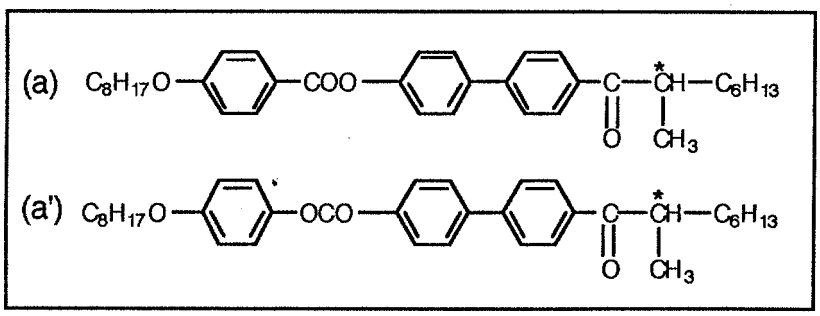

(a) I 136 °C SmA* 108 SmC* 49 SmC_A*

(a') I 132° C SmA* 100 SmC* no SmC_A*

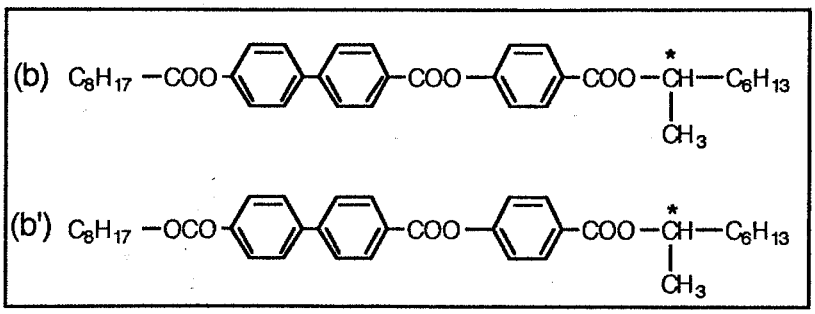

(a) I 145 °C SmA* 115 SmC* 103 SmC_A*

(a') I 101 °C SmA* 92 SmC* no SmC_A*

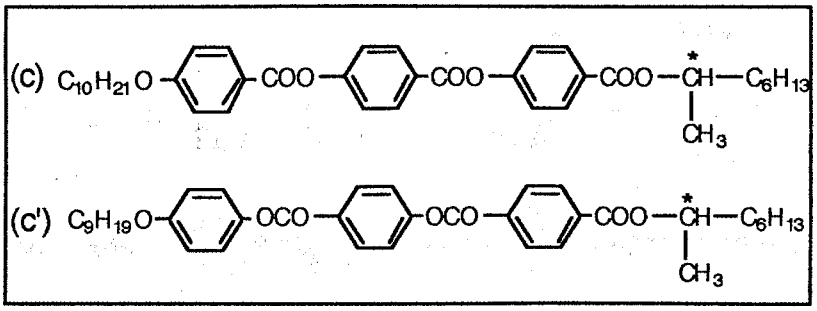

(c) I 137 °C SmA* 115 SmC* 96 SmC_A*

(c') I 105 °C SmA* 102 SmC* no SmC_A*

Fig. 1.4.15 Effect of the direction of the ester group on the appearance of SmC_A* phase

(3) Effect of the Direction of Ester Functionalities

It is important for the appearance of the SmC_A^* phase to align the ester groups in the molecule along a certain direction. For example, the compounds (a), (b), and (c) exhibit the SmC_A^* phase, whereas the compounds (a'), (b') and (c') do not[95, 99-100] (see Fig. 1.4.15).

(4) Effect of Fluorine on the Formation of Antiferroelectric Phases

The effect of the introduction of fluorine atom(s) at the chiral centre on the stability of the SmC_A^* phase was investigated for various materials, the phase transitions for which can be compared in Fig. 1.4.16[101-102].

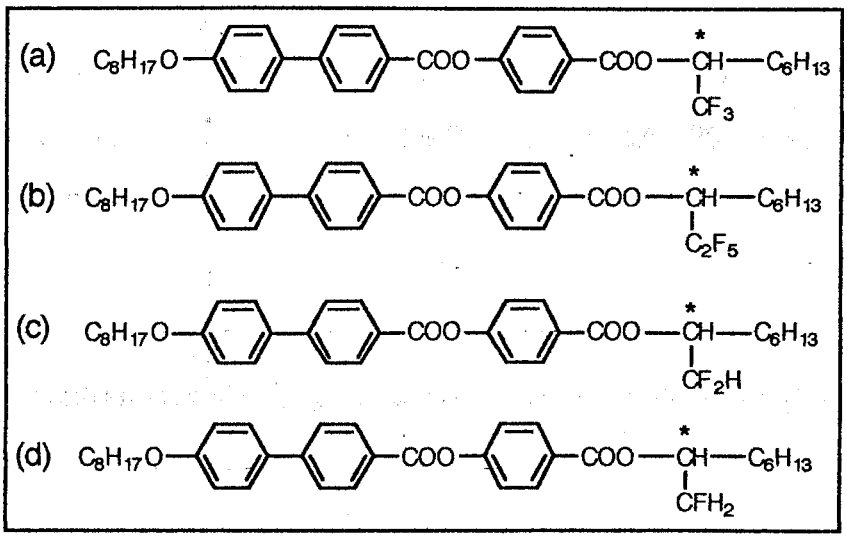

(a) I 121.0 °C SmA* 109 SmC_A^*

(b) I 85.5 °C SmA* 76.8 SmC_A^*

(c) I 125.0 °C SmA* 113.5 SmC* (no SmC_A^*)

(d) I 132.8 °C SmA* 105.5 SmC* (no SmC_A^*)

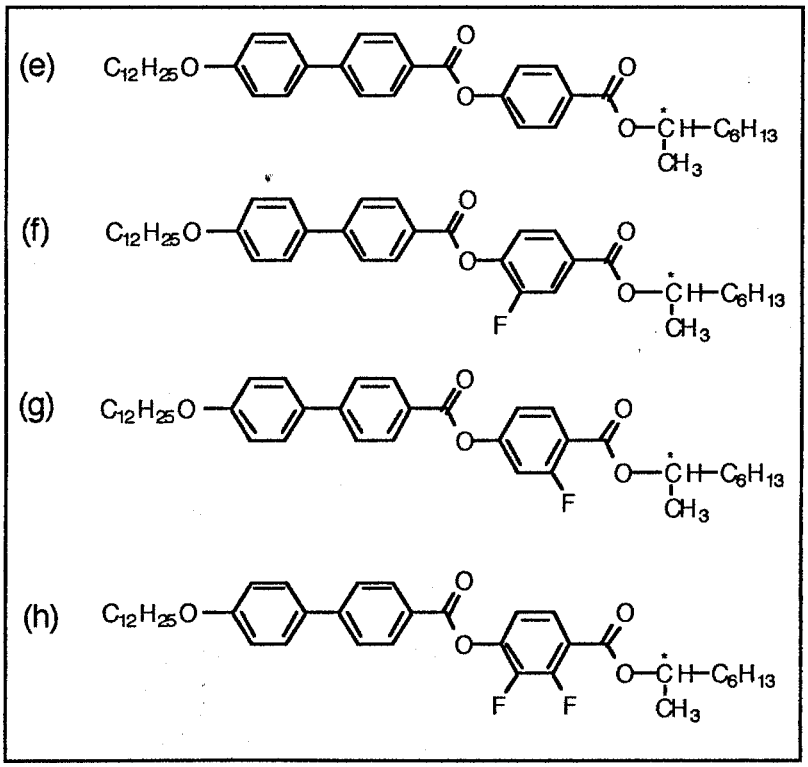

(e) I 129 °C SmA* 122 SmC_α* 117 SmC* 103.5 SmC_γ* 100 SmC_A* (mp 73)

(f) I 106 °C SmA* - - 91 SmC* 82 SmC_γ* 78 SmC_A* (mp 53)

(g) I 127 °C SmA* - - - - 119 SmC_γ* 108.4 SmC_A* (mp 40)

(h) I 111 °C SmA* - - 100 SmC* 95 SmC_γ* 94 SmC_A* (mp 53)

Fig. 1.4.16 Effect of introducing fluorine atoms on the stability of the SmC_A* phase

1.4.6 Antiferroelectric Structure in Non-chiral Liquid Crystals

Most materials that exhibit antiferroelectric properties are highly chiral and therefore have helical macro-structures. However, non-chiral materials which apparently exhibit a smectic phase that has antiferroelectric-like layer ordering were reported[97], suggesting that the formation of an antiferroelectric structure is due to the presence of dimeric molecular species.

In chiral systems, compounds have strong dipoles which act along the C_2 axis of the SmC* phase. Therefore the dipoles can couple to produce a macroscopic spontaneous polarization. Conversely, pairing of the molecules will compensate for the strong lateral dipoles along the C_2 axis and reduce the value of the spontaneous polarization. This pairing causes the molecules in adjacent layers to tilt in opposite directions to one another as shown in Fig. 1.4.17 (a), forming a zigzag layer ordering.

In the case of racemic modifications, it is thought that like chiral materials aggregate together to give an inhomogeneous distribution of (*S*)-(*S*) and (*R*)-(*R*) pairs. Therefore, an inhomogeneous zigzag antiferroelectric structure is obtained as shown in Fig. 1.4.17 (b).

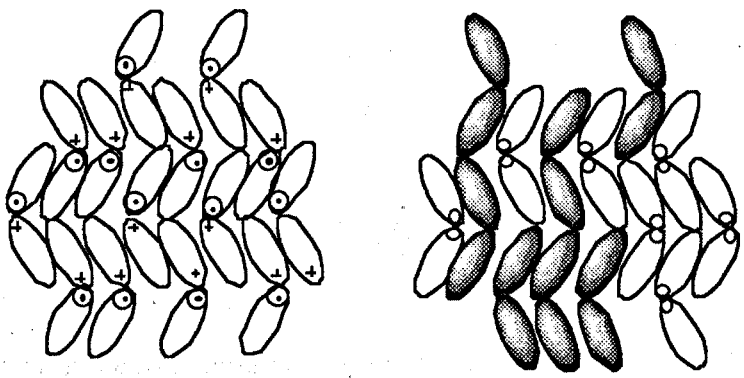

Fig . 1.4.17 (a) Chiral molecules pairing which have opposing dipole directions. (b) pairing in a racemic modification.

For example, Nishiyama *et al.* found that compound 1-propylbutyl 4'-(4-n-nonyloxyphenylpropioloyloxy)biphenyl-4-carboxylate (see Fig. 1.4.18) showed a similar structure to the antiferroelectric phase even though it is not chiral. The branching atom is sp^3 hybridized. Therefore the forked tail of the molecule is no longer co-planar with the molecular core but bent at an angle with respect to the long axis. The bending of the swallow tail would be expected to cause the formation of either bent or zigzag shaped dimers.

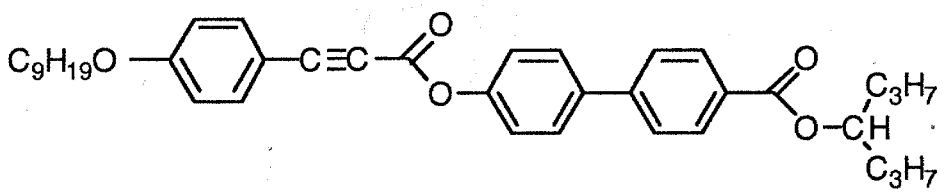

I 70.0 °C SmA 54.8 SmC_{Alt} 41.7 K

Fig. 1.4.18 Structure of 1-propylbutyl 4'-(4-n-nonyloxyphenylpropioloyloxy)biphenyl-4-carboxylate and its transition temperature.

As illustrated in Fig. 1.4.19, interdigitation of end chains orients the rigid parts of the molecules in adjacent layers to have opposing tilt. The packing together of bent dimeric species may result in the formation of antiferroelectric structures.

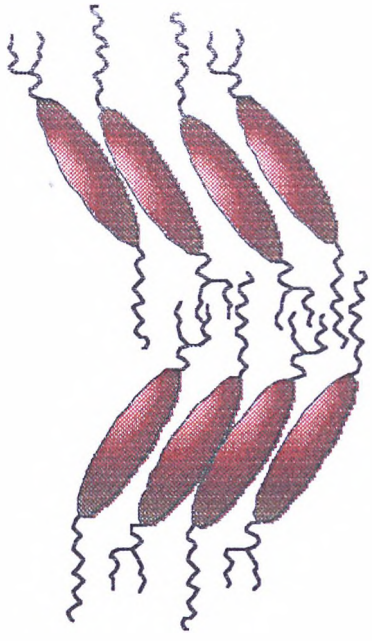

Fig. 1.4.19 Alternating smectic C (SmC_{Alt}) phase

(1) Effect of the Central Linkage on Alternating Tilt Phases[103]

An investigation of the non-chiral, racemic swallow-tailed molecules is shown in Fig. 1.4.20. This shows that the stability of the phase of SmC_{Alt} is influenced to a larger extent by the character of the linking group.

When the linking group is dimethylene (see Fig. 1.4.20 (c)), the transitions are low in temperature and monotropic. There is free rotation around this bond and the increase in number of possible conformations may reduce the mesomorphic character of the compound either through an increase in the apparent width of the molecule or by a decrease in linearity. Alternatively the linkage could effectively reduce the size of the rigid core by quasi disconnection of the phenyl groups of the core. In comparison the ethenyl linkage (see Fig. 1.4.20 (b)), has a high barrier to the rotation from the *trans* configuration and there is extended delocalisation of electrons across the whole of the

core. Hence polarization is possible through the double bond from the phenyl group. Therefore a long rigid core which has a zigzag structure is important in enhancing the antiferroelectric phase. The ethynyl linkage (see Fig. 1.4.20 (a)) is more linear; this may have the effect of increasing the core interaction and hence the melting point so that phase transitions are monotropic. The strong localisation of electrons in the triple bond may also have the effect of reducing transition temperatures.

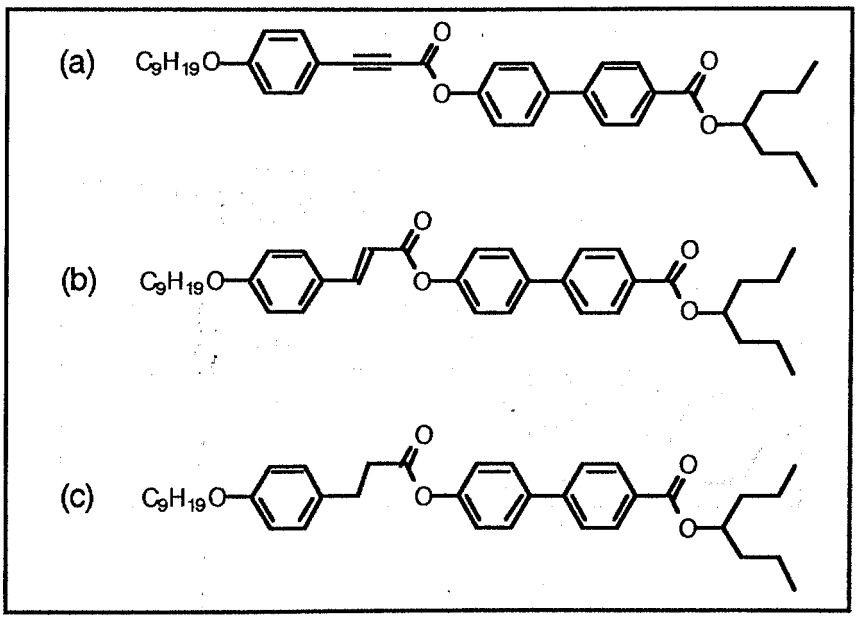

(a)	I	70 °C	SmA	54.8	SmC_{Alt}	41.7 K	(mp 73)
(b)	I	126 °C	SmA	112	SmC_{Alt}	106.5 K	(mp 106.5)
(c)	I	40 °C	SmA	35	SmC/K		(mp 60)

Fig. 1.4.20 Effect of the central linkage on alternating tilt phases

(2) Effect of Swallow Tail Structures on Alternating Tilt Phases[104]

If molecules have the a bent structure, the distance between the transverse dipole moments of the molecules belonging to adjacent layers may be shorter, which is suitable for the pairing of molecules that stabilize the antiferroelectric liquid crystal phase.

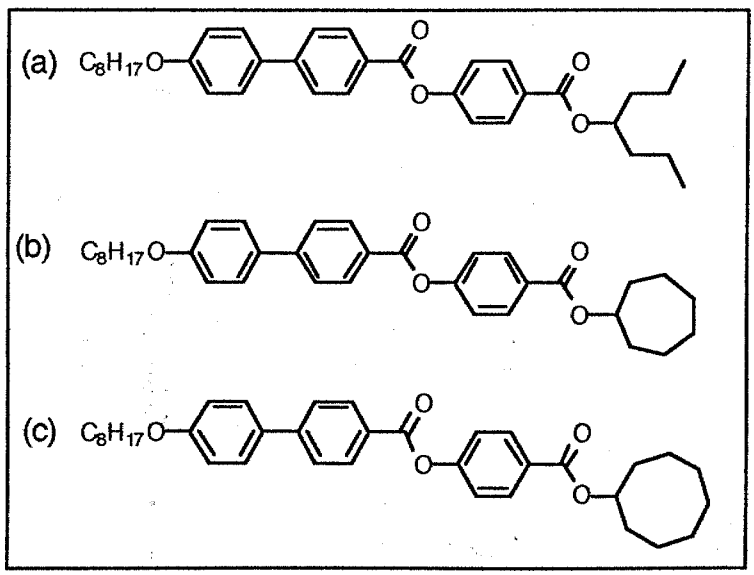

(a)	I	119.7 °C	SmA	103.2	SmC_{Alt}	(mp 80)
(b)	I	176.7 °C	SmA	134.3	SmC	(mp 106.6)
(c)	I	171.5 °C	SmA	140	SmC	(mp 102.8)

Fig. 1.4.21 Effect of the swallow tail structure on SmC_{Alt} properties

In Fig. 1.4.21, a swallow tailed compound is shown which was found to exhibit an alternating tilt SmC phase whereas the ring tailed compounds shows only SmC phases. This indicates that the steric interaction between the molecules *via* the terminal alkyl

chains is also necessary for pairing to occur. For ring tailed compounds (in Fig. 1.4.21 (b), (c)), overlap is difficult. The steric interaction of terminal aliphatic chain overlap which produce the alternating layer structure may be weak. If this is the case, the pairing of ring tailed molecules can not be enhanced by steric interactions and SmC_{Alt} phases do not appear. This demonstrates the need for inter layer interactions of the molecules in stabilizing the zigzag structure of the antiferroelectric-like phase.

1.5 References

1. F. Reinitzer, Monatsh, *Chem.*, 1888, **9**, 421
2. O. Z. Lehmann, *Phys. Chem.* (Leipzig), 1889, **4**, 462
3. D. Volander, *Ber. Deut. Chem. Ges.*, 1921, **54**, 2261
4. G. Friedel, *Ann. Physique.*, 1922, **18**, 273
5. R. Williams, *J. Chem. Phys.*, 1963, **39**, 384
6. A. P. Kapustin and L. K. Vistin, *Kristallografiya*, 1965, **10**, 118
7. G. H. Heilmeir, L. A. Zanoni and L. A. Barton, *Appl. Phys. Lett.*, 1968, **13**, 46
8. M. Schadt and W. Helfrich, *Appl. Phys. Lett.*, 1971, **18**, 127
9. J. L. Fergason, *Appl. Optics.*, 1968, **7**, 1729
10. G. W. Gray, K. J. Harrison and J. A. Nash, *Electron Lett.*, 1973, **9**, 130
11. G. W. Gray, *J. Phys.* (Paris), 1975, **36**, 337
12. T. J. Scheffer, and J. Nehring, *Appl. Phys. Lett.*, 1984, **45**, 1021
13. N. A. Clark and S. T. Lagerwall, *Appl. Phys. Lett.*, 1980, **36**, 899
14. P.J. Collings and M. Hird, '*Introduction to Liquid Crystals*', Taylor and Francis 1997
15. K. J. Toyne, '*Thermotropic Liquid Crystals*' ed G. W. Gray, Wiley, Chichester, 1987
16. H. Sackmann and D. Demus, *Mol. Cryst. Liq. Cryst.*, 1966, **2**, 81
17. S. L. Arora, J. L. Ferason and A. Saupe, *Mol. Cryst. Liq. Cryst.*, 1970, **10**, 243
18. A. Saupe, *Mol. Cryst. Liq. Cryst.*, 1969, **7**, 59
19. G. W. Gray and J. W. Goodby, '*Smectic Liquid Crystals*', Leonard Hill, Glasgow, 1984
20. P. G. de Gennes, '*The Physics of Liquid Crystals*', Clarendon press, Oxford, 1974
21. A. Losche and S. Grande, *18th Ampere Congress*, Nottingham, England, 1974, 201
22. A. Losche, S. Grande and K. Eider, *1st Specialised Colloque Ampere*, Krakow,

Poland, 1973, 103

23. N. A. Clark and S. T. Lagerwall, '*Ferroelectric Liquid Crystals*' Vol 7, Gordon and Breach Science Publishers, 1991
24. A. de Vries, *Mol. Cryst. Liq. Cryst.*, 1970, **10**, 219
25. W. L. McMillan, *Phys. Rev.*, 1973, **8**, 1921
26. A. Wulf, *Phys. Rev.*, 1975, **11A**, 365
27. B. W. Van der Meer and G. Vertogen, *J. Phys.*, 1979, **40**, C3-222
28. R. G. Priest, *J. Phys.*, 1975, **36**, 437
29. W. J. A. Goossens, *J. Phys.*, 1985, **46**, 1411
30. G. W. Gray and D. G. McDonnell, *Mol. Cryst. Liq. Cryst.*, 1977, **34**, 211-217
31. G. W. Gray and D. Coates, *Phys. Lett.*, 1973, **45A**, 115
32. D. Demus, S. Diele, S. Grande and H. Sackmann, *Adv. Liq. Cryst.*, 1983, **6**, 1
33. J. Valasek, *Phys. Rev.*, 1921, **17**, 475
34. R. B. Meyer, L. Liebert, L. Strzele and P. Keller, *J. Phys. Lett.*, 1975, **36**, L69
35. R. B. Meyer, *Mol. Cryst. Liq. Cryst.*, 1977, **40**, 33
36. H. B. Brand, P. E. Cladis and P. L. Finn, *Phys. Rev.* A, 1985, **31**, 361
37. J. S. Patel and J. W. Goodby, *Opt. Eng.*, 1987, **26**, 373
38. R. S. Cahn, C. K. Ingold and V. Prelog, *Angew. Chem. Int. Ed.*, 1966, **5**, 385
39. R. S. Cahn and C. K. Ingold, *J. Chem. Soc.*,1951, 612
40. J. W. Goodby, E. Chin, T. M. Leslie, J. M. Geary and J. S. Patel, *J. Am. Chem. Soc.*, 1986, **108**, 4729
41. J. W. Goodby and E. Chin, *J. Am. Chem. Soc.*, 1986, **108**, 4736
42. J. W. Goodby and T. M. Leslie, *Mol. Cryst. Liq. Cryst.*, 1984, **110**. 175
43. S. T. Lagerwall, N. A. Clark, J. Dijon, J. F. Clerc, *Ferroelectrics*, 1989, **94**, 1205
44. T. Geelhaar, *Ferroelectrics*, 1988, **85**, 329
45. M. A. Handscky and N. A. Clark., *Appl. Phys. Lett.*, 1982, **41**, 39
46. M. J. Bradshaw, V. Brimmell and E. P. Raynes, *Liq. Cryst.*, 1987, **2**, 107

47. L. K. M. Chan, G. W. Gray, D. Lacey, R. M. Scrowston, I. G. Shenouda, K. J. Toyne, *Mol. Cryst. Liq. Cryst.*, 1989, **172**, 125

48. M. Born, *Optik*, Springer Verlag, Berlin-Heidelberg-New York 1972

49. D. M. Walba, S. C. Slater, W. N. Thurmes, N. A. Clark, M. A. Handschy and F. Supon, *J. Am. Chem. Soc.*, 1986, **108**, 5210

50. H. Stegemeyer, R. Meister, U. Hoffmann and W. Kuczynski, *Liq. Cryst.*, 1991, **10**, No. 3, 295

51. B. Urbanc and B. Zeks, *Liq. Cryst.*, 1989, **5**, No. 24, 1075

52. J. Dijon, '*Liquid Crystals Applications and Uses*' Vol.1 Edi. by B. Bahadur, World Scientific Publishing Co. Pte. Ltd, 1990

53. K. Sharp, *Ferroelectrics*, 1988, **84**, 119

54. Ph. Mattinot-Lagarde, *J. Phys. Lett.*, 1977, **38**, L-17

55. W. Kuczynski and Ber. Bunsenges, *Phys. Chem.*, 1981, **85**, 234

56. M. I. Barnik, V. A. Baikalov, V. G. Chigrinov and E. P. Pozhidaev, *Mol. Cryst. Liq. Cryst.*, 1987, **143**, 101

57. P. Pieranski, E. Guyon, P. Keller, L. Liebert, W. Kuczynski and P. Pieranski, *Mol. Cryst. Liq. Cryst.*, 1977, **38**, 275

58. C. Escher, T. Geelhaar and E. Bohm, *Liq. Cryst.*, 1988, **3**, No.4, 469

59. S. A. Pikin, '*Structural Trnasformations in Liquid Crystals*' (In Russian), M., Nauka, 1981

60. M. A. Handschy and N. A. Clark, *Ferroelectrics*, 1984, **59**, 69

61. N. A. Clark, M. A. Handschy and S. T. Lagerwall, *Mol. Cryst. Liq. Cryst.*, 1983, **94**, 213

62. N. A. Clark and S. T. Lagerwall, *Ferroelectrics*, 1984, **59**, 25

63. E. P. Pozhidayev, L. M. Blinov, L. A. Beresnev and V. V. Belyaev, *Mol. Cryst. Liq. Cryst.*, 1985, **124**, 359

64. H. R. Duebal, C. Escher, D. Guenther, W. Hemmerling, Y. Inoguchi, I. Mueller, M.

Murakami, D. Ohlendorf and R. Wingen, *Jpn. J. Appl. Phys.*, 1988, 27, L.2241

65. J. Dijon, C. Ebel, C. Vauchier, F. Baume, J. F. Clerc, M. Estor, T. Leroux, P. Maltese and L. Mulatier, *SID'88 DI-GEST*, 1988, 246
66. G. W. Gray, M. Hird, D. Lacey and K. Toyne, *J. Chem. Soc., Perkin Trans II*, 1989, 2041
67. A. M. Levelut, C. Germain, P. Keller, L. Liebert and J. Billard, *J. Phys.* (Paris), 1983, **44**, 623
68. Y. Galerne and L. Liebert, *Phys. Rev. Lett.*, 1990, **64**, 906
69. N. Hiji, A. D. L. Chandani, S. Nishiyama and Y. Ouchi, H. Takezoe and A. Fukuda, *Ferroelectrics*, 1988, **85**, 99
70. K. Furukawa, K. Terashima, M. Ichihashi, S. Saitoh, K. Miyazawa and T. Inukai, *Ferroelectrics*, 1988, **85**, 451
71. A. D. L. Chandani, E. Gorecka, Y. Ouchi, H. Takezoe and A. Fukuda, *Jpn. J. Appl. Phys.*, 1989, **28**, L1265
72. J. W. Goodby and E. Chin, *Liq. Cryst.*, 1988, **3**, 1245
73. M. Yamawaki, Y. Yamada, N. Yamamoto, K. Mori, H. Hayashi, Y. Suzuki, Y. S. Negi , T. Hagiwara, I. Kawamura, H. Orihara and Y. Ishibashi, *Proc. 9th Int. Display Research Conf.*, Japan Display'89, Kyoto, 1989, P.26
74. Y. Suzuki, T. Hagiwara, I. Kawamura, N. Okamura, T. Kitazume, M. Kakimoto, Y. Imai, Y. Ouchi, H. Takezoe and A. Fukuda, *Liq. Cryst.*, 1989, **6**, 167
75. Y. Yamada, N. Yamamoto, K. Mori, K. Nakamura, T. Hagiwara, Y. Suzuki, I. Kawamura, H. Orihara and Y. Ishibashi, *Jpn. J. Appl. Phys.*, 1990, **29**, 1757
76. Ch. Bahr and D. Fliegner, *Phys. Rev. Lett.*, 1993, **70**, 1842
77. Y. Galerne and L. Liebert, *Phys. Rev. Lett.*, 1990, **64**, 906
78. Y. Galerne and L. Liebert, *Phys. Rev. Lett.*, 1991, **66**, 2891
79. T. Isozaki, T. Fujikawa, H. Takezoe, A. Fukuda, T. Hagiwara, Y. Suzuki and I. Kawamura, *Phys. Rev.* B, 1993, **48**, 13439

80. A. Fukuda, Y. Takanishi, T. Isozaki, K. Ishikawa and H. Takezoe, *J. Mater. Chem.*, 1994, **4**, 997

81. A. D. L. Chandani, Y. Ouchi, H. Takezoe, A. Fukuda, K. Terashima, K. Furukawa and A. Kishi, *Jpn. J. Appl. Phys.*, 1989, **28**, L1261

82. K. Ema, H. Yao, I. Kawamura, T. Chan and C. W. Garland, *Phys. Rev.* E, 1993, **47**, 1203

83. Y. Takanishi, K. Hiraoka, V. K. Agrawal, H. Takezoe, A. Fukuda and M. Matsushita, *Jpn. J. Appl. phys.*, 1991, 30, 2023

84. T. Isozaki, K. Hiraoka, Y. Takanishi, H. Takezoe, A. Fukuda, Y. Suzuki and I. Kawamura, *Liq. Cryst.*, 1992, **12**, 59

85. S. Inui, N. Iimura, T. Suzuki, H. Iwane, K. Miyachi, Y. Takanishi and A. Fukuda, *J. Mater. Chem.*, 1996, **6** (4), 671

86. A. Fukuda, *Proc. of Asia Display'95*, 1995, 61-64

87. K. Miyasto, S. Abe, H. Takezoe, A. Fukuda and E. Kuze, *Jpn. J. Appl. Phys.*, 1983, **22**, L661

88. J. Lee, A. D. L. Chandani, K. Itoh, Y. Ouchi, H. Takezoe and A. Fukuda, *Jpn. J. Appl. Phys.*, 1990, **29**, L1122

89. Y. Takanish, H. Takezoe, A. Fukuda, H. Komura and J. Watanabe, *J. Mater. Chem.*, 1992, **1** (2), 71

90. A. Fukuda, Y. Takanishi, T. Isozaki, K. Ishikawa and H. Takezoe, *J. Mater. Chem.*, 1994, **4** (7), 997

91. M. Yamayaki, Y. Yamada, N. Yamamoto, K. Mori, H. Hayashi, Y. Suzuki, Y. S. Negi, T. Hagiwara, I. Kawamura, H. Orihara and Y. Ishibashi, *Proc. of Japan Display'89*, 1989, p26

92. H. Takezoe, J. Lee, A. D. L. Chandani, E. Gorecka, Y. Ouchi, A. Fukuda, K. Terashima and K. Furukawa, *Ferroelectrics*, 1991, **114**, 187

93. Y. Yamada, K. Mori, N. Yamamoto, H. Hayashi, K. Nakamura, M. Yamawaki, H.

Orihara and Y. Ishibashi, *Jpn. J. Appl. Phys.*, 1989, **28**, L1606

94. N. Hiji, A. D. L. Chandani, S. Nishiyama, Y. Ouchi, H. Takezoe and A. Fukuda, *Ferroelectrics*, 1988, **85**, 99
95. I. Nishiyama, A. Yoshizawa, M. Fukumasa and T. Hirai, *Jpn. J. Appl. Phys.*, 1989, **28**, L2248
96. I. Nishiyama, *Jpn. J. Appl. Phys.*, 1989, 28, **L**.2248
97. I. Nishiyama and J. W. Goodby, *J. Mater. Chem.*, 1992, **2** (10), 1015
98. I. Nishiyama, *Ph. D. Thesis*, 1992, Hull University
99. T. Hagiwara, Y. Suzuki, Y. Aihara, Y. Sadamune, Y. S. Negi, I. Kawamura, Y. Yamada, N. Yamamoto and K. Mori, *15th Jpn. Liq. Cryst. Conf., (Eki*sho-Tohronkai, Osaka), 1989, p304 (in Japanese)
100. H. Takeda, H. Miyake, S. Takenaka and S. Kusabayashi, *16th Jpn. Liq. Cryst. Conf., (E*kisho-Tohronkai, Hiroshima) 1990, p134 (in Japanese)
101. Y. Suzuki, T. Hagiwara, Y. Aihara, Y. Sadamune, I. Kawamura, N. Okamura, T. Kitazume, M. Kakimoto, Y. Imai, Y. Yamada, N. Yamamoto and K. Mori, *15th Jpn. Liq. Cryst. Conf.,* (Ekisho-Tohronkai, Osaka) 1989, p302 (in Japanese)
102. T. Hagiwara, Y. Suzuki, Y. Aihara, Y. Sadamune, Y. S. Negi, I. Kawamura, Y. Yamada, N. Yamamoto and K. Mori, *15th Jpn, Liq. Cryst. Conf.*, (Ekisho-Tohronkai, Osaka) 1989, p304 (in Japanese)
103. R. Tuffin, J. W. Goodby, D. Bennemann, G. Heppke, D. Lotzsch and G. Scherowsky, *Mol. Cryst. Liq. Cryst.*, 1995, **260**, 51
104. Y. Ouchi, Y. Yoshioka, H. Ishi, K. Seki, M. Kitamura, R. Noyoru, Y. Takanishi and I. Nishiyama, *J. Mater. Chem.*, 1995, **5** (12), 2297

2 Aims of the Project

If a man will begin with certainties, he shall end in doubts; but if he will be content to begin with doubts, he shall end in certainties.

Francis Bacon

in "The Advancement of Learning" (1605)

2. Aims of the Project

As noted previously, the number and the variety of the central rigid core sections found in antiferroelectric liquid crystals are limited. However, the cores that are used are of a type that have high reorientational viscosities which in devices leads to slow response time. This is because the core structures contain polar groups (COO, O *etc*), and these are bent in shape.

Therefore, it will be interesting to see if the high viscosities are simply associated with the core types, or if they are related to the fact that polar or sterically bent core structures are required to stabilise the antiferroelectric and ferrielectric phases. In the first case there is a good possibility that the reorientational viscosity can be lowered by changing the core, hence leading to desirable switching speeds, but if the second idea proves correct then no improvement in switching speeds might be expected from the core alteration. Thus, work has centred on the investigation of the ability of the following difluoroterphenyl systems as suitable for forming antiferroelectric properties.

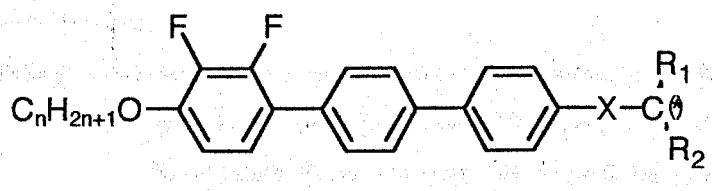

where chiral or achiral branches are attached to the core *via* linking group X

Difluoroterphenyl systems are known to exhibit low viscosity and fast switching ferroelectric phases when doped with suitable chiral materials. They also have reasonable temperature range of SmC phases and negative dielectric anisotropy.

Modification of the end groups was utilised in order to generate antiferroelectric materials.

Ether and ester linking systems of molecular architecture in Fig. 2.1.1 (a) and (b) were investigated.

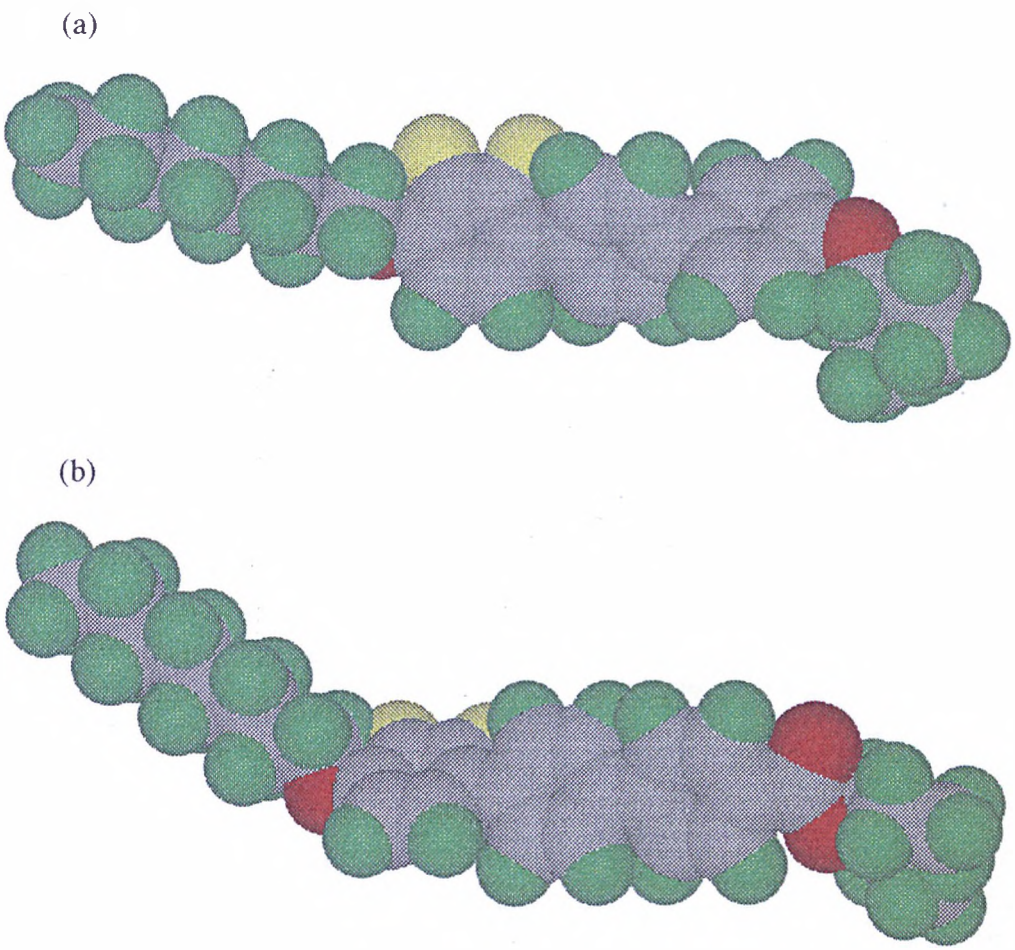

Fig. 2.1.1 Molecular modelling of (a) ether linking (b) ester linking difluoroterphenyl systems

3 Experimental

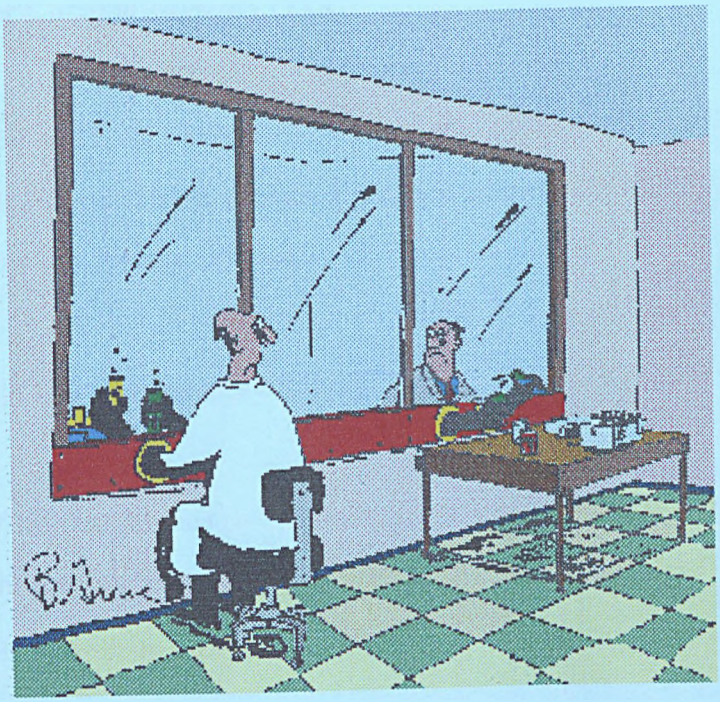

3 Experimental

3.1 Chromatography

3.1.1 Column Chromatography

Purification of materials was carried out by using flash column chromatography over Kieselgel 60 (230-400 mesh) silica gel (Merck, Darmstadt) with various eluents.

3.1.2 Thin Layer Chromatography (TLC)

The intermediates and final products were examined by TLC using Kieselgel 60 F254 (Merck, Darmstadt) and various eluents. Detection of products was normally achieved by UV irradiation (λ = 254 and 365 nm).

3.1.3 Gas-Liquid Chromatography (GLC)

The progress of many reactions (where indicated), was monitored using a Chrompack CP-9001 gas chromatograph fitted with a 10 m x 0.25 mm id, 0.12 μm CP-Sil 5CB fused coating silica capillary column.

3.1.4 High Performance Liquid Chromatography (HPLC)

HPLC was used to check the purity of all final compounds and the system consisted of the following modules: (a) a Kontron 420 pump, (b) a Must Multi-port Stream Switch, (c) a Perkin-Elmer ISS-100 Auto Sampler, (d) a Dynamax microsorb C18 Reverse

Phase column, (e) a Spectroflow 757 Absorbance Detector, (f) a Chessell chart recorder, (g) a Polymer Labs calibre software.

Reverse phase chromatography was carried out over octadecylsiloxane (5 mm particle size, 25 x 0.46 cm, C18 column) using acetonitrile or acetonitrile/chloroform as the eluent. Detection of the eluting products was achieved using a Spectroflow 757 absorbance detector ($\lambda = 254$ nm).

3.2 Differential Scanning Calorimetry (DSC)

All final products were subjected to thermal analysis by using a Perkin-Elmer DSC7 differential scanning calorimeter coupled to a data station using 7Series/UNIX Thermal Analysis software. Nitrogen was used for the purge and the glove box gas. Differential scanning thermograms were obtained at a scanning rate of 10 °C min^{-1} after the sample was encapsulated in aluminium pans; the calorimeter was standardised with respect to indium (literature values : onset = 156.60 °C, $\Delta H = 28.45$ J g^{-1})[1].

3.3 Polarizing Optical Microscopy

Phase identification and transition temperatures of all final products were determined with the use of an Olympus BH-2 polarizing microscope in conjunction with a Mettler FP52 heating stage and FP5 temperature control unit. Photomicrographs were taken using a Zeiss Universal polarizing light microscope equipped with an Olympus C-35AD camera. Homeotropic samples were prepared by simply using clean microscope glass cover slips and slides (washed with water, concetrated nitric acid and acetone).

3.4 Electrooptic Measurements

3.4.1 General Information

Electrooptic measurements were carried out using homogeneously aligned cells (Linkam and DERA) which were constructed from electrically-conducting indium tin oxide (ITO) coated glass, treated with unidirectional, parallel-buffed polyimde (PI) coating layers so as to give sites for planar, homogeneous growth of the liquid crystalline phase. The cell gap (5-10 μm) maintained by glass spacers was verified by uv-vis interferometry using a Philips PU H720 uv-vis scanning spectrometer. The effective electrode areas of the cells used were 0.25, 0.81 and 1.0 cm^2. The temperature was controlled by using a Mettler FP82 attached to an FP90 central processor. The cells were filled by capillary action at atmospheric pressure, with the liquid crystalline materials in the isotropic liquid state. Good alignment was achieved by slowly cooling (< 0.1 °C min^{-1}) from the isotropic liquid into the required liquid crystalline phase while applying an electric field (square wave form, Vrms = 90 V and 200 Hz).

3.4.2 Direct Measurement of Spontaneous Polarization

Typically, spontaneous polarization values have been measured by one of the following methods;

(a) The Sawyer-Tower method[2], which is standard for solid ferroelectrics, has been used most commonly in ferroelectric liquid crystals[3-8].

(b) The indirect method, based on the electric field dependence of the dielectric constant[9] has been employed.

(c) The measurement of the current induced by rapidly reversing a field[10].

However the triangular wave method[11] used in this research has advantages over the conventional methods mentioned above. The use of a triangular wave allows for a fairly accurate measure of spontaneous polarization because the excess charge flow through the circuit due to polarization reversal appears on a straight baseline. The total polarization, $\mathbf{P}_{tot}$, is given by

$$\mathbf{P}_{tot} = \mathbf{P} + \mathbf{P}_{ind} \tag{3.1}$$

where $\mathbf{P}$ is the ferroelectric polarization and $\mathbf{P}_{ind}$ is the induced polarization.

$$\mathbf{P}_{ind} = \Delta\varepsilon\varepsilon_0(\mathbf{n}\cdot\mathbf{E})\mathbf{n} + (\varepsilon_\perp - 1)\varepsilon_0\mathbf{E}. \tag{3.2}$$

In equation 3.2, $\Delta\varepsilon = \varepsilon_\parallel - \varepsilon_\perp$ is the difference between the dielectric constants measured parallel and perpendicular to the director $\mathbf{n}$, respectively, ε_0 is the vacuum permittivity (8.854×10^{-12} $J^{-1}C^2m^{-1}$) and E is the applied electric field. When a voltage U (in the z direction) is applied to a ferroelectric liquid crystal cell, the induced current I is

$$I = U/R + C\,(dU/dt) + A\,(d\mathbf{P}_{tot}/dt)\mathbf{e}z \tag{3.3}$$

where R is the ohmic resistance of the liquid crystal layer, C is the capacity of the empty cell, A is the area of the electrode. The use of a triangular wave voltage has the advantage that the ohmic and capacitive contributions to I(t) in equation 3.3 give straight lines with the slope directly indicating the ohmic resistance and therefore they can be easily subtracted from the total current. Moreover, the triangular wave method clearly reveals that a threshold voltage for deforming the helix does not exist. The triangular waveform for the electric field was generated by a Hewlett Packard 33120A 15 MHz function generator with a maximum amplitude of ±10 V and a 32±0.2 ns rise

time. The output signal was amplified by a fixed gain (x50) amplifier with a maximum amplitude of ±175 V, 16.5±0.3 ms rise time and 1 kHz waveform capability. A triangular voltage with 5-65 Vrms at 20 Hz was applied to the cell placed in the hot-stage. An optical polarizing microscope was used for observing textural changes during the measurements. The current was measured by detecting the voltage change across a resistor of 100 kΩ, which was sufficiently small compared with the impedance of the cell connected in series, and amplified by the means of a variable gain operational amplifier with an input impedance >>100 kΩ, therefore the current loss for the measurement is negligible. The voltage was digitized using a Hewlett Packard 54600B 100 MHz, 1 M digitizing oscilloscope. The data was analysed on a 486 SX 40 MHz microcomputer using acquisition and analysis software. The experimental arrangement for the measurement of spontaneous polarization is illustrated in Fig. 3.4.1.

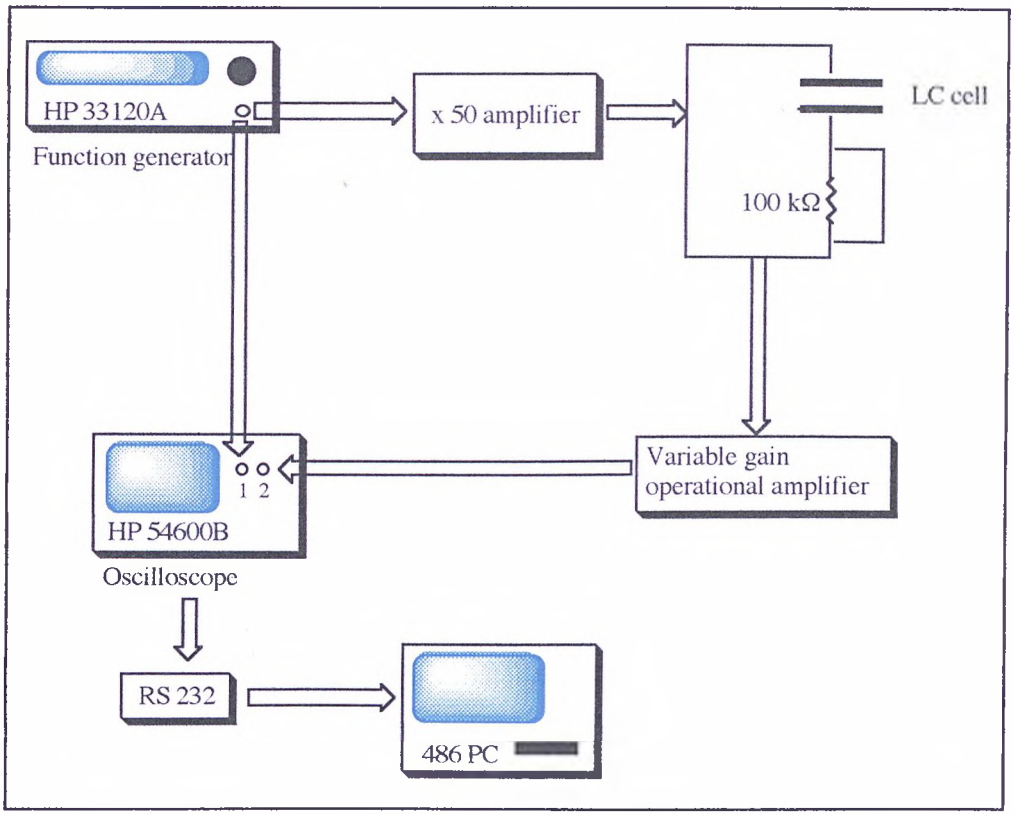

Fig. 3.4.1 Diagram of the experimental setup for the measurement of spontaneous polarization

3.4.3 Determination of the Direction of the Spontaneous Polarization

The unswitched cell is heated into the SmA phase in the microscope oven. The sample is rotated until the aligned focal conic or planar homogeneous domains are aligned with the reference direction. Extinction is obtained along the reference direction by rotation of the polarizer and analyzer. The material is then cooled into its ferroelectric phase, and a weak form of extinction is obtained in the same direction as the SmA phase because of the formation of helical ordering in the direction. The sample is then subjected to a DC voltage (75.0 V) of known polarity and normally the top plate is positively charged. The helix unwinds and the material becomes poled in a uniform direction with its spontaneous polarization being coupled to the applied field. The extinction direction is

now at an angle relative to the reference axis. The sample is then rotated through the minimum angle required to return it to extinction along the reference direction. The sense of the rotation of the sample, as shown in Fig. 3.4.2, defines the direction in which the molecules are tilted with respect to the layer normal, and thus the direction of the spontaneous polarization.

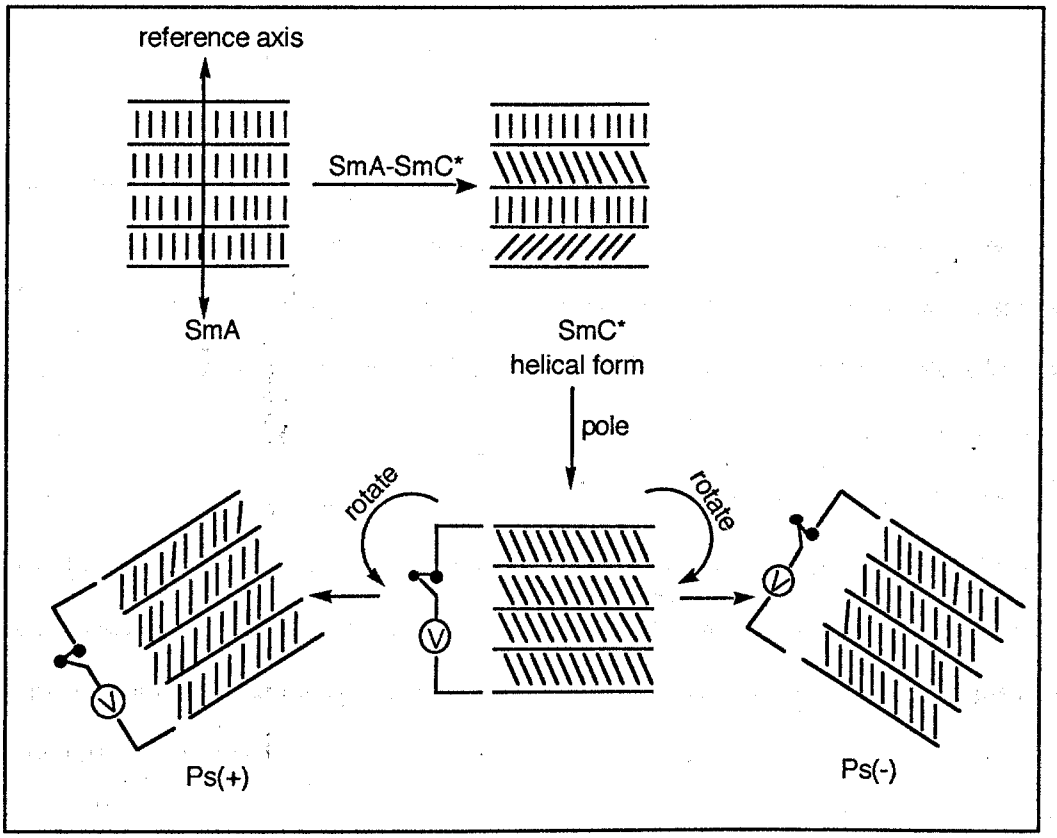

Fig. 3.4.2 Diagram for the determination of the direction of the spontaneous polarization

3.4.4 Measurement of the Switched Tilt Angle

The switched tilt angle, which is defined as the angle between the layer normal and the direction for the SmC* phase was determined by finding the extinction direction using

polarized light microscopy. When 50 Vrms square waves at 10 mHz were applied to the cells. The cone angle of the ferroelectric phase as a function of temperature was obtained and is twice the switched tilt angle.

3.5 Molecular Modelling

Molecular modelling studies were performed on a Silicon Graphics workstation (Indigo XS 24, 4000) using Cerius2 software.

The Dreiding[12] force field developed by Mayo, Olafson and Goddard was used for structure prediction and energy calculation of group molecules. The Drieding force field allows reasonable predictions for a very large number of structures because the general force constants and geometry parameters are based on simple hybridizations rather than on specific combinations of atoms. During an energy minimization, the atomic coordinates are adjusted in order to reduce the molecular energy using the current force field expression. The minimization is terminated when the root mean square (RMS) force is below a specified convergence value. The RMS force is a direct measure of the tolerance applied to the energy gradient (d^2E/dt^2), *i.e.* the rate of change of potential energy with step number.

3.6 Spectroscopy and Optical Analysis

3.6.1 Nuclear Magnetic Resonance Spectroscopy (NMR)

Proton nuclear resonance (^{1}HNMR) spectroscopy was carried out using a Jeol-GX270 FT NMR spectrometer.

3.6.2 Infra-red Spectroscopy (IR)

Infra-red spectroscopy was carried out using a Perkin-Elmer 783 infra-red spectrometer.

3.6.3 Mass Spectrometry (MS)

Mass spectra were recorded using a Finnigan-MAT 1020 automated GC/MS spectrometer.

3.6.4 Optical Rotation (OR)

Optical rotations of chiral materials were determined using a Bendix-NPL control unit. Values were measured in chloroform at the sodium D-line (λ = 589 nm) and at room temperature.

3.7 Drying and Purification of Solvents

Diethyl ether and toluene were dried over sodium wire.
Dichloromethane was distilled from phosphorus pentoxide.
Tetrahydrofuran was distilled from sodium and benzophenone.

3.8 Nomenclature and Abbreviations

The IUPAC system of nomenclature has been used as a guide throughout this thesis and the abbreviations in the text have the meanings given below;
mp = melting point; bp = boiling point,

K = crystalline solid phase; I = isotropic liquid phase; N = nematic liquid crystal mesophase; Ch = cholesteric liquid crystal mesophase; Sm = smectic liquid crystal mesophase (*e.g.*, SmA, SmC) with subscript letters to identify the subphases (*e.g.*, SmCα)

DCM = dichloromethane; DMAP = 4-(*N*,*N*-dimethylamino)pyridine; DCC = *N*,*N*'-dicyclohexylcarbodiimide; DCU = *N*,*N*'-dicyclohexylurea; DEAD = diethyl azodicarboxylate; DME = 1,2-dimethoxyethane; DMF = *N*,*N*-dimethylformamide; THF = tetrahydrofuran; LDA = lithium diisopropylamide; TPP = triphenylphosphine; Bn = benzyl, $C_6H_5CH_2$

The multiplicities of nmr signals are given as s = singlet; d = doublet; t = triplet; q = quartet; quint = quintet; sext = sextet; sept = septet; m = mutiplet.

3.9 Synthesis

3.9.1 Synthetic Scheme 1 and Materials Prepared (1-11)

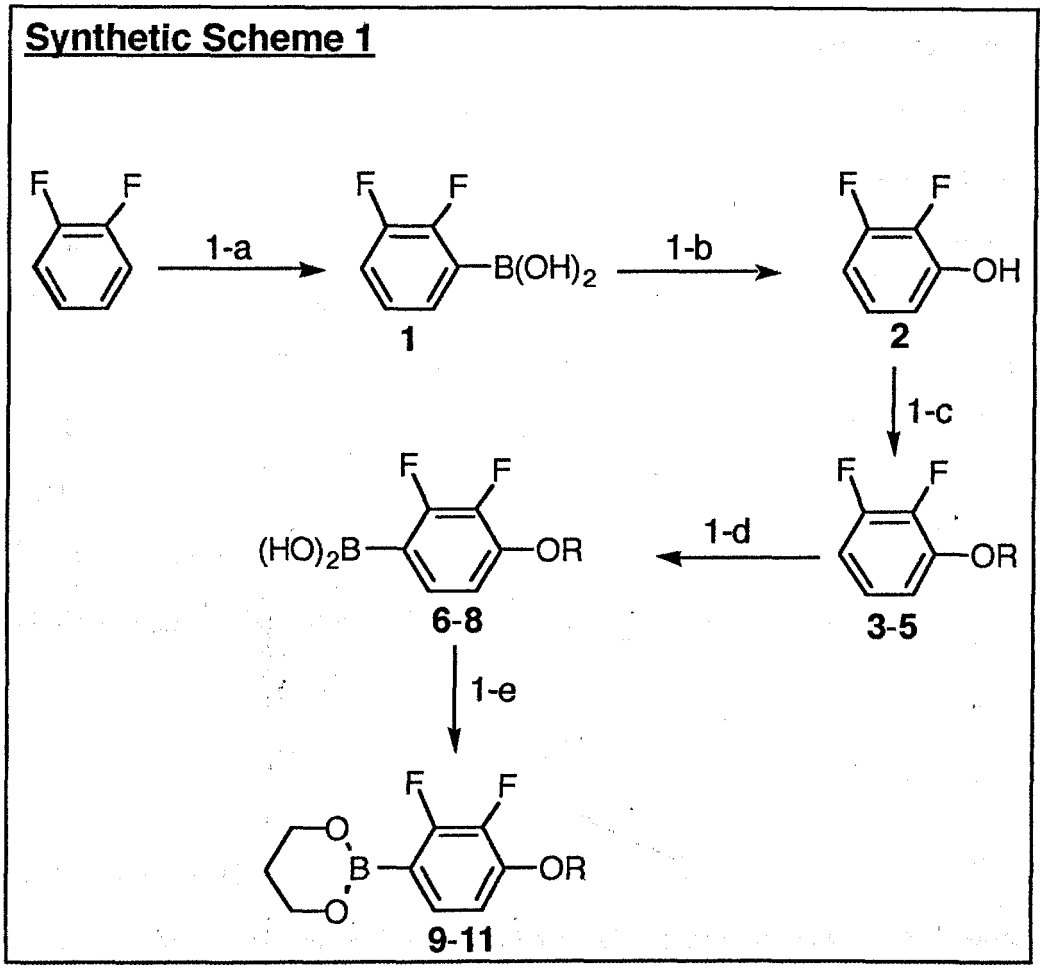

No.	3, 6, 9	4, 7, 10	5, 8, 11
R	C_8H_{17}	$C_{10}H_{21}$	C_6H_{13}

1-a ··· (i) n-BuLi, THF; (ii) $(MeO)_3B$, THF; (iii) 10 % HCl

1-b ··· 10 % H_2O_2, Et_2O

1-c ··· RBr (R = C_6H_{13}, C_8H_{17}, $C_{10}H_{21}$), K_2CO_3, butanone

1-d ··· (i) n BuLi, THF; (ii) $(MeO)_3B$, THF ; (iii) 10 % HCl

1-e ··· $HO(CH_2)_3OH$, petroleum (bp 40-60 °C)

2,3-Difluorophenylboronic acid (1)

n-Butyllithium (7.0 ml, 10.0 M in hexane, 70.0 mmol) was added dropwise to a solution of 1,2-difluorobenzene (7.50 g, 65.7 mmol) in dry THF (100 ml) with stirring at -78 °C under dry nitrogen. The reaction mixture was maintained under these conditions for 1 hour before trimethyl borate (13.7 g, 132 mmol) was added dropwise at -78 °C. The reaction mixture was allowed to warm to room temperature overnight. 10% Hydrochloric acid (50 ml) was then added and the reaction mixture was stirred for a further 1 hour before being washed with diethyl ether (3 x 200 ml). The combined ethereal washings were washed with water (50 ml) and dried ($MgSO_4$). The solvent was removed *in vacuo* to afford a white solid which was used in the next step without further purification.

Yield 9.36 g (91 %); mp = 235-237 °C

IR (KBr) ν_{max} 3600-3000 (H-bonded OH), 1620 (C=C), 1470, 1350, 1265 (B-O) cm^{-1}

MS m/z 158 (M^+, 50 %), 140, 127, 114, 94 (100 %)

2,3-Difluorophenol (2)

10% Aqueous hydrogen peroxide (100 ml) was added dropwise to a stirred refluxing mixture of compound **1** (9.21 g, 58.3 mmol) in diethyl ether (100 ml) under dry nitrogen. The reaction was heated under reflux for a further 4 hours. TLC analysis showed a complete reaction. The product was extracted into diethyl ether (3 x 50 ml) and the combined ethereal extracts were dried ($MgSO_4$). The solvent was removed *in vacuo* and the residue was distilled at room temperature to give a yellow liquid.

Yield 7.20 g (95 %); bp = 120-125 °C

^{1}HNMR ($CDCl_3$) δ 6.64-6.80 (2H, m), 6.87-6.98 (1H, m), phenolic proton was not detected.

IR (KBr) ν_{max} 3600-3000 (H-bonded OH), 1620 (C=C), 1510, 1480, 1380,

1260 (C-O) cm^{-1}

MS *m/z* 130 (M^+, 100 %), 110

***1,2-Difluoro-3-octyloxybenzene* (3)**

1-Bromooctane (11.8 g, 60.9 mmol) was added to a refluxing suspension of compound **2** (7.20 g, 55.4 mmol) and potassium carbonate (11.5 g, 83.1 mmol) in butanone (90 ml). The reaction was heated under reflux overnight and TLC analysis showed a complete reaction. The reaction was cooled and the insoluble inorganic material was removed by filtration. The filtrate was evaporated to give a yellow residue which was purified by column chromatography [DCM/petroleum (bp 40-60 °C), 3:7] and distilled to give a colourless liquid.

Yield 7.30 g (55 %); bp = 150 °C/15 mmHg

^{1}HNMR ($CDCl_3$) δ 0.89 (3H, t), 1.20-1.52 (10H, m), 1.82 (2H, quint), 4.02 (2H, t), 6.67-6.79 (2H, m), 6.89-7.00 (1H, m)

IR (KBr) ν_{max} 3040 (aryl C-H), 2980/2860 (aliphatic C-H), 1620 (C=C), 1460 (CH_2), 1350 (CH_3), 1265 (C-O) cm^{-1}

MS *m/z* 242 (M^+, 95 %), 130, 112, 56 (100 %)

The following compounds (**4** and **5**) were prepared using the same general procedure used for the preparation of compound **3**.

***1-Decyloxy-2,3-difluorobenzene* (4)**

Quantities used: 1-Bromodecane (38.3 g, 173 mmol), compound **2** (20.4 g, 157 mmol), potassium carbonate (32.5 g, 235 mmol)

Yield 19.7 g (46 %)

^{1}HNMR ($CDCl_3$) δ 0.88 (3H, t), 1.19-1.53 (14H, m), 1.82 (2H, quint), 4.03 (2H, t), 6.68-6.80 (2H, m), 6.90-7.01(1H, m)

IR (KBr) ν_{max} 3040 (aryl C-H), 2960/2880 (aliphatic C-H), 1625 (C=C), 1465 (CH_2), 1340 (CH_3), 1265 (C-O) cm^{-1}

MS *m/z* 270 (M^+, trace), 140, 130 (100 %)

***1,2-Difluoro-3-hexyloxybenzene* (5)**

Quantities used: 1-Bromohexane (7.27 g, 44.0 mmol), compound **2** (5.20 g, 40.0 mmol), potassium carbonate (32.5 g, 60.0 mmol)

Yield 5.83 g (68 %); bp = 125 °C/15 mmHg

^{1}HNMR ($CDCl_3$) δ 0.90 (3H, t), 1.30 (4H, m), 1.40 (2H, quint), 1.80 (2H, quint), 4.00 (2H, m), 6.67-6.79 (2H, m), 6.90-7.00 (1H, m)

IR (KBr) ν_{max} 3040 (aryl C-H), 2980/2880 (aliphatic C-H), 1630 (C=C), 1480 (CH_2), 1350 (CH_3), 1265 (C-O) cm^{-1}

MS *m/z* 214 (M^+, 45 %), 130 (100 %)

***2,3-Difluoro-4-octyloxyphenylboronic acid* (6)**

n-Butyllithium (3.2 ml, 10.0 M in hexane, 32.0 mmol) was added dropwise to a solution of compound **3** (7.32 g, 30.2 mmol) in dry THF (40 ml) with stirring at -78 °C. The reaction mixture was maintained under these conditions for 1 hour before trimethyl borate (6.44 g, 62.0 mmol) was added dropwise at -78 °C. The reaction mixture was then allowed to warm to room temperature overnight. 10% Hydrochloric acid (30 ml) was then added and the mixture was stirred for a further 1 hour before being washed with diethyl ether (3 x 200 ml). The combined ethereal washings were washed with water and dried ($MgSO_4$). The solvent was removed to give a yellow solid which was dried *in vacuo*.

Yield 7.96 g (92 %)

^{1}HNMR (DMSO) δ 0.87 (3H, t), 1.20-1.50 (10H, m), 1.74 (2H, quint), 4.08 (2H, t), the aromatic protons were not clearly defined.

IR (KBr) ν_{max} 3500-3000 (H-bonded OH), 2920/2860 (aliphatic C-H), 1620 (C=C), 1460 (CH_2), 1350 (CH_3), 1265 (C-O) cm^{-1}

MS *m/z* 286 (M^+, 5 %), 174 (100 %)

The following compounds (**7** and **8**) were prepared using the same general procedure used for the preparation of compound **6** and were then used in the next step without further purification.

***4-Decyloxy-2,3-difluorophenylboronic acid* (7)**

Quantities used: n-Butyllithium (33.2 ml, 2.50 M in hexane, 82.9 mmol), compound **4** (18.8 g, 69.5 mmol), trimethyl borate (15.0 g, 144 mmol)

Yield 19.8 g (91 %)

***2,3-Difluoro-4-hexyloxyphenylboronic acid* (8)**

Quantities used: n-Butyllithium (12.5 ml, 2.50 M in hexane, 31.2 mmol), compound **5** (5.81 g, 27.1 mmol), trimethyl borate (5.63 g, 54.2 mmol)

Yield 6.70 g (96 %)

***2-(2,3-Difluoro-4-octyloxyphenyl)-1,3,2-dioxaborinane* (9)**

Propan-1,3-diol (5.98 g, 78.6 mmol) in petroleum (bp 40-60 °C, 300 ml) was added to compound **6** (7.50 g, 26.2 mmol) and the mixture was stirred overnight at room temperature. Analysis by GLC showed a complete reaction. The water layer was removed using a separation funnel and the petroleum layer was dried ($MgSO_4$), the solvent was evaporated *in vacuo* and the residue was recrystallised (methanol) to give a white solid.

Yield 6.40 g (75 %); mp = 37-40 °C

^{1}HNMR (DMSO) δ 0.89 (3H, t), 1.20-1.53 (10H, m), 1.82 (2H, quint), 2.08 (2H,

quint), 4.04 (2H, t), 4.18 (4H, 2 x t) 6.69 (1H, ddd), 7.34 (1H, ddd)

IR (KBr) ν_{max} 2920/2870 (aliphatic C-H), 1620 (C=C), 1460 (CH_2), 1380 (CH_3), 1320/1290/1270, 1210 cm^{-1}

MS *m/z* 326(M^+, trace), 214(100 %), 156, 127, 112

The following compounds (**10** and **11**) were prepared using the same general procedure used for the preparation of compound **9**.

***2-(4-Decyloxy-2,3-difluorophenyl)-1,3,2-dioxaborinane* (10)**

Quantities used: Propan-1,3-diol (13.4 ml, 176 mmol), compound **7** (18.5 g, 58.7 mmol)

Yield 14.1 g (68 %); mp = 38-41 °C

^{1}HNMR ($CDCl_3$) δ 0.88 (3H, t), 1.20-1.53 (14H, m), 1.82 (2H, quint), 2.08 (2H, quint), 4.05 (2H, t), 4.18 (4H, t), 6.69 (1H, ddd), 7.33 (1H, ddd)

IR (KBr) ν_{max} 2920/2870 (aliphatic C-H), 1620 (C=C), 1460 (CH_2), 1380 (CH_3), 1320/1290/1270, 1210 cm^{-1}

MS *m/z* 354 (M^+, trace), 214(100 %), 156, 127, 112

***2-(2,3-Difluoro-4-hexyloxyphenyl)-1,3,2-dioxaborinane* (11)**

Quantities used: Propan-1,3-diol (6.60 ml, 86.7 mmol), compound **8** (7.50 g, 28.9 mmol)

Yield 6.20 g (72 %)

^{1}HNMR ($CDCl_3$) δ 0.88 (3H, t), 1.20-1.52 (6H, m), 1.82 (2H, quint), 2.08 (2H, quint), 4.03 (2H, t), 4.18 (4H, t), 6.68 (1H, ddd), 7.34 (1H, ddd)

IR (KBr) ν_{max} 2920/2870 (aliphatic C-H), 1605 (C=C), 1450 (CH_2), 1390 (CH_3), 1310/1290/1270, 1200 cm^{-1}

MS *m/z* 298 (M^+, trace), 214(100 %), 156, 127, 112

3.9.2 Synthetic Scheme 2 and Materials Prepared (12-27)

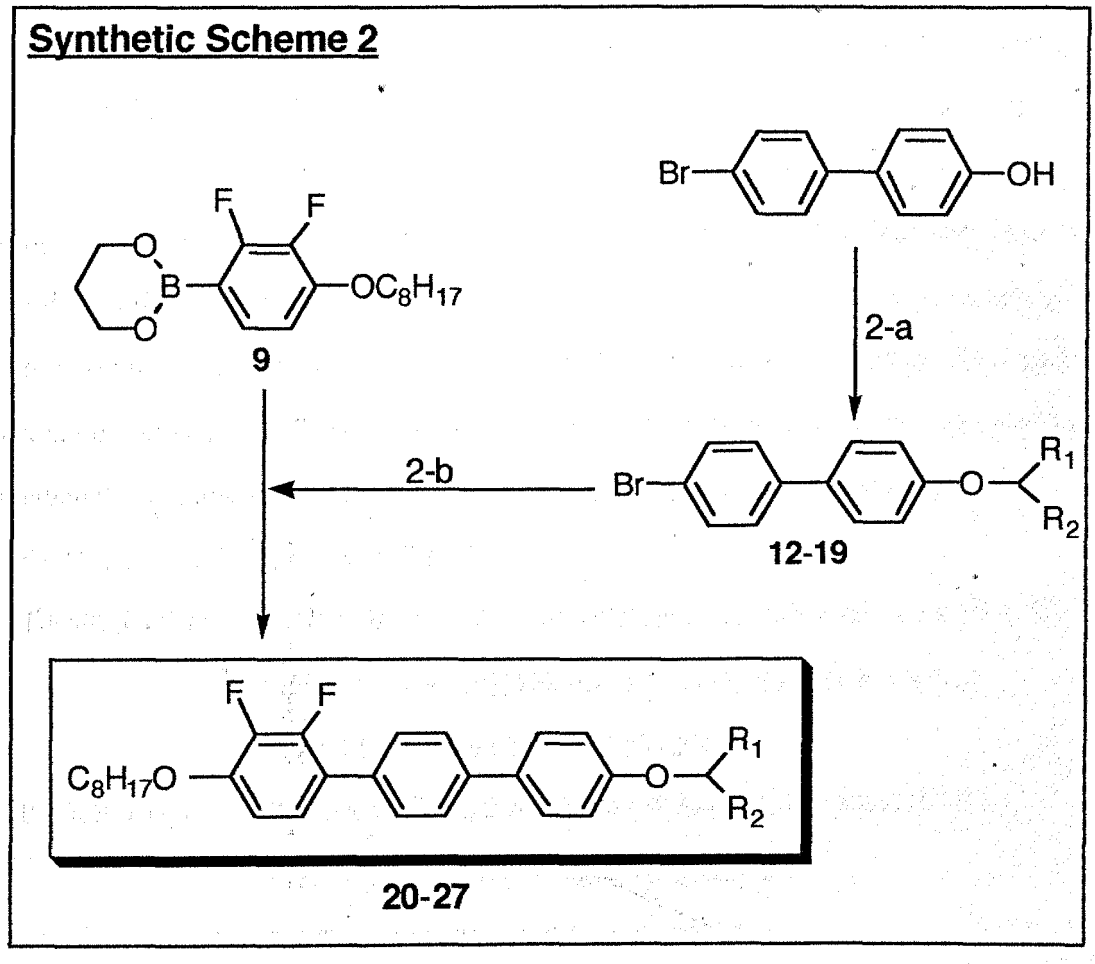

Compounds					Compounds				
No.	No.	R_1	R_2	Config.	No.	No.	R_1	R_2	Config.
12	**20**	CH_3	C_5H_{11}		**16**	**24**	C_2H_5	C_3H_7	
13	**21**	CH_3	C_6H_{13}	(*R*)-	**17**	**25**	C_2H_5	C_5H_{11}	
14	**22**	CH_3	C_6H_{13}	(*S*)-	**18**	**26**	C_3H_7	C_3H_7	
15	**23**	C_2H_5	C_2H_5		**19**	**27**	C_4H_9	C_4H_9	

2-a ··· R_1R_2CHOH, DEAD, TPP, THF

2-b ··· $Pd(PPh_3)_4$, 2M-Na_2CO_3, DME

***4-Bromo-4'-(1-methylhexyloxy)biphenyl* (12)**

DEAD (4.35 g, 25.0 mmol) in THF (10 ml) was added dropwise to a solution of 4-bromo-4'-hydroxybiphenyl (6.23 g, 25.0 mmol), TPP (6.56 g, 25.0 mmol) and heptan-2-ol (2.91 g, 25.0 mmol) in THF (200 ml) at room temperature under dry nitrogen. The reaction was held under these conditions overnight when TLC analysis revealed a complete reaction and the mixture was filtered. The filtrate was washed with ether (2 x 50 ml) and the combined ethereal extracts were washed with water and dried ($MgSO_4$). The solvent was removed *in vacuo* and the residue was purified by column chromatography [DCM/petroleum (bp 40-60 °C), 1:9]. The product was recrystallised (methanol/ethyl acetate, 3:1) to yield a white solid which was dried *in vacuo*.

Yield 2.14 g (25 %); mp = 70-72 °C

^{1}HNMR ($CDCl_3$)	δ 0.89 (3H, t), 1.26-1.46 (9H, m; including a 3H, d), 1.50-1.65 (1H, m), 1.69-1.81(1H, m), 4.39 (1H, sext), 6.94 (2H, d), 7.41(2H, d), 7.46 (2H, d), 7.53 (2H, d)
IR (KBr) ν_{max}	3060 (aryl C-H), 2940/2860 (aliphatic C-H), 1600 (C=C), 1480 (CH_2), 1380 (CH_3), 1250 (C-O) cm^{-1}
MS *m/z*	348/346 (M^+, 20 %), 250/248 (100 %)

The following compounds (**13-19**) were prepared using the same general procedure used for the preparation of compound **12.**

(R)-(+)-*4-Bromo-4'-(1-methylheptyloxy)biphenyl* (13)

Quantities used: DEAD (2.80 g, 16.1 mmol), 4-bromo-4'-hydroxybiphenyl (4.00 g, 16.1 mmol), TPP (4.22 g, 16.1 mmol), (*S*)-(+)-octan-2-ol (2.10 g, 16.1 mmol)

Yield 2.21 g (38 %); mp = 76-79 °C

^{1}HNMR ($CDCl_3$)	δ 0.90 (3H, t), 1.26-1.46 (11H, m; including a 3H, d at 1.32), 1.50-1.65 (1H, m), 1.69-1.81(1H, m), 4.39 (1H, sext),

6.94 (2H, d), 7.41 (2H, d), 7.46 (2H, d), 7.53 (2H, d)

IR (KBr) ν_{max} 3050 (aryl C-H), 2920/2840 (aliphatic C-H), 1600 (C=C), 1480 (CH_2), 1375 (CH_3), 1250 (C-O) cm^{-1}

MS *m/z* 362/360 (M^+, 20 %), 250/248 (100 %)

$[\alpha]_D^{22°C}$ +0.28°

(S)-(-)-*4-Bromo-4'-(1-methylheptyloxy)biphenyl* (14)

Quantities used: DEAD (2.80 g, 16.1 mmol), 4-bromo-4'-hydroxybiphenyl (4.00 g, 16.1 mmol), TPP (4.22 g, 16.1 mmol), (*R*)-(-)-octan-2-ol (2.10 g, 16.1 mmol)

Yield 2.19 g (38 %); mp = 76-79 °C

^{1}HNMR ($CDCl_3$) δ 0.88 (3H, t), 1.26-1.46 (11H, m; including a 3H, d at 1.32), 1.50-1.65 (1H, m), 1.69-1.81 (1H, m), 4.39 (1H, sext), 6.95 (2H, d), 7.41 (2H, d), 7.46 (2H, d), 7.52 (2H, d)

IR (KBr) ν_{max} 3060 (aryl C-H), 2930/2850 (aliphatic C-H), 1600 (C=C), 1480 (CH_2), 1375 (CH_3), 1250 (C-O) cm^{-1}

MS *m/z* 362/360 (M^+, 10 %), 250/248 (100 %)

$[\alpha]_D^{22°C}$ -0.25°

***4-Bromo-4'-(1-ethylpropoxy)biphenyl* (15)**

Quantities used: DEAD (2.80 g, 16.1 mmol), 4-bromo-4'-hydroxybiphenyl (4.00 g, 16.1 mmol), TPP (4.22 g, 16.1 mmol), pentan-3-ol (1.42 g, 16.1 mmol)

Yield 1.47 g (29 %); mp = 68-71 °C

^{1}HNMR ($CDCl_3$) δ 0.98 (6H, 2 x t), 1.70 (4H, d/q), 4.16 (1H, quint), 6.96 (2H, d), 7.40 (2H, d), 7.46 (2H, d), 7.52 (2H, d)

IR (KBr) ν_{max} 3050 (aryl C-H), 2940/2870 (aliphatic C-H), 1600 (C=C), 1480 (CH_2), 1380 (CH_3), 1250 (C-O) cm^{-1}

MS *m/z* 320/318 (M^+, 15 %), 250/248 (100 %)

***4-Bromo-4'-(1-ethylbutoxy)biphenyl* (16)**

Quantities used: DEAD (4.35 g, 25.0 mmol), 4-bromo-4'-hydroxybiphenyl (6.23 g, 25.0 mmol), TPP (6.56 g, 25.0 mmol), hexan-3-ol (2.55 g, 25.0 mmol)

Yield 3.22 g (39 %); mp = 69-71 °C

^{1}HNMR ($CDCl_3$)	δ 0.95 (3H, t), 0.97 (3H, t), 1.25-1.77 (6H, m), 4.22 (1H, quint), 6.95 (2H, d), 7.41(2H, d), 7.46 (2H, d), 7.53 (2H, d)
IR (KBr) ν_{max}	3050 (aryl C-H), 2940/2860 (aliphatic C-H), 1600 (C=C), 1480 (CH_2), 1380 (CH_3), 1250 (C-O) cm^{-1}
MS *m/z*	334/332 (M^+, 10 %), 250/248 (100 %)

***4-Bromo-4'-(1-ethylhexyloxy)biphenyl* (17)**

Quantities used: DEAD (2.80 g, 16.1 mmol), 4-bromo-4'-hydroxybiphenyl (4.00 g, 16.1 mmol), TPP (4.22 g, 16.1 mmol), octan-3-ol (2.10 g, 16.1 mmol)

Yield 2.80 g (48 %); mp = 42-44 °C

^{1}HNMR ($CDCl_3$)	δ 0.89 (3H, t), 0.97 (3H, t), 1.22-1.49 (6H, m), 1.60-1.75 (4H, m), 4.20 (1H, quint), 6.95 (2H, d), 7.40 (2H, d), 7.46 (2H, d), 7.52 (2H, d)
IR (KBr) ν_{max}	3050 (aryl C-H), 2930/2850 (aliphatic C-H), 1600 (C=C), 1480 (CH_2), 1380 (CH_3), 1250 (C-O) cm^{-1}
MS *m/z*	362/360 (M^+, 10 %), 250/248 (100 %)

***4-Bromo-4'-(1-propylbutoxy)biphenyl* (18)**

Quantities used: DEAD (2.80 g, 16.1 mmol), 4-bromo-4'-hydroxybiphenyl (4.00 g, 16.1 mmol), TPP (4.22 g, 16.1 mmol), heptan-4-ol (1.87 g, 16.1 mmol)

Yield 2.42 g (43 %); mp = 64-65 °C

^{1}HNMR ($CDCl_3$)	δ 0.98 (6H, 2xt), 1.24-1.77 (8H, m), 4.28 (1H, quint), 6.95 (2H, d),

7.41(2H, d), 7.46 (2H, d), 7.53 (2H, d)

IR (KBr) ν_{max} 3050 (aryl C-H), 2940/2850 (aliphatic C-H), 1600 (C=C), 1470 (CH_2), 1380 (CH_3), 1250 (C-O) cm^{-1}

MS *m/z* 348/346 (M^+, trace), 250/248 (100 %)

***4-Bromo-4'-(1-butylpentoxy)biphenyl* (19)**

Quantities used: DEAD (2.80 g, 16.1 mmol), 4-bromo-4'-hydroxybiphenyl (4.00 g, 16.1 mmol), TPP (4.22 g, 16.1 mmol), nonan-5-ol (2.32 g, 16.1 mmol)

Yield 2.80 g (46 %); mp = 49-50 °C

^{1}HNMR ($CDCl_3$) δ 0.90 (6H, t), 1.25-1.76 (12H, m), 4.25 (1H, quint), 6.94 (2H, d), 7.41(2H, d), 7.46 (2H, d), 7.52 (2H, d)

IR (KBr) ν_{max} 3050 (aryl C-H), 2950/2850 (aliphatic C-H), 1600 (C=C), 1470 (CH_2), 1380 (CH_3), 1250 (C-O) cm^{-1}

MS *m/z* 376/374 (M^+, 5 %), 250/248 (100 %)

***2,3-Difluoro-4"-(1-methylhexyloxy)-4-octyloxyterphenyl* (20)**

To a rapidly stirred solution of tetrakis(triphenylphosphine)palladium(0) (0.20 g, 0.17 mmol) and compound **12** (2.00 g, 5.76 mmol) in DME (50 ml) and aqueous 2M- sodium carbonate (50 ml) at 80-100 °C was added compound **9** (2.07 g, 6.34 mmol) in DME (20 ml) under dry nitrogen. The reaction mixture was heated under reflux overnight when TLC showed a complete reaction. The product was extracted into ether (3 x 200 ml) and the combined ethereal extracts were washed with water and dried ($MgSO_4$). The solvent was removed *in vacuo* and the product was purified by column chromatography [DCM/petroleum (bp 40-60 °C), 3:7] and recrystallisation (ethanol) to give a white solid.

Yield 1.58 g (54 %); mp = 65 °C

^{1}HNMR ($CDCl_3$) δ 0.89 (6H, 2 x t), 1.20-1.68 (20H, m; including a 3H, d at 1.35),

	1.68-1.92 (3H, m), 4.08 (2H, t), 4.41(1H, sext), 6.81(1H, ddd), 6.97 (2H, d), 7.14 (1H, ddd), 7.50-7.65 (6H, m)
IR (KBr) ν_{max}	3040 (aryl C-H), 2940/2860 (aliphatic C-H), 1600 (C=C), 1480 (CH_2), 1380 (CH_3), 1250 (C-O) cm^{-1}
MS *m/z*	508 (M^+, 50 %), 410, 298 (100 %)
HPLC (C18)	99.5 % (in acetonitrile)

The following compounds (**21** and **27**) were prepared using the same general procedure used for the preparation of compound **20**.

(R)-(+)-*2,3-Difluoro-4"-(1-methylheptyloxy)-4-octyloxyterphenyl* (21)

Quantities used: tetrakis(triphenylphosphine)palladium(0) (0.16 g, 0.14 mmol), compound **13** (1.65 g, 4.56 mmol), compound **9** (1.64 g, 5.02 mmol), 2M- sodium carbonate (50 ml)

Yield 0.60 g (25 %); mp = 85 °C

^{1}HNMR ($CDCl_3$)	δ 0.89 (6H, 2 x t), 1.21-1.68 (22H, m; including a 3H, d at 1.35), 1.68-1.92 (3H, m), 4.09 (2H, t), 4.41(1H, sext), 6.81(1H, ddd), 6.97 (2H, d), 7.14 (1H, ddd), 7.50-7.66 (6H, m)
IR (KBr) ν_{max}	3040 (aryl C-H), 2940/2850 (aliphatic C-H), 1610 (C=C), 1485 (CH_2), 1375 (CH_3), 1250 (C-O) cm^{-1}
MS *m/z*	522 (M^+, 20 %), 410, 298 (100 %)
$[\alpha]_D^{22°C}$	+2.69°
HPLC (C18)	99.6 % (in acetonitrile)

(S)-(-)-*2,3-Difluoro-4"-(1-methylheptyloxy)-4-octyloxyterphenyl* (**22**)

Quantities used: tetrakis(triphenylphosphine)palladium(0) (0.16 g, 0.14 mmol), compound **14** (1.65 g, 4.56 mmol), compound **9** (1.64 g, 5.02 mmol), 2M- sodium carbonate (50 ml)

Yield 1.39 g (58 %); mp = 85 °C

^{1}HNMR ($CDCl_3$)	δ 0.89 (6H, 2 x t), 1.21-1.68 (22H, m; including a 3H, d at 1.34), 1.68-1.92 (3H, m), 4.08 (2H, t), 4.41 (1H, sext), 6.81 (1H, ddd), 6.97 (2H, d), 7.13 (1H, ddd), 7.50-7.65 (6H, m)
IR (KBr) ν_{max}	3040 (aryl C-H), 2920/2850 (aliphatic C-H), 1610 (C=C), 1465 (CH_2), 1370 (CH_3), 1250 (C-O) cm^{-1}
MS *m/z*	522 (M^+, 25 %), 410, 298 (100 %)
$[\alpha]_D^{22°C}$	-2.22°
HPLC(C18)	99.5 % (in acetonitrile)

4"-(1-Ethylpropoxy)-2,3-difluoro-4-octyloxyterphenyl (**23**)

Quantities used: tetrakis(triphenylphosphine)palladium(0) (0.16 g, 0.14 mmol), compound **15** (1.45 g, 4.56 mmol), compound **9** (1.64 g, 5.02 mmol), 2M- sodium carbonate (50 ml)

Yield 0.54 g (25 %); mp = 72 °C

^{1}HNMR ($CDCl_3$)	δ 0.90 (3H, t), 0.99 (6H, 2 x t), 1.23-1.54 (10H, m), 1.72 (4H, d/q), 1.85 (2H, quint), 4.08 (2H, t), 4.17 (1H, quint), 6.82 (1H, ddd), 6.98 (2H, d), 7.13 (1H, ddd), 7.50-7.66 (6H, m)
IR (KBr) ν_{max}	3040 (aryl C-H), 2930/2840 (aliphatic C-H), 1610 (C=C), 1465 (CH_2), 1380 (CH_3), 1250 (C-O) cm^{-1}
MS *m/z*	480 (M^+, 35 %), 410, 298 (100 %)
HPLC (C18)	99.5 % (in acetonitrile)

4"-(1-Ethylbutoxy)-2,3-difluoro-4-octyloxyterphenyl (**24**)

Quantities used: tetrakis(triphenylphosphine)palladium(0) (0.28 g, 0.24 mmol), compound **16** (2.70 g, 8.10 mmol), compound **9** (2.91 g, 8.91 mmol), 2M- sodium carbonate (100 ml)

Yield 2.54 g (64 %); mp = 62 °C

^{1}HNMR ($CDCl_3$)	δ 0.90(3H, t), 0.95 (3H, t), 0.98 (3H, t), 1.24-1.53 (12H, m), 1.59-1.77 (4H, m), 1.85 (2H, quint), 4.08 (2H, t), 4.23 (1H, quint), 6.81 (1H, ddd), 6.98 (2H, d) 7.14 (1H, ddd), 7.51-7.65 (6H, m)
IR (KBr) ν_{max}	3040 (aryl C-H), 2940/2850 (aliphatic C-H), 1610 (C=C), 1465 (CH_2), 1380 (CH_3), 1250 (C-O) cm^{-1}
MS *m/z*	494 (M^+, 25 %), 410, 298 (100 %)
HPLC (C18)	98.8 % (in acetonitrile)

4"-(1-Ethylhexyloxy)-2,3-difluoro-4-octyloxyterphenyl (**25**)

Quantities used: tetrakis(triphenylphosphine)palladium(0) (0.16 g, 0.14 mmol), compound **17** (1.65 g, 4.56 mmol), compound **9** (1.64 g, 5.02 mmol), 2M- sodium carbonate (50 ml)

Yield 1.51 g (64 %); mp = 52 °C

^{1}HNMR ($CDCl_3$)	δ 0.89 (6H, 2 x t), 0.98 (3H, t) 1.24-1.52 (16H, m), 1.61-1.78 (4H, m), 1.85 (2H, quint), 4.09 (2H, q), 4.22 (1H, quint), 6.81 (1H, ddd), 6.97 (2H, d) 7.14 (1H, ddd), 7.50-7.66 (6H, m)
IR (KBr) ν_{max}	3040 (aryl C-H), 2930/2850 (aliphatic C-H), 1610 (C=C), 1465 (CH_2), 1385 (CH_3), 1240 (C-O) cm^{-1}
MS *m/z*	522 (M^+, trace), 410, 298, 57 (100 %)
HPLC (C18)	99.8 % (in acetonitrile)

***2,3-Difluoro-4-octyloxy-4"-(1-propylbutoxy)terphenyl* (26)**

Quantities used: tetrakis(triphenylphosphine)palladium(0) (0.23 g, 0.20 mmol), compound **18** (2.30 g, 6.63 mmol), compound **9** (2.38 g, 7.29 mmol), 2M- sodium carbonate (80 ml)

Yield 1.22 g (36 %); mp = 68 °C

^{1}HNMR ($CDCl_3$)	δ 0.89 (3H, t), 0.95 (6H, t) 1.24-1.53 (14H, m), 1.57-1.76 (4H, d/t), 1.85 (2H, quint), 4.09 (2H, t), 4.30 (1H, quint), 6.81 (1H, ddd), 6.97 (2H, d), 7.13 (1H, ddd), 7.50-7.66 (6H, m)
IR (KBr) ν_{max}	3040 (aryl C-H), 2940/2850 (aliphatic C-H), 1600 (C=C), 1460 (CH_2), 1380 (CH_3), 1250 (C-O) cm^{-1}
MS *m/z*	508 (M^+, 10 %), 410, 298 (100 %)
HPLC (C18)	99.7 % (in acetonitrile)

***4"-(1-Butylpentoxy)-2,3-difluoro-4-octyloxyterphenyl* (27)**

Quantities used: tetrakis(triphenylphosphine)palladium(0) (0.25 g, 0.22 mmol), compound **19** (2.70 g, 7.20 mmol), compound **9** (2.59 g, 7.92 mmol), 2M- sodium carbonate (100 ml)

Yield 1.25 g (32 %); mp = 54 °C

^{1}HNMR ($CDCl_3$)	δ 0.89 (3H, t), 0.90 (6H, t) 1.23-1.53 (18H, m), 1.67 (4H, d/t), 1.85 (2H, quint), 4.08 (2H, q), 4.26 (1H, quint), 6.81 (1H, ddd), 6.97 (2H, d) 7.14 (1H, ddd), 7.50-7.65 (6H, m)
IR (KBr) ν_{max}	3040 (aryl C-H), 2940/2870 (aliphatic C-H), 1610 (C=C), 1465 (CH_2), 1385 (CH_3), 1240 (C-O) cm^{-1}
MS *m/z*	536 (M^+, 40 %), 410, 298 (100 %)
HPLC (C18)	99.8 % (in acetonitrile)

3.9.3 Synthetic Scheme 3 and Materials Prepared (28-60)

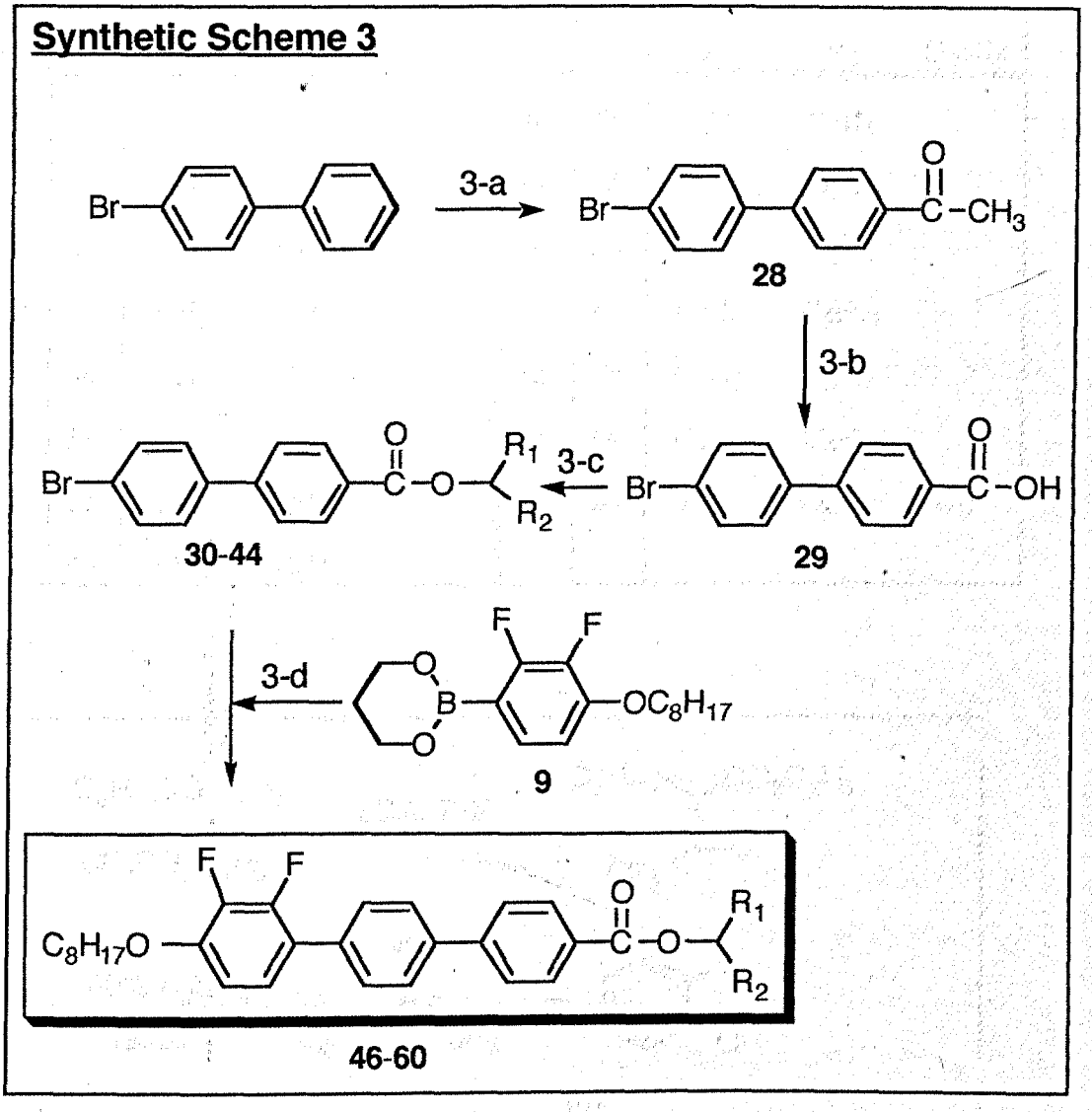

3-a ··· CH_3COCl, $AlCl_3$, DCM

3-b ··· NaOCl, $Na_2S_2O_5$, $[CH_3(CH_2)_3]_4NI$, dioxane

3-c ··· R_1R_2CHOH or $CF_3C_6H_{13}CHOH$, DCC, DMAP

3-d ··· $Pd(PPh_3)_4$, K_3PO_4, DMF

Compounds					Compounds				
No.	No.	R_1	R_2	Config	No.	No.	R_1	R_2	Config
30	**46**	CH_3	CH_3		**38**	**54**	C_2H_5	C_2H_5	
31	**47**	CH_3	C_4H_9		**39**	**55**	C_2H_5	C_3H_7	
32	**48**	CH_3	C_5H_{11}	(*S*)-	**40**	**56**	C_2H_5	C_4H_9	
33	**49**	CH_3	C_5H_{11}		**41**	**57**	C_2H_5	C_5H_{11}	
34	**50**	CH_3	C_6H_{13}	(*R*)-	**42**	**58**	C_3H_7	C_3H_7	
35	**51**	CH_3	C_6H_{13}		**43**	**59**	C_4H_9	C_4H_9	
36	**52**	CH_3	C_7H_{15}		**44**	**60**	CF_3	C_6H_{13}	(*R*)-
37	**53**	CH_3	C_8H_{17}						

‡

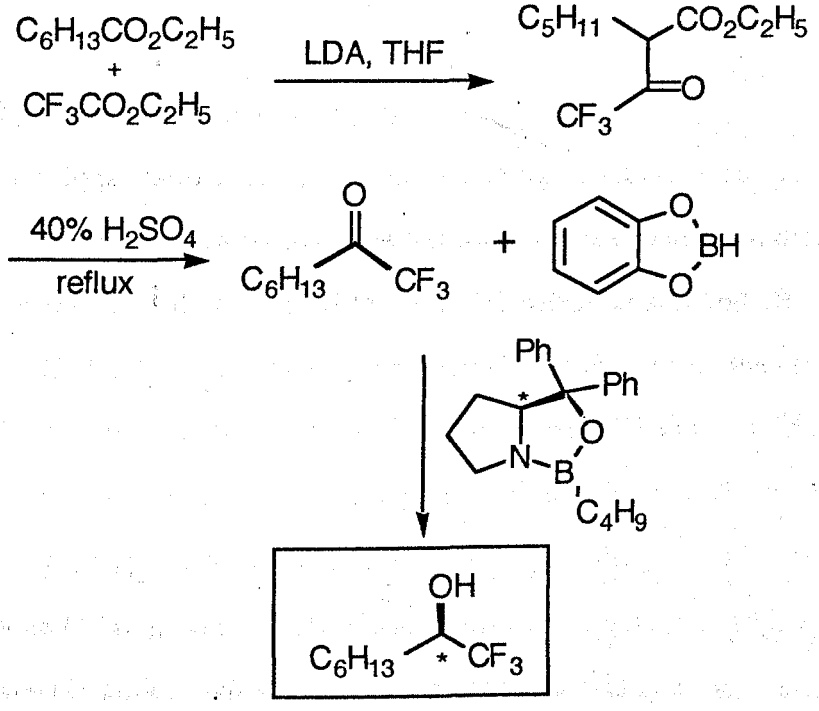

45

***4-Acetyl-4'-bromobiphenyl* (28)**

Acetyl chloride (9.26 g, 118 mmol) was added dropwise to a stirred, cooled (0 °C) solution of 4-bromobiphenyl (25.0 g, 107 mmol) and aluminium chloride (15.7 g, 118 mmol) in DCM (500 ml); the solution was stirred for a further hour at 0 °C. The stirred mixture was heated under reflux for 2 hours, and then cooled before dilute hydrochloric acid (water:conc. HCl = 1:1, 200 ml) was added. The product was extracted into DCM (2 x 200 ml) and the combined organic solvents were washed with water. The solvent was evaporated *in vacuo* and the product was recrystallised (ethanol) to give an orange solid.

Yield 14.4 g (49 %); mp = 122-124 °C

^{1}HNMR ($CDCl_3$)	δ 2.64 (3H, s), 7.49 (2H, d), 7.60 (2H, d), 7.65 (2H, d), 8.03 (2H, d)
IR (KBr) ν_{max}	3060 (aryl C-H), 1665 (C=O), 1610 (C=C), 1350 (CH_3)
MS *m/z*	276/274 (M^+, 30 %), 261/259, 152 (100 %)

***4'-Bromobiphenyl-4-carboxylic acid* (29)**

Dilute sodium hypochlorite was prepared by adding commercial sodium hypochlorite solution (containing 10-14% available chlorine) to water (30 ml) and dioxane (60 ml). The solution was stirred and heated to 50-60 °C before compound **28** (7.50n g, 27.3 mmol) was added. After the exothermic reaction had commenced, the temperature was maintained at 60-70 °C by frequent cooling in an ice bath. The mixture was stirred for a further 30 min before tetra-n-butylammonium iodide (3.50 g, 9.48 mmol) was added. The excess of hypochlorite was destroyed by adding a solution of sodium metabisulphite (5.00 g, 26.3 mmol). Conc. hydrochloric acid was added slowly to the mixture cooled in an ice bath to acidify the mixture to pH3 and then the crude product was filtered off. The product was dissolved in ether and washed with water and the ether

solvent was dried ($MgSO_4$). The solvent was removed *in vacuo* to give a pale yellow solid.

Yield 3.30g (44 %); mp = 260 °C (decomposed)

^{1}HNMR (DMSO+$CDCl_3$) δ 7.51(2H, d), 7.60 (2H, d), 7.63 (2H, d), 8.11(2H, d); the carboxylic acid proton was not detected.

IR (KBr) ν_{max} 3200-2500 (OH of carboxylic acid), 3060 (aryl C-H), 1675 (C=O), 1605 (C=C), 1295 (C-O) cm^{-1}

MS *m/z* 278/276 (M^+, 10 %), 261/259, 152 (100 %)

***1-Methylethyl 4'-bromobiphenyl-4-carboxylate* (30)**

DCC (2.10 g, 9.96 mmol) was added in one portion to a stirred solution of compound **29** (2.5 g, 9.00 mmol), propan-2-ol (0.50 g, 8.33 mmol) and DMAP (0.30 g, 2.50 mmol) in dry DCM (50 ml) and the mixture was stirred at room temperature overnight. The DCU was filtered off and the filtrate was washed successively with water, 5 % acetic acid and water. The solution was dried ($MgSO_4$) and the solvent was removed *in vacuo*. The product was purified by column chromatography [DCM/petroleum (bp 40-60 °C), 2:8] to give a white solid.

Yield 2.25 g (85 %); mp = 97-99 °C

^{1}HNMR ($CDCl_3$) δ 1.39 (6H, 2 x d), 5.28 (1H, septet), 7.48 (2H, d), 7.59 (2H, d), 7.61 (2H, d), 8.10 (2H, d)

IR (KBr) ν_{max} 3060 (aryl C-H), 2980/2930 (aliphatic C-H), 1700 (C=O), 1605 (C=C), 1465 (CH_2), 1370 (CH_3), 1275 (C-O) cm^{-1}

MS *m/z* 320/318 (M^+, 5 %), 278/276, 261/259, 152 (100 %)

The following compounds (**31-44**) were prepared using the same general procedure used for the preparation of compound **30**.

***1-Methylpentyl 4'-bromobiphenyl-4-carboxylate* (31)**

Quantities used: DCC (1.70 g, 8.22 mmol), DMAP (0.26 g, 2.06 mmol), compound **29** (2.10 g, 7.54 mmol), hexan-2-ol (0.70 g, 6.85 mmol)

Yield 1.76 g (71 %); mp = 59-61 °C

^{1}HNMR ($CDCl_3$)	δ 0.91 (3H, t), 1.23-1.81 (9H, m: including 3H, d at 1.37), 5.18 (1H, sext) 7.49 (2H, d), 7.58 (2H, d), 7.62 (2H, d), 8.11 (2H, d)
IR (KBr) ν_{max}	3050 (aryl C-H), 2955/2865 (aliphatic C-H), 1700 (C=O), 1610 (C=C), 1470 (CH_2), 1380 (CH_3), 1280 (C-O) cm^{-1}
MS *m/z*	362/360 (M^+, 5 %), 278/276, 261/259, 152 (100 %)

(S)-(+)-*1-Methylhexyl 4'-bromobiphenyl-4-carboxylate* (32)

Quantities used: DCC (4.26 g, 20.7 mmol), DMAP (0.63 g, 5.16 mmol), compound **29** (5.25 g, 18.9 mmol), (*S*)-(+)- heptan-2-ol (2.00 g, 17.2 mmol)

Yield 3.30 g (51 %); mp = 44-45 °C

^{1}HNMR ($CDCl_3$)	δ 0.88 (3H, t), 1.20-1.80 (11H, m: including 3H, d at 1.36), 5.19 (1H, sext), 7.48 (2H, d), 7.57 (2H, d), 7.62 (2H, d), 8.10 (2H, d)
IR (KBr) ν_{max}	3050 (aryl C-H), 2925/2865 (aliphatic C-H), 1720 (C=O), 1610 (C=C), 1470 (CH_2), 1385 (CH_3), 1275 (C-O) cm^{-1}
MS *m/z*	376/374 (M^+, trace), 278/276, 261/259, 152 (100 %)
$[\alpha]_D^{22°C}$	+ 32.7°

***1-Methylhexyl 4'-bromobiphenyl-4-carboxylate* (33)**

Quantities used: DCC (2.35 g, 11.4 mmol), DMAP (0.35 g, 2.84 mmol), compound **29** (2.89 g, 10.4 mmol), heptan-2-ol (1.10 g, 9.48 mmol)

Yield 1.92 g (54 %); mp = 61-62 °C

^{1}HNMR ($CDCl_3$) δ 0.89 (3H, t), 1.24-1.82 (11H, m: including 3H, d at 1.37), 5.18 (1H, sext), 7.48 (2H, d), 7.58 (2H, d), 7.62 (2H, d), 8.11 (2H, d)

IR (KBr) ν_{max} 3050 (aryl C-H), 2930/2860 (aliphatic C-H), 1700 (C=O), 1610 (C=C), 1470 (CH_2), 1380 (CH_3), 1280 (C-O) cm^{-1}

MS *m/z* 376/374 (M^+, 5 %), 278/276, 261/259, 152 (100 %)

(R)-(-)-*1-Methylheptyl 4'-bromobiphenyl-4-carboxylate* (34)

Quantities used: DCC (6.10 g, 29.5 mmol), DMAP (0.90 g, 7.38 mmol), compound **29** (7.53 g, 27.1 mmol), (*R*)-(-)-octan-2-ol (3.20 g, 24.6 mmol)

Yield 3.30 g (34 %); mp = 41-42 °C

^{1}HNMR ($CDCl_3$) δ 0.88 (3H, t), 1.25-1.82 (13H, m: including 3H, d at 1.36), 5.17 (1H, sext), 7.48 (2H, d), 7.59 (2H, d), 7.62 (2H, d), 8.11 (2H, d)

IR (KBr) ν_{max} 3060 (aryl C-H), 2920/2855 (aliphatic C-H), 1710 (C=O), 1610 (C=C), 1470 (CH_2), 1390 (CH_3), 1290 (C-O) cm^{-1}

MS *m/z* 390/388 (M^+, 5 %), 278/276, 261/259, 152 (100 %)

$[\alpha]_D^{22°C}$ -31.1°

***1-Methylheptyl 4'-bromobiphenyl-4-carboxylate* (35)**

Quantities used: DCC (1.90 g, 9.22 mmol), DMAP (0.28 g, 2.31 mmol), compound **29** (2.35 g, 8.45 mmol), octan-2-ol (1.00 g, 7.68 mmol)

Yield 2.41g (81 %); mp = 34-35 °C

^{1}HNMR ($CDCl_3$) δ 0.88 (3H, t), 1.23-1.83 (13H, m: including 3H, d at 1.37), 5.18 (1H, sext), 7.48 (2H, d), 7.59 (2H, d), 7.61 (2H, d), 8.11 (2H, d)

IR (KBr) ν_{max} 3060 (aryl C-H), 2930/2860 (aliphatic C-H), 1715 (C=O),

1610 (C=C), 1480 (CH_2), 1390 (CH_3), 1280 (C-O) cm^{-1}

MS *m/z* 390/388 (M^+, 5 %), 278/276, 261/259, 152 (100 %)

***1-Methyloctyl 4'-bromobiphenyl-4-carboxylate* (36)**

Quantities used: DCC (5.1 g, 24.9 mmol), DMAP (0.76 g, 6.24 mmol), compound **29** (6.3 g, 22.9 mmol), nonan-2-ol (3.0 g, 20.8 mmol)

Yield 3.6 g (44 %); mp = 45-48 °C

^{1}HNMR ($CDCl_3$) δ 0.88 (3H, t), 1.21-1.82 (15H, m: including 3H, d at 1.36), 5.18 (1H, sext), 7.48 (2H, d), 7.59 (2H, d), 7.62 (2H, d), 8.11 (2H, d)

IR (KBr) ν_{max} 3055 (aryl C-H), 2920/2850 (aliphatic C-H), 1705 (C=O), 1610 (C=C), 1470 (CH_2), 1380 (CH_3), 1290 (C-O) cm^{-1}

MS *m/z* 404/402 (M^+, trace), 278/276, 261/259, 152 (100 %)

***1-Methylnonyl 4'-bromobiphenyl-4-carboxylate* (37)**

Quantities used: DCC (4.70 g, 22.8 mmol), DMAP (0.70 g, 5.69 mmol), compound **29** (5.80 g, 20.9 mmol), decan-2-ol (3.00 g, 19.0 mmol)

Yield 3.30 g (42 %); mp = 28-29 °C

^{1}HNMR ($CDCl_3$) δ 0.88 (3H, t), 1.20-1.85 (17H, m: including 3H, d at 1.35), 5.18 (1H, sext), 7.47 (2H, d), 7.58 (2H, d), 7.63 (2H, d), 8.10 (2H, d)

IR (KBr) ν_{max} 3050 (aryl C-H), 2920/2850 (aliphatic C-H), 1705 (C=O), 1610 (C=C), 1480 (CH_2), 1380 (CH_3), 1275 (C-O) cm^{-1}

MS *m/z* 418/416 (M^+, trace), 278/276, 261/259, 152 (100 %)

***1-Ethylpropyl 4'-bromobiphenyl-4-carboxylate* (38)**

Quantities used: DCC (6.10 g, 29.5 mmol), DMAP (0.30 g, 2.10 mmol), compound **29** (7.53 g, 27.1 mmol), pentan-2-ol (2.20 g, 24.6 mmol)

Yield 2.70 g (32 %)

^{1}HNMR ($CDCl_3$) δ 0.95 (6H, 2 x t), 1.34-1.77 (4H, m), 5.12 (1H, quint), 7.47 (2H, d), 7.58 (2H, d), 7.62 (2H, d), 8.11 (2H, d)

IR (KBr) ν_{max} 3060 (aryl C-H), 2970/2930 (aliphatic C-H), 1710 (C=O), 1605 (C=C), 1470 (CH_2), 1390 (CH_3), 1275 (C-O) cm^{-1}

MS *m/z* 348/346 (M^+, trace), 278/276, 261/259, 152 (100 %)

***1-Ethylbutyl 4'-bromobiphenyl-4-carboxylate* (39)**

Quantities used: DCC (2.43 g, 11.8 mmol), DMAP (0.36 g, 2.94 mmol), compound **29** (3.00 g, 10.8 mmol), hexan-3-ol (1.00 g, 9.80 mmol)

Yield 1.93 g (55 %)

^{1}HNMR ($CDCl_3$) δ 0.95 (6H, 2 x t), 1.32-1.79 (6H, m), 5.12 (1H, quint), 7.48 (2H, d), 7.58 (2H, d), 7.62 (2H, d), 8.11 (2H, d)

IR (KBr) ν_{max} 3050 (aryl C-H), 2965/2935 (aliphatic C-H), 1715 (C=O), 1610 (C=C), 1470 (CH_2), 1390 (CH_3), 1275 (C-O) cm^{-1}

MS *m/z* 362/360 (M^+, trace), 278/276, 261/259, 152 (100 %)

***1-Ethylpentyl 4'-bromobiphenyl-4-carboxylate* (40)**

Quantities used: DCC (6.36 g, 30.9 mmol), DMAP (0.94 g, 7.74 mmol), compound **29** (7.90 g, 28.4 mmol), heptan-3-ol (3.00 g, 25.8 mmol)

Yield 3.60 g (37 %)

^{1}HNMR ($CDCl_3$) δ 0.95 (6H, 2 x t), 1.30-1.74 (8H, m), 5.11 (1H, quint), 7.48 (2H, d), 7.58 (2H, d), 7.61 (2H, d), 8.11 (2H, d)

IR (KBr) ν_{max} 3055 (aryl C-H), 2935/2860 (aliphatic C-H), 1710 (C=O),

1610 (C=C), 1470 (CH_2), 1390 (CH_3), 1275 (C-O) cm^{-1}

MS *m/z* 376/374 (M^+, trace), 278/276, 261/259, 152 (100 %)

***1-Ethylhexyl 4'-bromobiphenyl-4-carboxylate* (41)**

Quantities used: DCC (6.10 g, 29.5 mmol), DMAP (0.90 g, 7.38 mmol), compound **29** (7.53 g, 27.1 mmol), octan-3-ol (3.20 g, 24.6 mmol)

Yield 7.0 g (73 %)

^{1}HNMR ($CDCl_3$) δ 0.86 (3H, t), 0.96 (3H, t), 1.27-1.71 (10H, m), 5.10 (1H, quint), 7.48 (2H, d), 7.58 (2H, d), 7.61 (2H, d), 8.11 (2H, d)

IR (KBr) ν_{max} 3050 (aryl C-H), 2930/2860 (aliphatic C-H), 1710 (C=O), 1610 (C=C), 1470 (CH_2), 1390 (CH_3), 1275 (C-O) cm^{-1}

MS *m/z* 390/388 (M^+, 5 %), 278/276, 261/259, 152 (100 %)

***1-Propylbutyl 4'-bromobiphenyl-4-carboxylate* (42)**

Quantities used: DCC (1.98 g, 9.59 mmol), DMAP (0.29 g, 2.40 mmol), compound **29** (2.44 g, 8.79 mmol), heptan-4-ol (0.93 g, 7.99 mmol)

The product was purified by column chromatography to give a colourless liquid.

Yield 1.00 g (34 %)

^{1}HNMR ($CDCl_3$) δ 0.94 (6H, t), 1.35-1.74 (8H, m), 5.19 (1H, quint), 7.47 (2H, d), 7.58(2H, d), 7.62(2H, d), 8.11(2H, d)

IR (KBr) ν_{max} 3050 (aryl C-H), 2955/2865 (aliphatic C-H), 1710 (C=O), 1610 (C=C), 1470 (CH_2), 1380 (CH_3), 1270 (C-O) cm^{-1}

MS *m/z* 376/374(M^+, trace), 278/276, 152 (100 %)

***1-Butylpentyl 4'-bromobiphenyl-4-carboxylate* (43)**

Quantities used: DCC (2.43 g, 11.8 mmol), DMAP (0.36 g, 2.94 mmol), compound **29** (3.00 g, 10.8 mmol), nonan-5-ol (1.40 g, 9.72 mmol)

The product was purified by column chromatography to give a colourless liquid.

Yield 2.80 g (71 %)

^{1}HNMR ($CDCl_3$)	δ 0.95 (6H, t), 1.34-1.75 (12H, m), 5.15 (1H, quint), 7.47 (2H, d), 7.58 (2H, d), 7.62 (2H, d), 8.11(2H, d)
IR (KBr) ν_{max}	3040 (aryl C-H), 2955/2860 (aliphatic C-H), 1715 (C=O), 1610 (C=C), 1470 (CH_2), 1380 (CH_3), 1275 (C-O) cm^{-1}
MS *m/z*	404/402 (M^+, trace), 278/276, 261/259, 152 (100 %)

(R)-(-)-*1-Trifluoromethylheptyl 4'-bromobiphenyl-4-carboxylate* (44)

Quantities used: DCC (0.60 g, 2.80 mmol), DMAP (0.09 g, 0.70 mmol), compound **29** (0.71 g, 2.56 mmol), compound **45** (0.43 g, 2.33 mmol)

Yield 0.70 g (68 %)

^{1}HNMR ($CDCl_3$)	δ 0.87 (3H, t), 1.23-1.47 (8H, m), 1.89 (2H, d/t), 5.57 (1H, sext), 7.50 (2H, d), 7.60(2H, d), 7.67 (2H, d), 8.14 (2H, d)
IR (KBr) ν_{max}	3050 (aryl C-H), 2960/2930/2860 (aliphatic C-H), 1730 (C=O), 1610 (C=C), 1480 (CH_2), 1390 (CH_3), 1260 (C-O), 1180 (C-F) cm^{-1}
MS *m/z*	444/442 (M^+, trace), 278/276, 261/259, 152 (100 %)
$[\alpha]_D^{22°C}$	-42.2°

‡**(R)-(+)-*1,1,1-Trifluorooctan-2-ol* (45)**

This compound was supplied by Dr. R. A. Lewis and had been prepared by following the procedure reported in Reference 13.

^{1}HNMR ($CDCl_3$)	δ 0.88 (3H, t), 1.25-1.45 (6H, m), 1.50-1.60 (2H, m), 1.60-1.78 (2H, m), 2.05 (1H, d), 3.91 (1H, m)
IR (KBr) ν_{max}	3100-3600 (H-bonded OH), 2960/2940/2860 (aliphatic C-H), 1710, 1470 (CH_2), 1390 (CH_3), 1280 (C-O), 1170, 1140

MS *m/z*	Molecular ion was not detected by electron impact ionization.
$[\alpha]_D^{22°C}$	+16.4° (methanol)

***1-Methylethyl 2",3"-difluoro-4"-octyloxyterphenyl-4-carboxylate* (46)**

To a rapid stirred solution of tetrakis(triphenylphosphine)palladium(0) (0.22 g, 0.19 mmol), compound **30** (1.20 g, 3.76 mmol) and potassium phosphate (1.20 g, 5.64 mmol) in DMF (100 ml) was added compound **9** (1.35 g, 4.14 mmol) in dry DMF (20 ml) under dry nitrogen at 80-100 °C; the reaction mixture was maintained overnight at this temperature and GLC and TLC analysis then showed a complete reaction. Water (200 ml) was added and the product was extracted into diethyl ether (4 x 200 ml) by thorough washing. The combined ethereal extracts were washed with water (10 ml) and the solvent was removed *in vacuo*. The product was purified by column chromatography [DCM/petroleum (bp 40-60 °C), 1:4] and recrystallisation (methanol/ethyl acetate, 3:1) to give a white solid.

Yield 0.99 g (55 %); mp = 85 °C

^{1}HNMR ($CDCl_3$)	δ 0.90 (3H, t), 1.28-1.53 (16H, m: including a 6H, 2 x d at 1.39), 1.85 (2H, quint), 4.09 (2H, t), 5.29 (1H, sept), 6.83 (1H, ddd), 7.14 (1H, ddd), 7.58-7.73 (6H, m), 8.12 (2H, d)
IR (KBr) ν_{max}	3050 (aryl C-H), 2920/2850 (aliphatic C-H), 1710 (C=O), 1610 (C=C), 1470 (CH_2), 1390 (CH_3), 1275 (C-O) cm^{-1}
MS *m/z*	480 (M^+, 20 %), 421, 368, 326 (100 %), 308
HPLC (C18)	100 % (in acetonitrile)

The following compounds (**47-60**) were prepared using the same general procedure used for the preparation of compound **46.**

***1-Methylpentyl 2",3"-difluoro-4"-octyloxyterphenyl-4-carboxylate* (47)**

Quantities used: tetrakis(triphenylphosphine)palladium(0) (0.23 g, 0.20 mmol), compound **31** (1.40 g, 3.88 mmol), compound **9** (1.40 g, 4.29 mmol), potassium phosphate (1.24 g, 5.85 mmol)

Yield 0.8 g (39 %); mp = 43 °C

^{1}HNMR ($CDCl_3$)	δ 0.90 (6H, 2 x t), 1.27-1.69 (18H, m: including a 3H, d at 1.36), 1.70-1.90 (3H, m), 4.09 (2H, t), 5.18 (1H, sext), 6.83 (1H, ddd), 7.14 (1H, ddd), 7.58-7.73 (6H, m), 8.13 (2H, d)
IR (KBr) ν_{max}	3050 (aryl C-H), 2925/2855 (aliphatic C-H), 1720 (C=O), 1610 (C=C), 1470 (CH_2), 1380 (CH_3), 1275 (C-O) cm^{-1}
MS *m/z*	522 (M^+, 30 %), 411, 326 (100 %)
HPLC (C18)	100 % (in 90 % acetonitrile +10 % chloroform)

(S)-(+)-*1-Methylhexyl 2",3"-difluoro-4"-octyloxyterphenyl-4-carboxylate* (48)

Quantities used: tetrakis(triphenylphosphine)palladium(0) (0.15 g, 0.13 mmol), compound **32** (1.00 g, 2.66 mmol), compound **9** (0.96 g, 2.93 mmol), potassium phosphate (0.85 g, 3.99 mmol)

Yield 0.87 g (62 %); mp = 58 °C

^{1}HNMR ($CDCl_3$)	δ 0.89 (6H, 2 x t), 1.24-1.69 (20H, m: including a 3H, d at 1.37), 1.69-1.92 (3H, m), 4.09 (2H, t), 5.18 (1H, sext), 6.83 (1H, ddd), 7.14 (1H, ddd), 7.59-7.74 (6H, m), 8.13 (2H, d)
IR (KBr) ν_{max}	3050 (aryl C-H), 2925/2855 (aliphatic C-H), 1720 (C=O), 1610 (C=C), 1470 (CH_2), 1395 (CH_3), 1275 (C-O) cm^{-1}
MS *m/z*	536 (M^+, 20 %), 425, 326 (100 %), 309
$[\alpha]_D^{22°C}$	+20.5°
HPLC (C18)	100 % (in acetonitrile)

***1-Methylhexyl 2",3"-difluoro-4"-octyloxyterphenyl-4-carboxylate* (49)**

Quantities used: tetrakis(triphenylphosphine)palladium(0) (0.28 g, 0.24 mmol), compound **33** (1.80 g, 4.80 mmol), compound **9** (1.73 g, 5.28 mmol), potassium phosphate (1.53 g, 7.20 mmol)

Yield 1.33 g (52 %); mp = 43 °C

^{1}HNMR ($CDCl_3$)	δ 0.89 (6H, 2 x t), 1.24-1.69 (20H, m: including a 3H, d at 1.37), 1.69-1.93 (3H, m), 4.09 (2H, t), 5.19 (1H, sext), 6.83 (1H, ddd), 7.15 (1H, ddd), 7.58-7.74 (6H, m), 8.13 (2H, d)
IR (KBr) ν_{max}	3050 (aryl C-H), 2925/2855 (aliphatic C-H), 1720 (C=O), 1610 (C=C), 1470 (CH_2), 1385 (CH_3), 1275 (C-O) cm^{-1}
MS *m/z*	536 (M^+, 20 %), 425, 326 (100 %), 309
HPLC (C18)	99.7 % (in acetonitrile)

(R)-(-)-*1-Methylheptyl 2",3"-difluoro-4"-octyloxyterphenyl-4-carboxylate* (50)

Quantities used: tetrakis(triphenylphosphine)palladium(0) (0.25 g, 0.22 mmol), compound **34** (1.73 g, 4.43 mmol), compound **9** (1.59 g, 4.87 mmol), potassium phosphate (1.41 g, 6.65 mmol)

Yield 0.62 g (25 %); mp = 59 °C

^{1}HNMR ($CDCl_3$)	δ 0.88 (6H, 2 x t), 1.22-1.69 (22H, m: including a 3H, d at 1.38), 1.69-1.92 (3H, m), 4.09 (2H, t), 5.19 (1H, sext), 6.83 (1H, ddd), 7.14 (1H, ddd), 7.56-7.74 (6H, m) 8.13 (2H, d)
IR (KBr) ν_{max}	3050 (aryl C-H), 2920/2855 (aliphatic C-H), 1710 (C=O), 1610 (C=C), 1470 (CH_2), 1390 (CH_3), 1275 (C-O) cm^{-1}
MS *m/z*	550 (M^+, 60 %), 438, 421, 326 (100 %), 309
$[\alpha]_D^{22°C}$	-24.0°.
HPLC (C18)	99.9 % (in acetonitrile)

***1-Methylheptyl 2",3"-difluoro-4"-octyloxyterphenyl-4-carboxylate* (51)**

Quantities used: tetrakis(triphenylphosphine)palladium(0) (0.31 g, 0.27 mmol), compound **35** (2.08 g, 5.34 mmol), compound **9** (1.92 g, 5.87 mmol), potassium phosphate (1.70 g, 8.01 mmol)

Yield 0.75 g (26 %); mp = 54 °C

^{1}HNMR ($CDCl_3$)	δ 0.89 (6H, 2 x t), 1.22-1.69 (22H, m: including a 3H, d at 1.34), 1.69-1.89 (3H, m), 4.10 (2H, t), 5.14 (1H, sext), 6.87 (1H, ddd), 7.19 (1H, ddd), 7.59-7.76 (6H, m) 8.11 (2H, d)
IR (KBr) ν_{max}	3060 (aryl C-H), 2920/2850 (aliphatic C-H), 1710 (C=O), 1610 (C=C), 1470 (CH_2), 1380 (CH_3), 1270 (C-O) cm^{-1}
MS *m/z*	550 (M^+, 10 %), 421, 326 (100 %), 308
HPLC (C18)	99.0 % (in 90 % acetonitrile +10 % chloroform)

***1-Methyloctyl 2",3"-difluoro-4"-octyloxyterphenyl-4-carboxylate* (52)**

Quantities used: tetrakis(triphenylphosphine)palladium(0) (0.14 g, 0.12 mmol), compound **36** (1.00 g, 2.48 mmol), compound **9** (0.89 g, 2.73 mmol), potassium phosphate (0.79 g, 3.72 mmol)

Yield 0.40 g (29 %); mp = 54 °C

^{1}HNMR ($CDCl_3$)	δ 0.88 (6H, 2 x t), 1.25-1.65 (24H, m: including a 3H, d at 1.35), 1.69-1.90 (3H, m), 4.09 (2H, t), 5.18 (1H, sext), 6.83 (1H, ddd), 7.14 (1H, ddd), 7.58-7.73 (6H, m) 8.12 (2H, d)
IR (KBr) ν_{max}	3050 (aryl C-H), 2920/2850 (aliphatic C-H), 1710 (C=O), 1610 (C=C), 1470 (CH_2), 1395 (CH_3), 1275 (C-O) cm^{-1}
MS *m/z*	564 (M^+, 25 %), 452, 422, 326 (100 %), 308
HPLC (C18)	99.4 % (in 90 % acetonitrile +10 % chloroform)

1-Methylnonyl 2",3"-difluoro-4"-octyloxyterphenyl-4-carboxylate (**53**)

Quantities used: tetrakis(triphenylphosphine)palladium(0) (0.14 g, 0.12 mmol), compound **37** (1.00 g, 2.40 mmol), compound **9** (0.86 g, 2.64 mmol), potassium phosphate (0.76 g, 3.60 mmol)

Yield 0.64 g (46 %); mp = 52 °C

^{1}HNMR ($CDCl_3$)	δ 0.89 (6H, 2 x t), 1.23-1.69 (26H, m: including a 3H, d at 1.38), 1.69-1.80 (3H, m), 4.09 (2H, t), 5.18 (1H, sext), 6.83 (1H, ddd), 7.13 (1H, ddd), 7.58-7.73 (6H, m) 8.15 (2H, d)
IR (KBr) ν_{max}	3050 (aryl C-H), 2920/2850 (aliphatic C-H), 1710 (C=O), 1610 (C=C), 1470 (CH_2), 1390 (CH_3), 1275 (C-O) cm^{-1}
MS *m/z*	578 (M^+, 25 %), 439, 421, 326 (100 %), 308
HPLC (C18)	100 % (in 90 % acetonitrile +10 % chloroform)

1-Ethylpropyl 2",3"-difluoro-4"-octyloxyterphenyl-4-carboxylate (**54**)

Quantities used: tetrakis(triphenylphosphine)palladium(0) (0.12 g, 0.10 mmol), compound **38** (0.76 g, 2.20 mmol), compound **9** (0.79 g, 2.42 mmol), potassium phosphate (0.70 g, 3.30 mmol)

Yield 0.63 g (56 %); mp = 57 °C

^{1}HNMR ($CDCl_3$)	δ 0.89 (3H, t), 0.98 (6H, 2 x t), 1.24-1.53 (10H, m), 1.74 (4H, d/q), 1.85 (2H, quint), 4.09 (2H, t), 5.06 (1H, quint), 6.82 (1H, ddd), 7.15 (1H, ddd), 7.57-7.74 (6H, m), 8.15 (2H, d)
IR (KBr) ν_{max}	3050 (aryl C-H), 2930/2860 (aliphatic C-H), 1720 (C=O), 1610 (C=C), 1470 (CH_2), 1390 (CH_3), 1275 (C-O) cm^{-1}
MS *m/z*	508 (M^+, 65 %), 421, 396, 326 (100%), 309
HPLC (C18)	99.9 % (in acetonitrile)

***1-Ethylbutyl 2",3"-difluoro-4"-octyloxyterphenyl-4-carboxylate* (55)**

Quantities used: tetrakis(triphenylphosphine)palladium(0) (0.25 g, 0.22 mmol), compound **39** (1.59 g, 4.40 mmol), compound **9** (1.58 g, 4.84 mmol), potassium phosphate (1.40 g, 6.60 mmol)

Yield 0.75 g (33 %); mp = 52 °C

^{1}HNMR ($CDCl_3$)	δ 0.90 (6H, 2 x t) , 0.98 (3H, t), 1.24-1.53 (12H, m), 1.60-1.79 (4H, m), 1.86 (2H, quint), 4.09 (2H, t), 5.02 (1H, quint), 6.83 (1H, ddd), 7.14 (1H, ddd), 7.58-7.76 (6H, m), 8.14 (2H, d)
IR (KBr) ν_{max}	3050 (aryl C-H), 2925/2860 (aliphatic C-H), 1720 (C=O), 1600 (C=C), 1465 (CH_2), 1380 (CH_3), 1275 (C-O) cm^{-1}
MS *m/z*	522 (M^+, 35 %), 421, 410, 326 (100 %), 309
HPLC (C18)	98.5 % (in acetonitrile)

***1-Ethylpentyl 2",3"-difluoro-4"-octyloxyterphenyl-4-carboxylate* (56)**

Quantities used: tetrakis(triphenylphosphine)palladium(0) (0.15 g, 0.13 mmol), compound **40** (1.00 g, 2.67 mmol), compound **9** (0.90 g, 2.94 mmol), potassium phosphate (0.85 g, 4.01 mmol)

Yield 0.40 g (28 %); mp = 36 °C

^{1}HNMR ($CDCl_3$)	δ 0.89 (6H, 2 x t) , 0.97 (3H, t), 1.25-1.53 (14H, m), 1.63-1.78 (4H, m), 1.85 (2H, quint), 4.09 (2H, t), 5.11 (1H, quint), 6.83 (1H, ddd), 7.15 (1H, ddd), 7.58-7.73 (6H, m), 8.14 (2H, d)
IR (KBr) ν_{max}	3050 (aryl C-H), 2925/2855 (aliphatic C-H), 1715 (C=O), 1610 (C=C), 1470 (CH_2), 1395 (CH_3), 1275 (C-O) cm^{-1}
MS *m/z*	536 (M^+, 45 %), 421, 326 (100 %), 309
HPLC (C18)	100 % (in 90 % acetonitrile +10 % chloroform)

1-Ethylhexyl 2",3"-difluoro-4"-octyloxyterphenyl-4-carboxylate (**57**)

Quantities used: tetrakis(triphenylphosphine)palladium(0) (0.15 g, 0.13 mmol), compound **41** (1.00 g, 2.57 mmol), compound **9** (0.93 g, 2.83 mmol), potassium phosphate (0.82 g, 3.86 mmol)

Yield 0.32 g (23 %); mp = 31 °C

^{1}HNMR ($CDCl_3$)	δ 0.89 (6H, 2 x t), 0.97 (3H, t), 1.24-1.53 (16H, m), 1.62-1.78 (4H, m), 1.85 (2H, quint), 4.09 (2H, t), 5.10 (1H, quint), 6.83 (1H, ddd), 7.15 (1H, ddd), 7.58-7.75 (6H, m), 8.14 (2H, d)
IR (KBr) ν_{max}	3050 (aryl C-H), 2920/2850 (aliphatic C-H), 1705 (C=O), 1605 (C=C), 1465 (CH_2), 1390 (CH_3), 1270 (C-O) cm^{-1}
MS *m/z*	550 (M^+, 50 %), 438, 421, 326 (100 %), 309
HPLC (C18)	99.6 % (in acetonitrile)

1-Propylbutyl 2",3"-difluoro-4"-octyloxyterphenyl-4-carboxylate (**58**)

Quantities used: tetrakis(triphenylphosphine)palladium(0) (0.10 g, 0.09 mmol), compound **42** (0.70 g, 1.87 mmol), compound **9** (0.67 g, 2.06 mmol), potassium phosphate (0.59 g, 2.81 mmol)

Yield 0.62 g (62 %); mp = 60 °C

^{1}HNMR ($CDCl_3$)	δ 0.90 (3H, t), 0.95 (6H, 2 x t), 1.24-1.53 (14H, m), 1.68 (4H, d/t), 1.86 (2H, quint), 4.09 (2H, t), 5.10 (1H, quint), 6.83 (1H, ddd), 7.15 (1H, ddd), 7.58-7.75 (6H, m), 8.14 (2H, d)
IR (KBr) ν_{max}	3050 (aryl C-H), 2930/2860 (aliphatic C-H), 1705 (C=O), 1600 (C=C), 1465 (CH_2), 1380 (CH_3), 1275 (C-O) cm^{-1}
MS *m/z*	536 (M^+, 20 %), 438, 421, 326 (100 %), 309
HPLC (C18)	99.3 % (in acetonitrile)

***1-Butylpentyl 2",3"-difluoro-4"-octyloxyterphenyl-4-carboxylate* (59)**

Quantities used: tetrakis(triphenylphosphine)palladium(0) (0.31 g, 0.27 mmol), compound **43** (2.15 g, 5.33 mmol), compound **9** (1.92 g, 5.86 mmol), potassium phosphate (1.70 g, 8.00 mmol)

Yield 1.40 g (47 %); mp = 37 °C

^{1}HNMR ($CDCl_3$)	δ 0.88 (3H, t), 0.90 (6H, 2 x t), 1.23-1.54 (18H, m), 1.69 (4H, d/t),1.86 (2H, quint), 4.09 (2H, t), 5.16 (1H, quint), 6.83 (1H, ddd), 7.15 (1H, ddd), 7.58-7.74 (6H, m), 8.14 (2H, d)
IR (KBr) ν_{max}	3040 (aryl C-H), 2930/2850 (aliphatic C-H), 1710 (C=O), 1605 (C=C), 1460 (CH_2), 1385 (CH_3), 1275 (C-O) cm^{-1}
MS *m/z*	564 (M^+, 20 %), 452, 421, 326 (100 %), 308
HPLC (C18)	99.5 % (in acetonitrile)

***(R)-(-)-1-Trifluoromethylheptyl 2",3"-difluoro-4"-octyloxyterphenyl-4-carboxylate* (60)**

Quantities used: tetrakis(triphenylphosphine)palladium(0) (0.08 g, 0.07 mmol), compound **44** (0.60 g, 1.35 mmol), compound **9** (0.49 g, 1.49 mmol), potassium phosphate (0.43 g, 2.03 mmol)

Yield 0.45 g (54 %); mp = 55 °C

^{1}HNMR ($CDCl_3$)	δ 0.89 (6H, 2 x t), 1.20-1.53 (18H, m), 1.79-1.96 (4H, m), 4.10 (2H, t), 5.58 (1H, sext), 6.83 (1H, ddd) 7.15 (1H, ddd), 7.59-7.78 (6H, m), 8.16 (2H, d)
IR (KBr) ν_{max}	3050 (aryl C-H), 2925/2855 (aliphatic C-H), 1740 (C=O), 1610 (C=C), 1470 (CH_2), 1395 (CH_3), 1265 (C-O), 1180 (C-F) cm^{-1}
MS *m/z*	604 (M^+, 10 %), 493, 327 (100 %),
HPLC (C18)	100 % (in acetonitrile)
$[\alpha]_D^{22°C}$	-39.3°

3.9.4 Synthetic Scheme 4 and Materials Prepared (61-73)

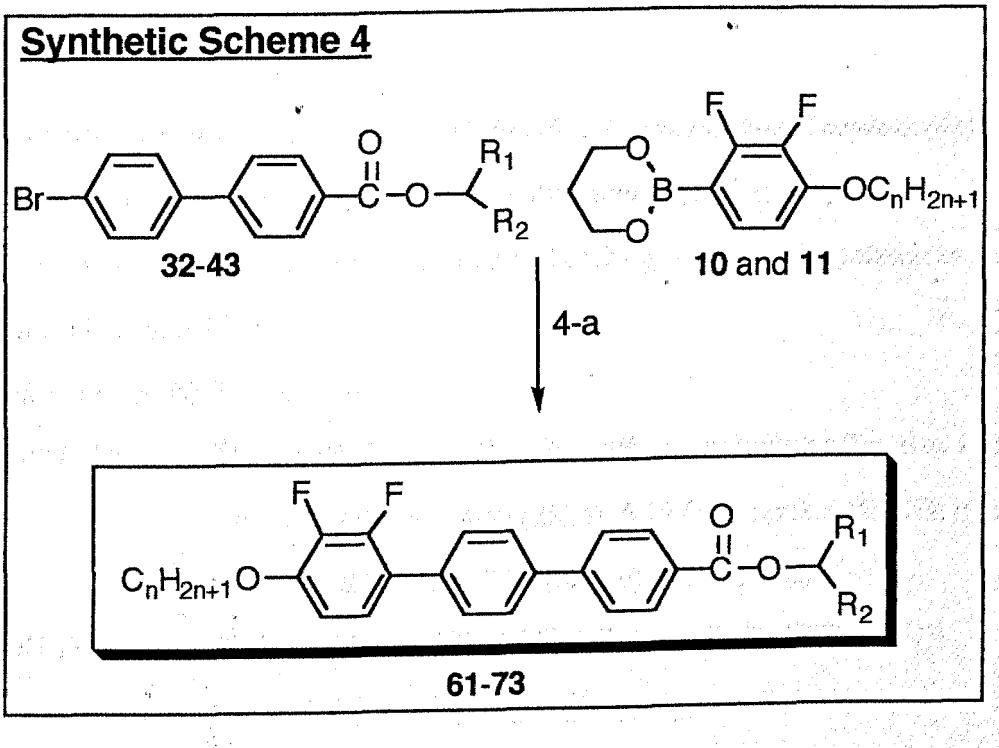

4-a ··· $Pd(PPh_3)_4$, K_3PO_4, DMF

Compounds					Compounds				
No.	n	R_1	R_2	Config.	No.	n	R_1	R_2	Config.
61	6	CH_3	C_6H_{13}	(*R*)-	**68**	10	C_2H_5	C_2H_5	
62	10	CH_3	C_5H_{11}	(*S*)-	**69**	10	C_2H_5	C_3H_7	
63	10	CH_3	C_5H_{11}		**70**	10	C_2H_5	C_4H_9	
64	10	CH_3	C_6H_{13}	(*R*)-	**71**	10	C_2H_5	C_5H_{11}	
65	10	CH_3	C_6H_{13}		**72**	10	C_3H_7	C_3H_7	
66	10	CH_3	C_7H_{15}		**73**	10	C_4H_9	C_4H_9	
67	10	CH_3	C_8H_{17}						

The following compounds (**61**-**73**) were prepared using the same general procedure used for the preparation of compound **46**.

***(R)-(+)-1-Methylheptyl 2",3"-difluoro-4"-hexyloxyterphenyl-4-carboxylate* (61)**

Quantities used: tetrakis(triphenylphosphine)palladium(0) (0.22 g, 0.19 mmol), compound **34** (1.50 g, 3.88 mmol), compound **11** (1.27 g, 4.25 mmol), potassium phosphate (1.23 g, 5.82 mmol)

Yield = 0.80 g (40 %); mp = 61 °C

^{1}HNMR ($CDCl_3$)	δ 0.88 (6H, 2 x t), 1.22-1.68 (18H, m: including a 3H, d at 1.39), 1.69-1.91 (3H, m), 4.10 (2H, t), 5.19 (1H, sext), 6.83 (1H, ddd), 7.15 (1H, ddd), 7.58-7.75 (6H, m), 8.13 (2H, d)
IR (KBr) ν_{max}	3040 (aryl C-H), 2920/2855 (aliphatic C-H), 1700 (C=O), 1610 (C=C), 1460 (CH_2), 1395 (CH_3), 1275 (C-O) cm^{-1}
MS *m/z*	522 (M^+, 45 %), 393, 327 (100 %), 309
$[\alpha]_D^{22°C}$	+27.0°
HPLC (C18)	100 % (in acetonitrile)

***(S)-(+)-1-Methylhexyl 4"-decyloxy -2",3"-difluoroterphenyl-4-carboxylate* (62)**

Quantities used: tetrakis(triphenylphosphine)palladium(0) (0.15 g, 0.13 mmol), compound **32** (1.00 g, 2.67 mmol), compound **10** (1.04 g, 2.94 mmol), potassium phosphate (0.85 g, 4.01 mmol)

Yield = 0.7 g (47 %); mp = 50 °C

^{1}HNMR ($CDCl_3$)	δ 0.89 (6H, 2 x t), 1.23-1.68 (24H, m: including a 3H, d at 1.37), 1.70-1.92 (3H, m), 4.10 (2H, t), 5.19 (1H, sext), 6.83 (1H, ddd), 7.15 (1H, ddd), 7.58-7.73 (6H, m), 8.13 (2H, d)
IR (KBr) ν_{max}	3040 (aryl C-H), 2920/2850 (aliphatic C-H), 1705 (C=O), 1600 (C=C), 1465 (CH_2), 1395 (CH_3), 1280 (C-O) cm^{-1}

MS *m/z*	564 (M^+, 30 %), 450, 424, 326 (100 %), 309
$[\alpha]_D^{22°C}$	+23. 2°
HPLC (C18)	100 % (in acetonitrile)

***1-Methylhexyl 4"-decyloxy-2",3"-difluoroterphenyl-4-carboxylate* (63)**

Quantities used: tetrakis(triphenylphosphine)palladium(0) (0.24 g, 0.21 mmol), compound **33** (1.60 g, 4.26 mmol), compound **10** (1.66 g, 4.69 mmol), potassium phosphate (1.36 g, 6.39 mmol)

Yield = 0.75 g (31 %); mp = 48 °C

^{1}HNMR ($CDCl_3$)	δ 0.88 (6H, 2 x t), 1.24-1.68 (24H, m: including a 3H, d at 1.36), 1.70-1.90 (3H, m), 4.09 (2H, t), 5.18 (1H, sext), 6.83 (1H, ddd), 7.14 (1H, ddd), 7.58-7.73 (6H, m), 8.12 (2H, d)
IR (KBr) ν_{max}	3050 (aryl C-H), 2920/2850 (aliphatic C-H), 1710 (C=O), 1610 (C=C), 1470 (CH_2), 1400 (CH_3), 1275 (C-O) cm^{-1}
MS *m/z*	564 (M^+, 10 %), 326 (100 %), 309
HPLC (C18)	99.7 % (in 90 % acetonitrile + 10 % chloroform)

(R)-(-)-*1-Methylheptyl 4"-decyloxy-2",3"-difluoroterphenyl-4-carboxylate* (64)

Quantities used: tetrakis(triphenylphosphine)palladium(0) (0.15 g, 0.13 mmol), compound **34** (1.00 g, 2.57 mmol), compound **10** (1.00 g, 2.83 mmol), potassium phosphate (0.82 g, 3.86 mmol)

Yield = 0.40 g (27 %); mp = 60 °C

^{1}HNMR ($CDCl_3$)	δ 0.89 (6H, 2 x t), 1.26-1.65 (26H, m: including a 3H, d at 1.36), 1.72-1.90 (3H, m), 4.09 (2H, t), 5.18 (1H, sext), 6.83 (1H, ddd), 7.15 (1H, ddd), 7.58-7.73 (6H, m), 8.12 (2H, d)
IR (KBr) ν_{max}	3050 (aryl C-H), 2920/2850 (aliphatic C-H), 1710 (C=O), 1610 (C=C), 1470 (CH_2), 1395 (CH_3), 1280 (C-O) cm^{-1}

MS *m/z*	578 (M^+, 10 %), 448, 326 (100 %)
$[\alpha]_D^{22°C}$	-21.9°
HPLC (C18)	98.9 % (in 90 % acetonitrile + 10 % chloroform)

1-Methylheptyl 4"-decyloxy-2",3"-difluoroterphenyl-4-carboxylate **(65)**

Quantities used: tetrakis(triphenylphosphine)palladium(0) (0.15 g, 0.13 mmol), compound **35** (1.00 g, 2.57 mmol), compound **10** (1.00 g, 2.83 mmol), potassium phosphate (0.82 g, 3.86 mmol)

Yield = 0.44 g (29 %); mp = 49 °C

^{1}HNMR ($CDCl_3$)	δ 0.89 (6H, 2 x t), 1.26-1.67 (26H, m: including a 3H, d at 1.35), 1.70-1.90 (3H, m), 4.09 (2H, t), 5.18 (1H, sext), 6.83 (1H, ddd), 7.15 (1H, ddd), 7.58-7.73 (6H, m), 8.12 (2H, d)
IR (KBr) ν_{max}	3040 (aryl C-H), 2920/2850 (aliphatic C-H), 1710 (C=O), 1610 (C=C), 1470 (CH_2), 1395 (CH_3), 1275 (C-O) cm^{-1}
MS *m/z*	578 (M^+, 10 %), 448, 326 (100 %), 308
HPLC (C18)	100 % (in 90 % acetonitrile + 10 % chloroform)

1-Methyloctyl 4"-decyloxy-2",3"-difluoroterphenyl-4-carboxylate **(66)**

Quantities used: tetrakis(triphenylphosphine)palladium(0) (0.14 g, 0.12 mmol), compound **36** (1.00 g, 2.48 mmol), compound **10** (0.97 g, 2.73 mmol), potassium phosphate (0.79 g, 3.72 mmol)

Yield = 0.30 g (20 %); mp = 51 °C

^{1}HNMR ($CDCl_3$)	δ 0.87 (6H, 2 x t), 1.26-1.67 (28H, m: including a 3H at 1.36), 1.69-1.90 (3H, m), 4.09 (2H, t), 5.18 (1H, sext), 6.81 (1H, ddd), 7.14 (1H, ddd), 7.58-7.73 (6H, m), 8.12 (2H, d)
IR (KBr) ν_{max}	3050 (aryl C-H), 2920/2850 (aliphatic C-H), 1705 (C=O), 1610 (C=C), 1470 (CH_2), 1395 (CH_3), 1275 (C-O) cm^{-1}

MS *m/z* 592 (M^+, 20 %), 449, 326 (100 %), 308

HPLC (C18) 100 % (in 90 % acetonitrile + 10 % chloroform)

***1-Methylnonyl 4"-decyloxy-2",3"-difluoroterphenyl-4-carboxylate* (67)**

Quantities used: tetrakis(triphenylphosphine)palladium(0) (0.14 g, 0.12 mmol), compound **37** (1.00 g, 2.40 mmol), compound **10** (0.94 g, 2.64 mmol), potassium phosphate (0.76 g, 3.60 mmol)

Yield = 0.30 g (21 %); mp = 51 °C

^{1}HNMR ($CDCl_3$) δ 0.88 (6H, 2 x t), 1.26-1.65 (30H, m: including a 3H, d at 1.36), 1.72-1.90 (3H, m), 4.09 (2H, t), 5.18 (1H, sext), 6.83 (1H, ddd), 7.16 (1H, ddd), 7.58-7.73 (6H, m), 8.12 (2H, d)

IR (KBr) ν_{max} 3050 (aryl C-H), 2920/2850 (aliphatic C-H), 1705 (C=O), 1610 (C=C), 1470 (CH_2), 1395 (CH_3), 1275 (C-O) cm^{-1}

MS *m/z* 606 (M^+, 25 %), 326 (100 %)

HPLC (C18) 99.3 % (in 80 % acetonitrile + 20 % chloroform)

***1-Ethylpropyl 4"-decyloxy-2",3"-difluoroterphenyl-4-carboxylate* (68)**

Quantities used: tetrakis(triphenylphosphine)palladium(0) (0.14 g, 0.12 mmol), compound **38** (0.80 g, 2.31 mmol), compound **10** (0.90 g, 2.54 mmol), potassium phosphate (0.74 g, 3.47 mmol)

Yield = 0.50 g (40 %); mp = 63 °C

^{1}HNMR ($CDCl_3$) δ 0.89 (3H, t), 0.98 (6H, 2 x t), 1.22-1.53 (14H, m), 1.73 (4H, d/q), 1.86 (2H, quint), 4.09 (2H, t), 5.05 (1H, quint), 6.83 (1H, ddd), 7.15 (1H, ddd), 7.58-7.74 (6H, m), 8.15 (2H, d)

IR (KBr) ν_{max} 3060 (aryl C-H), 2920/2850 (aliphatic C-H), 1710 (C=O), 1605 (C=C), 1470 (CH_2), 1395 (CH_3), 1275 (C-O) cm^{-1}

MS *m/z* 536 (M^+, 15 %), 326 (100 %), 308

HPLC (C18) 99.9 % (in acetonitrile)

***1-Ethylbutyl 4"-decyloxy-2",3"-difluoroterphenyl-4-carboxylate* (69)**

Quantities used: tetrakis(triphenylphosphine)palladium(0) (0.13 g, 0.11 mmol), compound **39** (0.80 g, 2.22 mmol), compound **10** (0.87 g, 2.44 mmol), potassium phosphate (0.71 g, 3.33 mmol)

Yield = 0.30 g (25 %); mp = 42 °C

^{1}HNMR ($CDCl_3$) δ 0.89 (3H, t), 0.98 (6H, 2 x t), 1.22-1.53 (16H, m), 1.57-1.79 (4H, m) 1.85 (2H, quint), 4.09 (2H, t), 5.13 (1H, quint), 6.83 (1H, ddd), 7.15 (1H, ddd), 7.58-7.74 (6H, m), 8.14 (2H, d)

IR (KBr) ν_{max} 3050 (aryl C-H), 2920/2850 (aliphatic C-H), 1710 (C=O), 1605 (C=C), 1470 (CH_2), 1400 (CH_3), 1275 (C-O) cm^{-1}

MS *m/z* 550 (M^+, 10 %), 326 (100 %), 308

HPLC (C18) 98.8 % (in acetonitrile)

***1-Ethylpentyl 4"-decyloxy-2",3"-difluoroterphenyl-4-carboxylate* (70)**

Quantities used: tetrakis(triphenylphosphine)palladium(0) (0.15 g, 0.13 mmol), compound **40** (1.00 g, 2.67 mmol), compound **10** (1.04 g, 2.94 mmol), potassium phosphate (0.85 g, 4.01 mmol)

Yield = 0.40 g (27 %); mp = 38 °C

^{1}HNMR ($CDCl_3$) δ 0.89 (3H, t), 0.97 (6H, 2 x t), 1.26-1.54 (18H, m), 1.63-1.78 (4H, m), 1.85 (2H, quint), 4.09 (2H, t), 5.11 (1H, quint), 6.83 (1H, ddd), 7.14 (1H, ddd), 7.58-7.73 (6H, m), 8.13 (2H, d)

IR (KBr) ν_{max} 3050 (aryl C-H), 2925/2850 (aliphatic C-H), 1715 (C=O), 1610 (C=C), 1470 (CH_2), 1395 (CH_3), 1275 (C-O) cm^{-1}

MS *m/z* 564 (M^+, 30 %), 326 (100 %), 309

HPLC (C18) 100 % (in 90 % acetonitrile + 10 % chloroform)

***1-Ethylhexyl 4"-decyloxy-2",3"-difluoroterphenyl-4-carboxylate* (71)**

Quantities used: tetrakis(triphenylphosphine)palladium(0) (0.15 g, 0.13 mmol), compound **41** (1.00 g, 2.57 mmol), compound **10** (1.00 g, 2.83 mmol), potassium phosphate (0.82 g, 3.86 mmol)

Yield = 0.30 g (21 %); mp = 32 °C

^{1}HNMR ($CDCl_3$)	δ 0.89 (3H, t), 0.98 (6H, 2 x t), 1.24-1.53 (20H, m), 1.61-1.77 (4H, m), 1.85 (2H, quint), 4.09 (2H, t), 5.12 (1H, quint), 6.83 (1H, ddd), 7.14 (1H, ddd), 7.58-7.73 (6H, m), 8.14 (2H, d)
IR (KBr) ν_{max}	3050 (aryl C-H), 2925/2850 (aliphatic C-H), 1705 (C=O), 1610 (C=C), 1465 (CH_2), 1385 (CH_3), 1275 (C-O) cm^{-1}
MS *m/z*	578 (M^+, 15 %), 326 (100 %), 309
HPLC (C18)	98.5 % (in 90 % acetonitrile + 10 % chloroform)

***1-Propylbutyl 4"-decyloxy-2",3"-difluoroterphenyl-4-carboxylate* (72)**

Quantities used: tetrakis(triphenylphosphine)palladium(0) (0.15 g, 0.13 mmol), compound **42** (1.00 g, 2.67 mmol), compound **10** (1.00 g, 2.94 mmol), potassium phosphate (0.85 g, 4.01 mmol)

Yield = 0.50 g (33 %); mp = 55 °C

^{1}HNMR ($CDCl_3$)	δ 0.89 (3H, t), 0.94 (6H, 2 x t), 1.24-1.53 (18H, m), 1.58 -1.78 (4H, m), 1.86 (2H, quint), 4.09 (2H, t), 5.20 (1H, quint), 6.83 (1H, ddd), 7.15 (1H, ddd), 7.58-7.74 (6H, m), 8.14 (2H, d)
IR (KBr) ν_{max}	3050 (aryl C-H), 2920/2850 (aliphatic C-H), 1705 (C=O), 1610 (C=C), 1470 (CH_2), 1400 (CH_3), 1290 (C-O) cm^{-1}
MS *m/z*	564 (M^+, 15 %), 326 (100 %), 309
HPLC (C18)	100 % (in 90 % acetonitrile + 10 % chloroform)

***1-Butylpentyl 4"-decyloxy-2",3"-difluoroterphenyl-4-carboxylate* (73)**

Quantities used: tetrakis(triphenylphosphine)palladium(0) (0.24 g, 0.21 mmol), compound **43** (1.72 g, 4.27 mmol), compound **10** (1.67 g, 4.70 mmol), potassium phosphate (1.36 g, 6.39 mmol)

Yield = 0.85 g (34 %); mp = 45 °C

^{1}HNMR ($CDCl_3$)	δ 0.88 (3H, t), 0.90 (6H, 2 x t), 1.22-1.53 (22H, m), 1.58 -1.78 (4H, m), 1.86 (2H, quint), 4.10 (2H, t), 5.17 (1H, quint), 6.83 (1H, ddd), 7.15 (1H, ddd), 7.58-7.74 (6H, m), 8.14 (2H, d)
IR (KBr) ν_{max}	3050 (aryl C-H), 2925/2855 (aliphatic C-H), 1710 (C=O), 1605 (C=C), 1470 (CH_2), 1380 (CH_3), 1275 (C-O) cm^{-1}
MS *m/z*	592 (M^+, 15 %), 325 (100 %), 309
HPLC (C18)	99.9 % (in 90 % acetonitrile + 10 % chloroform)

3.9.5 Synthetic Scheme 5 and Materials Prepared (74-111)

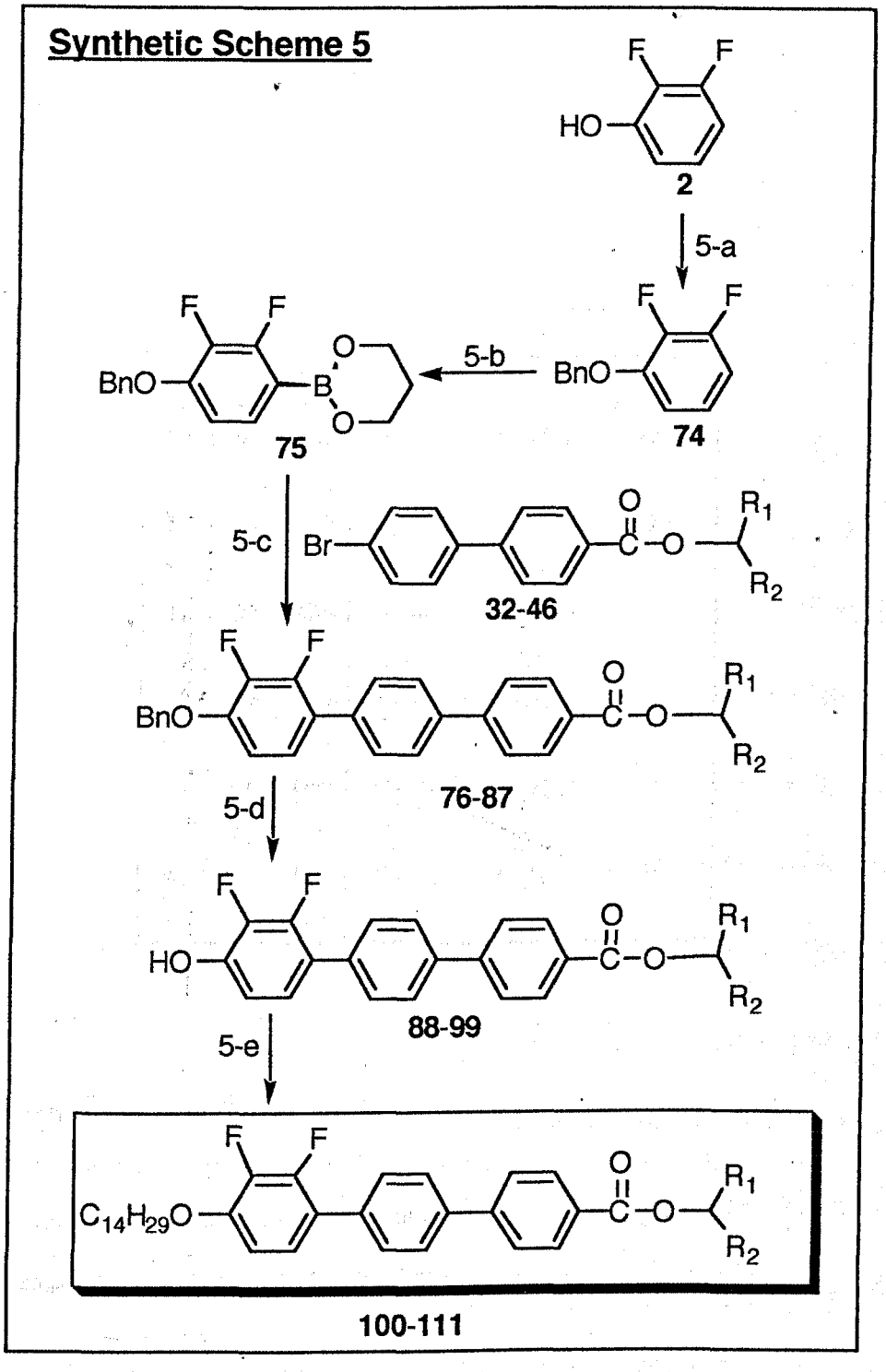

5-a ··· $PhCH_2Cl$, K_2CO_3, butanone

5-b ··· (i) n-BuLi, THF ; (ii) $(MeO)_3B$, THF ; (iii) 10 % HCl

5-c ··· $Pd(PPh_3)_4$, K_3PO_4, DMF

5-d ··· H_2, Pd/C, ethyl acetate

5-e ··· $C_{14}H_{29}Br$, K_2CO_3, butanone

Compounds					
No.	No.	No.	R_1	R_2	Config.
76	**88**	**100**	CH_3	C_5H_{11}	(*S*)-
77	**89**	**101**	CH_3	C_5H_{11}	
78	**90**	**102**	CH_3	C_6H_{13}	(*R*)-
79	**91**	**103**	CH_3	C_6H_{13}	
80	**92**	**104**	CH_3	C_7H_{15}	
81	**93**	**105**	CH_3	C_8H_{17}	
82	**94**	**106**	C_2H_5	C_2H_5	
83	**95**	**107**	C_2H_5	C_3H_7	
84	**96**	**108**	C_2H_5	C_4H_9	
85	**97**	**109**	C_2H_5	C_5H_{11}	
86	**98**	**110**	C_3H_7	C_3H_7	
87	**99**	**111**	C_4H_9	C_4H_9	

1-Benzyloxy-2,3-difluorobenzene **(74)**

This compound was prepared using the same general procedure used for the preparation of compound **3** and the product was distilled.

Quantities used: benzyl chloride (43.0 g, 340 mmol), compound **2** (40.0 g, 310 mmol), potassium carbonate (64.8 g, 470 mmol)

Yield = 39.0 g (57 %); bp 108 °C/0.035 mmHg

^{1}HNMR ($CDCl_3$) δ 5.15 (2H, s), 6.70-6.81 (2H, m), 6.88 -6.99 (1H, m),

	7.29-7.47 (5H, m)
IR (KBr) ν_{max}	3065/3025 (aryl C-H), 2930/2870 (aliphatic C-H), 1610 (C=C), 1500, 1470, 1380, 1250 (C-O) cm^{-1}
MS *m/z*	220 (M^+, 5 %), 101, 91 (100 %)

***2-(4-Benzyloxy-2,3-difluorophenyl)-1,3,2-dioxaborinane* (75)**

This compound was prepared using the same general procedure used for the preparation of compound **9** and was recrystallized (MeOH).

Quantities used: n-butyllithium (73.0 ml, 2.50M in hexane, 183 mmol), compound **74** (35.0 g, 159 mmol), trimethyl borate (33.0 g, 318 mmol), propan-1,3-diol (36.3 g, 477 mmol)

Yield = 26.0 g (54 %); mp = 71 °C

^{1}HNMR ($CDCl_3$)	δ 2.06 (2H, quint), 4.16 (4H, 2 x t), 5.16 (1H, s), 6.20-6.76 (1H, m), 7.25-7.43 (6H, m)
IR (KBr) ν_{max}	3060/3020 (aryl C-H), 2960/2900 (aliphatic C-H), 2360, 1630 (C=C), 1510, 1485, 1460 (CH_2), 1385 (CH_3), 1320/1300/1275, 1210 cm^{-1}
MS *m/z*	304 (M^+, 5 %), 91(100 %)

The following compounds (**76-87**) were prepared using the same general procedure used for the preparation of compound **46** and the solids or liquids were hydrogenolysed without purification.

(S)-*1-Methylhexyl 4"-benzyloxy-2",3"-difluoroterphenyl-4-carboxylate* (76)

Quantities used: tetrakis(triphenylphosphine)palladium(0) (0.20 g, 0.17 mmol), compound **32** (1.25 g, 3.33 mmol), compound **75** (1.11 g, 3.66 mmol), potassium phosphate (1.06 g, 5.00 mmol)

Yield = 0.95 g (56 %)

1-Methylhexyl 4"-benzyloxy-2",3"-difluoroterphenyl-4-carboxylate **(77)**

Quantities used: tetrakis(triphenylphosphine)palladium(0) (0.14 g, 0.12 mmol), compound **33** (0.87 g, 2.32 mmol), compound **75** (0.78 g, 2.55 mmol), potassium phosphate (0.74 g, 3.48 mmol)

Yield = 0.86 g (72 %)

(R)-*1-Methylheptyl 4"-benzyloxy-2",3"-difluoroterphenyl-4-carboxylate* **(78)**

Quantities used: tetrakis(triphenylphosphine)palladium(0) (0.14 g, 0.12 mmol), compound **34** (0.95 g, 2.44 mmol), compound **75** (0.81 g, 2.68 mmol), potassium phosphate (0.78 g, 3.66 mmol)

Yield = 0.55 g (43 %)

1-Methylheptyl 4"-benzyloxy-2",3"-difluoroterphenyl-4-carboxylate **(79)**

Quantities used: tetrakis(triphenylphosphine)palladium(0) (0.33 g, 0.28 mmol), compound **35** (2.19 g, 5.60 mmol), compound **75** (1.87 g, 6.15 mmol), potassium phosphate (1.79 g, 8.40 mmol)

Yield = 1.30 g (43 %)

1-Methyloctyl 4"-benzyloxy-2",3"-difluoroterphenyl-4-carboxylate **(80)**

Quantities used: tetrakis(triphenylphosphine)palladium(0) (0.15 g, 0.13 mmol), compound **36** (1.05 g, 2.61 mmol), compound **75** (0.87 g, 2.87 mmol), potassium phosphate (0.83 g, 3.92 mmol)

Yield = 0.90 g (64 %)

***1-Methylnonyl 4"-benzyloxy-2",3"-difluoroterphenyl-4-carboxylate* (81)**

Quantities used: tetrakis(triphenylphosphine)palladium(0) (0.20 g, 0.17 mmol), compound **37** (1.40 g, 3.36 mmol), compound **75** (1.12 g, 3.70 mmol), potassium phosphate (1.07 g, 5.04 mmol)

Yield = 1.00 g (53 %)

***1-Ethylpropyl 4"-benzyloxy-2",3"-difluoroterphenyl-4-carboxylate* (82)**

Quantities used: tetrakis(triphenylphosphine)palladium(0) (0.16 g, 0.14 mmol), compound **38** (1.00 g, 2.88 mmol), compound **75** (0.96 g, 3.17 mmol), potassium phosphate (0.92 g, 4.32 mmol)

Yield = 0.90 g (64 %)

***1-Ethylbutyl 4"-benzyloxy-2",3"-difluoroterphenyl-4-carboxylate* (83)**

Quantities used: tetrakis(triphenylphosphine)palladium(0) (0.14 g, 0.12 mmol), compound **39** (0.88 g, 2.44 mmol), compound **75** (0.81 g, 2.68 mmol), potassium phosphate (0.78 g, 3.66 mmol)

Yield = 0.85 g (70 %)

***1-Ethylpentyl 4"-benzyloxy-2",3"-difluoroterphenyl-4-carboxylate* (84)**

Quantities used: tetrakis(triphenylphosphine)palladium(0) (0.12 g, 0.10 mmol), compound **40** (0.75 g, 2.00 mmol), compound **75** (0.67 g, 2.20 mmol), potassium phosphate (0.64 g, 3.00 mmol)

Yield = 0.60 g (58 %)

1-Ethylhexyl 4"-benzyloxy-2",3"-difluoroterphenyl-4-carboxylate (**85**)

Quantities used: tetrakis(triphenylphosphine)palladium(0) (0.15 g, 0.13 mmol), compound **41** (1.00 g, 2.57 mmol), compound **75** (0.86 g, 2.83 mmol), potassium phosphate (0.82 g, 3.86 mmol)

Yield = 0.70 g (51 %)

1-Propylbutyl 4"-benzyloxy-2",3"-difluoroterphenyl-4-carboxylate (**86**)

Quantities used: tetrakis(triphenylphosphine)palladium(0) (0.14 g, 0.12 mmol), compound **42** (0.92 g, 2.45 mmol), compound **75** (0.82 g, 2.70 mmol), potassium phosphate (0.78 g, 3.68 mmol)

Yield = 0.60 g (48 %)

1-Butylpentyl 4"-benzyloxy-2",3"-difluoroterphenyl-4-carboxylate (**87**)

Quantities used: tetrakis(triphenylphosphine)palladium(0) (0.14 g, 0.12 mmol), compound **43** (0.98 g, 2.43 mmol), compound **75** (0.81 g, 2.67 mmol), potassium phosphate (0.77 g, 3.65 mmol)

Yield = 0.70 g (53 %)

Compounds **76-87** were hydrogenolysed over 10% Pd/C in ethyl acetate and the reactions were monitored by GLC to obtain the compounds **88-99** which were then alkylated to give compounds **100-111.**

The following compounds (**100-111**) were prepared using the same general procedure used for the preparation of compound **3.**

(S)-(+)-*1-Methylhexyl 2",3"-difluoro-4"-tetradecyloxyterphenyl-4-carboxylate* (**100**)

Quantities used : 1-bromotetradecane (0.57 g, 2.04 mmol), compound **88** (0.78 g, 1.85 mmol), potassium carbonate (0.38 g, 2.78 mmol)

Yield = 0.20 g (18 %); mp = 69 °C

^{1}HNMR ($CDCl_3$)	δ 0.89 (6H, 2 x t), 1.23-1.68 (32H, m: including a 3H, d at 1.37), 1.69-1.92 (3H, m), 4.09 (2H, t), 5.18 (1H, sext), 6.83 (1H, ddd), 7.14 (1H, ddd), 7.58-7.74 (6H, m), 8.13 (2H, d)
IR (KBr) ν_{max}	3050 (aryl C-H), 2920/2850 (aliphatic C-H), 1720 (C=O), 1610 (C=C), 1470 (CH_2), 1395 (CH_3), 1290 (C-O) cm^{-1}
MS *m/z*	620 (M^+, 20 %), 326 (100 %)
$[\alpha]_D^{22°C}$	+18.8°
HPLC (C18)	95.5 % (in 90 % acetonitrile + 10 % chloroform)

1-Methylhexyl 2",3"-difluoro-4"-tetradecyloxyterphenyl-4-carboxylate (**101**)

Quantities used: 1-bromotetradecane (0.51 g, 1.84 mmol), compound **89** (0.71 g, 1.67 mmol), potassium carbonate (0.35 g, 2.51 mmol)

Yield = 0.50 g (48 %); mp = 52 °C

^{1}HNMR ($CDCl_3$)	δ 0.88 (6H, 2 x t), 1.22-1.69 (32H, m: including a 3H, d at 1.37), 1.69-1.92 (3H, m), 4.09 (2H, t), 5.18 (1H, sext), 6.83 (1H, ddd), 7.15 (1H, ddd), 7.58-7.73 (6H, m), 8.13 (2H, d)
IR (KBr) ν_{max}	3050 (aryl C-H), 2920/2850 (aliphatic C-H), 1710 (C=O), 1605 (C=C), 1470 (CH_2), 1395 (CH_3), 1290 (C-O) cm^{-1}
MS *m/z*	620 (M^+, 45 %), 506, 425, 326 (100 %)
HPLC (C18)	100 % (in 90 % acetonitrile + 10 % chloroform)

(R)-(-)-*1-Methylheptyl 2",3"-difluoro-4"-tetradecyloxyterphenyl-4-carboxylate* (102)

Quantities used: 1-bromotetradecane (0.32 g, 1.14 mmol), compound **90** (0.46 g, 1.04 mmol), potassium carbonate (0.22 g, 1.56 mmol)

Yield = 0.15 g (23 %); mp = 65 °C

^{1}HNMR ($CDCl_3$)	δ 0.88 (6H, 2 x t), 1.22-1.69 (34H, m: including a 3H, d at 1.38), 1.69-1.92 (3H, m), 4.09 (2H, t), 5.18 (1H, sext), 6.83 (1H, ddd), 7.15 (1H, ddd), 7.58-7.74 (6H, m), 8.13 (2H, d)
IR (KBr) ν_{max}	3050 (aryl C-H), 2920/2850 (aliphatic C-H), 1720 (C=O), 1605 (C=C), 1470 (CH_2), 1395 (CH_3), 1290 (C-O) cm^{-1}
MS *m/z*	634 (M^+, 20 %), 505, 326 (100 %), 309
$[\alpha]_D^{22°C}$	-19.9°
HPLC (C18)	99.5 % (in 80 % acetonitrile + 20 % chloroform)

***1-Methylheptyl 2",3"-difluoro-4"-tetradecyloxyterphenyl-4-carboxylate* (103)**

Quantities used: 1-bromotetradecane (0.75 g, 2.71 mmol), compound **91** (1.08 g, 2.46 mmol), potassium carbonate (0.51 g, 3.69 mmol)

Yield = 0.25 g (16 %); mp = 57 °C

^{1}HNMR ($CDCl_3$)	δ 0.88 (6H, 2 x t), 1.24-1.68 (34H, m: including a 3H, d at 1.36), 1.70-1.90 (3H, m), 4.09 (2H, t), 5.18 (1H, sext), 6.83 (1H, ddd), 7.15 (1H, ddd), 7.58-7.73 (6H, m), 8.13 (2H, d)
IR (KBr) ν_{max}	3050 (aryl C-H), 2920/2850 (aliphatic C-H), 1710 (C=O), 1605 (C=C), 1470 (CH_2), 1395 (CH_3), 1290 (C-O) cm^{-1}
MS *m/z*	634 (M^+, 20 %), 326 (100 %), 308
HPLC (C18)	100 % (in 80 % acetonitrile + 20 % chloroform)

***1-Methyloctyl 2",3"-difluoro-4"-tetradecyloxyterphenyl-4-carboxylate* (104)**

Quantities used: 1-bromotetradecane (0.51 g, 1.83 mmol), compound **92** (0.75 g, 1.66 mmol), potassium carbonate (0.34 g, 2.49 mmol)

Yield = 0.35 g (32 %); mp = 53 °C

^{1}HNMR ($CDCl_3$)	δ 0.88 (6H, 2 x t), 1.23-1.65 (36H, m: including a 3H, d at 1.36), 1.70-1.90 (3H, m), 4.09 (2H, t), 5.18 (1H, sext), 6.83 (1H, ddd), 7.15 (1H, ddd), 7.58-7.73 (6H, m), 8.12 (2H, d)
IR (KBr) ν_{max}	3050 (aryl C-H), 2920/2850 (aliphatic C-H), 1720 (C=O), 1605 (C=C), 1470 (CH_2), 1395 (CH_3), 1290 (C-O) cm^{-1}
MS *m/z*	648 (M^+, 20 %), 326 (100 %)
HPLC (C18)	100 % (in 80 % acetonitrile + 20 % chloroform)

***1-Methylnonyl 2",3"-difluoro-4"-tetradecyloxyterphenyl-4-carboxylate* (105)**

Quantities used: 1-bromotetradecane (0.55 g, 1.98 mmol), compound **93** (0.84 g, 1.80 mmol), potassium carbonate (0.37 g, 2.70 mmol)

Yield = 0.39 g (33 %); mp = 54 °C

^{1}HNMR ($CDCl_3$)	δ 0.88 (6H, 2 x t), 1.24-1.63 (38H, m: including a 3H, d at 1.36), 1.70-1.90 (3H, m), 4.09 (2H, t), 5.18 (1H, sext), 6.82 (1H, ddd), 7.14 (1H, ddd), 7.58-7.72 (6H, m), 8.12 (2H, d)
IR (KBr) ν_{max}	3050 (aryl C-H), 2920/2850 (aliphatic C-H), 1720 (C=O), 1605 (C=C), 1470 (CH_2), 1395 (CH_3), 1290 (C-O) cm^{-1}
MS *m/z*	662 (M^+, 20%), 326 (100 %)
HPLC (C18)	99.3 % (in 80 % acetonitrile + 20 % chloroform)

***1-Ethylpropyl 2",3"-difluoro-4"-tetradecyloxyterphenyl-4-carboxylate* (106)**

Quantities used: 1-bromotetradecane (0.57 g, 2.04 mmol), compound **94** (0.73 g, 1.85 mmol), potassium carbonate (0.38 g, 2.78 mmol)

Yield = 0.20 g (18 %); mp = 41 °C

^{1}HNMR ($CDCl_3$)	δ 0.88 (3H, t), 0.98 (6H, 2 x t), 1.23-1.52 (22H, m), 1.74 (4H, d/q), 1.85 (2H, quint), 4.09 (2H, t), 5.05 (1H, quint), 6.83 (1H, ddd), 7.15 (1H, ddd), 7.58-7.74 (6H, m), 8.14 (2H, d)
IR (KBr) ν_{max}	3040 (aryl C-H), 2920/2850 (aliphatic C-H), 1710 (C=O), 1605 (C=C), 1465 (CH_2), 1395 (CH_3), 1270 (C-O) cm^{-1}
MS *m/z*	592 (M^+, trace), 397, 326, 43 (100 %)
HPLC (C18)	100 % (in 80 % acetonitrile + 20 % chloroform)

***1-Ethylbutyl 2",3"-difluoro-4"-tetradecyloxyterphenyl-4-carboxylate* (107)**

Quantities used: 1-bromotetradecane (0.52 g, 1.87 mmol), compound **95** (0.70 g, 1.70 mmol), potassium carbonate (0.35 g, 2.55 mmol)

Yield = 0.30 g (29 %); mp = 57 °C

^{1}HNMR ($CDCl_3$)	δ 0.89 (3H, t), 0.98 (6H, 2 x t), 1.22-1.53 (24H, m), 1.58 -1.79 (4H, m), 1.86 (2H, quint), 4.09 (2H, t), 5.13 (1H, quint), 6.83 (1H, ddd), 7.14 (1H, ddd), 7.58-7.74 (6H, m), 8.14 (2H, d)
IR (KBr) ν_{max}	3050 (aryl C-H), 2920/2850 (aliphatic C-H), 1720 (C=O), 1610 (C=C), 1470 (CH_2), 1395 (CH_3), 1275 (C-O) cm^{-1}
MS *m/z*	606 (M^+, 45 %), 506, 425, 326 (100 %)
HPLC (C18)	99.5 % (in 80 % acetonitrile + 20 % chloroform)

***1-Ethylpentyl 2",3"-difluoro-4"-tetradecyloxyterphenyl-4-carboxylate* (108)**

Quantities used: 1-bromotetradecane (0.36 g, 1.29 mmol), compound **96** (0.50 g, 1.17 mmol), potassium carbonate (0.24 g, 1.76 mmol)

Yield = 0.40 g (55 %); mp = 46 °C

^{1}HNMR ($CDCl_3$)	δ 0.89 (3H, t), 0.97 (6H, 2 x t), 1.24-1.58 (26H, m), 1.71 (4H, d/t), 1.85 (2H, quint), 4.09 (2H, t), 5.11 (1H, quint), 6.83 (1H, ddd), 7.14 (1H, ddd), 7.58-7.73 (6H, m), 8.14 (2H, d)
IR (KBr) ν_{max}	3050 (aryl C-H), 2920/2850 (aliphatic C-H), 1720 (C=O), 1610 (C=C), 1470 (CH_2), 1385 (CH_3), 1275 (C-O) cm^{-1}
MS *m/z*	620 (M^+, 10 %), 505, 326 (100 %)
HPLC (C18)	99.3 % (in 80 % acetonitrile + 20 % chloroform)

***1-Ethylhexyl 2",3"-difluoro-4"-tetradecyloxyterphenyl-4-carboxylate* (109)**

Quantities used: 1-bromotetradecane (0.40 g, 1.46 mmol), compound **97** (0.58 g, 1.33 mmol), potassium carbonate (0.28 g, 2.00 mmol)

Yield = 0.30 g (36 %); mp = 42 °C

^{1}HNMR ($CDCl_3$)	δ 0.89 (3H, t), 0.98 (6H, 2 x t), 1.20-1.53 (28H, m), 1.73 (4H, d/t), 1.85 (2H, quint), 4.10 (2H, t), 5.10 (1H, quint), 6.83 (1H, ddd), 7.15 (1H, ddd), 7.58-7.73 (6H, m), 8.15 (2H, d)
IR (KBr) ν_{max}	3050 (aryl C-H), 2920/2850 (aliphatic C-H), 1720 (C=O), 1610 (C=C), 1470 (CH_2), 1395 (CH_3), 1275 (C-O) cm^{-1}
MS *m/z*	634 (M^+, 45 %), 506, 326 (100 %)
HPLC (C18)	100 % (in 80 % acetonitrile + 20 % chloroform)

***1-Propylbutyl 2",3"-difluoro-4"-tetradecyloxyterphenyl-4-carboxylate* (110)**

Quantities used: 1-bromotetradecane (0.36 g, 1.29 mmol), compound **98** (0.50 g, 1.17 mmol), potassium carbonate (0.24 g, 1.76 mmol)

Yield = 0.35 g (48 %); mp = 55 °C

^{1}HNMR ($CDCl_3$)	δ 0.89 (3H, t), 0.95 (6H, 2 x t), 1.23-1.54 (26H, m), 1.58 -1.79 (4H, m), 1.86 (2H, quint), 4.09 (2H, t), 5.20 (1H, quint), 6.83 (1H, ddd), 7.15 (1H, ddd), 7.58-7.74 (6H, m), 8.13 (2H, d)
IR (KBr) ν_{max}	3040 (aryl C-H), 2920/2850 (aliphatic C-H), 1710 (C=O), 1610 (C=C), 1465 (CH_2), 1350 (CH_3), 1270 (C-O) cm^{-1}
MS *m/z*	620 (M^+, 25 %), 505, 424, 326 (100 %)
HPLC (C18)	99.8 % (in 90 % acetonitrile + 10 % chloroform)

***1-Butylpentyl 2",3"-difluoro-4"-tetradecyloxyterphenyl-4-carboxylate* (111)**

Quantities used: 1-bromotetradecane (0.39 g, 1.42 mmol), compound **99** (0.58 g, 1.29 mmol), potassium carbonate (0.27 g, 1.94 mmol)

Yield = 0.25 g (30 %); mp = 39 °C

^{1}HNMR ($CDCl_3$)	δ 0.88 (3H, t), 0.90 (6H, t), 1.20-1.53 (30H, m), 1.69 (4H, d/t), 1.85 (2H, quint), 4.09 (2H, t), 5.17 (1H, quint), 6.83 (1H, ddd), 7.15 (1H, ddd), 7.58-7.75 (6H, m), 8.14 (2H, d)
IR (KBr) ν_{max}	3050 (aryl C-H), 2925/2850 (aliphatic C-H), 1710 (C=O), 1605 (C=C), 1470 (CH_2), 1380 (CH_3), 1275 (C-O) cm^{-1}
MS *m/z*	648 (M^+, 35 %), 506, 326 (100 %)
HPLC (C18)	99.4 % (in 80 % acetonitrile + 20 % chloroform)

3.10 References

1. " *CRC Handbook of Physics and Chemistry* ", ed R. C. Weast, 68th Ed. CRC Press, 1988.
2. H. Diamant, K. Drenck and R. Pepinsky, *Rev. Sci. Instr., 1957*, **28**, 30.
3. K. Yoshino, T. Uemoto and Y. Inuishi, *Jpn. J. Appl. Phys.*, 1977, **16**, 571.
4. J. Hoffmann, W. Kuczynski and J. Malecki, *Mol. Cryst. & Liq. Cryst.*, 1978, **44**, 287.
5. H. Matsumura, *Mol. Cryst. Liq. Cryst.*, 1978, **49**, 105.
6. W. Kuczynski and H. Stegemeyer, *Chem. Phys. Lett.*, 1980, **70**, 123.
7. T. Uemoto, K. Yoshino and Y. Inuishi, *Mol. Cryst. Liq. Cryst.*, 1981, **67**, 137.
8. M. Imasaki, T. Fujimoto, T. Nishihara, T. Yoshioka and Y. Narushige, *Jpn. J. Appl. Phys.*, 1982, **21**, 1100.
9. T. Uemoto, K. Yoshino and Y. Inuishi, *Jpn. J. Appl. Phys.*, 1979, **18**, 126.
10. Ph. Martinot-Lagarde, *J. de Phys.*, 1979, **18**, 1261
11. K. Miyasto, S. Abe, H. Takezoe, A. Fukuda and E. Kuze, *Jpn. J. Appl. Phys.*, 1983, **22**, L661.
12. S. L. Mayo, B. D. Olafson and W. A. Goddard, *J. Phys. Chem., 1990*, **94**, 8897.
13. P. V. Ramachandran, A. V. Teodorovic and H. C. Brown, *Tetrahedron*, 1993, **49**, No. 9, 1725

4 Results and Discussions

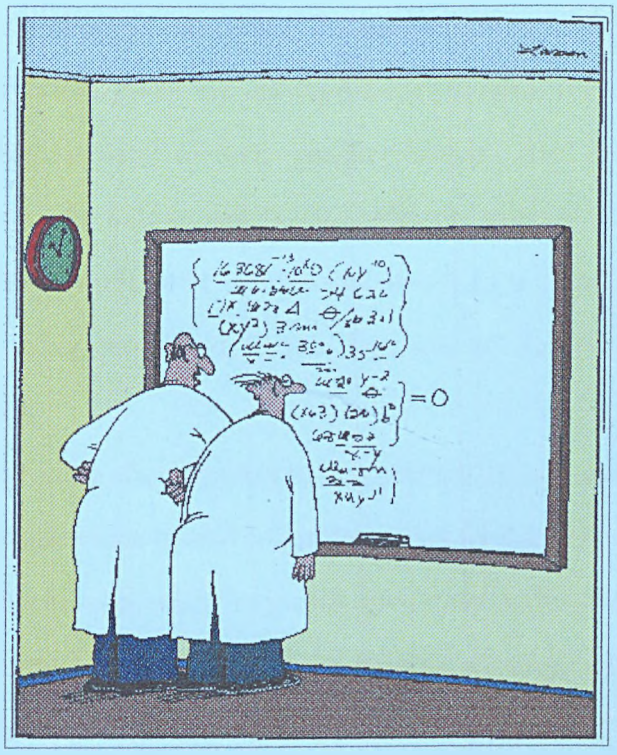

"No doubt about it, Ellington-we've mathematically expressed the purpose of the universe. God, how I love the thrill of scientific discovery"

4 Results and Discussions

4.1 Synthetic and Mechanistic Studies

4.1.1 Scheme 1

The boronic acid (compound **1**) can be easily prepared in excellent yield (> 95%) *via* lithiation *ortho* to an arylfluoro substituent, followed by treatment with trimethyl borate and hydrolysis of the borate ester with 10 % hydrochloric acid. The boronic acid is converted to a phenol (compound **2**) on oxidation with hydrogen peroxide and subsequent alkylation gives the alkoxydifluoro system (compounds **3**-**5**). A second lithiation can be used to form another boronic acid (compounds **6**-**8**). Lithiation is carried out below -60 °C in order to prevent the formation of fluorobenzynes. The boronic acid can be converted to a dioxaborinane system (compounds **9**-**11**) using propane-1,3-diol. The use of dioxaborinanes has the following advantages;

a) A boronic acid product often appears as a mixture of anhydrides and acid whereas the dioxaborinane is easy to purify to give a single product.

b) The spectra of the boronic acids frequently give little evidence confirming the boronic acid structure. Dioxaborinanes are capable of being fully characterisable and thus give clean spectra.

c) Exact quantities of dioxaborinane can be employed in further reactions, which is not the case for a boronic acid whose purity is variable.

4.1.2 Scheme 2 (Mitsunobu reaction)

Phenolic ethers were prepared by the reaction of alcohols with DEAD and PPh_3. The mechanism includes three steps[1] as shown in Fig. 4.1.1; (a) reaction of PPh_3 to form a salt wherein a phosphorus-nitrogen bond is formed. (b) reaction of the DEAD-

PPh_3 adduct with an alcohol to form an activated oxyphosphonium intermediate. (c) displacement *via* an SN_2 process to form the ether and triphenyl phosphine oxide. In the case of an optically active alcohol the reaction proceeds with inversion of configuration.

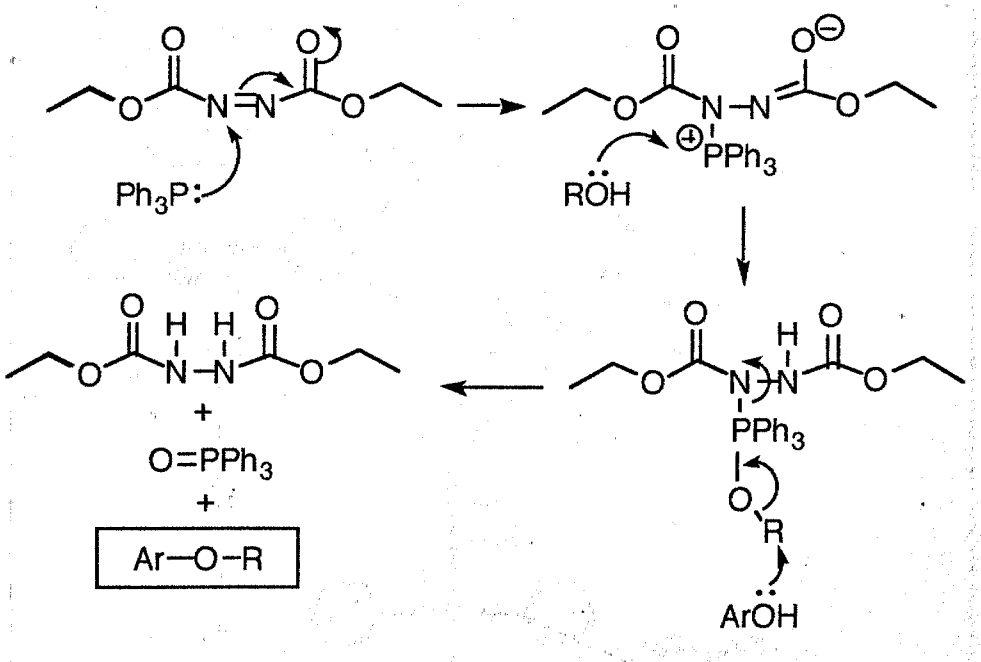

Fig. 4.1.1 The mechanism for the etherification of arylphenols

4.1.3 Scheme 3 (DCC reaction)

Esterification based on a requirement for both DCC and a catalytic quantity of aminopyridine allows the conversion of a carboxylic acid into an ester at room temperature and under essentially neutral conditions. There have been several mechanisms proposed[2], and most experimental evidence supports the process[3] shown in Fig. 4.1.2.

In this research, bromo-biphenyl-carboxylates were prepared from one equivalent of DCC, one equivalent of 4-bromo-biphenyl-carboxylic acid, the appropriate alcohol,

and 5 mol% of DMAP. The reaction proceeds at room temperature. The side product, DCU is easily removed by filtration. The yield of the isolated ester is reasonably high.

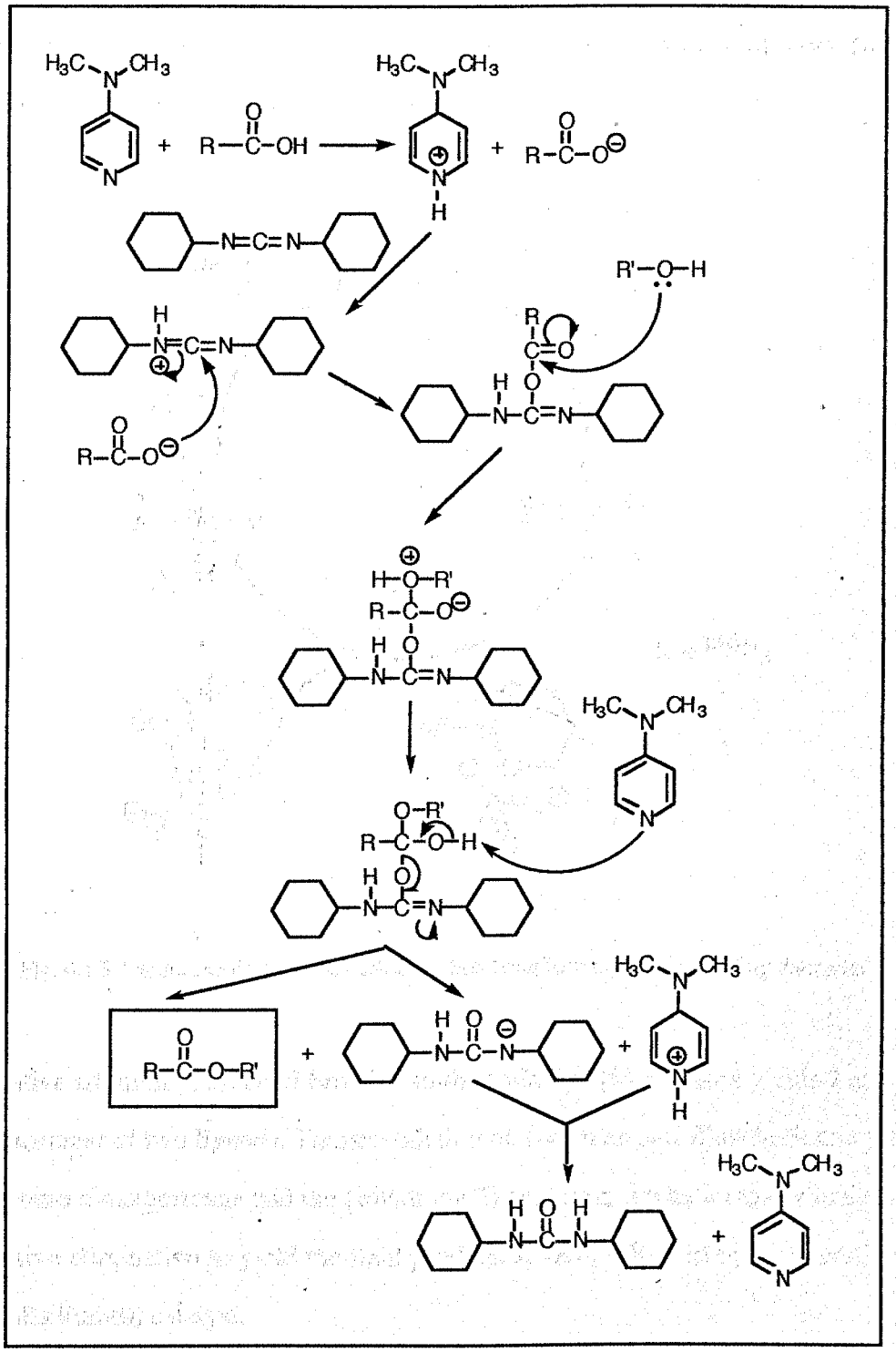

Fig. 4.1.2 The mechanism for the esterification of carboxylic acids

4.1.4 Schemes 2-5 (Coupling reaction)

Terphenyl systems (compounds **20-27, 46-60, 61-73, 100-111**) were prepared by the palladium catalysed cross coupling reaction of a dioxaborinane with an aryl bromide. A catalytic cyclic mechanism was proposed[4], and a process for the anhydrous coupling procedure is shown in Fig. 4.1.3.

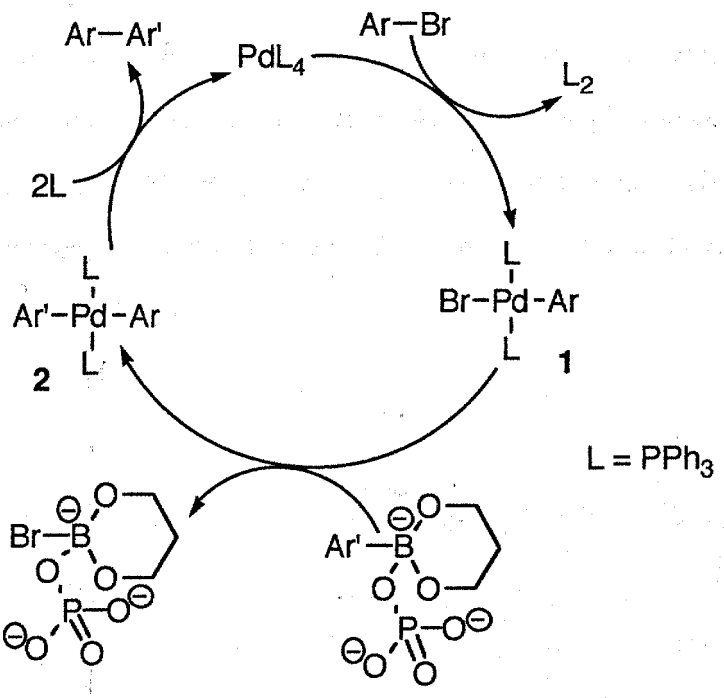

Fig. 4.1.3 The mechanism for the carbon-carbon bond forming cross-coupling reactions

Oxidative addition of an alkyl bromide to the palladium(0) complex yields **1** and the displacement of two ligands. Transmetalation of **1** with an aryl dioxaborinane yields the bromo dioxaborinane and the palladium(II) complex, **2** which rapidly undergoes reductive elimination to yield the final product, Ar-Ar', followed by regeneration of the palladium(0) catalyst.

The original procedure, using $Pd(PPh_3)_4$ and aqueous Na_2CO_3 in DME was found to be effective for aryl bromides which contain the ether linking group (compounds **12-19**). In the case of aryl bromides having an ester linkage (compounds **30-44**), K_3PO_4 in dry DMF as the base was employed to prevent hydrolysis of the ester[5].

The reaction between a sterically hindered aryl dioxaborinane such as 2-(2,3-difluoro-4-tetradecyloxyphenyl)-1,3,2-dioxaborinane and an aryl bromide gave either a very poor yield or no reaction at all. Therefore a different synthetic route was required (see scheme **5**). 1-Benzyloxy-2,3-difluorobenzene (compound **74**) was coupled with bromobiphenyl (compounds **32-46**). The benzyl protecting group was removed easily under mild catalytic hydrogenolysis conditions to give compounds **88-99** before being reacted with tetradecanyl bromide to obtain the final terphenyl system (compounds **100-111**).

4.2 MHPOBC study

The compounds, chiral (*R*)- and racemic MHPOBC were chosen and synthesized as reference materials to aid in this research.

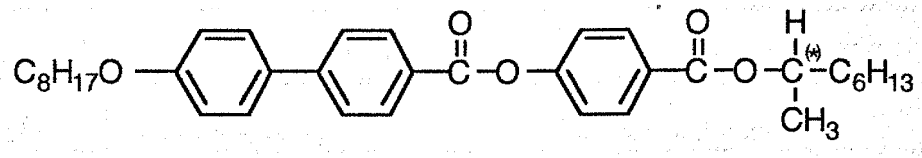

These compounds have been the focus of many experimental studies[6-11]. However, there is a need to investigate some of their properties which have not yet been clarified, for example comparisons of textures between chiral compound and racemate and temperature/field dependences of the spontaneous polarization.

4.2.1 Transition Temperatures and Defect Texture Studies

(*R*)- and racemic MHPOBC were investigated by thermal optical polarising microscopy on cooling from the isotropic liquid and the transition temperatures for the two materials were found to exhibit the following phase sequences;

Isomer	MHPOBC
(*R*)	I 149.1 °C SmA* 120.9 SmC_α* 119.3 SmC* 118.9 SmC_γ* 118.6 SmC_A* 66 SmI*
(±)	I 150.0 °C SmA - - 121.3 SmC - - 110.3 SmC_A 65.6 SmI

The chiral compound was apparently found to exhibit six mesophases whereas racemic compound did not show either the achiral analogues of the SmC_α and SmC_γ phases.

Understanding the role of optical purity in the formation of defect textures for various smectic phases is of particular interest, because the optically active isomer of MHPOBC appears to exhibit a different mesophase morphology to the racemate. The texture characteristics of these two isomers were compared in the Table 4.2.1.

	(*R*)-MHPOBC	(±)-MHPOBC
SmA(*)	usual focal conic	usual focal conic
SmC_{α}(*)	edges of the focal conic domains are coloured, weak bands across the focal conic fans	not detected
SmC(*)	banded focal conic defect texture	broken focal conic texture, 4-brushes singularities in a *schlieren* texture
SmC_{γ}(*)	increased band separation in the focal conic fan, highly mobile *schlieren*	not detected
SmC_{A}(*)	• in the higher temperature region ; broken focal conic domains, disappearance of the *schlieren* texture, similar to SmA phase • in the low temperature region ; banded focal conic texture, iridescent marbled *schlieren*	banded focal conic texture, marbled *schlieren* texture which is totally different from the SmC *schlieren*
SmI(*)	banded focal conic defects, non-iridescent *schlieren*	remained banded focal conic, marbled but streaky *schlieren*

Table 4.2.1 The textures of (*R*)- and (±)- MHPOBC

Plate 1 The SmA* phase of (*R*)-MHPOBC at 145 °C

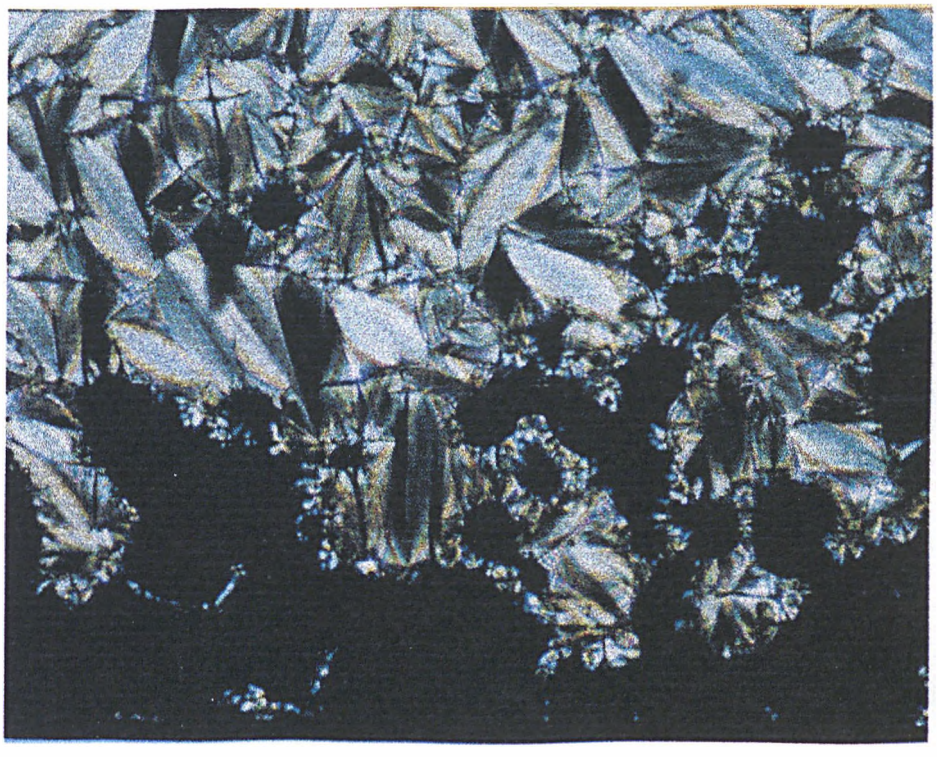

Plate 2 The SmC_{α}* phase of (*R*)-MHPOBC at 120 °C

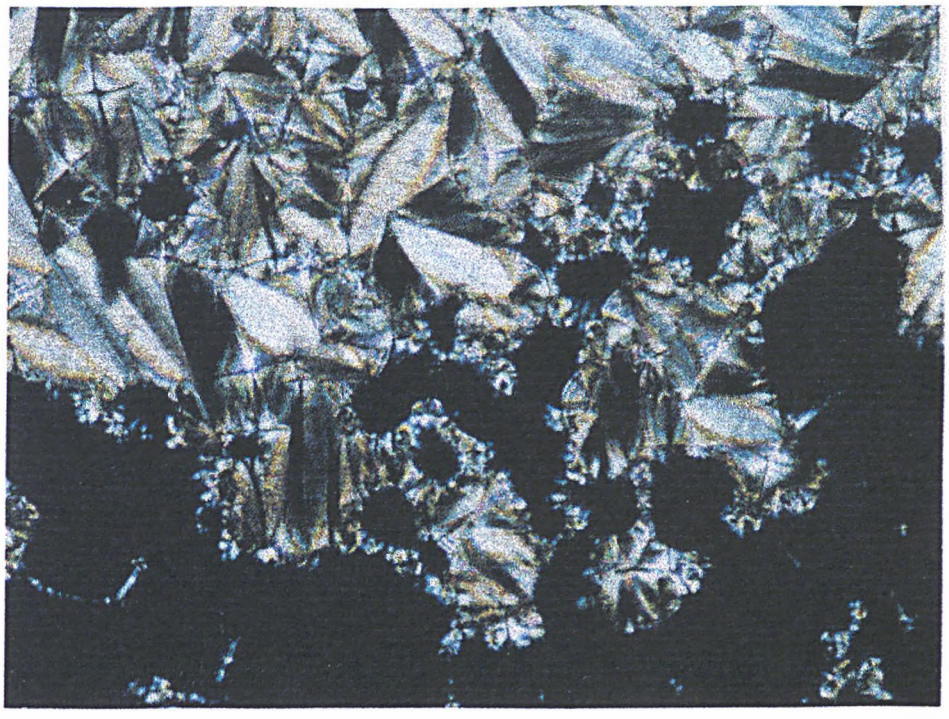

Plate 3 The SmC* phase of (*R*)-MHPOBC at 119 °C

Plate 4 The SmC_γ* phase of (*R*)-MHPOBC at 118.9 °C

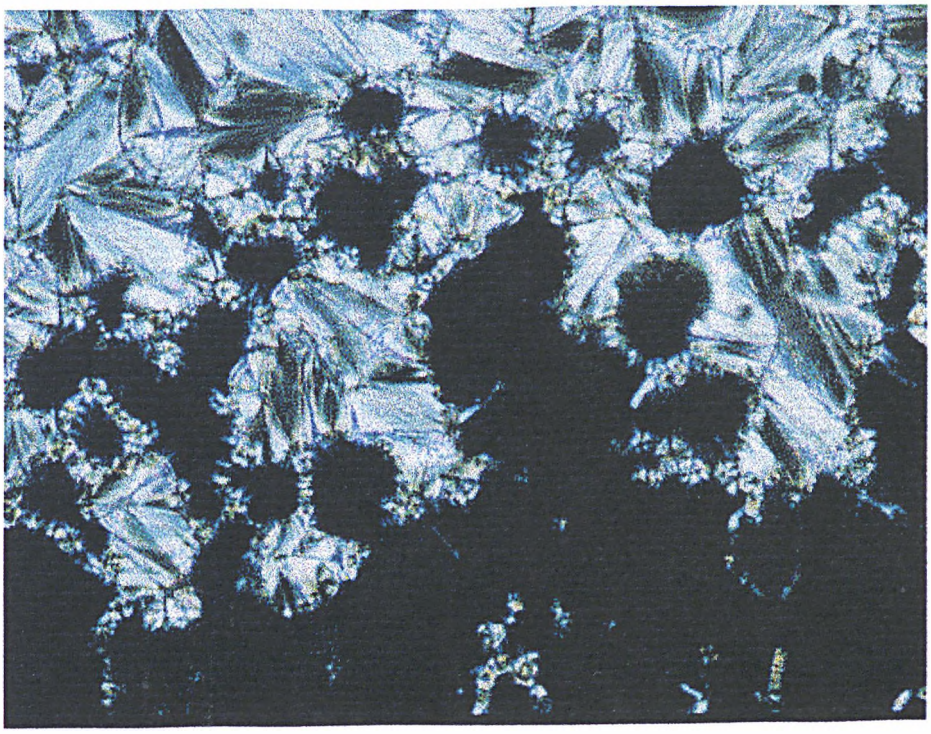

Plate 5 The SmC_A^* phase of (*R*)-MHPOBC at 118 °C

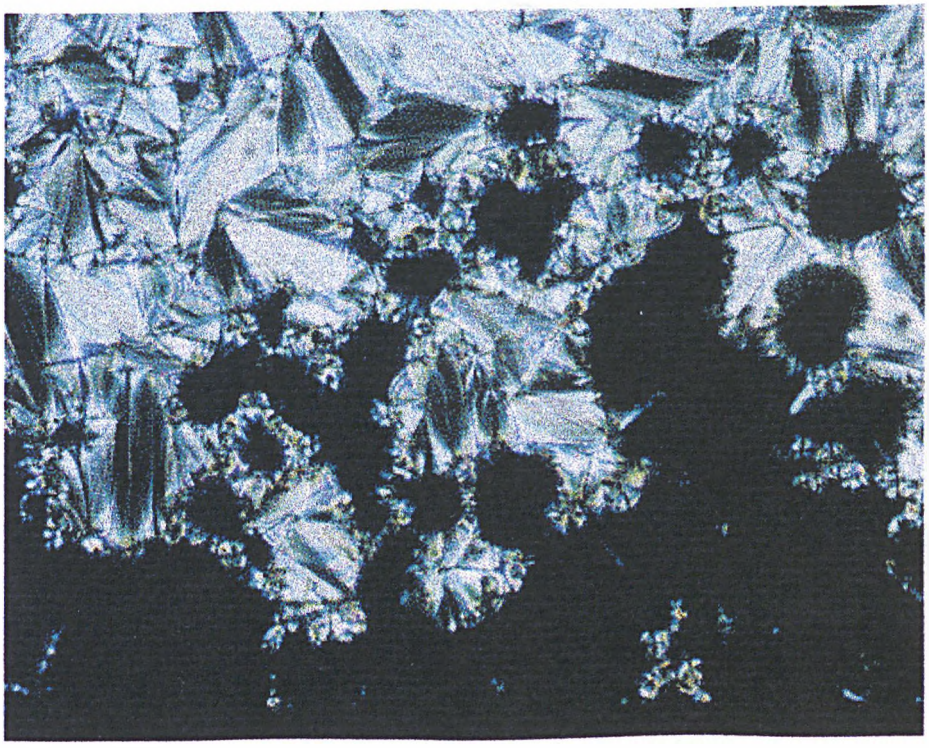

Plate 6 The SmC_A^* phase of (*R*)-MHPOBC at 100 °C

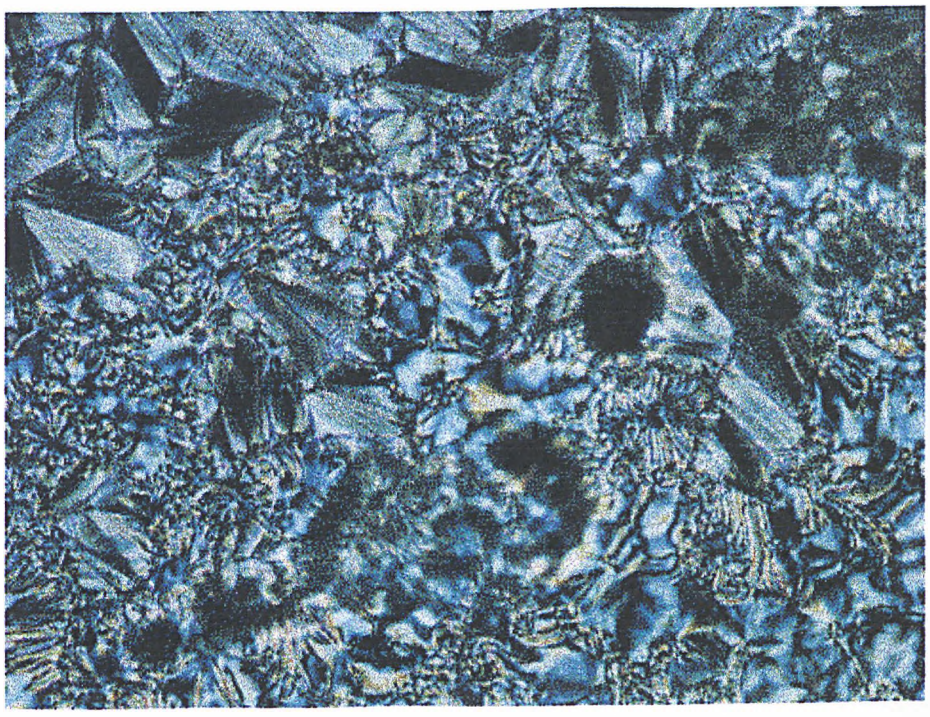

Plate 7 The SmC_A* phase of (*R*)-MHPOBC at 75 °C

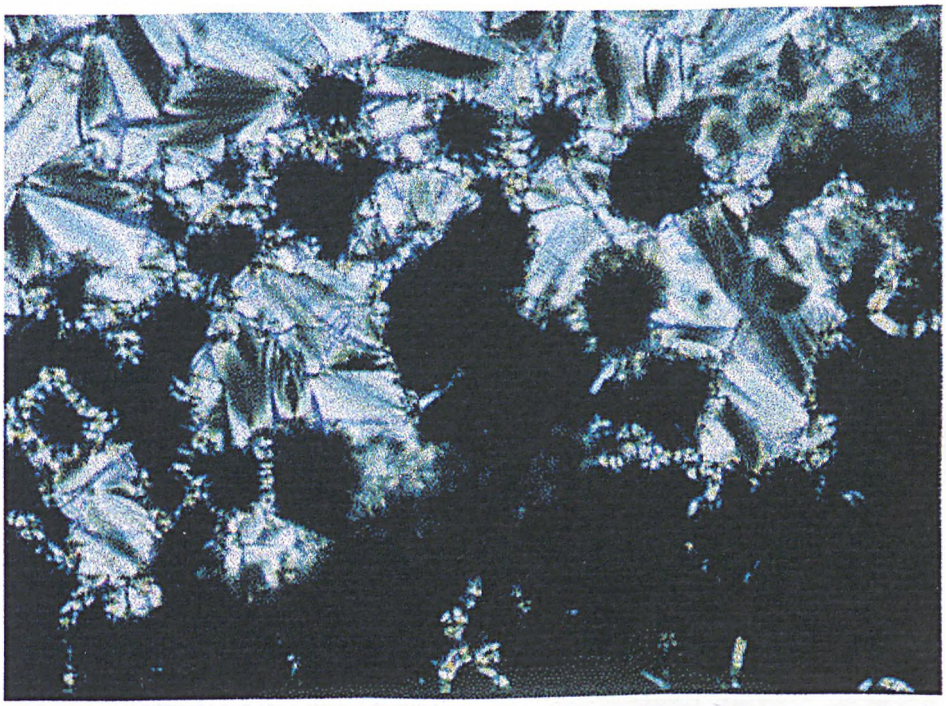

Plate 8 The SmI* phase of (*R*)-MHPOBC at 55 °C

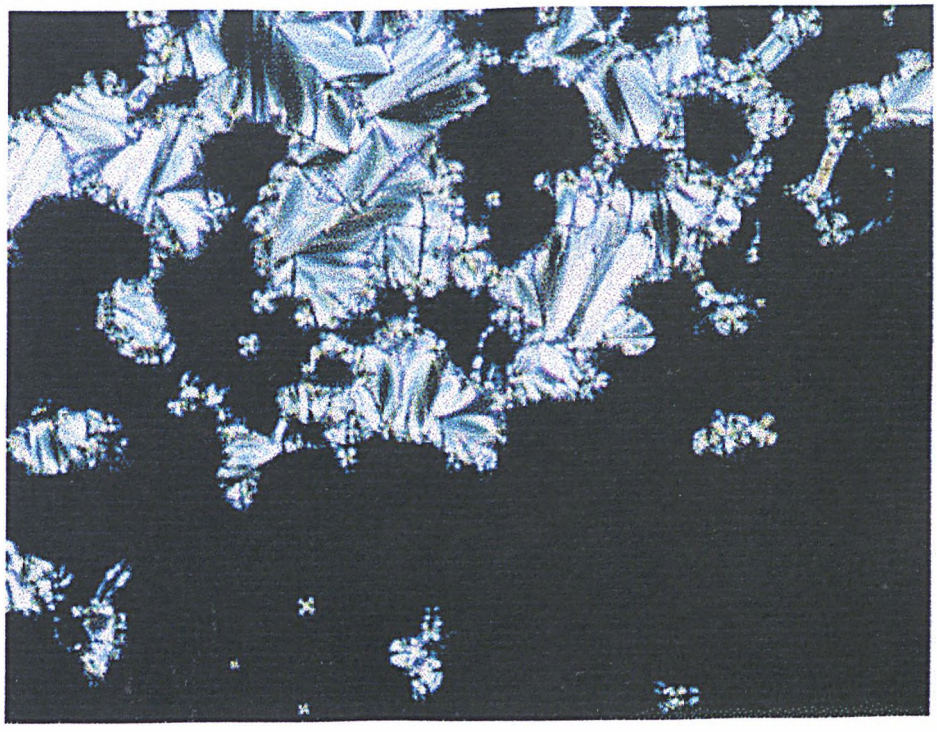

Plate 9 The SmA phase of (±)-MHPOBC at 149 °C

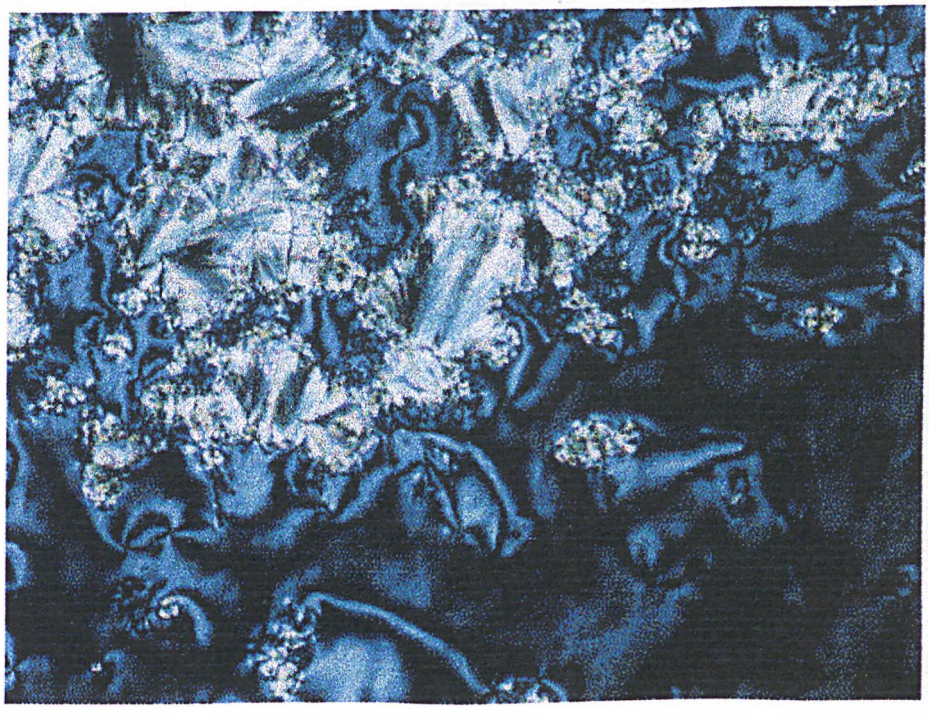

Plate 10 The SmC phase of (±)-MHPOBC at 120.9 °C

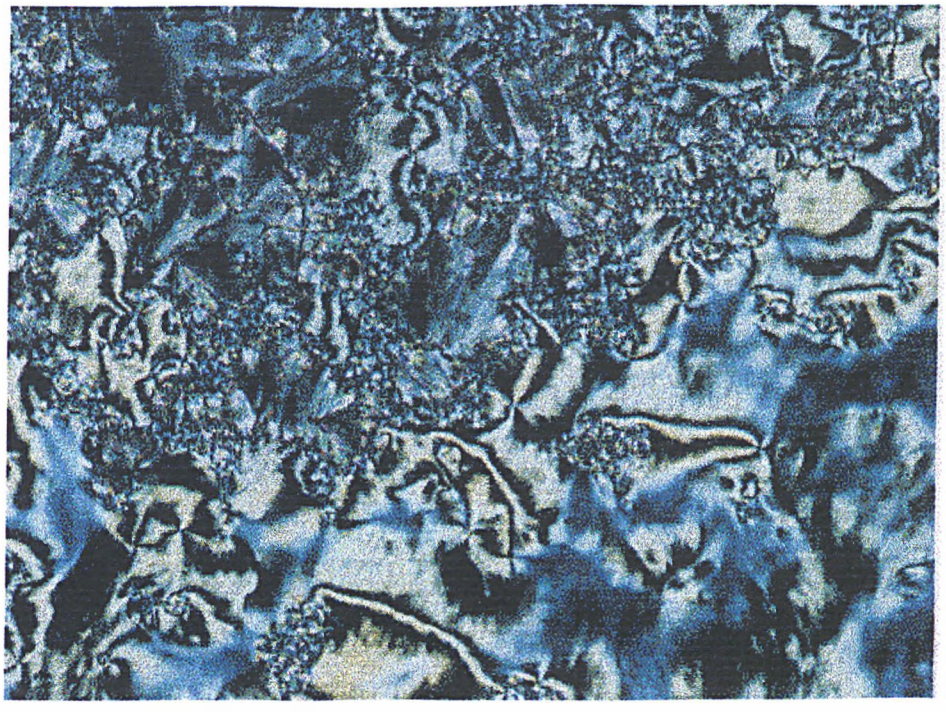

Plate 11 The SmC phase of (±)-MHPOBC at 113 °C

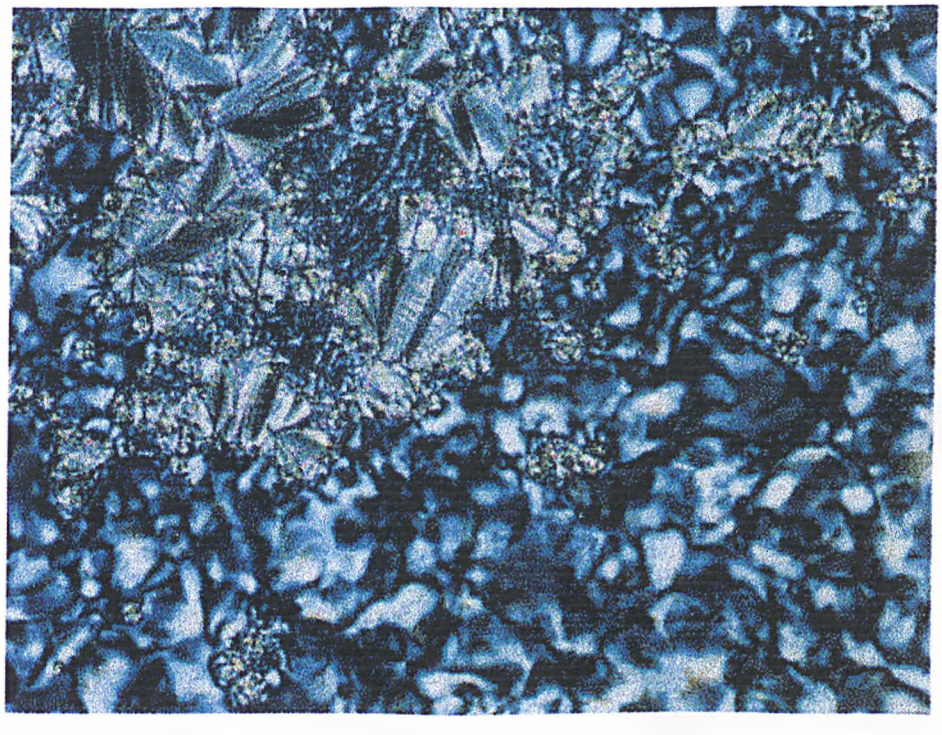

Plate 12 The SmC_{Alt} phase of (±)-MHPOBC at 110 °C

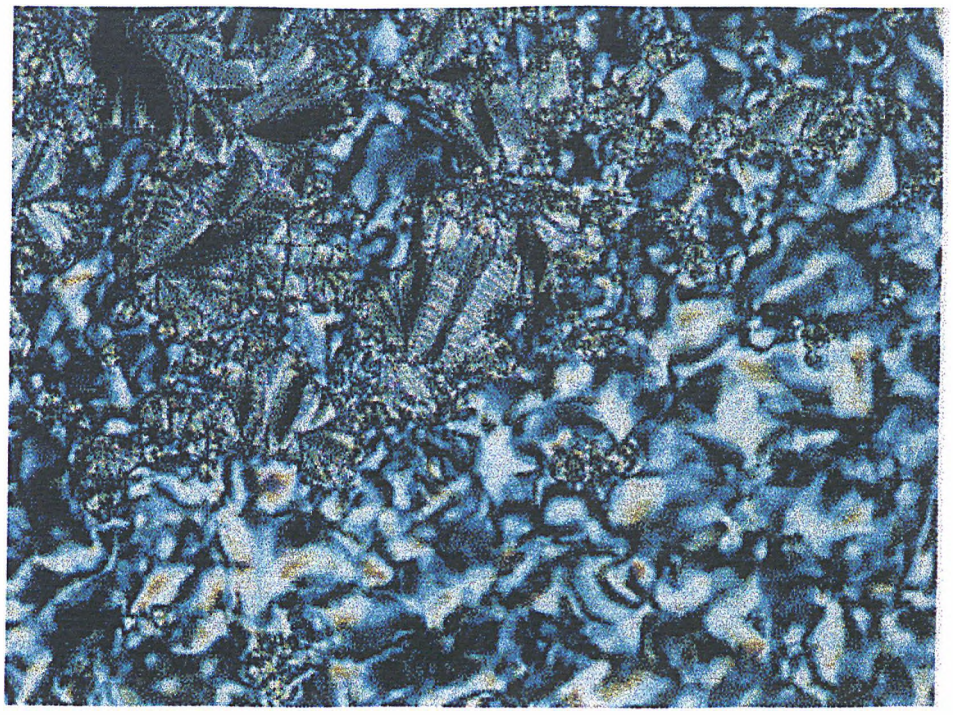

Plate 13 The SmC_{Alt} phase of (±)-MHPOBC at 70.5 °C

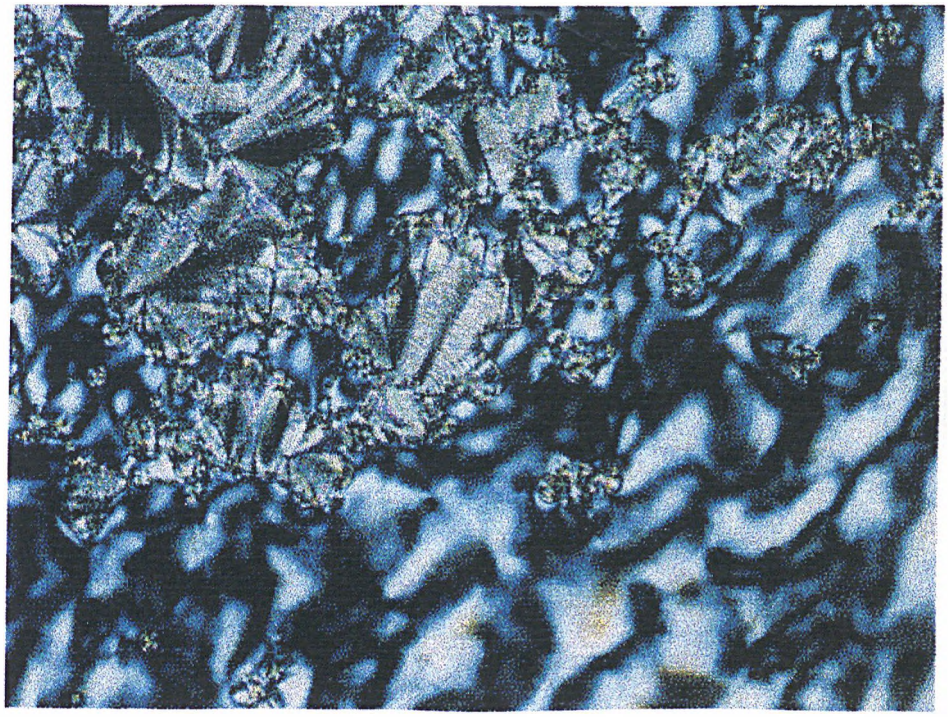

Plate 14 The SmI phase of (±)-MHPOBC at 64 °C

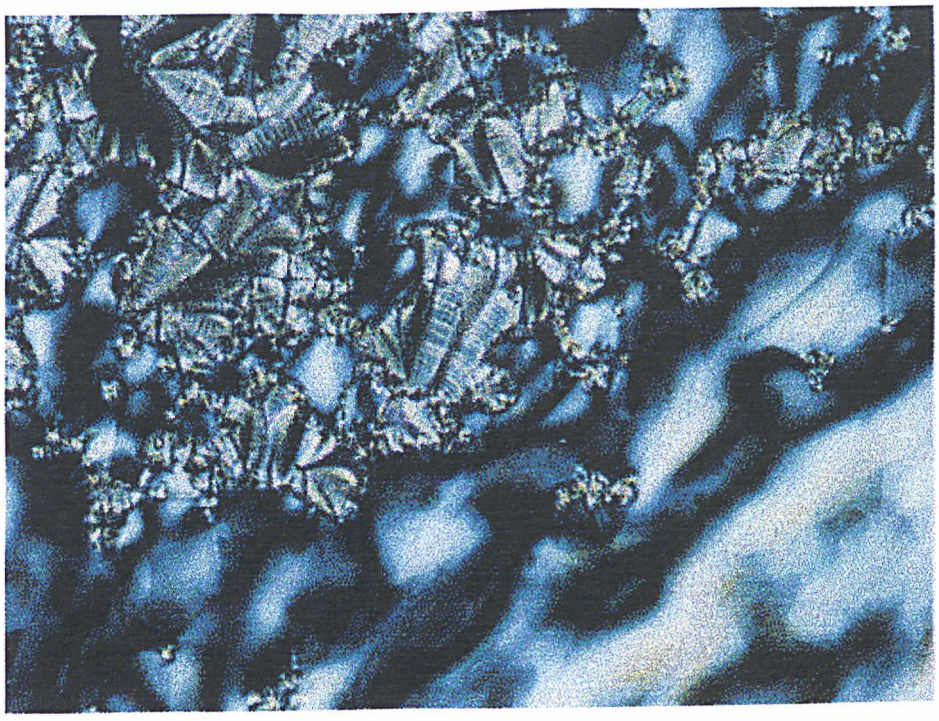

Plate 15 The SmI phase of (±)-MHPOBC at 43 °C

4.2.2 Spontaneous Polarization (Ps) of (*R*)-MHPOBC

The structural differences for the smectic phases of (*R*)-MHPOBC can be reflected in the different behaviours experienced under an applied electric field study. Thus, the temperature and the field dependence of the spontaneous polarization (Ps) are reported in this section.

The polarization reversal current was measured using a 9.66 μm, 1.0 cm^2 electrode area cell (DERA), on cooling.

Fig. 4.2.1 shows the overall trend of Ps for the smectic phases of (*R*)-MHPOBC at fixed applied voltage 6.7 V/μm, 20 Hz and a temperature range 115-50 °C. (The transition temperatures measured under the applied voltage were found to be slightly different to those measured under normal observation in the microscope oven.)

The values of the Ps, calculated from the total integrated area of the current peaks increase as the temperature falls and various changes can be seen on passing through the other phase transitions.

In the vicinity of the SmA*-SmC_α* transition (at 115 °C), a small peak begins to appear near zero field. The SmC_α* phase was reported as an intermediate phase between the SmA* and SmC* phases and it is antiferroelectric in nature at least at temperatures just below the phase transition from the SmA* to the SmC_α*[6]. In the next phase, the peaks increase remarkably in strength and combine to form one peak in the SmC* phase (at 100 °C). The SmC_γ* phase which is expected to have three peaks did not appear. This can be explained by the following two reasons; (a) the temperature range of the SmC_γ* phase is too narrow; (b) the unstable SmC_γ* may be induced by the field to the more stable either SmC* or SmC_A* phases. The switching current curves in the SmC_A* (at 100 °C) are marked by the appearance of

a second peak at higher field. The first peak around zero field is related to the field-induced transition from one of the ferroelectric states to the antiferroelectric state. The second peak is related to the further transition from the antiferroelectric state to the other ferroelectric state. However, these two peaks do not have the same shape. Asymmetry in the peaks is due to the energy required to overcome the surface pinning effects as the materials are switched from the ferroelectric to the antiferroelectric states. In the vicinity of the SmC_A*-SmI* (at 60 °C), the position of the second peak shifts gradually towards the first peaks, but both peaks require a higher electric field for switching to occur. This may result from a stabilization of the antiferroelectric ordering or the increased rotational viscosity of the compounds.

Each of the smectic phases mentioned above was measured in detail under various electric fields at a constant temperature.

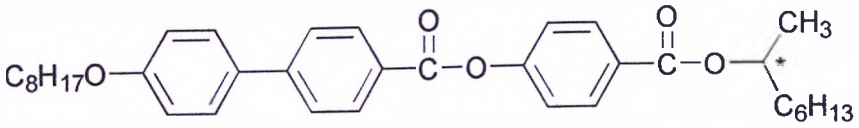

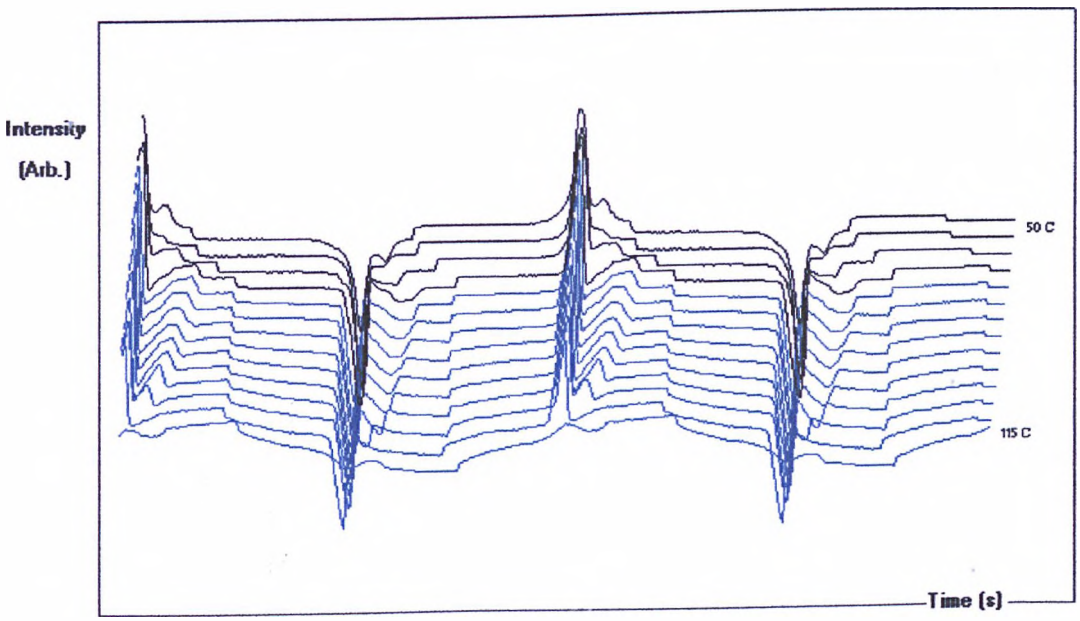

Temp. (°C)	Ps ($nCcm^{-2}$)	Temp. (°C)	Ps ($nCcm^{-2}$)
115	11.2	80	110
110	55.6	75	107
105	69.5	70	110
100	73.8	65	113
95	79.4	60	122
90	93.5	55	121
85	102	50	102

measured at 6.7 V/ μm, 20 Hz

Fig. 4.2.1 Switching current curves and Ps values of the smectic phases of (*R*)-MHPOBC

Fig. 4.2.2 shows the Ps of the SmC_{α}* phase under applied voltage 1.53-8.86 V/μm with 0.9 V/μm steps, 20 Hz and 115 °C.

At a lower applied voltage, the switching curves show split peaks, which indicates antiferroelectricity, but as the field increases, the split peaks get closer. Finally they merge into a single peak above 5.19 V/μm and the Ps values are saturated.

It is known that the thermally excited **c**-director disclination and the collective polarization fluctuation by a novel type of Coulomb interaction between the smectic layers causes the antiferroelecticity of the SmC_{α}*. But this inter-layer interaction is not strong because of the possibility of randomness in the tilt direction. Thus the split peaks at lower fields indicate the weak stability of antiferroelectric ordering. With increasing electric fields, the molecules in adjacent layers can more easily rotate in opposite directions and a ferroelectric state becomes dominant. As a result, direct switching between the two ferroelectric states occurs without passing through the antiferroelectric state.

Fig. 4.2.3 shows the Ps of the SmC* phase under an applied voltage of 2.44-9.16 V/μm with 0.6 V/μm steps, 20 Hz and 113 °C.

Simple single peaks appear for the SmC* phase. The Ps values are more or less saturated with respect to the electric field.

Fig. 4.2.4 shows the Ps of the SmC_A* phase under an applied voltage of 2.44-9.16 V/μm with 0.6 V/μm steps, 20 Hz and 100 °C.

At 2.44 V/μm, two peaks begin to appear but they have very small Ps values. At 3.05 V/μm, the first peak rose rapidly to show a sharp peak, followed by a very

broad second peak. As the applied voltage increased, the second peak shifted towards the first peak and the Ps values become saturated.

Fig. 4.2.5 shows the Ps of the SmI* phase under an applied voltage of 4.59-6.72 V/μm with 0.3 V/μm steps, 20 Hz and 55 °C.

At lower electric fields, the first peak appears around zero field and the second peak appears at the end of the high field, but the Ps is very small. As the electric field increases, the first peak moves towards higher field, conversely the second peak moves towards lower field and thus the two peaks get closer. However both peaks appear at higher field compared to other phases.

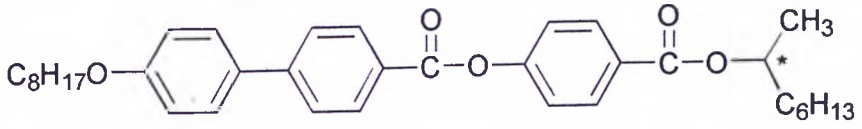

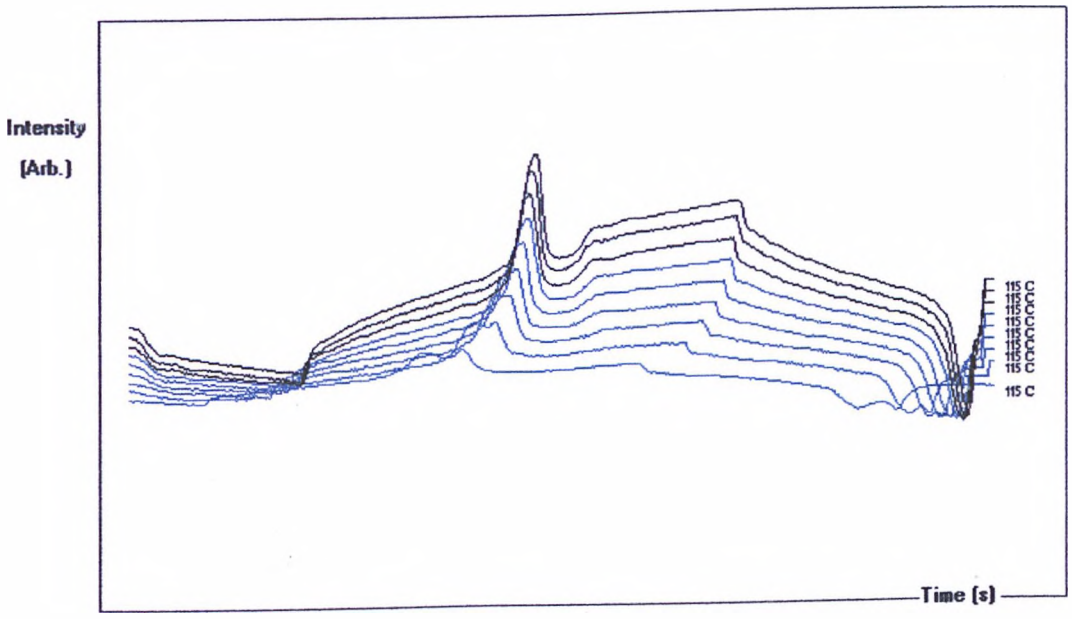

V/μm	Ps (nCcm^{-2})	V/μm	Ps (nCcm^{-2})
1.53	15.2	6.11	26.2
2.44	18.9	7.02	26.4
3.36	22.5	7.94	26.4
4.28	24.6	8.86	26.2
5.19	25.6		

measured at 115 °C

Fig. 4.2.2 Switching current curves and Ps values of the SmC_{α}* phase of (*R*)-MHPOBC

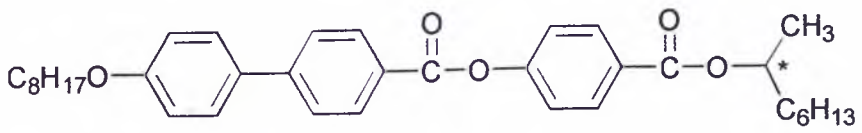

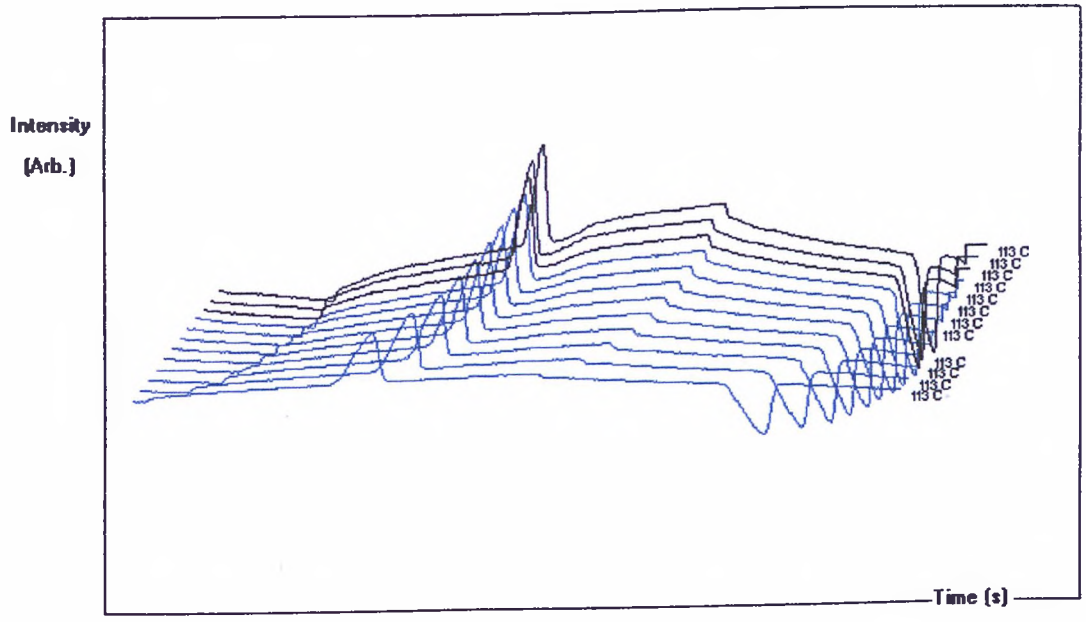

V/μm	Ps (nCcm^{-2})	V/μm	Ps (nCcm^{-2})
2.44	44.4	6.11	44.5
3.05	44.8	6.72	44.1
3.66	43.7	7.33	45.0
4.28	45.7	7.94	44.8
4.89	43.5	8.55	45.8
5.50	44.4	9.16	45.2

measured at 113 °C

Fig. 4.2.3 Switching current curves and Ps values of the SmC* phase of (*R*)-MHPOBC

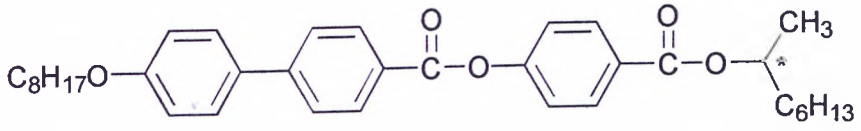

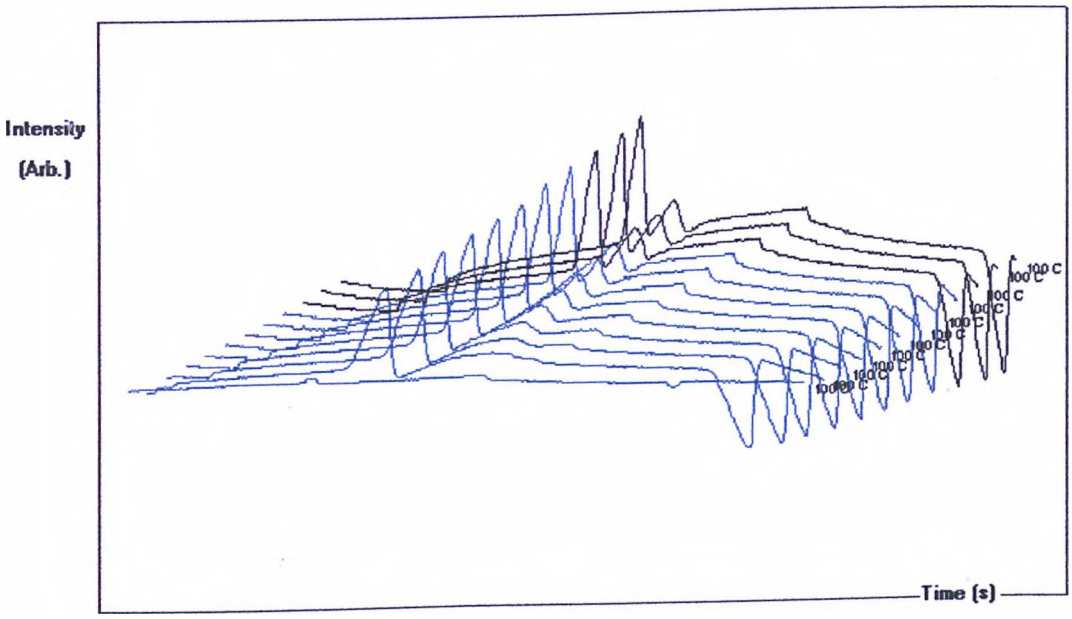

V/μm	Ps (nCcm^{-2})	V/μm	Ps (nCcm^{-2})
2.44	17.7	6.11	74.0
3.05	69.9	6.72	74.5
3.66	70.9	7.33	75.1
4.28	72.0	7.94	75.7
4.89	73.6	8.55	76.6
5.50	73.7	9.16	74.0

measured at 100 °C

Fig. 4.2.4 Switching current curves and Ps values of the SmC_A* phase of (*R*)-MHPOBC

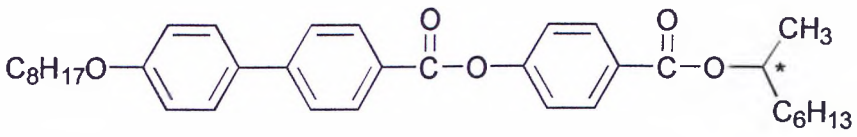

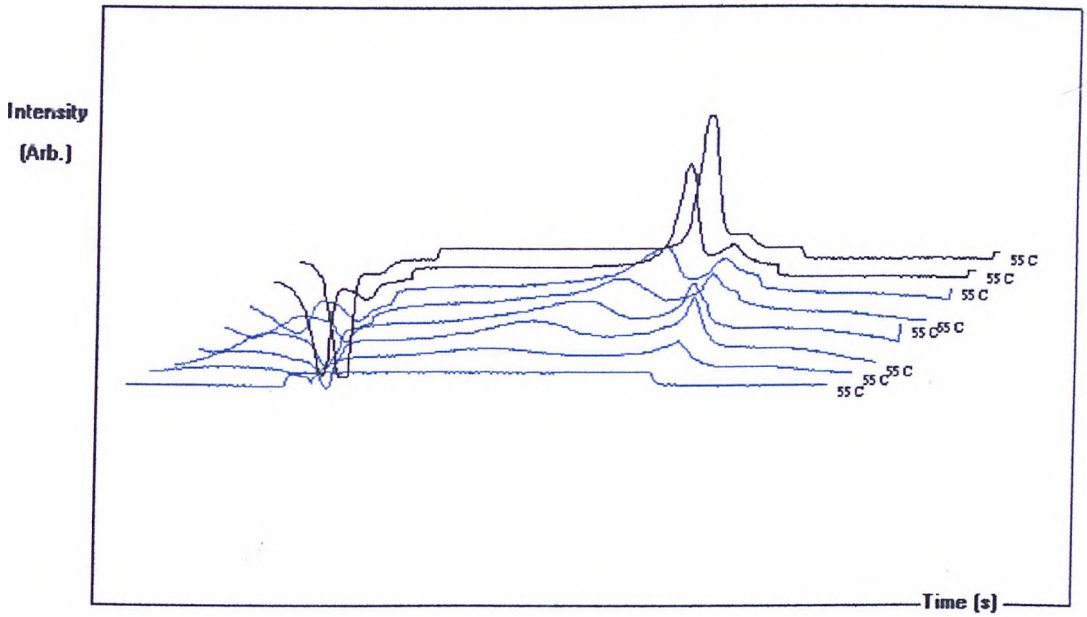

V/μm	Ps (nCcm^{-2})	V/μm	Ps (nCcm^{-2})
2.44	~0	6.11	64.5
3.05	~0	6.72	105
4.89	~0	8.55	110
5.50	~0	9.16	115

measured at 55 °C

Fig. 4.2.5 Switching current curves and Ps values of the SmI* phase of (*R*)-MHPOBC

4.2.3 Tilt Angle Measurements of (*R*)-MHPOBC

The temperature dependence of the apparent tilt angles of compound (*R*)-MHPOBC were measured using a 9.66 μm, 1.0 cm^2 electrode area cell (DERA), at 11.3 V/μm, 10 mHz (square wave). In Fig. 4.2.6, the electric field induced tilt angles versus temperature are plotted.

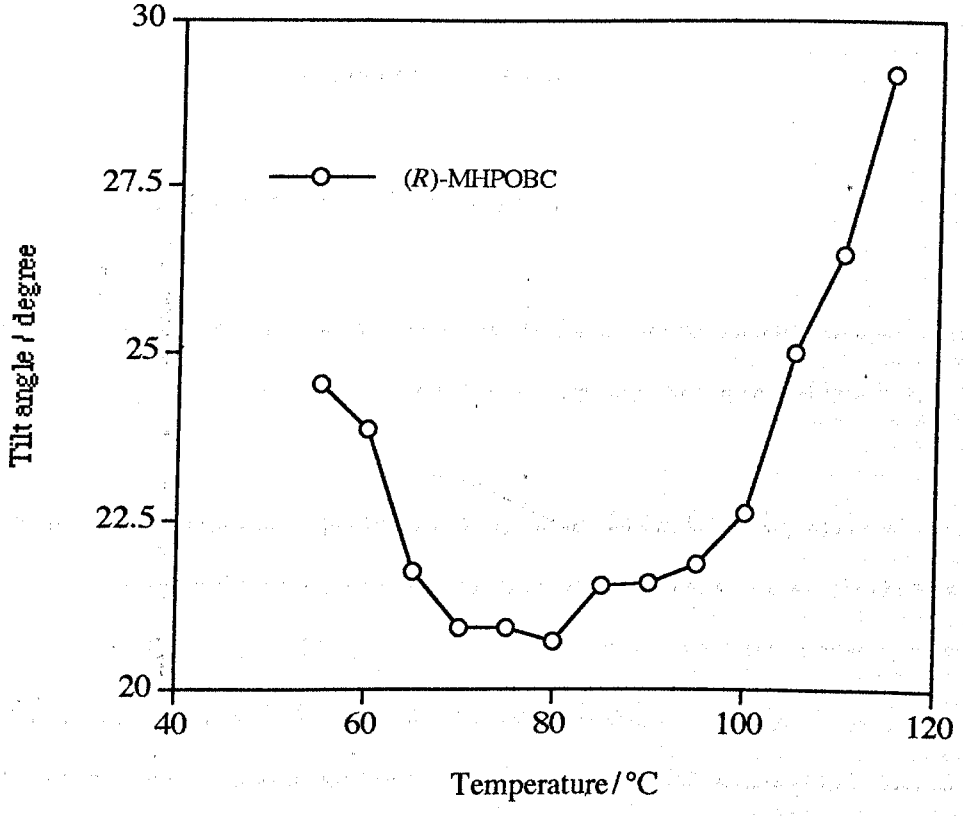

Fig. 4.2.6 Tilt angle versus temperature for the smectic phases of (*R*)-MHPOBC

Tilt angles decrease steeply from the SmC_α* phase at approx. 115 °C into the SmC_A* phase approx. at 105 °C. In the SmC_A* phase, the tilt angles show a small decrease until the phase change to the SmI* phase (65 °C). Tilt angles tend to increase below 65 °C in the SmI* phase.

4.3 Effect of the Ether Linkage on the Mesophase

In this section, the physical and electrooptical properties of the homologous series of chiral and racemic 4"-(1-alkylalkoxy)-2,3-difluoro-4-octyloxyterphenyls are reported.

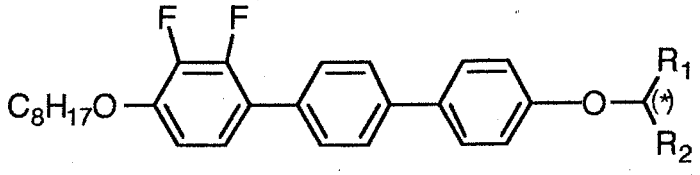

Compound **No**. (8, R_1, R_2)

4.3.1 Transition Temperatures and Phase Behaviour

The transition temperatures of the compounds **20**-**27** were measured by thermal optical polarizing microscopy on cooling. The results are shown in Table 4.3.1.

The N-SmC phase sequence appeared in compounds **20** (8, CH_3, C_5H_{11}) and **23** (8, C_2H_5, C_2H_5) whereas the chiral compounds **21*** and **22*** (8, CH_3, C_6H_{13}) showed blue phases in addition to the N*-SmC* phase sequences. The blue phases appeared over a range of less than 0.5 °C. The occurrence of these phases may be attributed to the fact that the rotation about the bonds attached to the chiral centre is restricted as the alkyl chain R_2 is increased. Therefore the effective "molecular chirality" of the system will be increased. The increased chirality causes a double twist structure of the blue phases as opposed to the N* phase which may be considered as a single twist system. Identification of the type of blue phase was not be determined.

Upon introducing an ethyl unit in the R_1 position, the mesophase stability is markedly decreased compared to a methyl unit in the R_1 position; compounds **24** (8,

C_2H_5, C_3H_7) and **25** (8, C_2H_5, C_5H_{11}) showed only short lived SmC or SmC_x phases on supercooling.

In the case of symmetrically branched swallow-tailed compounds, shorter chain compound **23** (8, C_2H_5, C_2H_5) showed only a 4.5 °C mesophase range and none of the longer chain compounds, **26** (8, C_3H_7, C_3H_7) and **27** (8, C_4H_9, C_4H_9) had a mesophase.

Compounds **20**-**27** were analyzed by DSC using heating and cooling rates of 10 °C min^{-1}; the transition temperatures and enthalpies are listed in Table 4.3.2 and their thermograms are shown in Fig. 4.3.1 (compounds **20**-**22**) and 4.3.2 (compounds **23**-**27**).

In Fig. 4.3.1, compound **20** (8, CH_3, C_5H_{11}) shows two broad peaks associated with the I-N and N-SmC transitions. For both of the chiral compounds **21*** and **22*** (8, CH_3, C_6H_{13}), two sharp peaks were observed which are associated with I-N* and N*-SmC* transitions respectively. The blue phases of these compounds were not detected by DSC. In Fig. 4.3.2, compound **23** (8, C_2H_5, C_2H_5) shows two smaller peaks for I-N and N-SmC transitions in comparison to those obtained for compound **20**. The transition from I to a short lived SmC phase for compound **24** (8, C_2H_5, C_3H_7) and an unidentified smectic phase in compound **25** (8, C_2H_5, C_5H_{11}) were not detected by DSC.

Summary

(a) Generally a symmetrically branched compounds tend to exhibit N/N* and SmC/C* sequences whereas symmetrically branched compounds do not have mesophases.

(b) Terminal ethers in difluoro systems do not exhibit antiferroelectric ordering.

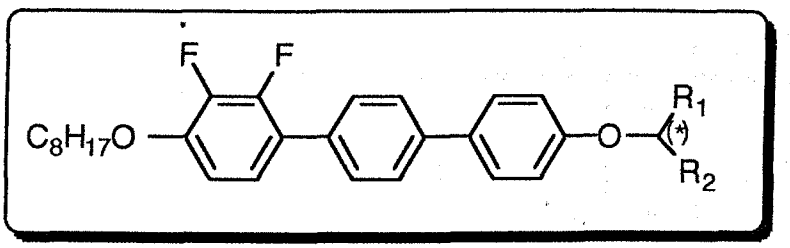

Compound **No.** (8, R_1, R_2)

Compounds		**Transition Temperatures / °C**								
No.	**R_1** **R_2**	**I**		**Blue (*)**		**N (*)**		**SmC (*)**		**K**
20	CH_3 C_5H_{11}	•	-	-	104.5	•	97.0	•	59.8	•
21*	CH_3 C_6H_{13}	•	98.2	•	97.9	•	94.7	•	70	•
22*	CH_3 C_6H_{13}	•	98.4	•	98.0	•	95.0	•	71	•
23	C_2H_5 C_2H_5	•	-	-	62.0	•	59.5	•	57.5	•
24	C_2H_5 C_3H_7	•	-	-	-	-	?[a]	•	59.7	•
25	C_2H_5 C_5H_{11}	•	-	-	-	-	?[b]	•	46.2	•
26	C_3H_7 C_3H_7	•	-	-	-	-	-	-	66.4	•
27	C_4H_9 C_4H_9	•	-	-	-	-	-	-	15.3	•

*.... Optically active: compound **21** (*R*)-, compound **22** (*S*)-

[a].... Short lived I to SmC [b].... Short lived I to S_X

Table 4.3.1 Transition temperatures for the 4"-(1-alkylalkoxy)-2,3-difluoro-4-octyloxyterphenyls determined by thermal optical polarized light microscopy, on cooling.

Compounds			Transition Temperatures[a] / °C and Associated Enthalpies[b] / [J/g]									
No.	R_1	R_2	I		Blue (*)		N (*)		SmC (*)		K	mp
20	CH_3	C_5H_{11}	•	-	-	101.8 [-2.19]	•	94.9 [-3.70]	•	51.3 [-38.2]	•	65
21*	CH_3	C_6H_{13}	•	- [-][c]	-	95.9 [-2.07]	•	92.3 [-4.24]	•	69.0 [-50.6]	•	85
22*	CH_3	C_6H_{13}	•	- [-][c]	-	96.2 [-2.51]	•	92.7 [-4.36]	•	68.3 [-51.5]	•	85
23	C_2H_5	C_2H_5	•	-	-	59.4 [-1.41]	•	57.1 [-2.84]	•	44.5 [-41.8]	•	72
24	C_2H_5	C_3H_7	•	-	-	-	-	- [-][c]	-	52.6 [-47.5]	•	62
25	C_2H_5	C_5H_{11}	•	-	-	-	-	- [-][c]	-	36.3 [-42.6]	•	52
26	C_3H_7	C_3H_7	•	-	-	-	-	-	-	57.4 [-60.3]	•	68
27	C_4H_9	C_4H_9	•	-	-	-	-	-	-	17.7 [-55.7]	•	54

[a].... Recorded at cooling rate of 10 °C min^{-1} [b].... Enthalpies of transition given in square brackets [c].... Transition not detected in DSC

Table 4.3.2 Transition temperatures for the 4"-(1-alkylalkoxy)-2,3-difluoro-4-octyloxyterphenyls determined by DSC measurements, on cooling.

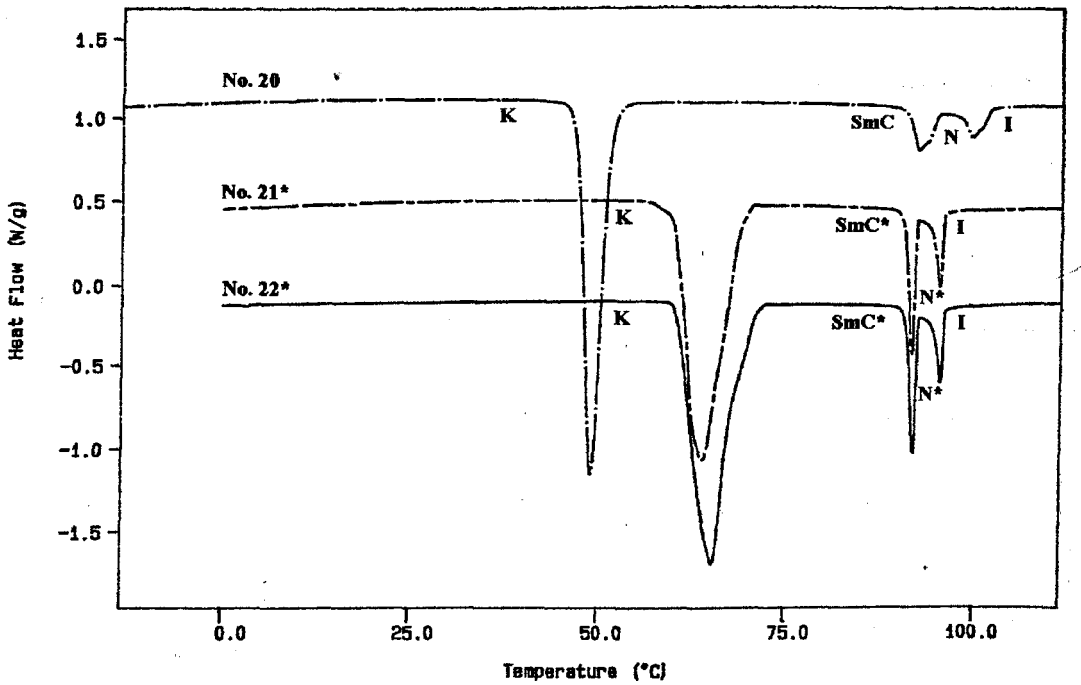

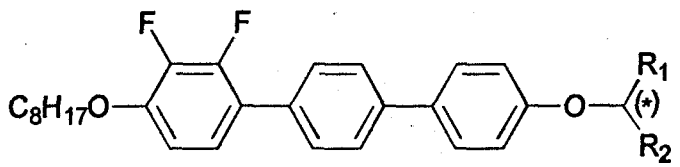

Compounds No.	R_1	R_2
20	CH_3	C_5H_{11}
21*	CH_3	C_6H_{13}
22*	CH_3	C_6H_{13}

Fig. 4.3.1 DSC thermograms of compounds **20-22***

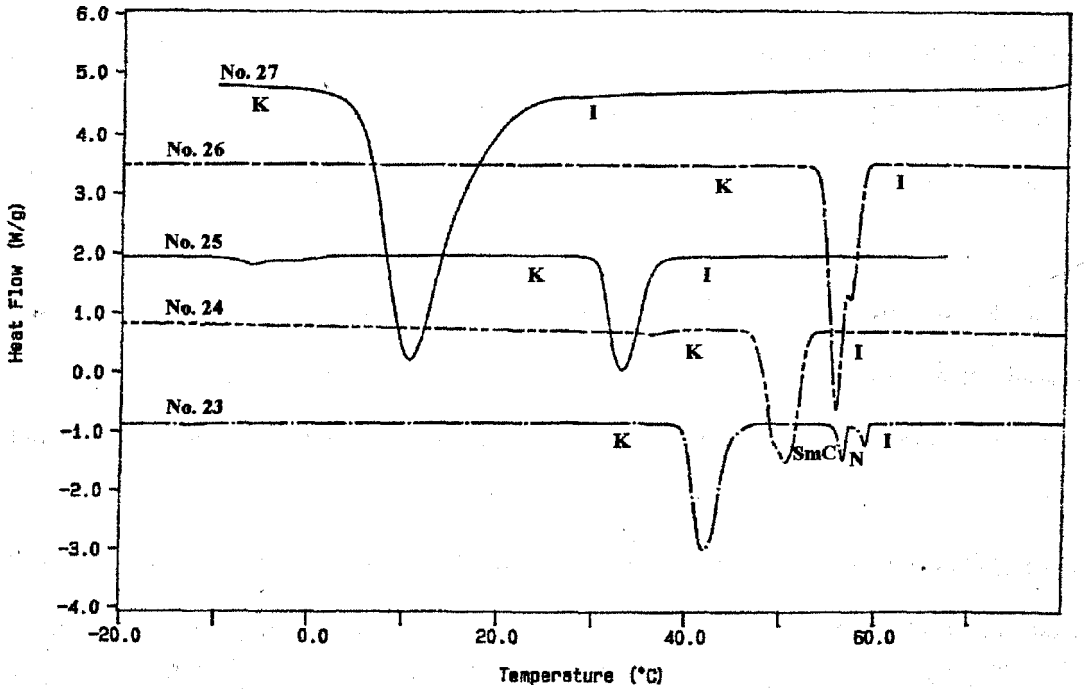

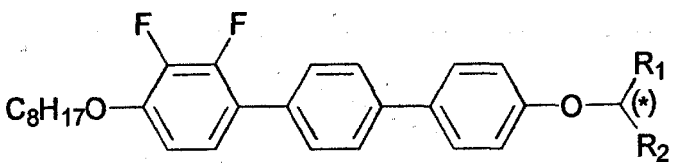

Compounds No.	R_1	R_2
23	C_2H_5	C_2H_5
24	C_2H_5	C_3H_7
25	C_2H_5	C_5H_{11}
26	C_3H_7	C_3H_7
27	C_4H_9	C_4H_9

Fig. 4.3.2 DSC thermograms of compounds **23-27**

4.3.2 Spontaneous Polarization and Tilt Angle Measurements

Fig. 4.3.3 shows temperature dependences of the Ps values of compound **22*** (8, CH_3, C_6H_{13}). The overall trend of Ps for the SmC* phase at fixed applied voltage 5.9 V/μm, 20 Hz and a temperature range of 91.5-79.5 °C is shown in Fig. 4.3.4.

The apparent tilt angle of compound **22*** (8, CH_3, C_6H_{13}) versus temperature under an electric field (10V/μm, square wave, 10 mHz) was measured (see Fig. 4.3.5). This electric field is high enough to cause full switching of the molecules.

The increase of the tilt angle with decreasing temperature is due to the well-known temperature dependence of the molecular tilt angle with respect to the layer normal. The saturated tilt angle below 84.5 °C was found to be relatively high (~34°).

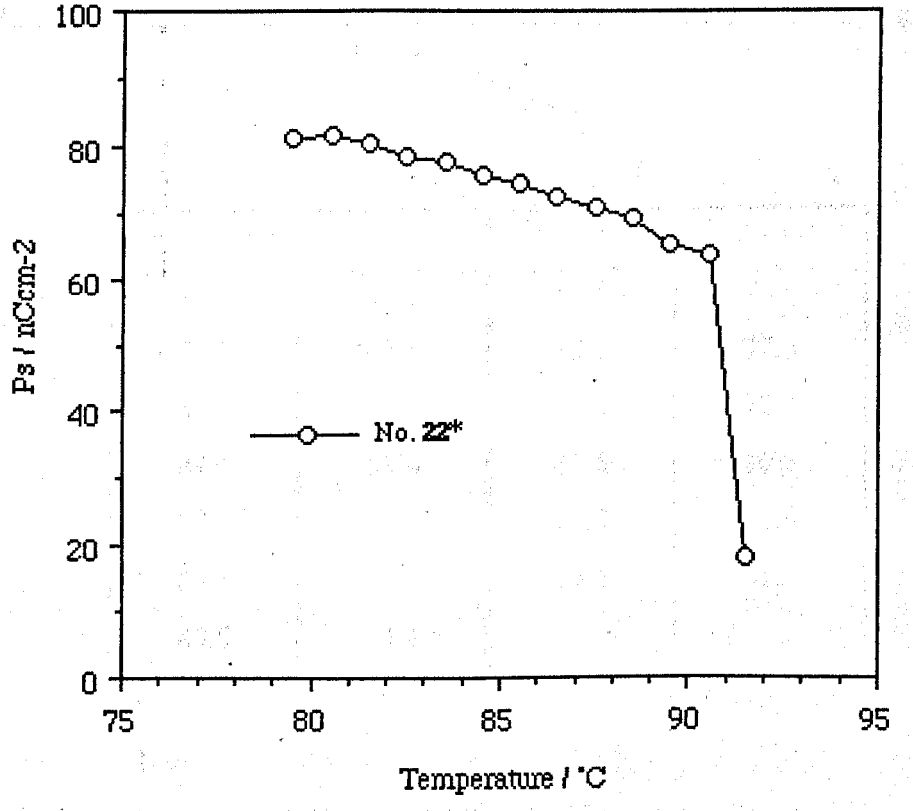

Fig. 4.3.3 Ps versus temperature for the SmC* phase of compound **22*** (8, CH_3, C_6H_{13})

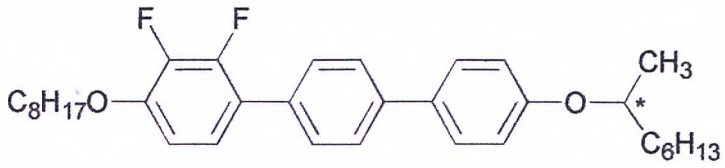

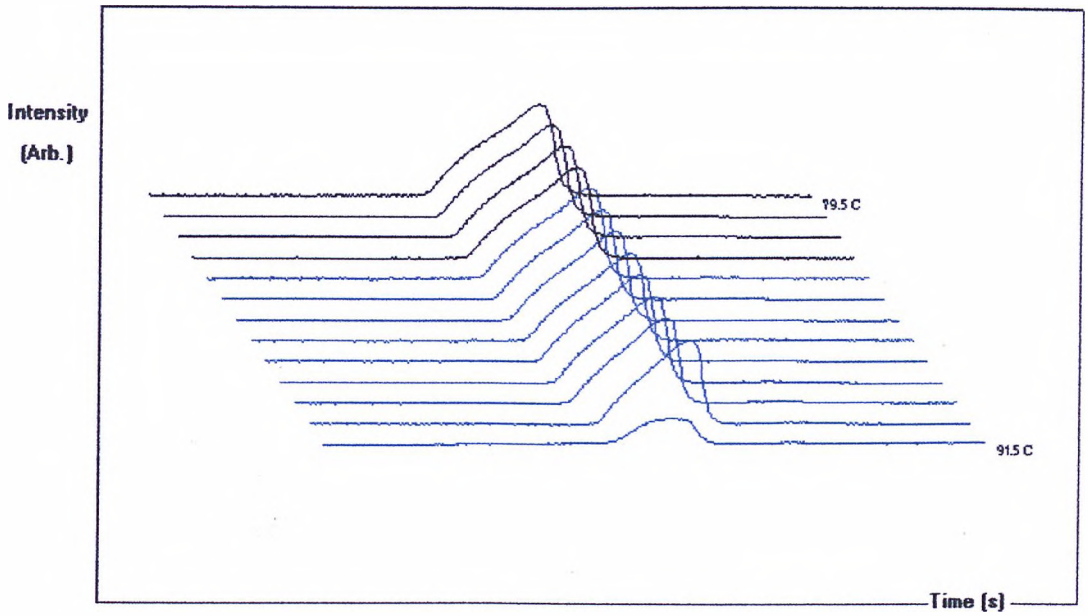

Temp. (°C)	Ps ($nCcm^{-2}$)	Temp. (°C)	Ps ($nCcm^{-2}$)
91.5	17.9	84.5	75.6
90.5	63.6	83.5	77.5
89.5	65.2	82.5	78.4
88.5	68.9	81.5	80.5
87.5	70.5	80.5	81.6
86.5	72.3	79.5	81.3
85.5	74.4		

measured at 5.9 V/ μm, 20 Hz

Fig. 4.3.4 Switching current curves and Ps values of the SmC* phase of compound **22*** (8, CH_3, C_6H_{13})

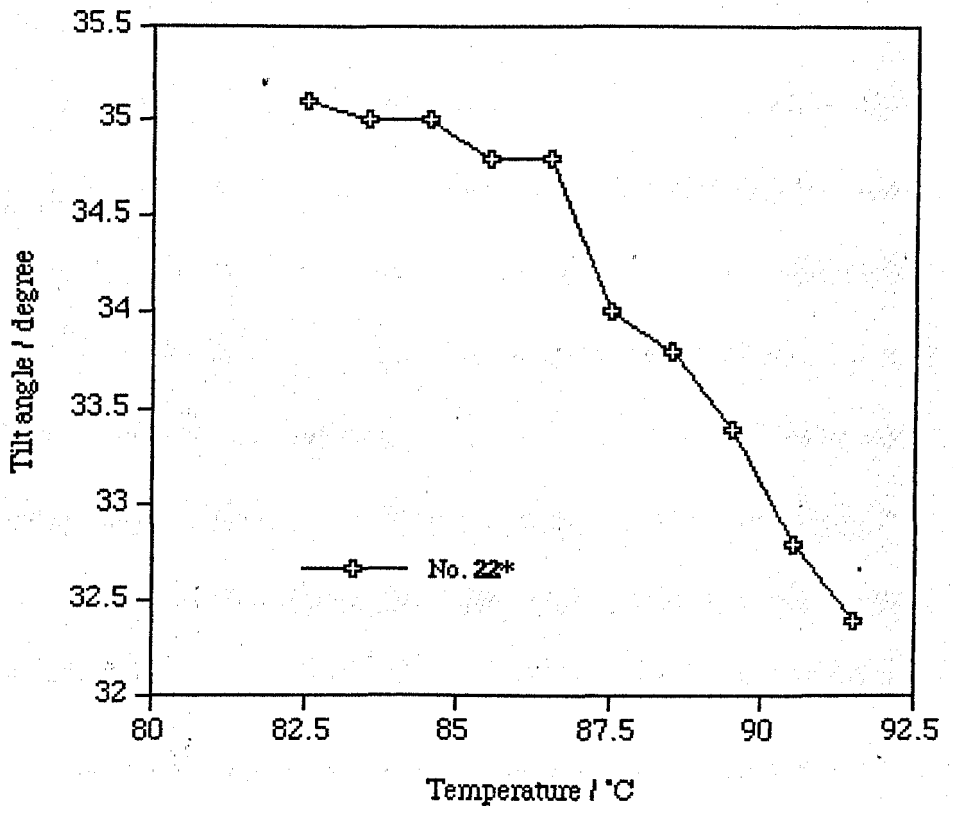

Temp. (°C)	Tilt angle (°)	Temp. (°C)	Tilt Angle (°)
91.5	32.4	86.5	34.8
90.5	32.8	85.5	34.8
89.5	33.4	84.5	35.0
88.5	33.8	83.5	35.0
87.5	34.0	82.5	35.1

measured at 10 V/μm, 10 mHz

Fig. 4.3.5 Tilt angle versus temperature for the SmC* phase of compound **22*** (8, CH_3, C_6H_{13})

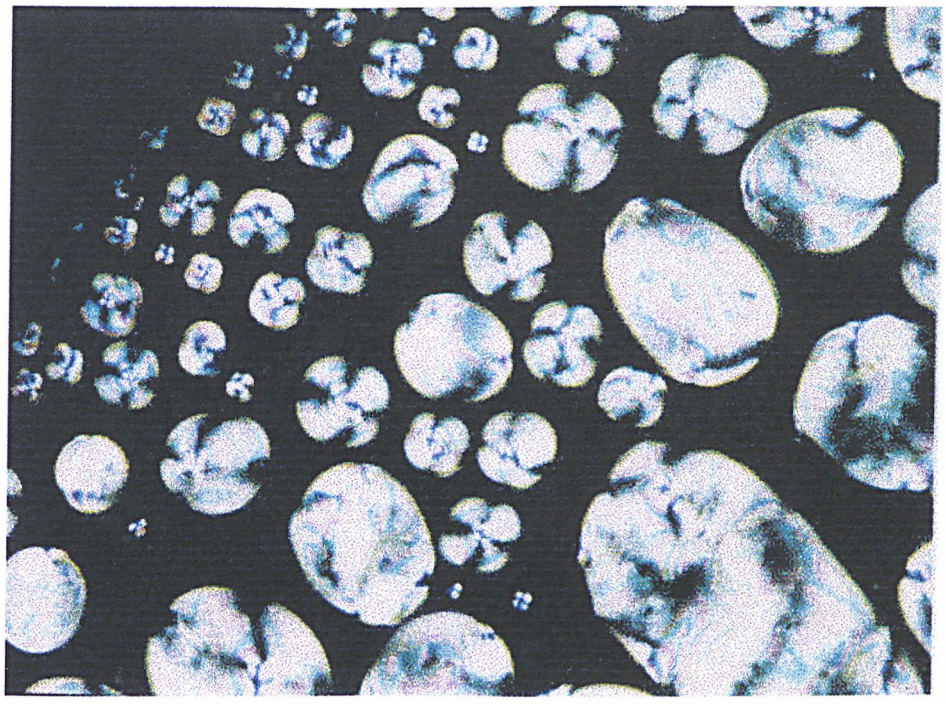

Plate 16 The Nematic phase of compound **20** (8, CH_3, C_5H_{11}) at 104.5 °C

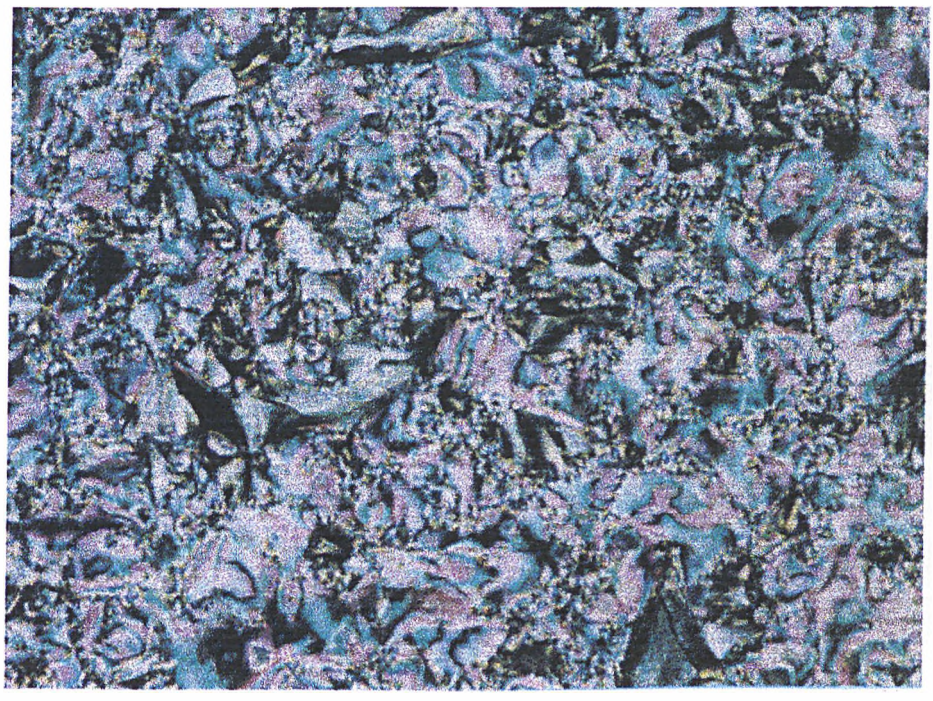

Plate 17 The SmC phase of compound **20** (8, CH_3, C_5H_{11}) at 92.3 °C

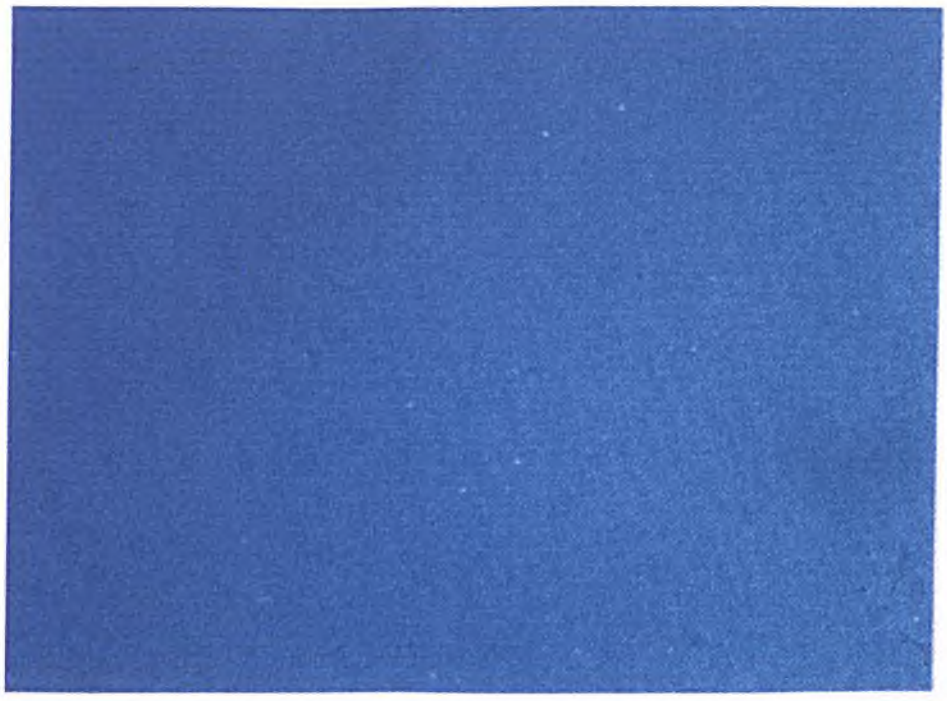

Plate 18 The Blue phase of compound **22*** (8, CH_3, C_6H_{13}) at 98.2 °C

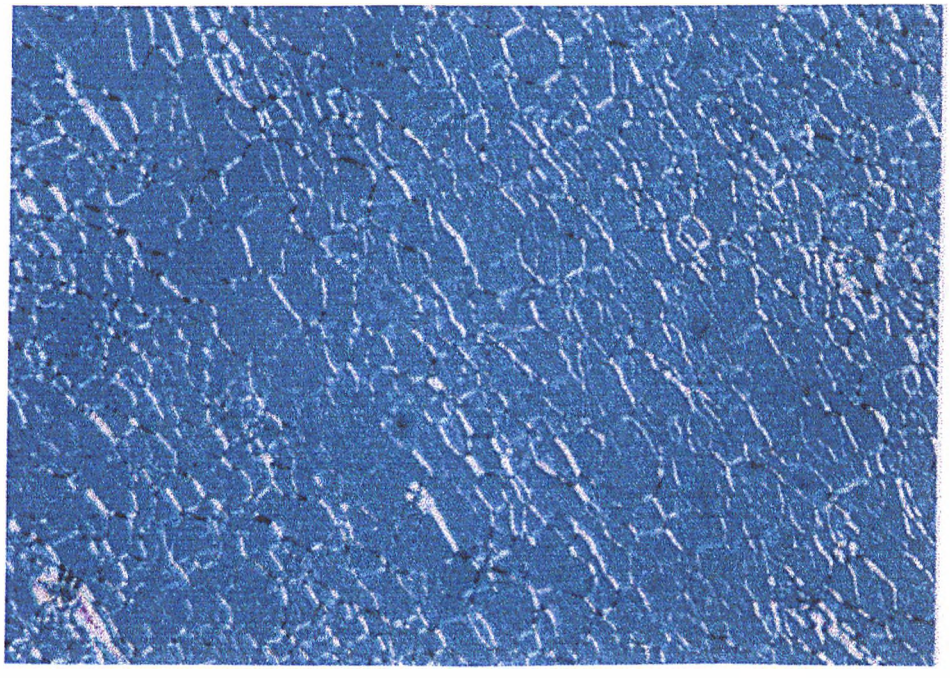

Plate 19 The Grandjean texture of compound **22*** (8, CH_3, C_6H_{13}) at 97.2 °C

4.4 Effect of the Ester Linkage on the Mesophase (C8)

In this section, the physical and electrooptical properties of the homologous series of chiral and racemic 1-alkylalkyl 2",3"-difluoro-4"-octyloxyterphenyl-4-carboxylates and (*R*)-trifluoromethylheptyl 2",3"-difluoro-4"-octyloxyterphenyl-4-carboxylate are reported.

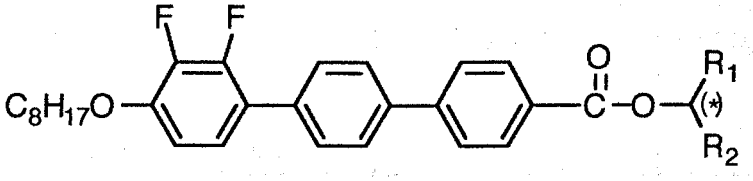

Compound **No**. (8, R_1, R_2)

4.4.1 Transition Temperatures and Phase Behaviour

The transition temperatures of the compounds **46-60*** were measured on cooling using thermal optical polarizing microscopy, and the results are listed in Table 4.4.1.

Compounds **46-60*** were analyzed by DSC using heating and cooling rates of 10 °C min^{-1}, the transition temperatures and enthalpies are listed in Table 4.4.2 (compounds **46-53**) and Table 4.4.3 (compounds **54-60***) and their thermograms are shown in Fig. 4.4.1 (compounds **46-53**), Fig. 4.4.2 (compounds **54-60***) and Fig. 4.4.3 (expanded).

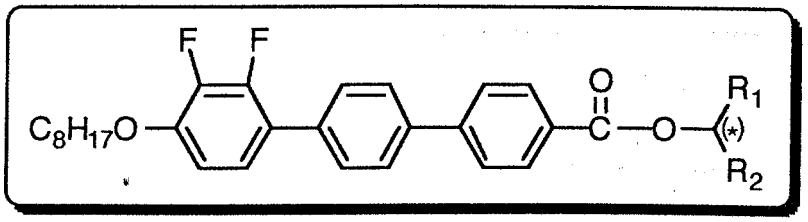

Compound **No.** (8, R_1, R_2)

Compounds			Transition Temperatures / °C								
No.	**R_1**	**R_2**	**I**		**SmA (*)**		**SmC (*)**		**SmC_A (*)**		**K**
46	CH_3	CH_3	•	151.5	•	-	-	-	-	41.5	•
47	CH_3	C_4H_9	•	109.4	•	-	-	42.3	•	25.0	•
48*	CH_3	C_5H_{11}	•	100.5	•	-	-	-	-	43.5	•
49	CH_3	C_5H_{11}	•	101.6	•	-	-	53.2	•	20.2	•
50*	CH_3	C_6H_{13}	•	93.3	•	-	-	-	-	42.1	•
51	CH_3	C_6H_{13}	•	99.9	•	-	-	36.5	•	28.7	•
52	CH_3	C_7H_{15}	•	97.5	•	-	-	33.2	•	24.7	•
53	CH_3	C_8H_{17}	•	94.2	•	-	-	24.5	•	-6.8	•
54	C_2H_5	C_2H_5	•	96.5	•	43.1	•	-	-	26.0	•
55	C_2H_5	C_3H_7	•	80.9	•	-	-	33.9	•	27.3	•
56	C_2H_5	C_4H_9	•	73.2	•	-	-	19.5	•	-10.0	•
57	C_2H_5	C_5H_{11}	•	64.7	•	-	-	-	-	-14.4	•
58	C_3H_7	C_3H_7	•	60.8	•	-	-	-	-	25.0	•
59	C_4H_9	C_4H_9	•	46.4	•	-	-	-	-	20.2	•
60*	CF_3	C_6H_{13}	•	72.1	•	-	-	-	-	26.0	•

*.... Optically active: compound **48**, **60** (*R*)-, compound **50** (*S*)-

Table 4.4.1 Transition temperatures for the 1-alkylakyl 2",3"-difluoro-4"-octyloxyterphenyl-4-carboxylates and 1-trifluoromethylheptyl 2",3"-difluoro-4"-octyloxyterphenyl-4-carboxylate determined by thermal optical polarized light microscopy, on cooling.

Compounds			Transition Temperatures[a] / °C and Associated Enthalpies[b] / [J/g]										
No.	R_1	R_2	I		SmA (*)		SmC (*)		SmC_A (*)		K	mp
46	CH_3	CH_3	•	147.2 [-13.3]	•	-	-	-	-	39.1 [-30.9]	•	85
47	CH_3	C_4H_9	•	106.4 [-9.51]	•	-	-	- [-][d]	-	-7.73 [-17.0]	•	43
48*	CH_3	C_5H_{11}	•	98.8 [-8.32]	•	-	-	58.5[c] [-0.03]	•	41.4 [-32.5]	•	58
49	CH_3	C_5H_{11}	•	99.4 [-9.19]	•	-	-	- [-][d]	-	-10.8 [-14.5]	•	43
50*	CH_3	C_6H_{13}	•	91.2 [-7.62]	•	-	-	-	-	27.8 [-24.4]	•	59
51	CH_3	C_6H_{13}	•	98.3 [-8.47]	•	-	-	- [-][d]	-	15.9 [-15.9]	•	54
52	CH_3	C_7H_{15}	•	94.2 [-8.65]	•	-	-	- [-][d]	-	-5.84 [-15.0]	•	54
53	CH_3	C_8H_{17}	•	91.0 [-8.47]	•	-	-	- [-][d]	-	-6.87 [-14.4]	•	52

[a].... Recorded at cooling rate of 10 °C min^{-1} [b].... Enthalpies of transition given in square brackets [c] .... Transition not detected in microscope [d].... Transition not detected in DSC

Table 4.4.2 Transition temperatures for the 1-alkylakyl 2",3"-difluoro-4"-octyloxyterphenyl-4-carboxylates determined by DSC measurements, on cooling.

Compounds			Transition Temperatures[a] / °C and Associated Enthalpies[b] / [J/g]									
No.	R_1	R_2	I		SmA (*)		SmC (*)		SmC_A (*)		K	mp
54	C_2H_5	C_2H_5	•	93.1 [-8.26]	•	41.4 [-0.06]	•	-	-	-8.93 [-19.9]	•	57
55	C_2H_5	C_3H_7	•	78.2 [-6.77]	•	-	-	- [-][d]	-	1.86 [-23.5]	•	52
56	C_2H_5	C_4H_9	•	70.2 [-6.23]	•	-	-	- [-][d]	-	-10.1 [-13.1]	•	36
57	C_2H_5	C_5H_{11}	•	60.9 [-5.97]	•	-	-	-	-	-14.4 [-9.60]	•	31
58	C_3H_7	C_3H_7	•	57.5 [-5.86]	•	-	-	-	-	25.9 [-25.3]	•	60
59	C_4H_9	C_4H_9	•	43.4 [-4.70]	•	-	-	-	-	- [-][e]	•	37
60*	CF_3	C_6H_{13}	•	68.7 [-6.05]	•	-	-	42.4[c] [-0.05]	•	20.4 [-30.4]	•	55

[a].... Recorded at cooling rate of 10 °C min^{-1} [b].... Enthalpies of transition given in square brackets [c].... Transition not detected in microscope [d].... Transition not detected in DSC [e] .... No recrystallisation on cooling to -50 °C

Table 4.4.3 Transition temperatures for the 1-alkylakyl 2",3"-difluoro-4"-octyloxyterphenyl-4-carboxylates and 1-trifluoromethylheptyl 2",3"-difluoro-4"-octyloxyterphenyl-4-carboxylate determined by DSC measurements, on cooling.

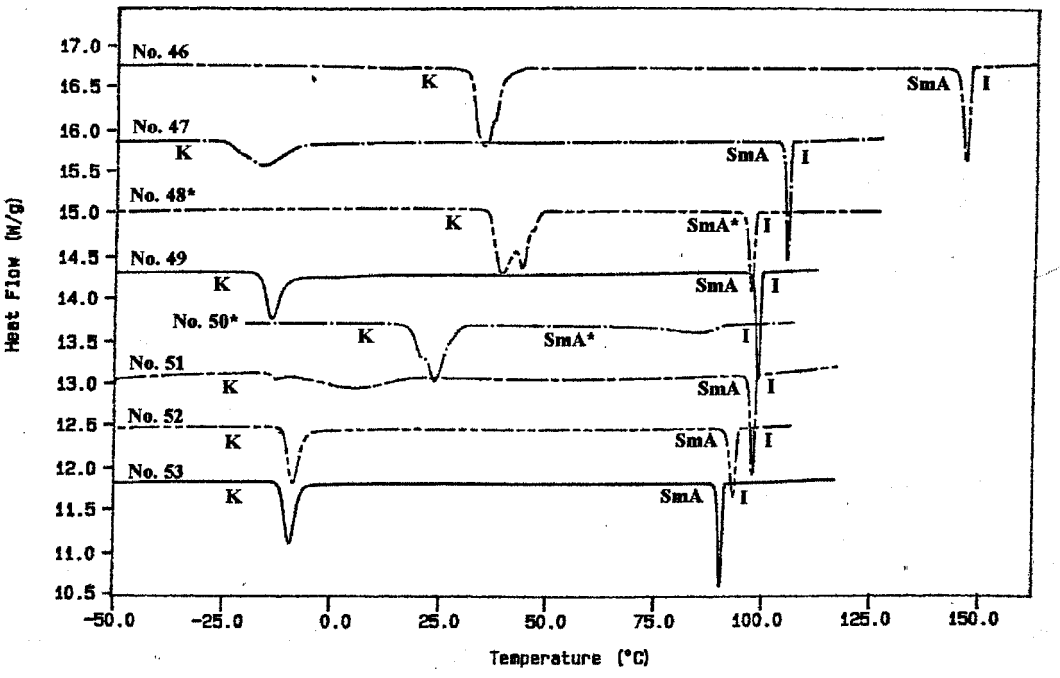

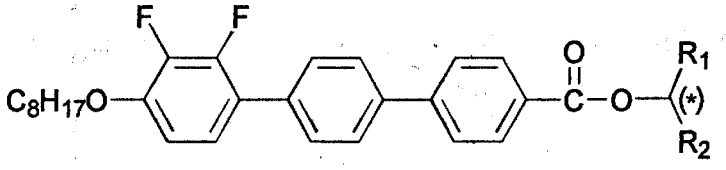

Compounds No.	R_1	R_2
46	CH_3	CH_3
47	CH_3	C_4H_9
48*	CH_3	C_5H_{11}
49	CH_3	C_5H_{11}
50*	CH_3	C_6H_{13}
51	CH_3	C_6H_{13}
52	CH_3	C_7H_{15}
53	CH_3	C_8H_{17}

Fig. 4.4.1 DSC thermograms of compounds **46-53**

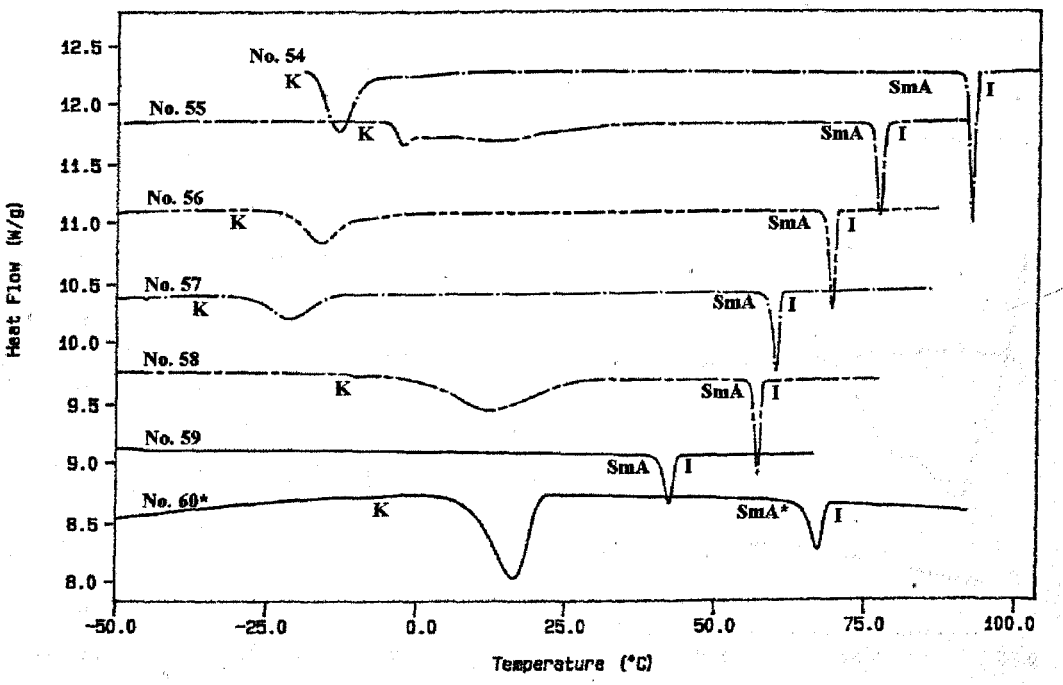

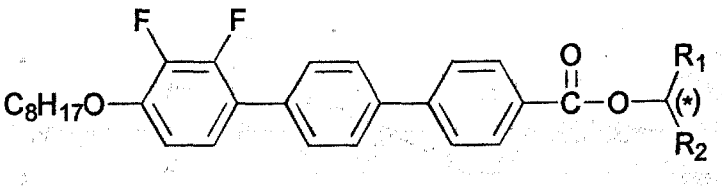

Compounds No.	R_1	R_2
54	C_2H_5	C_2H_5
55	C_2H_5	C_3H_7
56	C_2H_5	C_4H_9
57	C_2H_5	C_5H_{11}
58	C_3H_7	C_3H_7
59	C_4H_9	C_4H_9
60*	CF_3	C_6H_{13}

Fig. 4.4.2 DSC thermograms of compounds **54-60***

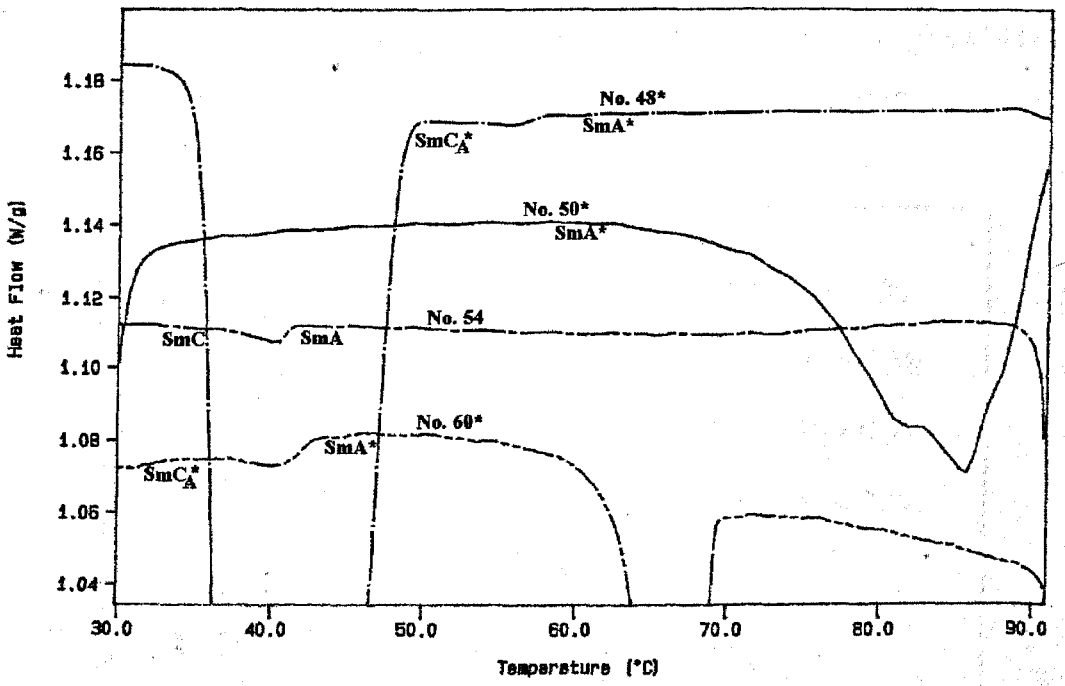

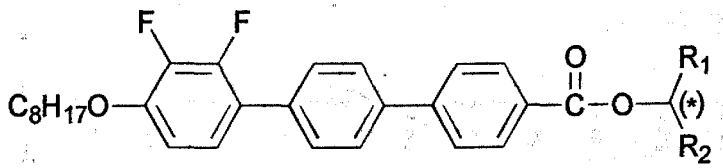

Compounds No.	R_1	R_2
48*	CH_3	C_5H_{11}
50*	CH_3	C_6H_{13}
54	C_2H_5	C_2H_5
60*	CF_3	C_6H_{13}

Fig. 4.4.3 Expanded DSC thermograms of compounds **48***, **50***, **54** and **60***

Every compound in this homologous series was found to exhibit a SmA (or SmA*) phase. In Fig. 4.4.4, the I-SmA transition temperatures for the racemic compounds as a function of the chain length, R_2 are plotted where R_1 = CH_3, C_2H_5, C_3H_7 and C_4H_9. As R_1 increases in length, the SmA phase becomes destabilized.

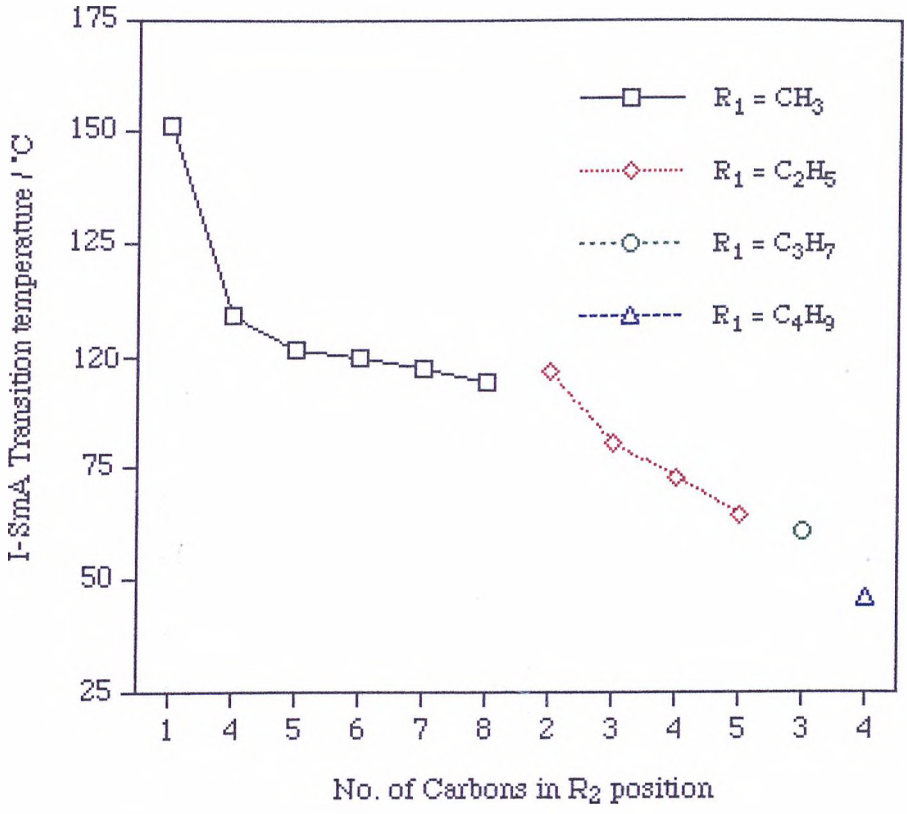

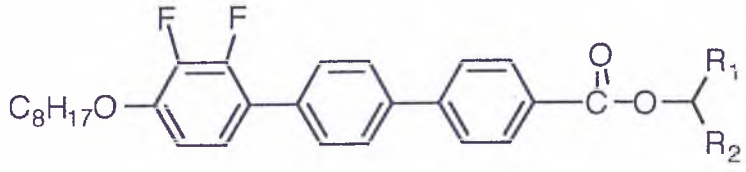

Fig. 4.4.4 I-SmA transition temperature as a function of the chain length of R_2

Compound **46** (8, CH_3, CH_3) which has the shortest chain length showed a very high I-SmA transition temperature and did not show any other mesophase. The SmC_{Alt} phase of the compound **47** (8, CH_3, C_4H_9) appeared in the microscope but the peak associated with an SmA-SmC_{Alt} transition was not detected by DSC.

The chiral compound **48*** (8, CH_3, C_5H_{11}) had no other mesophase below the SmA* phase in the microscope. However in DSC it showed a very small peak (ΔH = -0.03 J/g) at 58.5 °C, which is assumed to be related to the transition from SmA to SmC_A*. In the case of the racemic analogue **49** (8, CH_3, C_5H_{11}), a SmC_{Alt} phase was observed, but in this case the phase transition from SmA to SmC_{Alt} was not confirmed by DSC. In the same way, for the longer alkyl chain compounds **52** (8, CH_3, C_7H_{15}) and **53** (8, CH_3, C_8H_{17}), SmC_{Alt} phases observed by microscopy were not detected by DSC.

The chiral compound **50*** (8, CH_3, C_6H_{13}) was found to have a very unusual broad I-SmA* transition peak which occurred over a temperature range from 92 to 62 °C in the DSC thermogram. Conversely, the transition appeared to be very sharp in the microscope, *i.e.* the transition did not occur over a temperature range. Its racemic counterpart **51** (8, CH_3, C_6H_{13}) exhibited only an I-SmA transition peak and no further transitions ware detected by DSC. However, the material apparently exhibited a SmC_{Alt} phase as observed by microscopy.

When an ethyl group is introduced to the R_1 position, the symmetrically branched swallow-tailed compound **54** (8, C_2H_5, C_2H_5) exhibited a SmC phase and the second order SmA-SmC transition was detected as a very small enthalpy (ΔH = -0.06 J/g). However, asymmetric compounds **55** (8, C_2H_5, C_3H_7) and **56** (8, C_2H_5, C_4H_9) were found to possess SmC_{Alt} phases. As mentioned previously, the transition peaks associated with the SmA-SmC_{Alt} transition of the achiral compounds **55** and **56** were not detected by DSC.

The longer asymmetric and symmetric swallow-tailed compounds, **57** (8, C_2H_5, C_5H_{11}), **58** (8, C_3H_7, C_3H_7) and **59** (8, C_4H_9, C_4H_9) did not exhibit either SmC or SmC_{Alt} phases.

When R_1 is substituted by a CF_3 group, the I-SmA transition temperature of compound **60*** (8, CF_3, C_6H_{13}) falls remarkably compared to the compound **50*** (8, CH_3, C_6H_{13}). A SmC_A phase which was not observed in the microscope was apparent in the DSC (ΔH = -0.05 J/g).

Summary

(a) When $R_1 = CH_3$, the compounds tend to have SmC_{Alt} or SmC_A* phases. If the compound is chiral, the peak associated with the transition from SmA* to SmC_A* appears with an extremely small enthalpy. In the case of the corresponding achiral compounds, the peak vanishes.

(b) When $R_1 = C_2H_5$, the compounds tend to have SmC phases and peaks associated with the transition SmA-SmC appear even when they are achiral.

(c) When $R_1 = CF_3$, the compound shows stable antiferroelectric behaviour, and this will be discussed in more detail later.

4.5 Effect of the Ester Linkage on the Mesophase (C10)

In this section, the physical and electrooptical properties of the homologous series of chiral and racemic 1-alkylalkyl 2",3"-difluoro-4"-decyloxyterphenyl-4-carboxylates are related.

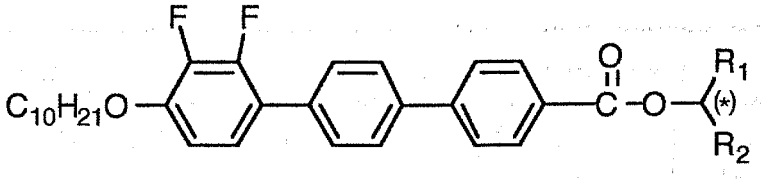

Compound **No.** (10, R_1, R_2)

4.5.1 Transition Temperatures and Phase Behaviour

The transition temperatures of the compounds **62*-73** were measured by thermal optical polarizing microscopy on cooling and these are listed in Table 4.5.1.

Compounds **62*-73** were analyzed by DSC using heating and cooling rates of 10 °C min^{-1}, the transition temperatures and enthalpies are listed in Table 4.5.2 (compounds **62*-67**) and Table 4.5.3 (compounds **68-73**) and their thermograms are seen in Fig. 4.5.1 (compounds **62*-67**), Fig. 4.5.2 (expanded), Fig. 4.5.3 (compounds **68-73**), and Fig. 4.5.4 (expanded).

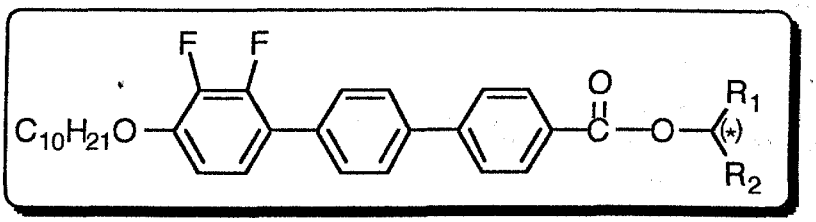

Compound **No.** (10, R_1, R_2)

Compounds			Transition Temperatures / °C								
No.	**R_1**	**R_2**	**I**		**SmA (*)**		**SmCα (*)**		**SmC (*)**		**K**
62*	CH_3	C_5H_{11}	•	94.6	•	-	-	-	-	37.0	•
63	CH_3	C_5H_{11}	•	96.9	•	-	-	69.9	•	23.8	•
64*	CH_3	C_6H_{13}	•	93.5	•	-	-	-	-	45.7	•
65	CH_3	C_6H_{13}	•	93.1	•	-	-	62.8	•	24.5	•
66	CH_3	C_7H_{15}	•	91.5	•	-	-	68.1	•	29.9	•
67	CH_3	C_8H_{17}	•	89.5	•	-	-	66.3	•	32.7	•
68	C_2H_5	C_2H_5	•	91.8	•	-	-	43.0	•	31.3	•
69	C_2H_5	C_3H_7	•	77.0	•	-	-	-	-	39.8	•
70	C_2H_5	C_4H_9	•	65.8	•	-	-	28.5	•	27.3	•
71	C_2H_5	C_5H_{11}	•	57.6	•	-	-	-	-	1.30	•
72	C_3H_7	C_3H_7	•	52.0	•	-	-	-	-	51.9	•
73	C_4H_9	C_4H_9	•	38.3	•	-	-	-	-	25.7	•

*.... Optically active: compound **62** (*R*)-, compound **64** (*S*)-

Table 4.5.1 Transition temperatures for the 1-alkylalkyl 2",3"-difluoro-4"-decyloxyterphenyl-4-carboxylates determined by thermal optical polarized light microscopy, on cooling.

Compounds			Transition Temperatures[a] / °C and Associated Enthalpies[b] / [J/g]									
No.	R_1	R_2	I		SmA (*)		SmC_α (*)		SmC (*)		K	mp
62*	CH_3	C_5H_{11}	•	92.6 [-7.56]	•	71.1[c] [-0.24]	•	-	-	34.3 [-30.6]	•	50
63	CH_3	C_5H_{11}	•	93.8 [-8.01]	•	-	-	67.1 [-0.14]	•	9.80 [-33.6]	•	48
64*	CH_3	C_6H_{13}	•	91.0 [-6.41]	•	69.3[c] [-0.07]	•	-	-	44.7 [-33.5]	•	60
65	CH_3	C_6H_{13}	•	90.8 [-7.83]	•	-	-	62.1 [-0.02]	•	-2.77 [-18.8]	•	49
66	CH_3	C_7H_{15}	•	88.9 [-7.65]	•	-	-	65.2 [-0.11]	•	24.3 [-21.6]	•	51
67	CH_3	C_8H_{17}	•	87.5 [-7.72]	•	-	-	64.2 [-0.09]	•	26.0 [-22.0]	•	51

[a].... Recorded at cooling rate of 10 °C min^{-1} [b].... Enthalpies of transition given in square brackets [c].... Transition not detected in microscope

Table 4.5.2 Transition temperatures for the 1-alkylakyl 2",3"-difluoro-4"-decyloxyterphenyl-4-carboxylates determined by DSC measurements, on cooling.

Compounds			Transition Temperatures[a] / °C and Associated Enthalpies[b] / [J/g]									
No.	**R_1**	**R_2**	**I**		**SmA (*)**		**SmC_α (*)**		**SmC (*)**		**K**	**mp**
68	C_2H_5	C_2H_5	•	88.8 [-6.71]	•	-	-	40.7 [-0.06]	•	26.8 [-41.6]	•	63
69	C_2H_5	C_3H_7	•	73.2 [-5.62]	•	-	-	-	-	36.0 [-49.8]	•	42
70	C_2H_5	C_4H_9	•	63.3 [-4.99]	•	-	-	26.4 [-0.04]	•	19.4 [-38.5]	•	38
71	C_2H_5	C_5H_{11}	•	54.9 [-4.63]	•	-	-	-	-	1.30 [-29.7]	•	32
72	C_3H_7	C_3H_7	•	49.1 [-3.20]	•	-	-	-	-	46.8 [-32.0]	•	55
73	C_4H_9	C_4H_9	•	35.1 [-3.60]	•	-	-	-	-	19.4 [-22.2]	•	45

[a].... Recorded at cooling rate of 10 °C min^{-1} [b].... Enthalpies of transition given in square brackets

Table 4.5.3 Transition temperatures for the 1-alkylakyl 2",3"-difluoro-4"-decyloxyterphenyl-4-carboxylates determined by DSC measurements, on cooling.

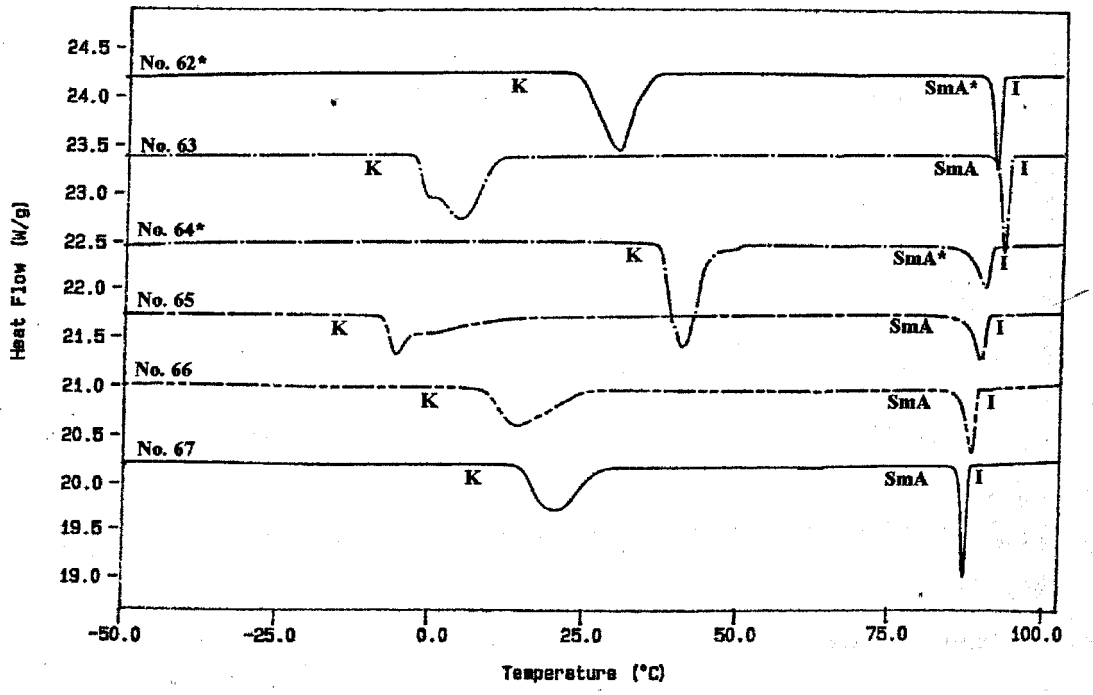

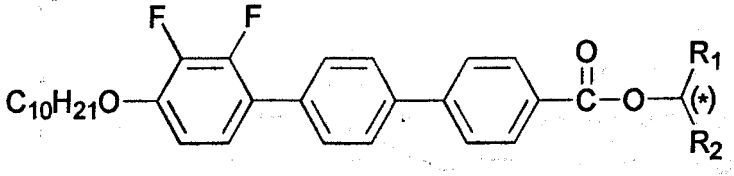

Compounds No.	R_1	R_2
62*	CH_3	C_5H_{11}
63	CH_3	C_5H_{11}
64*	CH_3	C_6H_{13}
65	CH_3	C_6H_{13}
66	CH_3	C_7H_{15}
67	CH_3	C_8H_{17}

Fig. 4.5.1 DSC thermograms of compounds **62*-67**

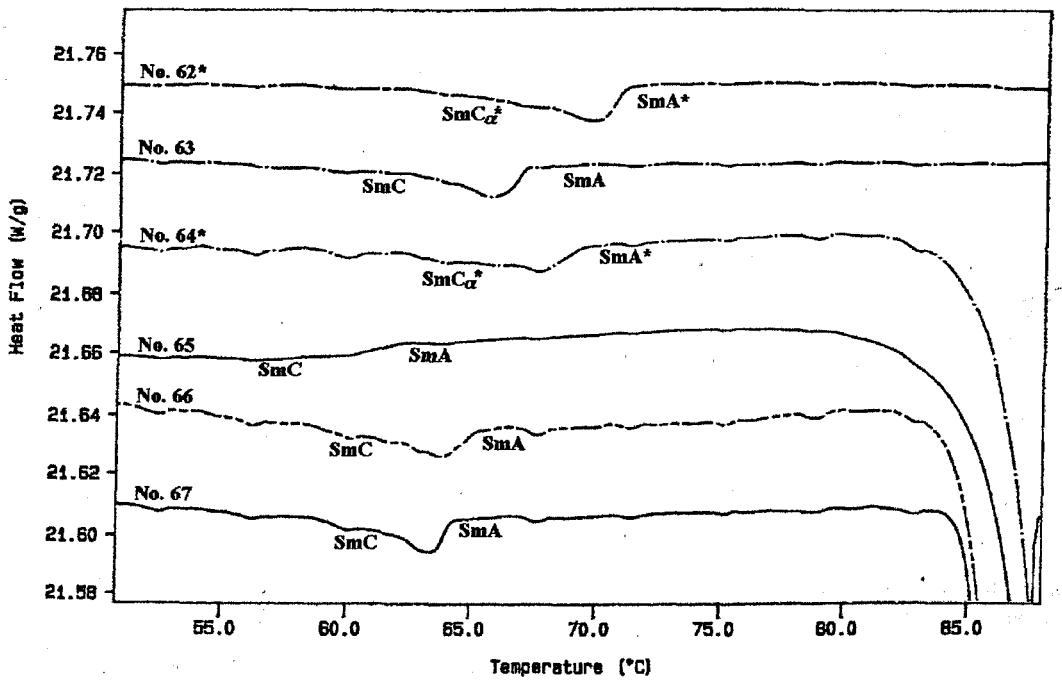

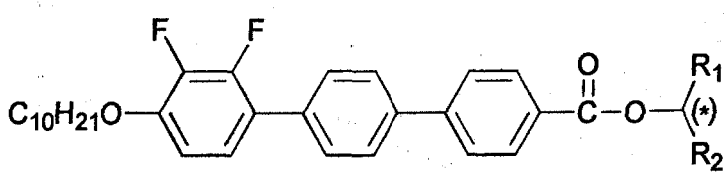

Compounds No.	R_1	R_2
62*	CH_5	C_5H_{11}
63	CH_3	C_5H_{11}
64*	CH_3	C_6H_{13}
65	CH_3	C_6H_{13}
66	CH_3	C_7H_{15}
67	CH_3	C_8H_{17}

Fig. 4.5.2 Expanded DSC thermograms of compounds **62*-67**

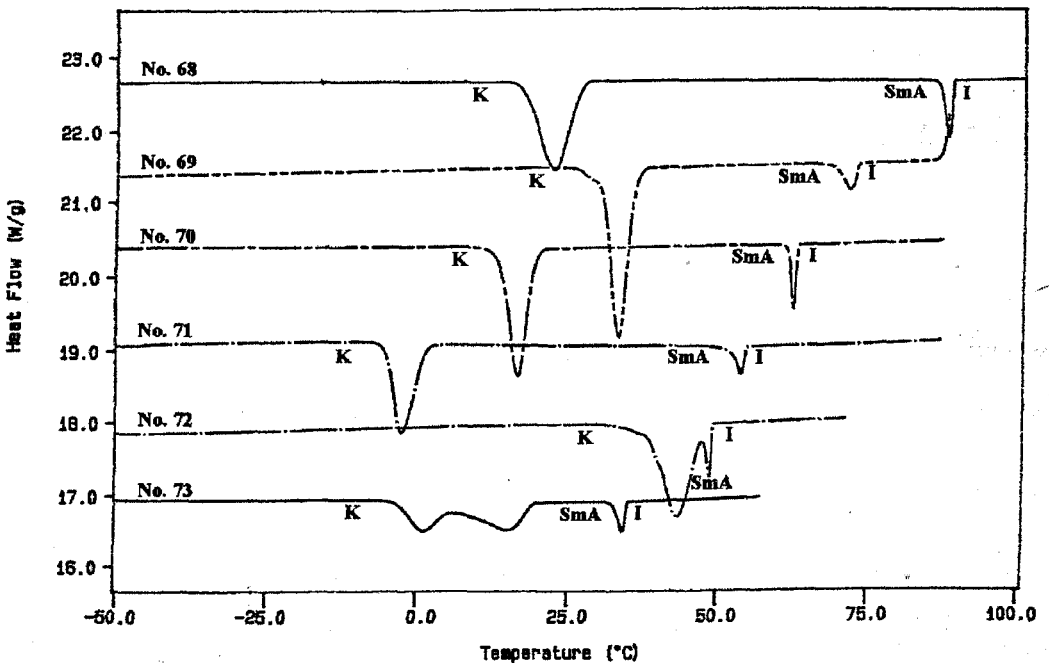

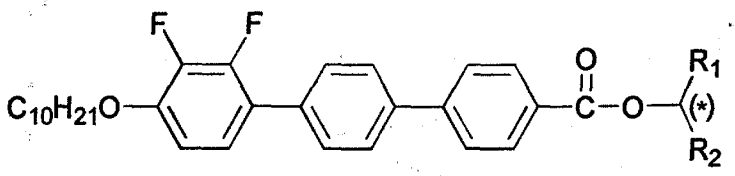

Compounds No.	R_1	R_2
68	C_2H_5	C_2H_5
69	C_2H_5	C_3H_7
70	C_2H_5	C_4H_9
71	C_2H_5	C_5H_{11}
72	C_3H_7	C_3H_7
73	C_4H_9	C_4H_9

Fig. 4.5.3 DSC thermograms of compounds **68-73**

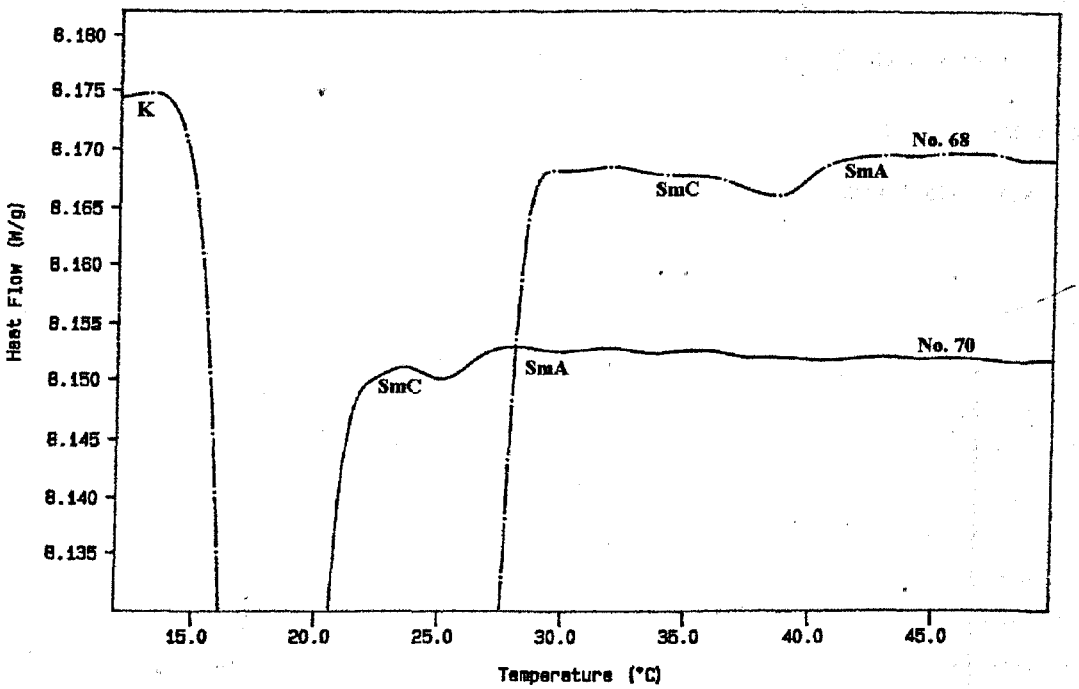

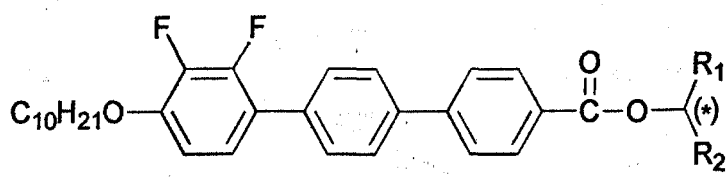

Compounds No.	R_1	R_2
68	C_2H_5	C_2H_5
70	C_2H_5	C_4H_9

Fig. 4.5.4 Expanded DSC thermograms of compounds **68** and **70**

Every compound in this homologous series was found to exhibit a SmA (or SmA*) phase. The I-SmA transition temperatures are lower compared to those observed for the octyloxy homologous series of compounds (8, R_1, R_2) (see Table 4.4.1). In Fig. 4.5.5, the I-SmA transition temperatures of the racemic compounds are plotted as a function of R_2 chain length where R_1 = CH_3, C_2H_5, C_3H_7 and C_4H_9. As R_1 increases in length, the SmA phase becomes destabilized.

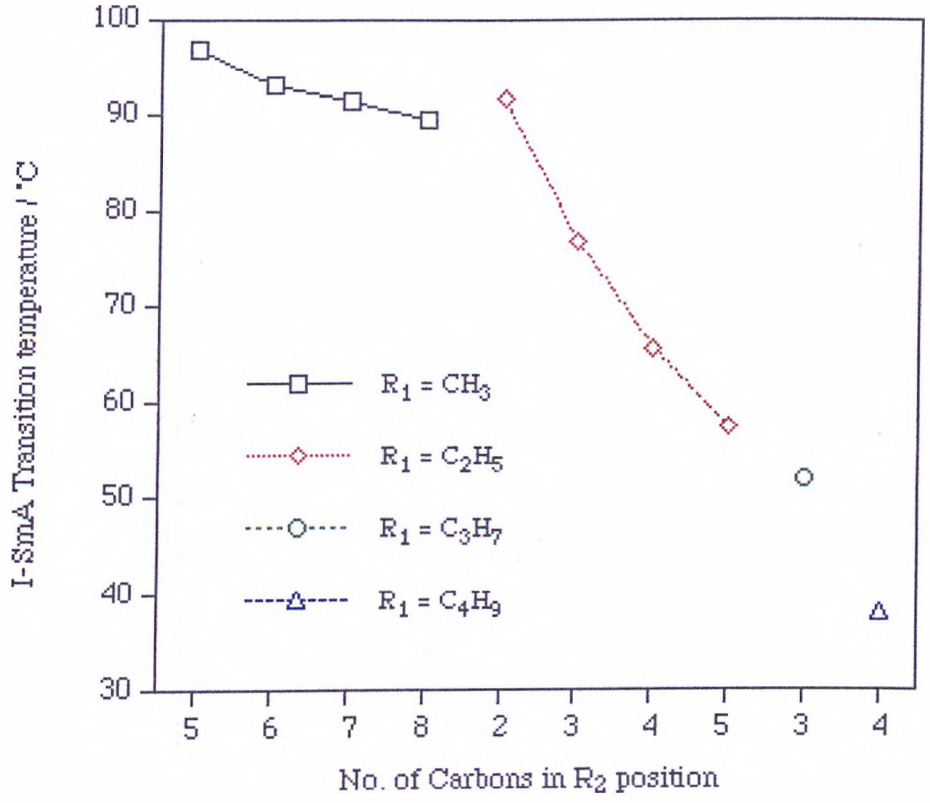

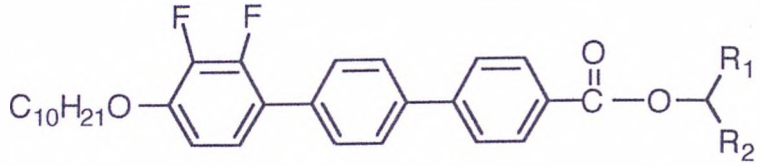

Fig. 4.5.5 I-SmA transition temperature versus R_2

In microscopy studies, racemic compounds **63** (10, CH_3, C_5H_{11}) and **65** (10, CH_3, C_6H_{13}) were found to have I-SmC sequences which showed very small enthalpies,

ΔH = -0.14 J/g and -0.02 J/g, respectively. In comparison to the compounds **49** (8, CH_3, C_5H_{11}) and **51** (8, CH_3, C_6H_{13}), increasing the alkoxy chain length suppresses as the antiferroelectric ordering, but opposing this trend, the SmC phase was enhanced by more than 16 °C as shown below:

Compounds **No.**								
49 (8, CH_3, C_5H_{11})	I	101.6 °C	SmA	-		53.2	SmC_{Alt}	20.2 K
63 (10, CH_3, C_5H_{11})	I	96.9	SmA	69.9	SmC	-		23.8 K
51 (8, CH_3, C_6H_{13})	I	99.9	SmA	-		36.5	SmC_{Alt}	28.7 K
65 (10, CH_3, C_6H_{13})	I	93.1	SmA	62.8	SmC	-		24.5 K

Their chiral counterparts compounds **62*** (10, CH_3, C_5H_{11}) and **64*** (10, CH_3, C_6H_{13}) exhibited peaks associated with a SmA*-SmC* phase transition which occurred *via* a SmC_α* phase as observed by DSC (The phase transitions were confirmed by means of electrical field studies which will be discussed later.) However, changes in the defect textures associated with the SmC_α* and the SmC* phases were not observed in the microscope.

The longer alkyl chain compounds, **66** (10, CH_3, C_7H_{15}) and **67** (10, CH_3, C_8H_{17}), were found not to exhibit antiferroelectric ordering, however, SmC phases were observed in the higher temperature region compared to SmC_{Alt} phases found for compounds **51** (8, CH_3, C_7H_{15}) and **52** (8, CH_3, C_7H_{15}).

Mesophase stability was significantly reduced for the symmetrically branched swallow-tailed compounds **72** (10, C_3H_7, C_3H_7) and **73** (10, C_4H_7, C_4H_7) in comparison to the unsymmetrically substituted systems. They were found to possess only very narrow SmA phases, which were monotropic. However, in the case of compound **68** (10, C_2H_5, C_2H_5), which had the shortest symmetrical branching

substituent, the mesophase behaviour was reasonably stable and as a consequence SmA and SmC phases were observed.

When an ethyl group is introduced for the R_1 position, *e.g.* compound **70** (10, C_2H_5, C_4H_9), only narrow SmC phases were observed. SmC phases were suppressed totally in compounds **69** (10, C_2H_5, C_3H_7) and **71** (10, C_2H_5, C_5H_{11}).

Summary

(a) In this homologous series (10, R_1, R_2), increasing the alkoxy chain decreases the I-SmA phase transition temperature compared to that seen in the homologous series (8, R_1, R_2).

(b) SmC phases are dominant, therefore, SmC_{Alt} phases are suppressed for the asymmetrically branched compounds.

(c) Interestingly, chiral compounds **62*** (10, CH_3, C_5H_{11}) and **64*** (10, CH_3, C_6H_{13}) show an intermediary state, SmC_α*, between the SmA* and SmC* phases. This implies that the SmC* structure is more competitive than the antiferroelectric ordering.

4.6 Effect of the Ester Linkage on Mesophase (C14)

In this section, the physical and electrooptic properties of the homologous series of chiral and racemic 1-alkylalkyl 2",3"-difluoro-4"-tetradecyloxyterphenyl-4-carboxylates are reported.

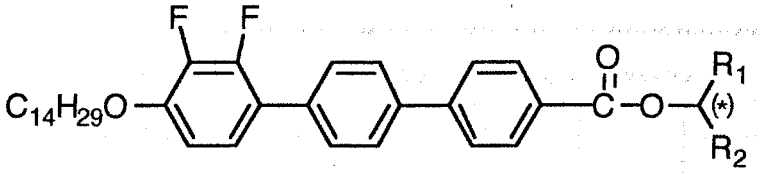

Compound **No**. (14, R_1, R_2)

4.6.1 Transition Temperatures and Phase Behaviour

The transition temperatures of the compounds **100*-111** were determined by thermal optical polarizing microscopy on cooling, and the results are given in Table 4.6.1.

Compounds **100*-111** were analyzed by DSC using heating and cooling rates of 10 °C min^{-1}, the transition temperatures and enthalpies are listed in Table 4.6.2 (compounds **100*-105**) and Table 4.6.3 (compounds **106-111**) and their thermograms are shown in Fig. 4.6.1 (compounds **100-105**), Fig. 4.6.2 (expanded) and Fig. 4.6.3 (compounds **106-111**).

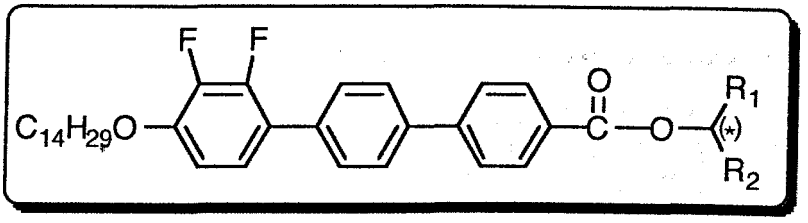

Compound **No.** (14, R_1, R_2)

Compounds			Transition Temperatures / °C								
No.	R_1	R_2	I		SmA (*)		SmC_α (*)		SmC (*)		K
100*	CH_3	C_5H_{11}	•	87.4	•	-	-	-	-	56.9	•
101	CH_3	C_5H_{11}	•	89.1	•	-	-	65.3	•	38.5	•
102*	CH_3	C_6H_{13}	•	86.5	•	-	-	-	-	47.7	•
103	CH_3	C_6H_{13}	•	87.5	•	-	-	71.0	•	32.5	•
104	CH_3	C_7H_{15}	•	84.9	•	-	-	73.1	•	36.9	•
105	CH_3	C_8H_{17}	•	83.3	•	-	-	72.6	•	35.8	•
106	C_2H_5	C_2H_5	•	87.3	•	-	-	-	-	33.2	•
107	C_2H_5	C_3H_7	•	72.0	•	-	-	-	-	38.1	•
108	C_2H_5	C_4H_9	•	61.1	•	-	-	-	-	29.7	•
109	C_2H_5	C_5H_{11}	•	53.5	•	-	-	-	-	30.2	•
110	C_3H_7	C_3H_7	•	48.2	•	-	-	-	-	43.7	•
111	C_4H_9	C_4H_9	•	34.4	•	-	-	-	-	24.8	•

*.... Optically active: compound **100** (*R*)-, compound **102** (*S*)-

Table 4.6.1 Transition temperatures for the 1-alkylakyl 2",3"-difluoro-4"-tetradecyloxyterphenyl-4-carboxylates determined by thermal optical polarized light microscopy, on cooling.

Compounds			Transition Temperatures[a] / °C and Associated Enthalpies[b] / [J/g]									
No.	R_1	R_2	I		SmA (*)		SmC_α (*)		SmC		K	mp
100*	CH_3	C_5H_{11}	•	86.3 [-6.43]	•	67.8[c] [-0.12]	•	-	-	47.6 [-65.1]	•	69
101	CH_3	C_5H_{11}	•	84.6 [-6.82]	•	-	-	62.3 [-0.04]	•	25.6 [-57.7]	•	52
102*	CH_3	C_6H_{13}	•	83.5 [-6.54]	•	-	-	69.4[c] [-0.16]	•	50.9 [-63.7]	•	65
103	CH_3	C_6H_{13}	•	86.3 [-7.53]	•	-	-	69.3 [-0.15]	•	28.8 [-57.3]	•	57
104	CH_3	C_7H_{15}	•	83.3 [-7.63]	•	-	-	71.1 [-0.22]	•	32.1 [-57.4]	•	53
105	CH_3	C_8H_{17}	•	82.1 [-7.50]	•	-	-	71.2 [-0.29]	•	28.6 [-56.4]	•	54

[a].... Recorded at cooling rate of 10 °C min^{-1} [b].... Enthalpies of transition given in square brackets [c].... Transition not detected in microscope

Table 4.6.2 Transition temperatures for the 1-alkylakyl 2",3"-difluoro-4"-tetradecyloxyterphenyl-4-carboxylates determined by DSC measurements, on cooling.

Compounds			Transition Temperatures[a] / °C and Associated Enthalpies[b] / [J/g]										
No.	R_1	R_2	I		SmA (*)		SmC_α (*)		SmC (*)		K	mp
106	C_2H_5	C_2H_5	•	84.5 [-6.72]	•	-	-	-	-	23.2 [-47.3]	•	41
107	C_2H_5	C_3H_7	•	69.2 [-5.45]	•	-	-	-	-	34.9 [-48.8]	•	57
108	C_2H_5	C_4H_9	•	59.2 [-4.94]	•	-	-	-	-	21.8 [-43.0]	•	46
109	C_2H_5	C_5H_{11}	•	51.6 [-4.10]	•	-	-	-	-	16.8 [-40.0]	•	42
110	C_3H_7	C_3H_7	•	44.4 [-4.16]	•	-	-	-	-	34.9 [-50.5]	•	55
111	C_4H_9	C_4H_9	•	31.4 [-3.63]	•	-	-	-	-	7.00 [-31.9]	•	39

[a].... Recorded at cooling rate of 10 °C min^{-1} [b].... Enthalpies of transition given in square brackets [c].... Transition not detected in microscope

Table 4.6.3 Transition temperatures for the 1-alkylakyl 2",3"-difluoro-4"-tetradecyloxyterphenyl-4-carboxylates determined by DSC measurements, on cooling.

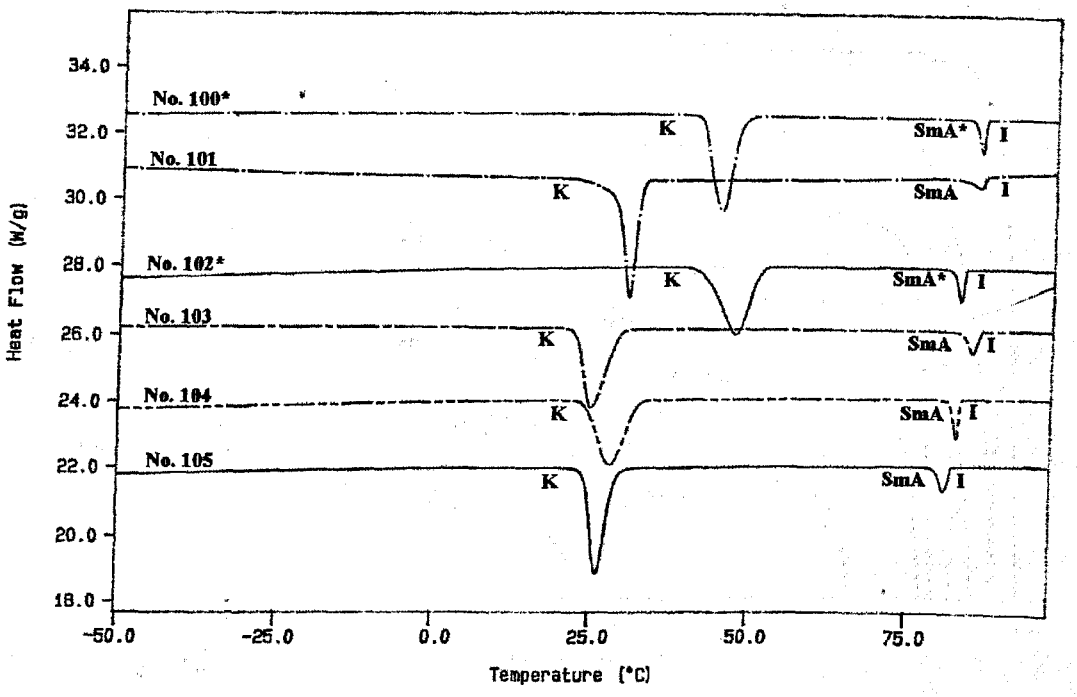

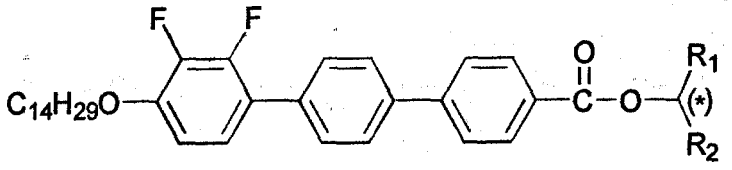

Compounds No.	R_1	R_2
100*	CH_3	C_5H_{11}
101	CH_3	C_5H_{11}
102*	CH_3	C_6H_{13}
103	CH_3	C_6H_{13}
104	CH_3	C_7H_{15}
105	CH_3	C_8H_{17}

Fig. 4.6.1 DSC thermograms of compounds **100*-105**

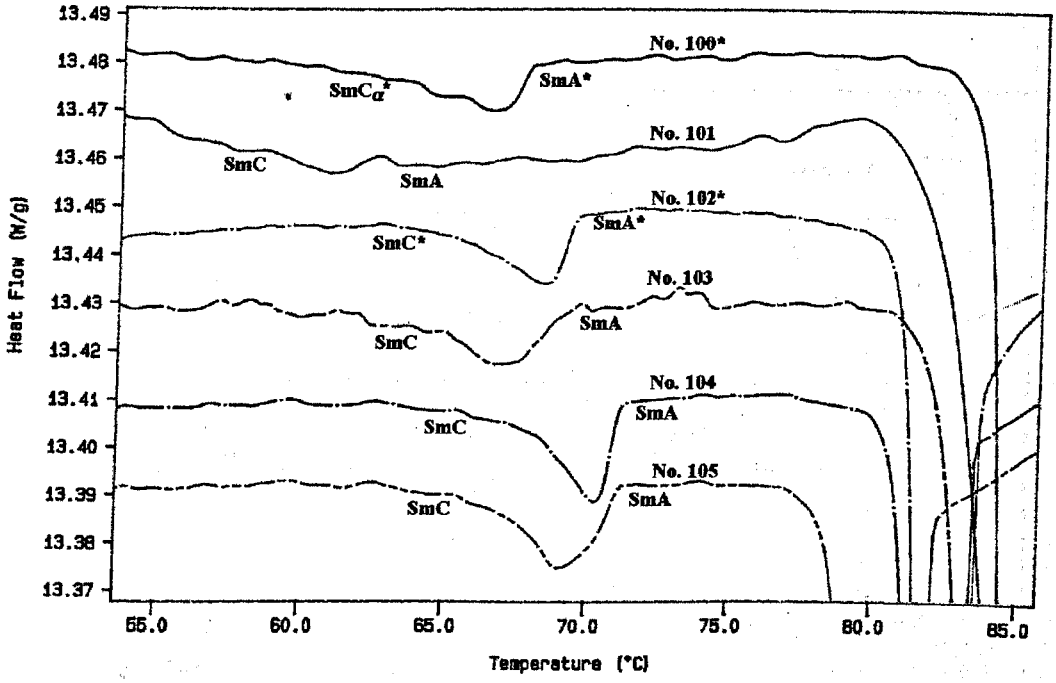

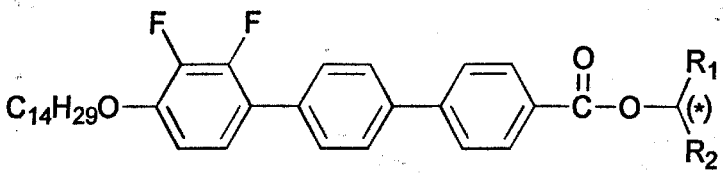

Compounds No.	R_1	R_2
100*	CH_3	C_5H_{11}
101	CH_3	C_5H_{11}
102*	CH_3	C_6H_{13}
103	CH_3	C_6H_{13}
104	CH_3	C_7H_{15}
105	CH_3	C_8H_{17}

Fig. 4.6.2 Expanded DSC thermograms of compounds **100*-105**

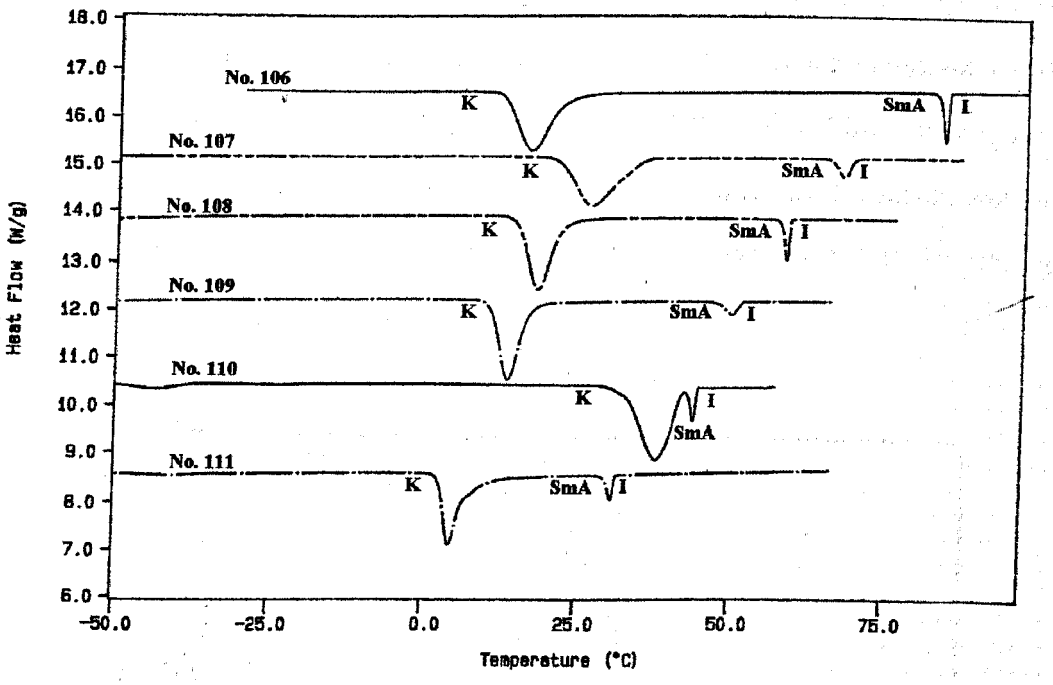

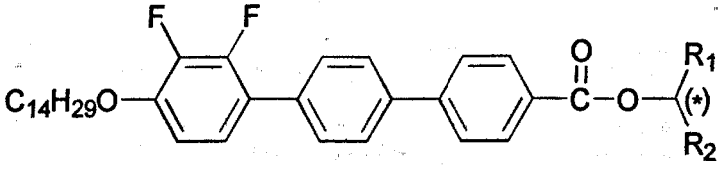

Compounds No.	R_1	R_2
106	C_2H_5	C_2H_5
107	C_2H_5	C_3H_7
108	C_2H_5	C_4H_9
109	C_2H_5	C_5H_{11}
110	C_3H_7	C_3H_7
111	C_4H_9	C_4H_9

Fig. 4.6.3 DSC thermograms of compounds **106-111**

Every compound in this homologous series was found to exhibit a SmA (or SmA*) phase. The I-SmA transition temperatures are the lowest in comparison to those observed for the homologous series of compounds (8, R_1, R_2) and compounds (10, R_1, R_2), see Tables 4.4.1 and 4.5.1. In Fig. 4.6.4, the I-SmA transition temperatures of the racemic compounds as a function of the chain length for the R_2 substituent are plotted when $R_1 = CH_3$, C_2H_5, C_3H_7 and C_4H_9. As R_1 increases in chain length, the SmA phase becomes destabilized.

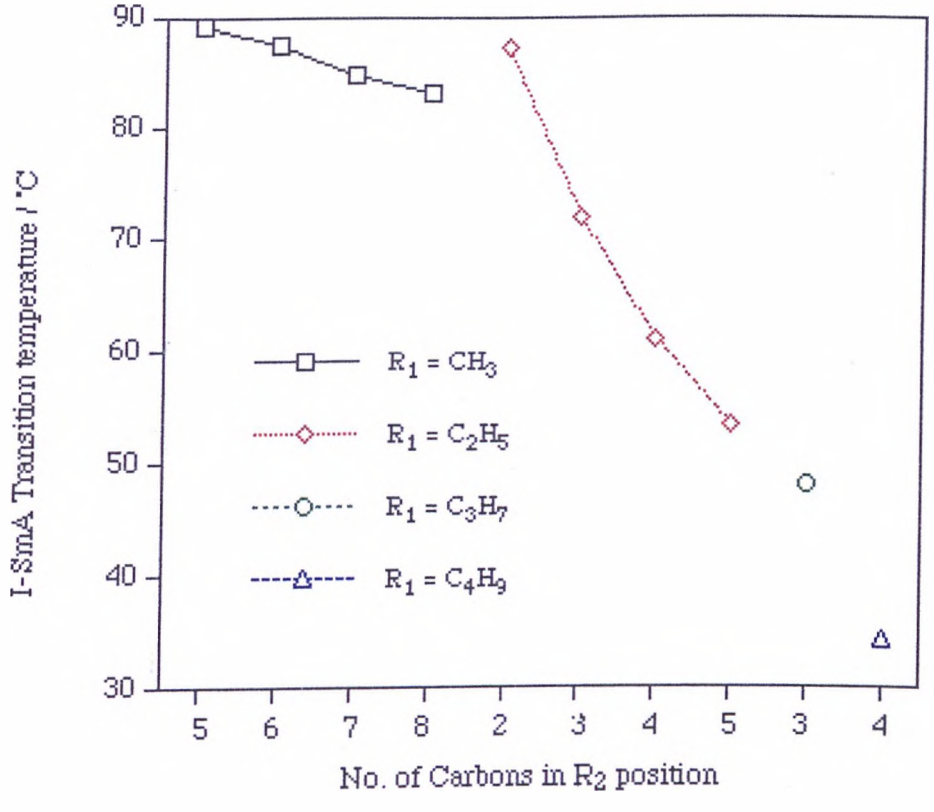

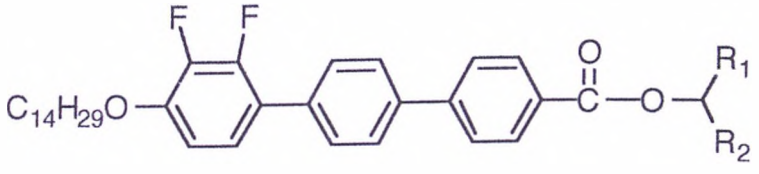

Fig. 4.6.4 I-SmA Transition temperature versus R_2

Chiral compound **100*** (14, CH_3, C_5H_{11}) exhibited a peak associated with the SmA*-SmC* transition which occurred *via* the formation of a SmC_α* phase in the DSC. In the same way as mentioned previously, the transition to the SmC* phase which was formed *via* formation of an intermediary phase was not confirmed by the microscopy. Its counterpart racemic compound **101** (14, CH_3, C_5H_{11}), was shown to possess a SmC phase by microscopy. Another chiral compound **103*** (14, CH_3, C_6H_{13}) exhibited a peak associated with the SmA*-SmC* transition, which was also ratified by electric field studies. For this compound, the SmC_α* phase could not be detected by DSC.

The compounds with longer chains at the asymmetric branching point, *e.g.* compounds **103** (14, CH_3, C_6H_{13}), **104** (14, CH_3, C_7H_{15}) and **105** (14, CH_3, C_8H_{17}) exhibited more stable SmC phases which are enhanced by more than 6 °C in comparison to those found in compounds **65** (10, CH_3, C_6H_{13}), **66** (10, CH_3, C_7H_{15}) and **67** (10, CH_3, C_8H_{17}) respectively (see Table 4.4.4).

Upon introducing an ethyl unit into the R_1 position, *e.g.* compounds **107** (14, C_2H_5, C_3H_7), **108** (14, C_2H_5, C_4H_9) and **109** (14, C_2H_5, C_5H_{11}), the *I*-SmA transition temperatures fell to the lowest point in comparison to those found for the homologous series (8, C_2H_5, R_2) and (10, C_2H_5, R_2). Thus, it is assumed that highly ordered smectic mesophases do not appear due to decreased mosophase stability.

The symmetrically branched compounds, **106** (14, C_2H_5, C_2H_5), **110** (14, C_3H_7, C_3H_7) and **111** (14, C_4H_9, C_4H_9) exhibited only SmA mesophases.

Summary

(a) The asymmetrically branched compounds show more stable SmC phases compared to those found for the homologous series (10, R_1, R_2).

(b) For the chiral compounds, compound **100*** (14, CH_3, C_5H_{11}) exhibited a

SmA*-SmC* phase transition which occurred *via* an intermediary state SmC_{α}* phase whereas for compound **102*** (14, CH_3, C_6H_{13}), the SmC_{α}* phase was not present.

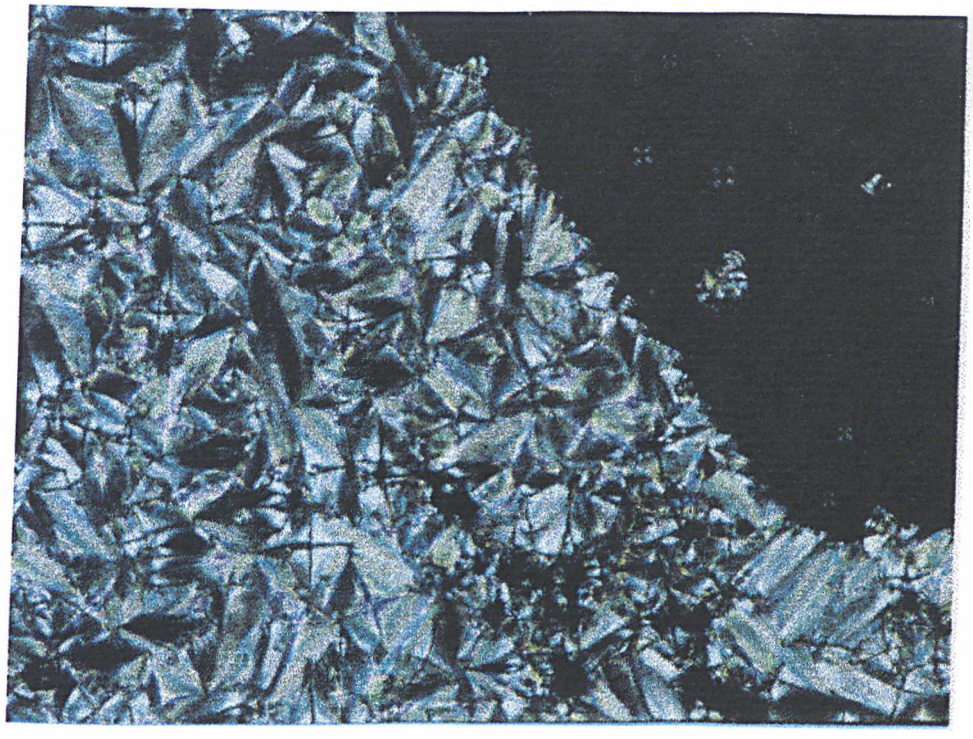

Plate 20 The banded focal conic defect texture (SmC_{Alt}) of compound **49** (8, CH_3, C_5H_{11}) at 48.2 °C

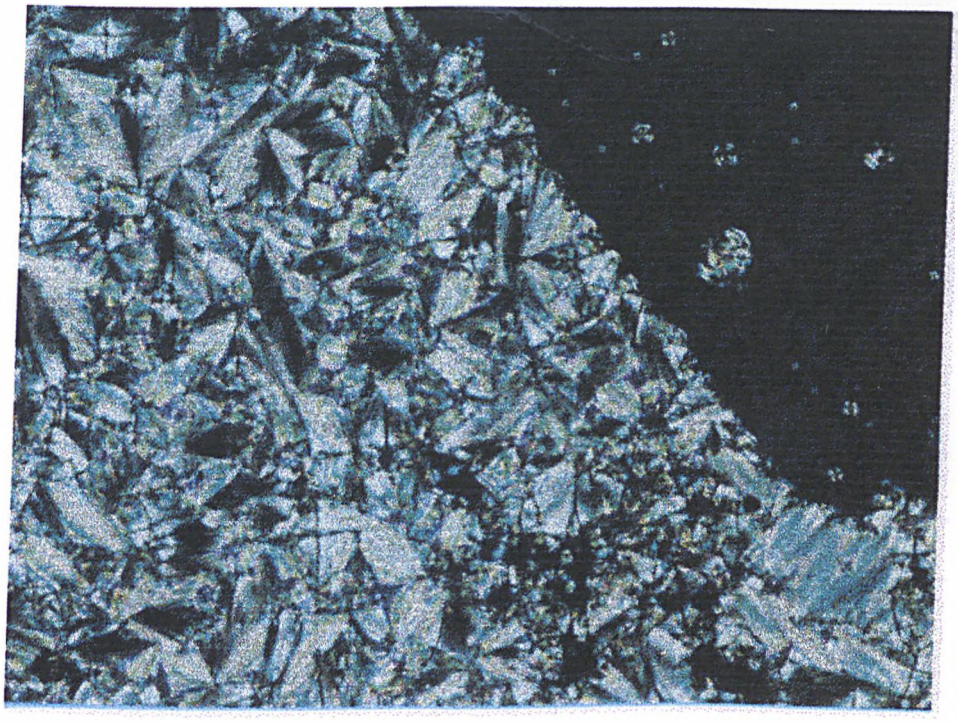

Plate 21 The banded focal conic defect and *schlieren* textures (SmC_{Alt}) of compound **49** (8, CH_3, C_5H_{11}) at 45.6 °C

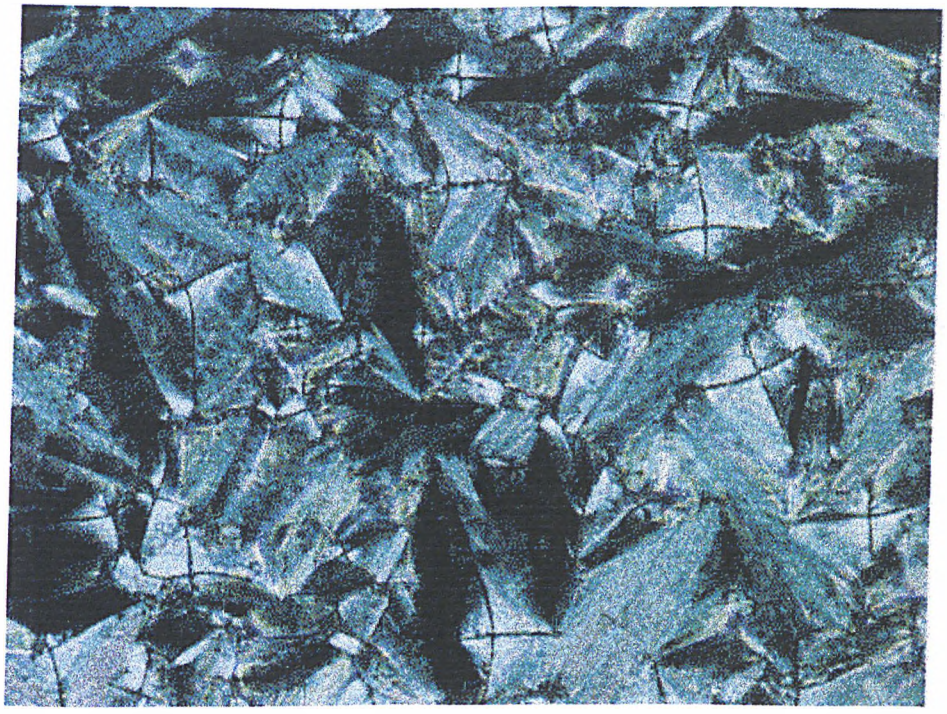

Plate 22 The banded focal conic defect texture (SmC_{Alt}) of compound **52** (8, CH_3, C_7H_{15}) at 32.7 °C

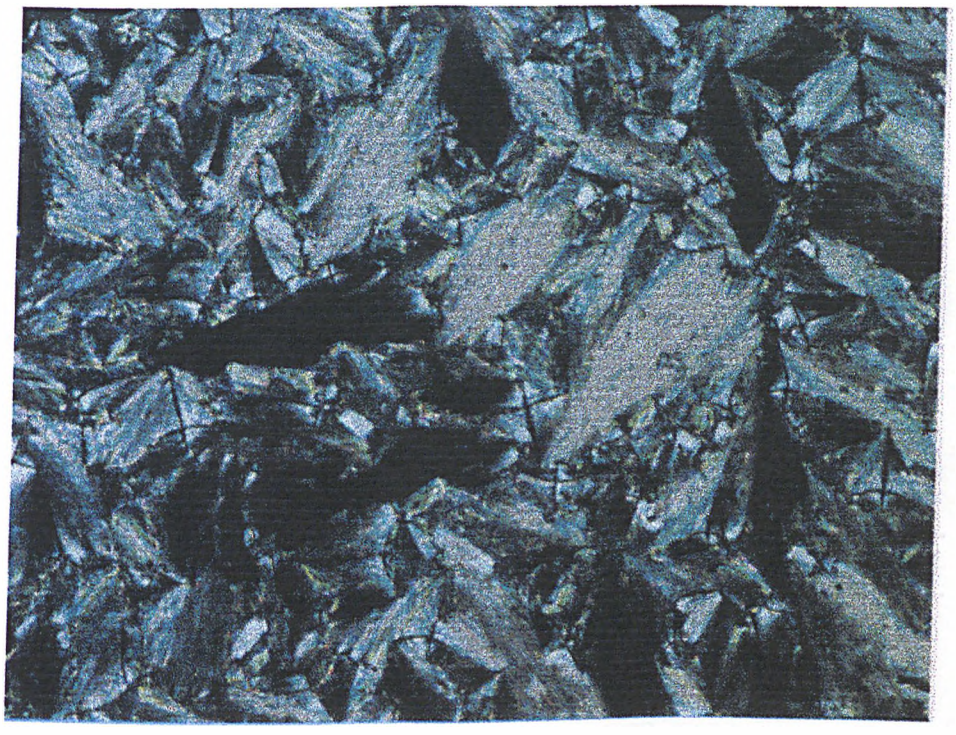

Plate 23 The broken focal conic defect texture (SmC) of compound **54** (8, C_2H_5, C_2H_5) at 43.0 °C

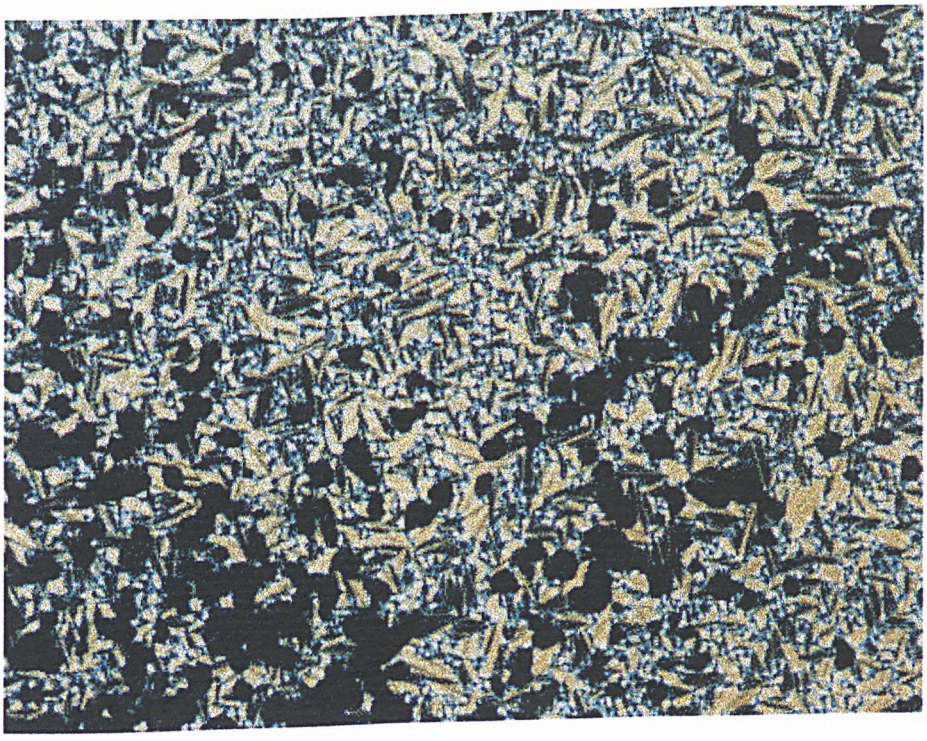

Plate 24 The focal conic defect texture of compound **60*** (8, CF_3, C_6H_{13}) at 40 °C

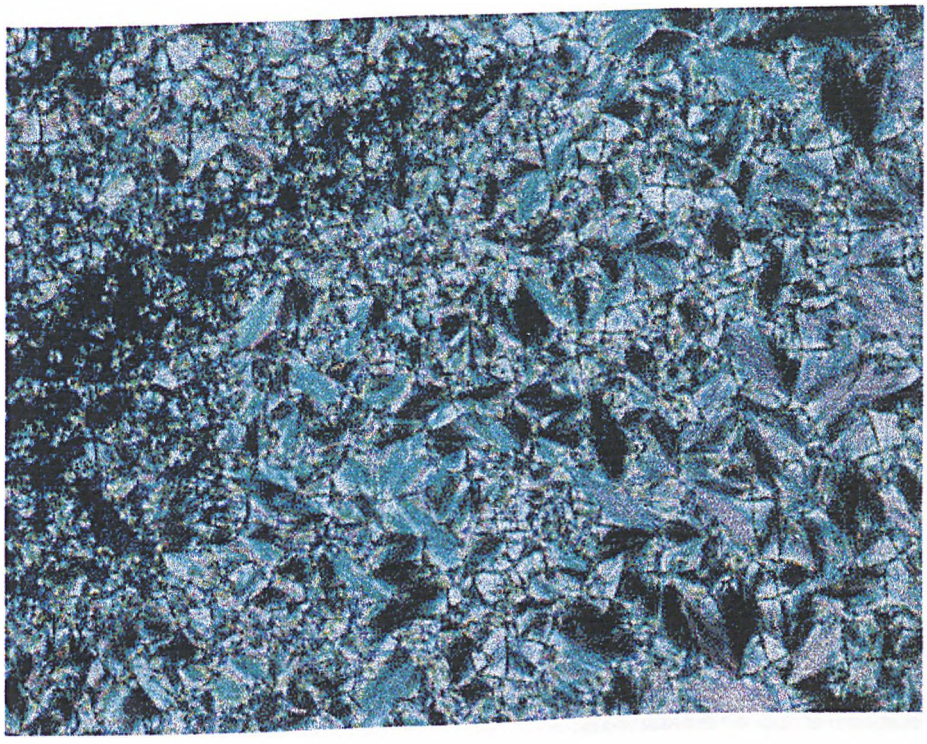

Plate 25 The broken focal conic defect texture (SmC) of compound **67** (10, CH_3, C_8H_{17}) at 65.4 °C

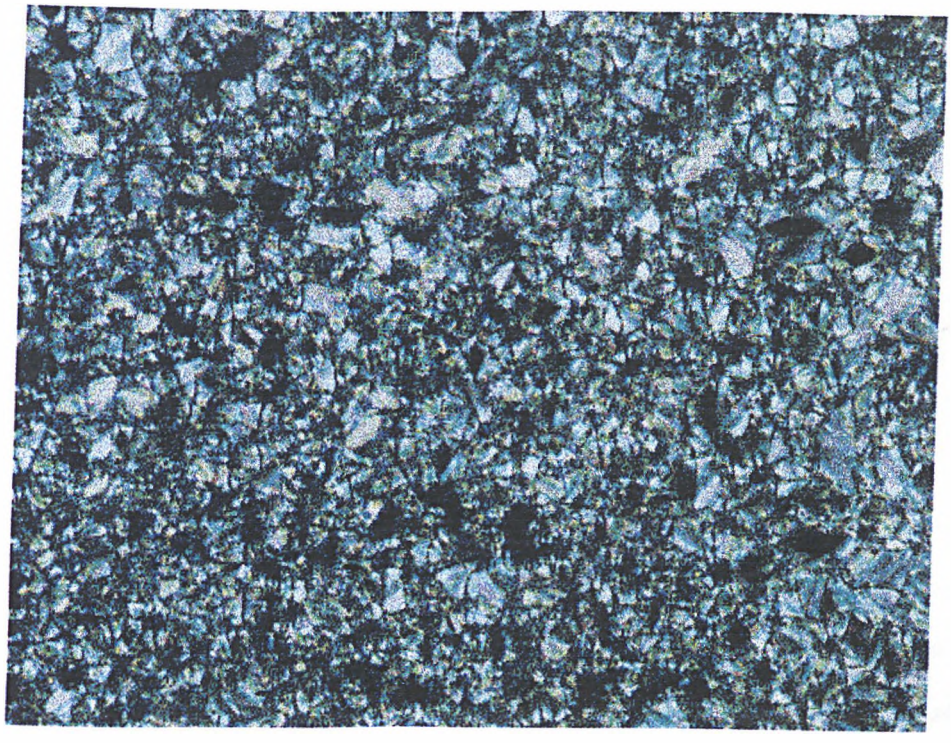

Plate 26 The broken focal conic defect texture (SmC) of compound **68** (10, C_2H_5, C_2H_5) at 42.5 °C

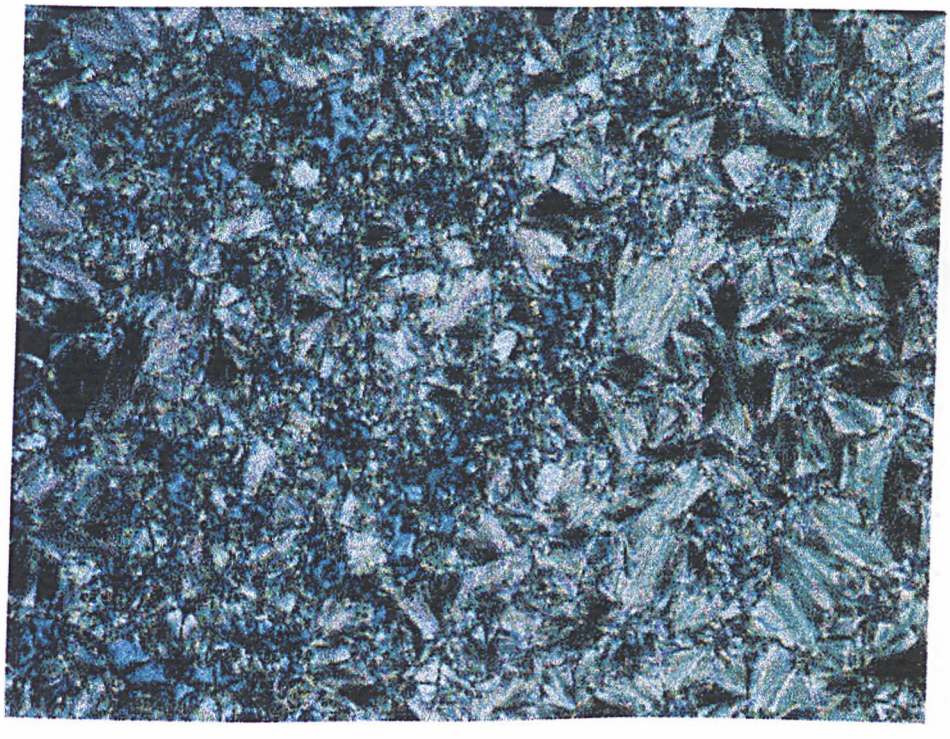

Plate 27 The broken focal conic defect and *schlieren* textures (SmC) of compound **104** (14, CH_3, C_7H_{15}) at 71.7 °C

4.7 Electrooptic Studies

The polarization reversal currents for compounds (**48***, **50***, **60***, **61***, **62***, **64***, **100*** and **102***) were measured on cooling using cells with 0.25 cm^2 electrode areas and plate separations of 5.0 μm.

Fig. 4.7.1 (a) shows the overall trend for the Ps of compound **48*** (8, CH_3, C_5H_{11}) at fixed applied voltage, 5.9 V/μm, 20 Hz and a temperature range 62.0-56.0 °C. A small peak begins to appear at 62 °C. This peak become bigger, and then splitting of the peaks occur at 58.0 °C at the SmC*-SmC_A* phase transition. At this transition temperature, the Ps value increases by 10.0 nC cm^{-2} compared to that observed at a temperature of 58.5 °C. Split peaks are unique and diagnostic for the presence of a SmC_A*. As most polarization reversal peaks observed for the typical SmC_A* phases are well-separated, the fact that the peaks are not well-separated for compound **48*** (8, CH_3, C_5H_{11}) indicates it may show very fast switching in a device.

Fig. 4.7.1 (b) shows the field dependence of the Ps for the SmC_A* phase of compound **48*** (8, CH_3, C_5H_{11}), using an applied voltage of 1.18-10.6 V/μm with 1.18 V/μm steps, 20 Hz and 56.0 °C. At the lower applied voltage, the split peaks show a broad signal followed by a small peak. As the applied voltage is increased, split peaks become sharper and more closer. Finally, the peaks appear as a single peak with a shoulder.

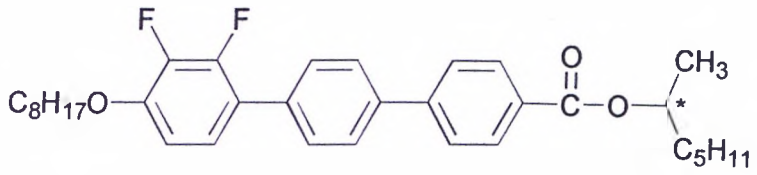

(a)

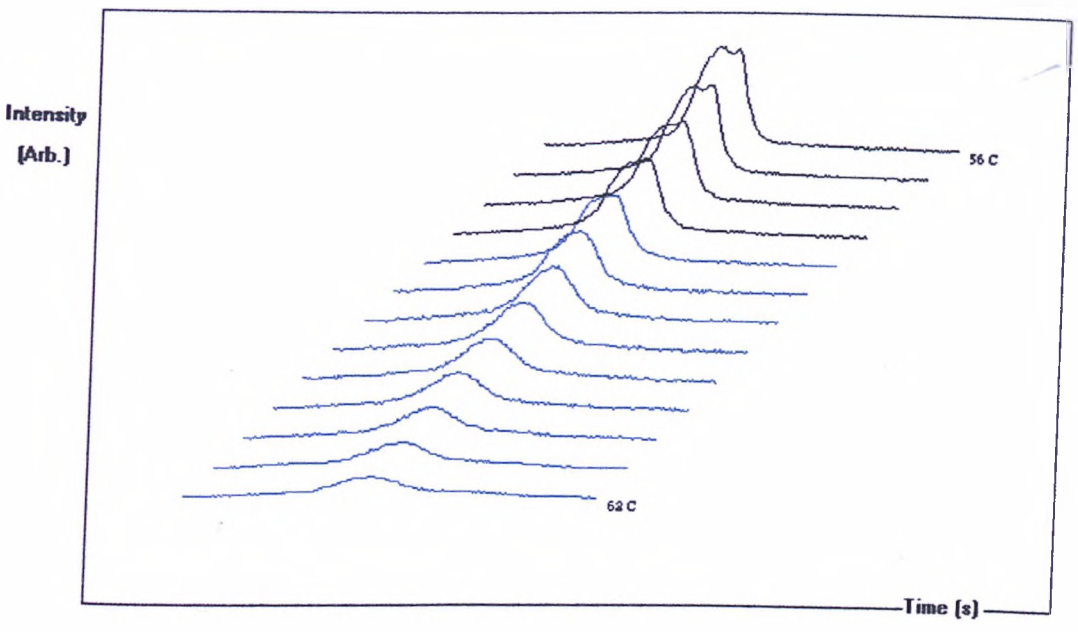

(a)

Temp. (°C)	Ps (nCcm^{-2})	Temp. (°C)	Ps (nCcm^{-2})
62.0	9.2	58.5	34.8
61.5	12.3	58.0	44.8
61.0	16.8	57.5	48.8
60.5	18.8	57.0	52.4
60.0	23.0	56.5	56.4
59.5	28.6	56.0	64.8
59.0	31.1		

measured at 5.9 V/μm, 20 Hz

Fig. 4.7.1 (a) Switching current curves and Ps values of the SmC_A* phase of compound **48*** (8, CH_3, C_5H_{11})

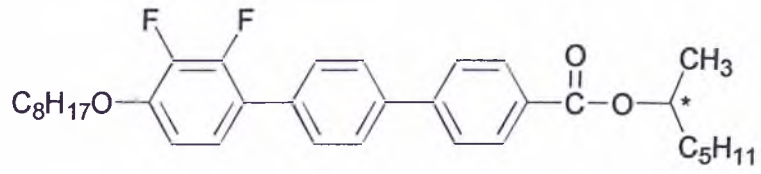

(b)

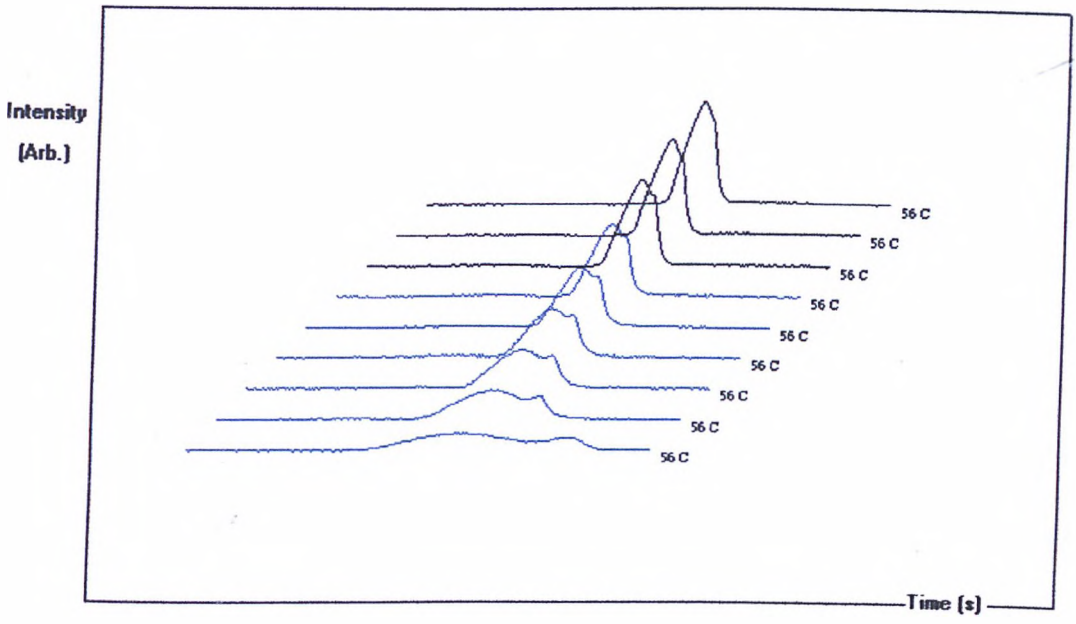

(b)

V/μm	Ps (nCcm^{-2})	V/μm	Ps (nCcm^{-2})
1.18	57.2	7.08	68.8
2.36	59.2	8.26	75.2
3.54	59.2	9.44	76.8
4.72	62.0	10.6	77.6
5.90	64.8		

measured at 56.0 °C

Fig. 4.7.1 (b) Switching current curves and Ps values of the SmC_A* phase of compound **48*** (8, CH_3, C_5H_{11})

Fig. 4.7.2 (a) shows the overall trend of the Ps for compound **50*** (8, CH_3, C_6H_{13}) at a fixed applied voltage of 5.9 V/m, 20 Hz and over a temperature range 70-52 °C. When the molecules are aligned in the cell under the electric field, textures are formed which have a spiral nature over a broad temperature range. At an ordinary Ch to SmA* transition, the helical ordering of Ch changes to give the layered structure of SmA* phase. However for a transition mediated by a twist grain boundary A phase (TUBA), there is competition between a helical structure and a layered structure. Thus the phase has small blocks of molecules of local SmA structure, forming a helix. The unusual alignment of compound **50*** (8, CH,) indicates that the phase is similar to TUBA phase. This is consistent with the observation of a very broad I-SmA* transition peak in DSc (see Fig. 4.4.3)

Finally, when the alignment is complete, the cell is found to have different domains which can be switched in different directions leading to very low measured values of Ps.

Fig. 4.7.2 (b) shows the field dependence of the Ps for the possible TUBA phase in compound **50*** (8, CH,), using an applied voltage of 4.13-10.6 V/μm with 0.60 V/μm steps at 20 Hz and a temperature of 55.0 °C. Even after increasing the voltage to 10.6 V/μm, the Ps is too low to detect.

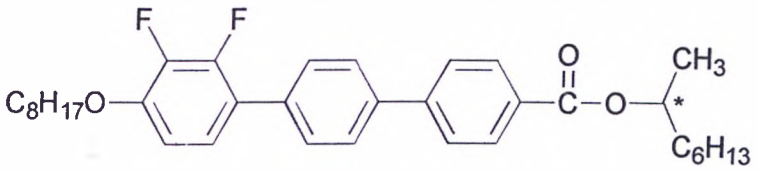

(a)

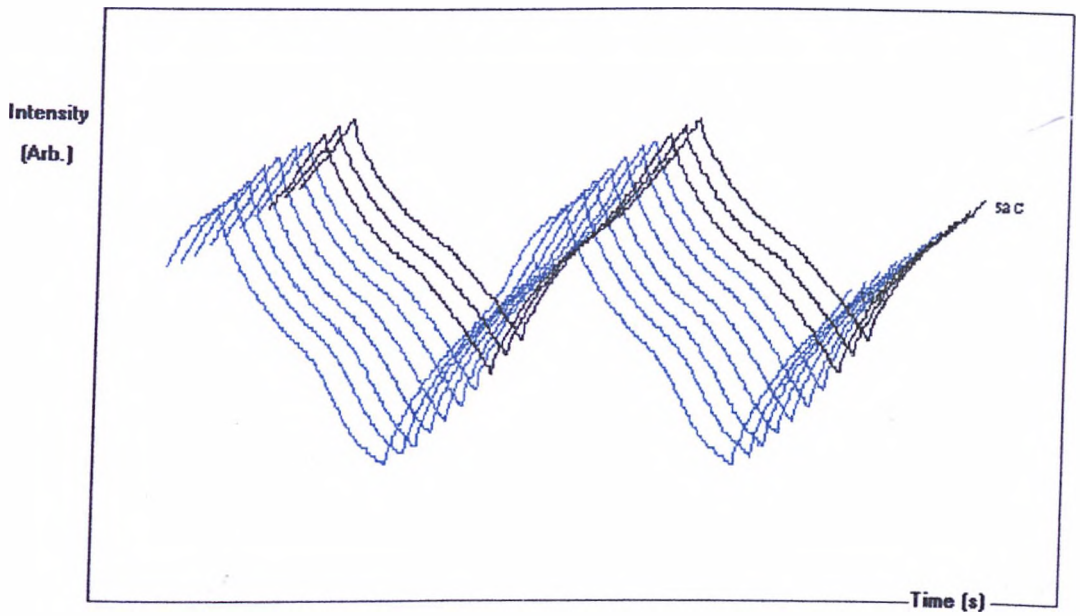

Fig. 4.7.2 (a) Switching current curves of compound **50*** (8, CH_3, C_6H_{13})

(b)

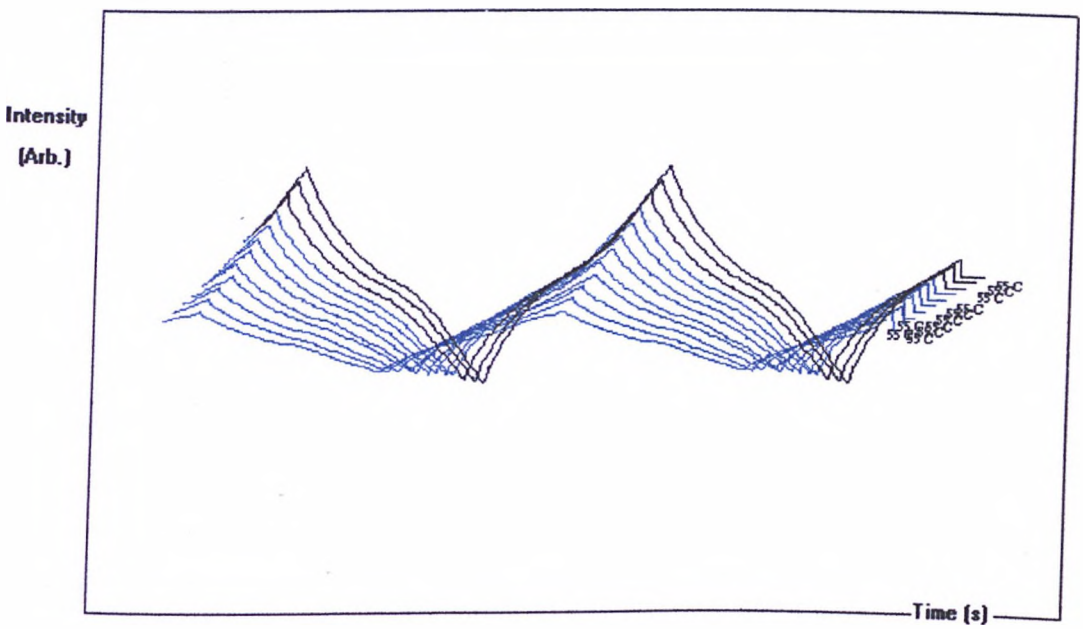

Fig. 4.7.2 (b) Switching current curves of compound **50*** (8, CH_3, C_6H_{13})

Fig. 4.7.3 (a) shows the overall trend for the Ps measured in the SmC_A^* phase of compound **60*** (8, CF_3, C_6H_{13}) at a fixed applied voltage, 8.85 V/μm, 20 Hz and over a temperature range 46-35 °C. As the temperature falls, the first peak moves to lower field and the second peak moves to higher field; thus the separation between the two peaks increases. This separation is due to the stabilization of the antiferroelectric ordering, and conversely the ferroelectric structure is destabilized.

Fig. 4.7.3 (b) shows the field dependence of the Ps in the SmC_A^* phase for compound **60*** (8, CF_3, C_6H_{13}), using an applied voltage 4.13-10.6 V/μm with 0.60 V/μm steps at 20 Hz and a temperature of 40 °C. As the applied field increases, the two peaks move closer and the Ps saturate. At higher fields, the stable antiferroelectric phase can be easily switched.

In the case of compound **61*** (6, CH_3, C_6H_{13}), it does not exhibit either ferroelectric or antiferroelectric phases. (Transition temperature by microscopy I 101.3 °C SmA* 45 K)

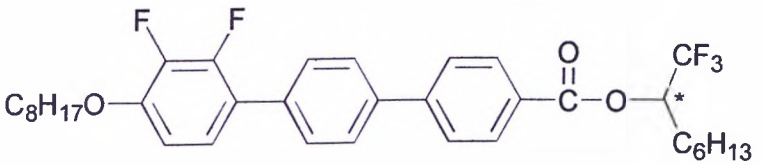

(a)

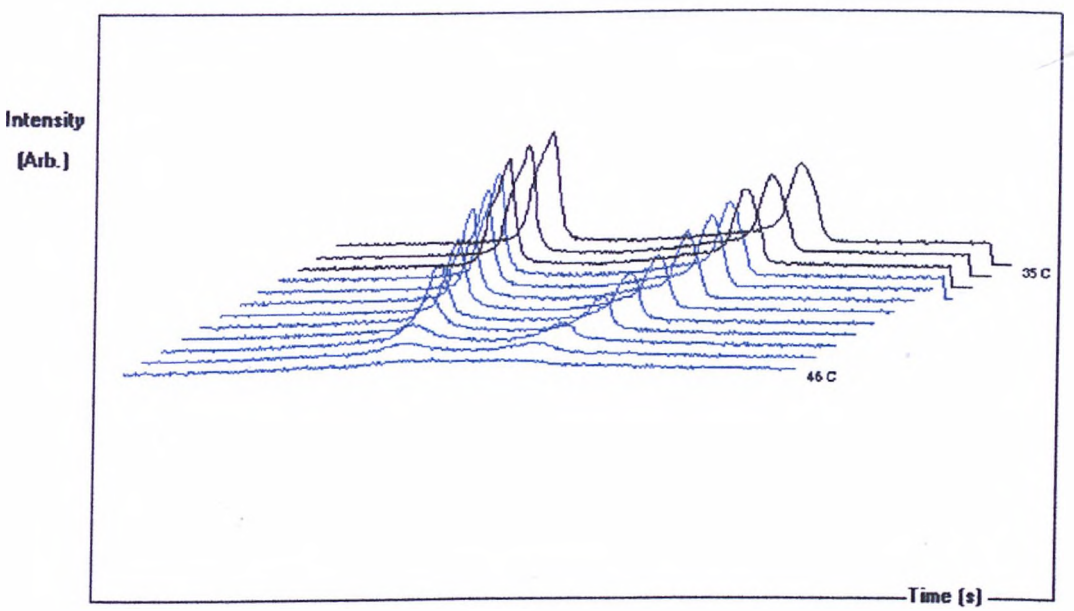

(a)

Temp. (°C)	Ps (nCcm^{-2})	Temp. (°C)	Ps (nCcm^{-2})
46	3.4	40	60.8
45	8.6	39	64.4
44	15.9	38	71.6
43	27.4	37	74.4
42	38.2	36	80.4
41	48.0	35	89.2

measured at 8.85 V/ μm, 20 Hz

Fig. 4.7.3 (a) Switching current curves and Ps values of the SmC_A* phase of compound **60*** (8, CF_3, C_6H_{13})

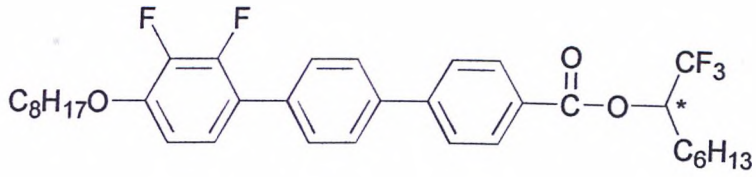

(b)

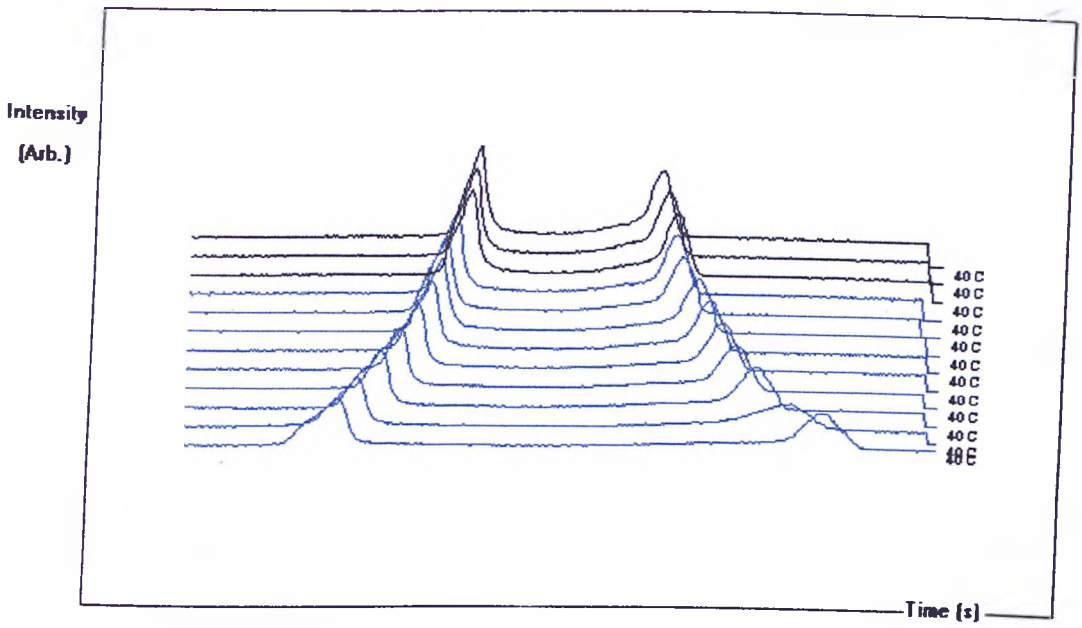

(b)

V/μm	Ps (nCcm^{-2})	V/μm	Ps (nCcm^{-2})
4.13	56	7.67	62.5
4.72	60.4	8.26	63.5
5.31	61.4	8.85	63.0
5.90	62.8	9.44	64.5
6.49	63.0	10.0	63.8
7.08	63.2	10.6	63.0

measured at 40 °C

Fig. 4.7.3 (b) Switching current curves and Ps values of the SmC_A* phase of compound **60*** (8, CF_3, C_6H_{13})

A comparison of temperature dependencies for the values of the Ps for compounds **48*** (8, CH_3, C_5H_{11}) and **60*** (8, CF_3, C_6H_{13}) is shown in Fig. 4.7.4.

A comparison of the apparent tilt angles for compounds **48*** (8, CH_3, C_5H_{11}) and **60*** (8, CF_3, C_6H_{13}) versus temperature under an applied electric field (10 V/μm, square wave, 10 mHz) is shown in Fig. 4.7.5. In the case of compound **48*** (8, CH_3, C_5H_{11}), the tilt angles initially increase in the higher temperature region (62-61.5 °C) of the phase and then decrease as the temperature is reduced. This is explained by the fact that compound **48*** (8, CH_3, C_5H_{11}) possesses ferroelectric ordering in the higher temperature region before the antiferroelectric structure becomes stabilized. However compound **60*** (8, CF_3, C_6H_{13}) showed that tilt angles tend to decrease over the entire temperature range as the antiferroelectric phase becomes more stabilized.

There appears to be no explanations in the literature for the decreased tilt angle with decreasing temperature observed in the two field induced ferroelectric states of a SmC* phase. The phenomena is presumably linked to the presence of the branched alkyl chains in antiferroelectric phase. On switching, both layers rotate to reach the ferroelectric state. Interdigitation of the branched terminal chains hinders this process. As the temperature decreases the energy barrier to rotation increases due to increasing the antiferroelectricity. To offset this, the tilt angle decreases in order that the steric contribution to the rotational energy barrier may be reduced.

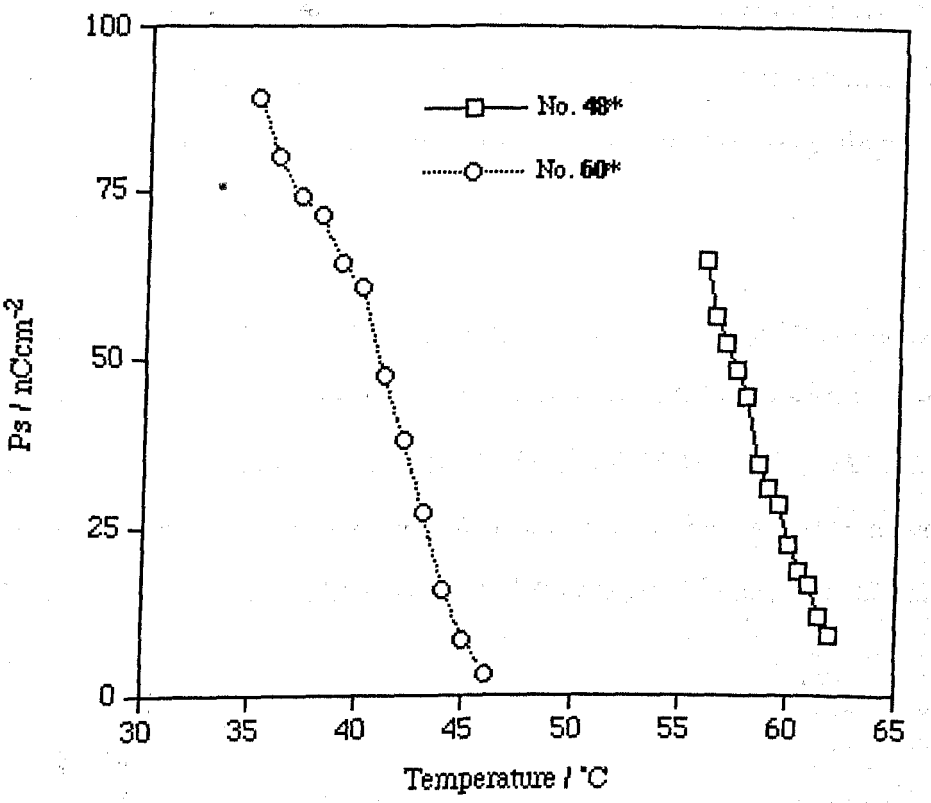

Fig. 4.7.4 Comparison of Ps values in compounds **48*** (8, CH_3, C_5H_{11}) and **60*** (8, CF_3, C_6H_{13})

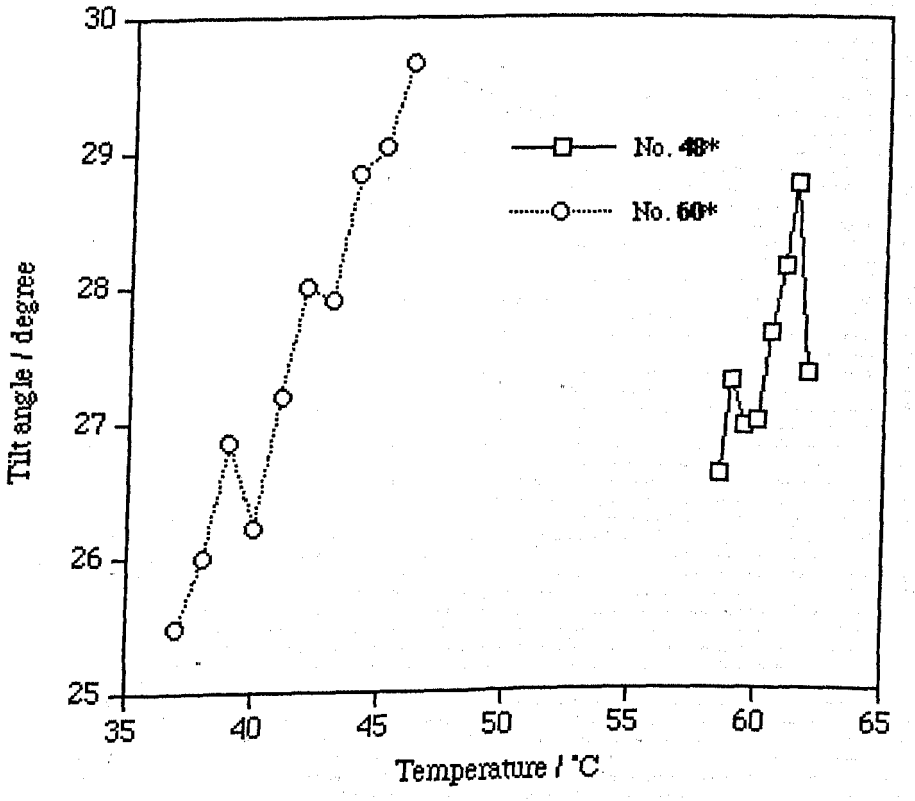

Fig. 4.7.5 Comparisons of tilt angles for compounds **48*** (8, CH_3, C_6H_{13}) and **60*** (8, CF_3, C_6H_{13})

Fig. 4.7.6 (a) shows the overall trend for the Ps for compound **62*** (10, CH_3, C_5H_{11}) at a fixed applied voltage of 5.9 V/μm at 20 Hz and over a temperature range 73-55 °C. Split peaks were found on cooling down to 71 °C, and then only single peaks were detected at lower temperatures.

Fig. 4.7.6 (b) and Fig. 4.7.6 (c) show the field dependence of the Ps of compound **62*** (10, CH_3, C_5H_{11}), using an applied voltage of 1.18-10.6 V/μm with 1.18 V/μm steps at 20 Hz, temperatures of 71 and 58 °C. In Fig. 4.7.6 (b), split peaks are seen over the entire range of the applied field. As can be seen in Fig. 4.7.6 (c), however, the split peaks disappeared totally even at the lower applied fields, and only single peaks were observed.

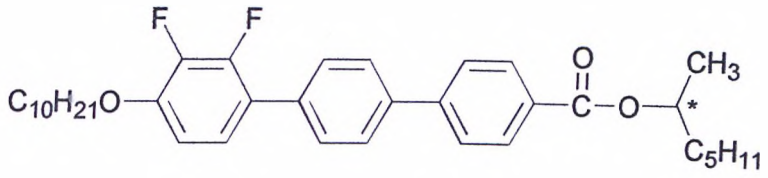

(a)

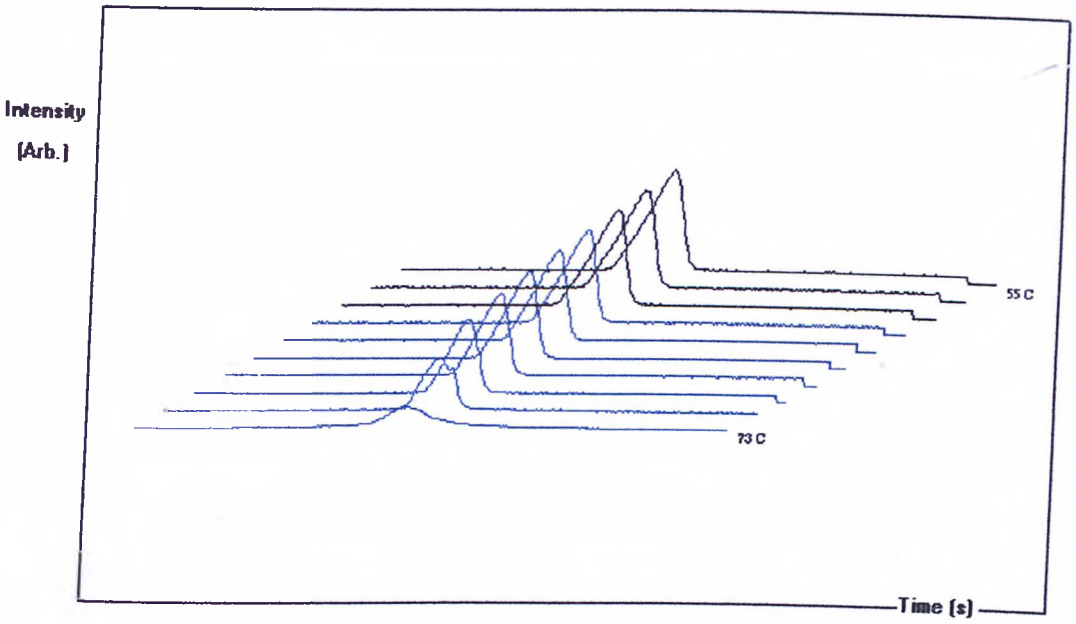

(a)

Temp. (°C)	Ps ($nCcm^{-2}$)	Temp. (°C)	Ps ($nCcm^{-2}$)
73	26.3	63	113
71	61.6	61	116
69	79.6	59	124
67	92.0	57	134
65	103	55	138

measured at 5.9 V/ μm, 20 Hz

Fig. 4.7.6 (a) Switching current curves and Ps values of compound **62*** (10, CH_3, C_5H_{11})

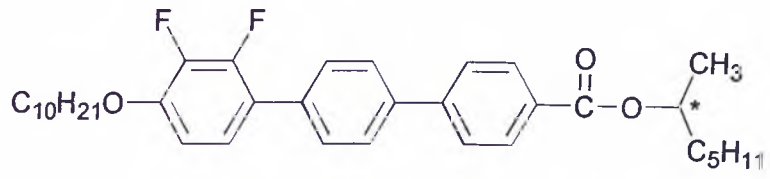

(b)

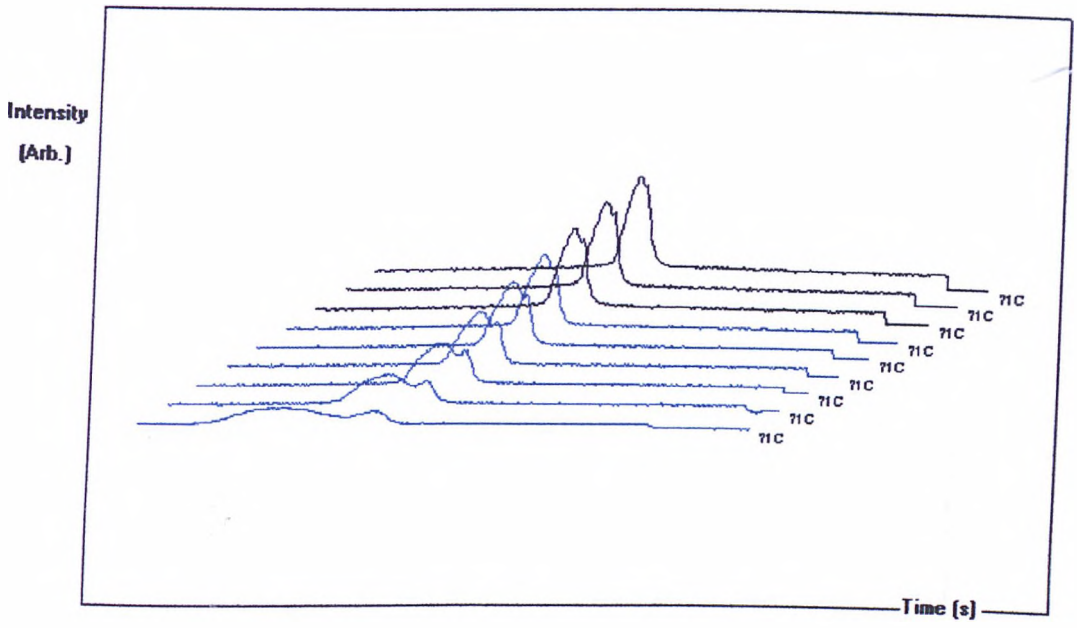

measured at 71 °C

(c)

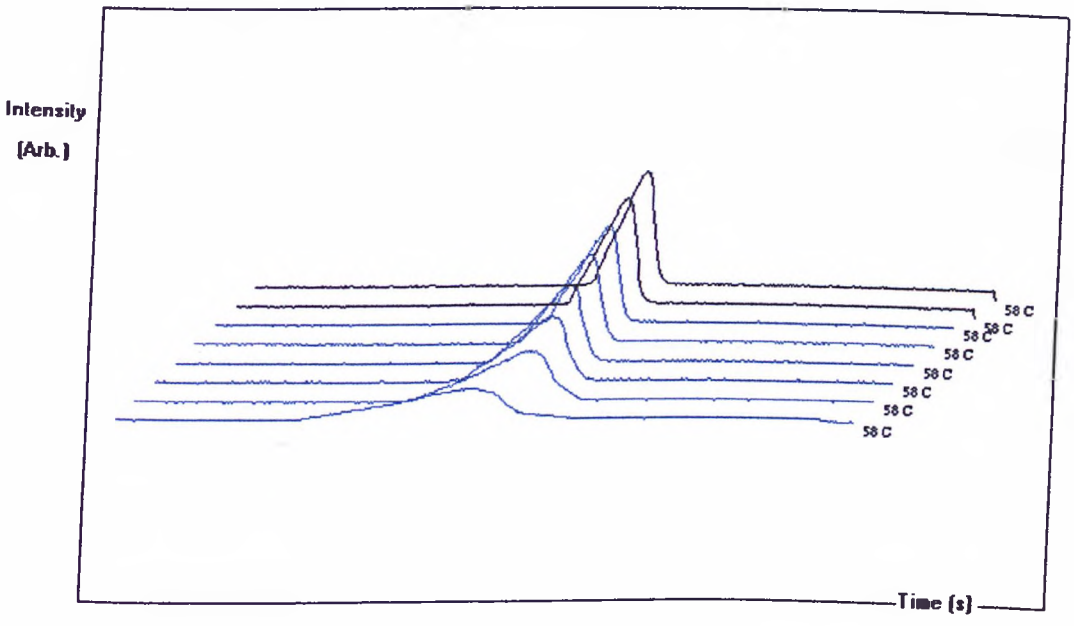

measured at 58 °C

(b)

V/μm	Ps (nCcm^{-2})	V/μm	Ps (nCcm^{-2})
1.18	53.6	7.08	62.0
2.36	54.6	8.26	62.0
3.54	55.6	9.44	62.4
4.72	58.0	10.6	62.8
5.90	61.2		

measured at 71 °C

(c)

V/μm	Ps (nCcm^{-2})	V/μm	Ps (nCcm^{-2})
1.18	118	7.08	130
2.36	124	8.26	130
3.54	126	9.44	130
4.72	128	10.6	130
5.90	130		

measured at 58 °C

Fig. 4.7.6 (b) and (c) Switching current curves and Ps values of compound **62*** (10, CH_3, C_5H_{11})

Fig. 4.7.7 (a) shows the overall trend of the Ps for compound **64*** (10, CH_3, C_6H_{13}) at a fixed applied voltage of 5.9 V/m at 20 Hz and over a temperature range of 72-59 °C. Split peaks were found on cooling until 69 °C and then only single peaks were observed in the lower temperature region.

Fig. 4.7.7 (b) and Fig. 4.7.7 (c) show the field dependence of the Ps for compound **64*** (10, CH_3, C_6H_{13}), using an applied voltage of 1.18-10.6 V/μm with 1.18 V/μm steps at 20 Hz and temperatures of 69 and 64 °C. In Fig. 4.7.7 (b), the switching curves show split peaks at lower applied field. With increasing applied voltage, direct switching between the two ferroelectric states occurred without passing through the antiferroelectric state. This different switching behaviour with varying field strength is material dependent. In the antiferroelectric phases of compounds **48*** (8, CH_3, C_5H_{11}) and **60*** (8, CF_3, C_6H_{13}), split peaks and two well separated peaks are clearly observed even at low applied fields.

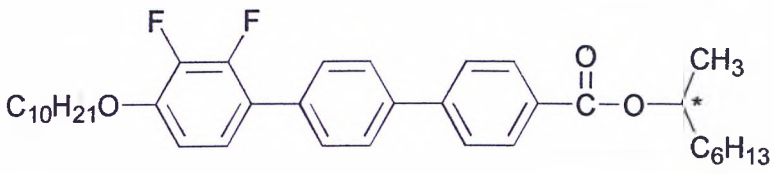

(a)

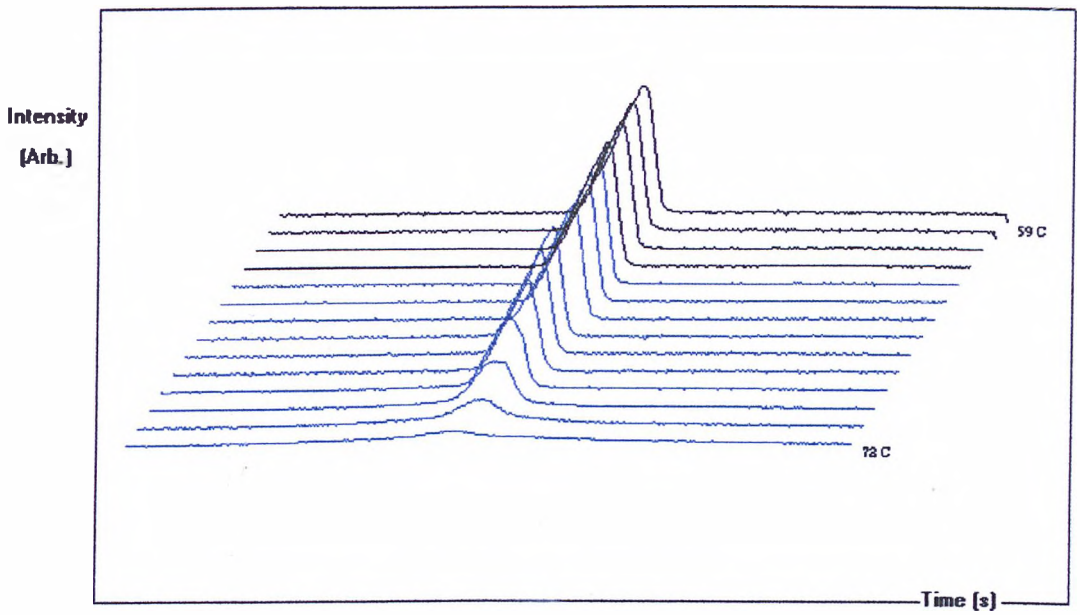

(a)

Temp. (°C)	Ps (nCcm^{-2})	Temp. (°C)	Ps (nCcm^{-2})
72	4.8	65	88.8
71	15.0	64	94.4
70	37.0	63	98.8
69	53.6	62	106
68	65.6	61	108
67	75.6	60	112
66	82.4	59	112

measured at 5.9 V/ μm, 20 Hz

Fig. 4.7.7 (a) Switching current curves and Ps values of compound **64*** (10, CH_3, C_6H_{13})

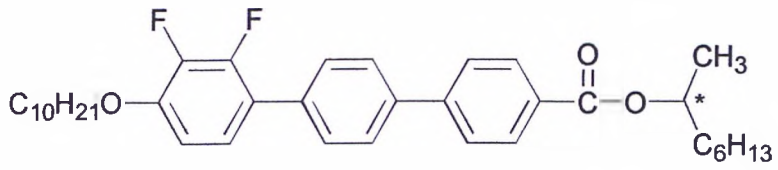

(b)

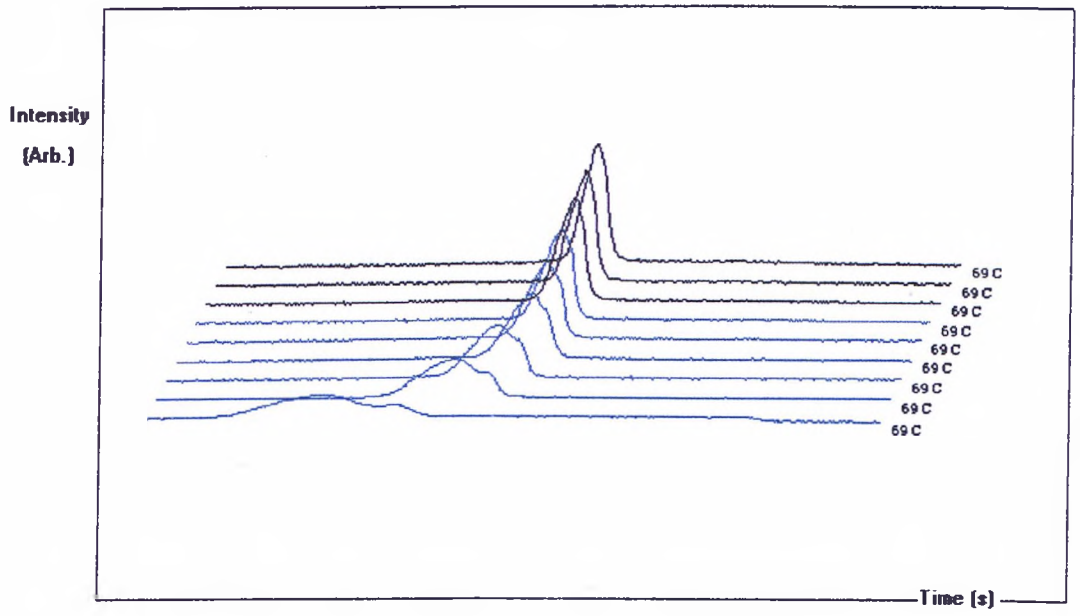

measured at 69 °C

(c)

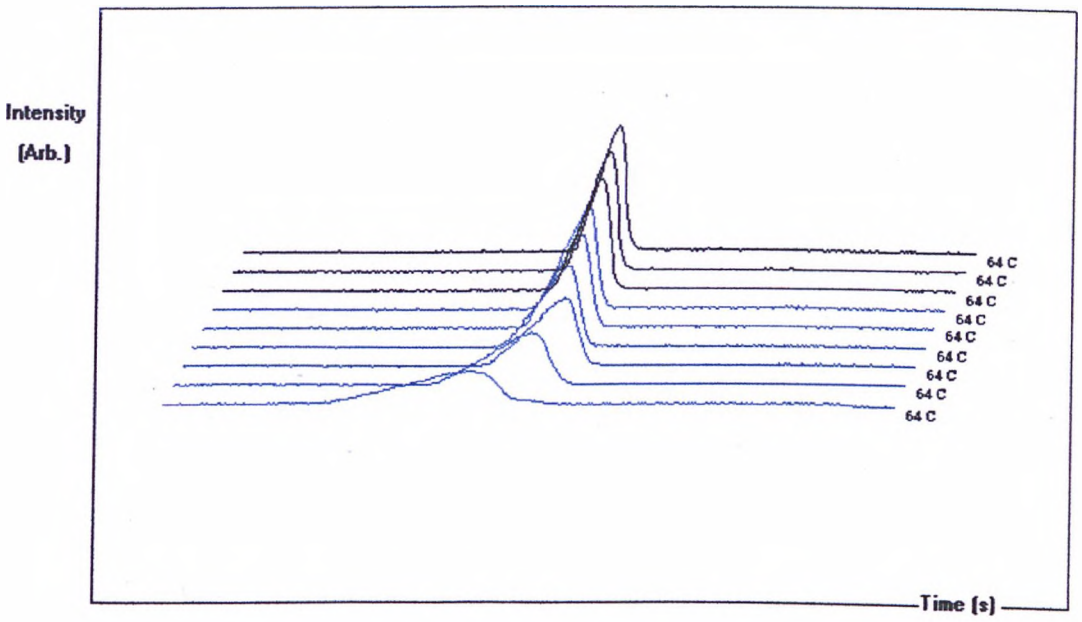

measured at 64 °C

(b)

V/μm	Ps (nCcm^{-2})	V/μm	Ps (nCcm^{-2})
1.18	50	7.08	58.4
2.36	52.4	8.26	60.4
3.54	51.6	9.44	60.4
4.72	53.6	10.6	62.4
5.90	55.6		

measured at 69 °C

(c)

V/μm	Ps (nCcm^{-2})	V/μm	Ps (nCcm^{-2})
1.18	91.2	7.08	94.4
2.36	94.4	8.26	97.6
3.54	96.0	9.44	98.4
4.72	94.4	10.6	97.2
5.90	94.8		

measured at 64 °C

Fig. 4.7.7 (b) and (c) Switching current curves and Ps values of compound **64*** (10, CH_3, C_6H_{13})

A comparison of the temperature dependent Ps values for compounds **62*** (10, CH_3, C_5H_{11}) and **64*** (10, CH_3, C_6H_{13}) is shown in Fig. 4.7.8.

A comparison of the apparent tilt angles for compounds **62*** (10, CH_3, C_5H_{11}) and **64*** (10, CH_3, C_6H_{13}) versus temperature under an applied electric field of 10 V/μm using a square wave of frequency 10 mHz is plotted in Fig. 4.7.9.

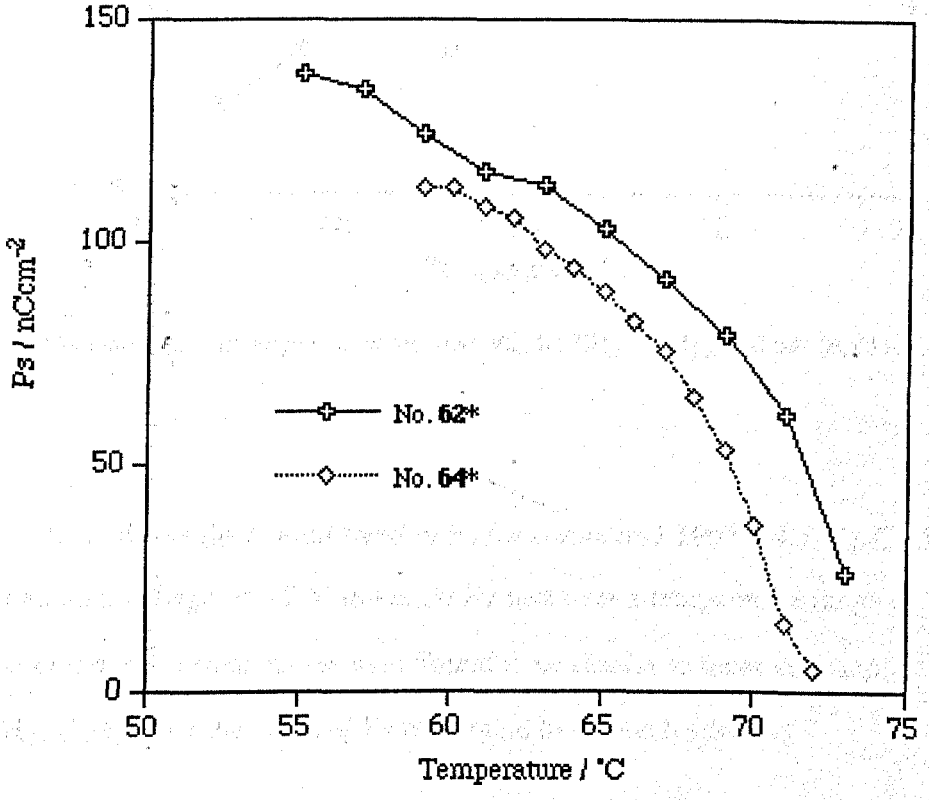

Fig. 4.7.8 Comparisons of Ps values in compounds **62*** (10, CH_3, C_5H_{11}) and **64*** (10, CH_3, C_6H_{13})

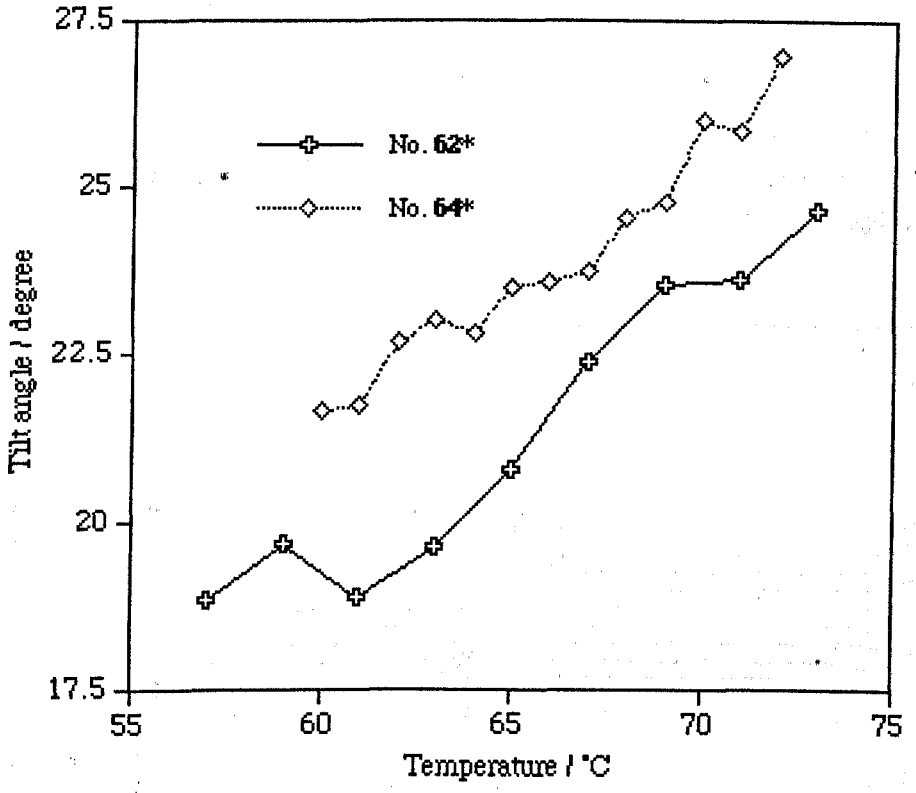

Fig. 4.7.9 Comparisons of tilt angles for compounds **62** (10, CH_3, C_5H_{11}) and **64*** (8, CH_3, C_6H_{13})

Fig. 4.7.10 (a) shows the overall trend of Ps for compound **100*** (14, CH_3, C_5H_{11}) at a fixed applied voltage of 5.9 V/μm at 20 Hz and over a temperature range of 71-63 °C. The switching current curves were found to be similar to those of compound **64*** (10, CH_3, C_6H_{13}) but the value of Ps was found to be much smaller.

Fig. 4.7.10 (b) and Fig. 4.7.10 (c) shows the field dependence of the Ps of compound **100*** (14, CH_3, C_5H_{11}), using an applied voltage of 1.18-10.6 V/μm with 1.18 V/μm steps at 20 Hz and temperatures of 68 and 65 °C.

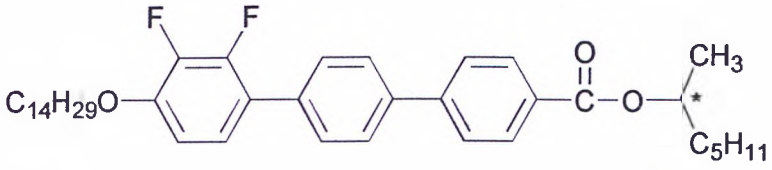

(a)

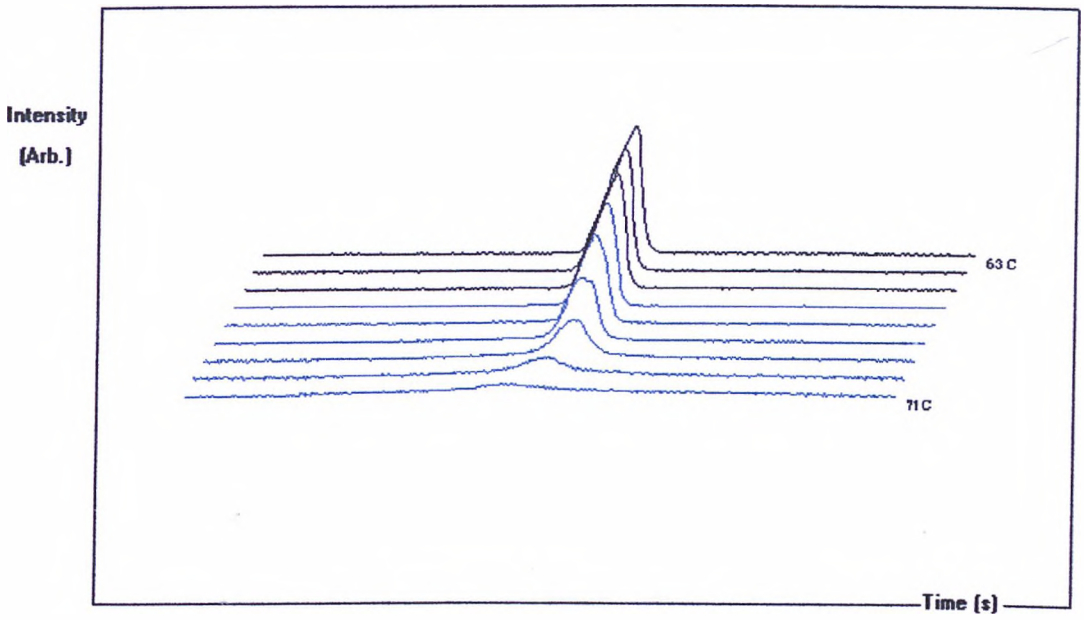

(a)

Temp. (°C)	Ps ($nCcm^{-2}$)	Temp. (°C)	Ps ($nCcm^{-2}$)
71	3.86	66	56.4
70	8.30	65	64.8
69	19.4	64	70.8
68	37.5	63	74
67	48.8		

measured at 5.9 V/ μm, 20 Hz

Fig. 4.7.10 (a) Switching current curves and Ps values of compound **100*** (14, CH_3, C_5H_{11})

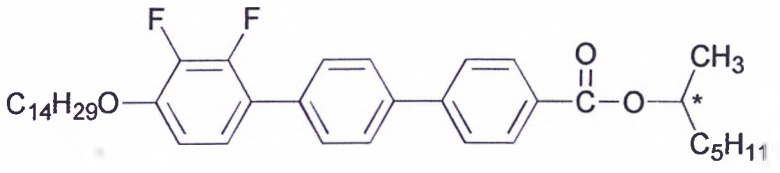

(b)

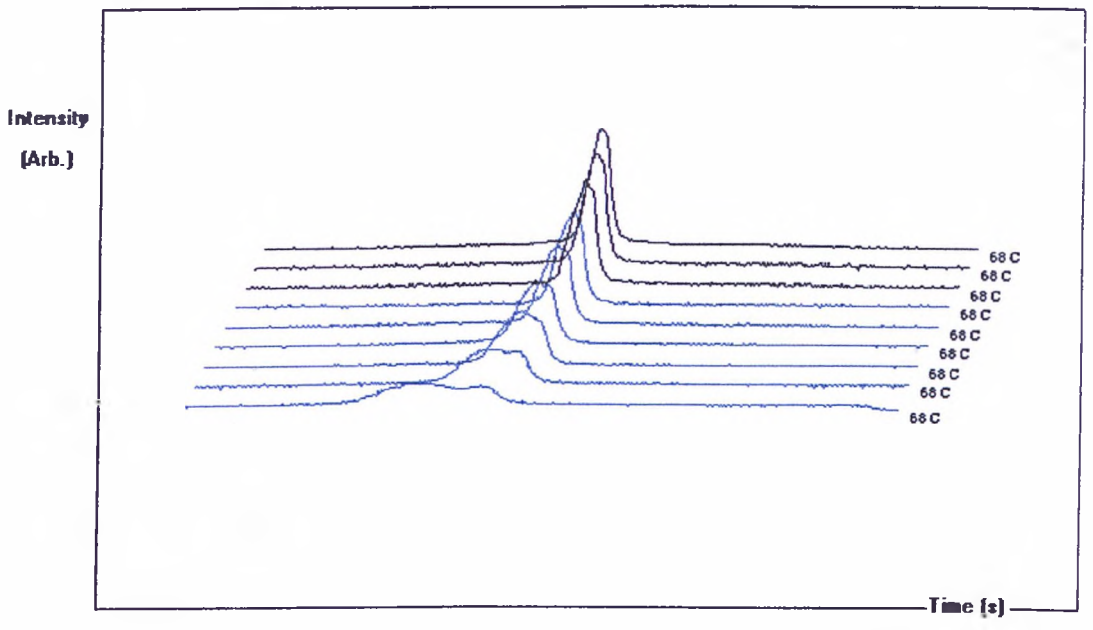

measured at 68 °C

(c)

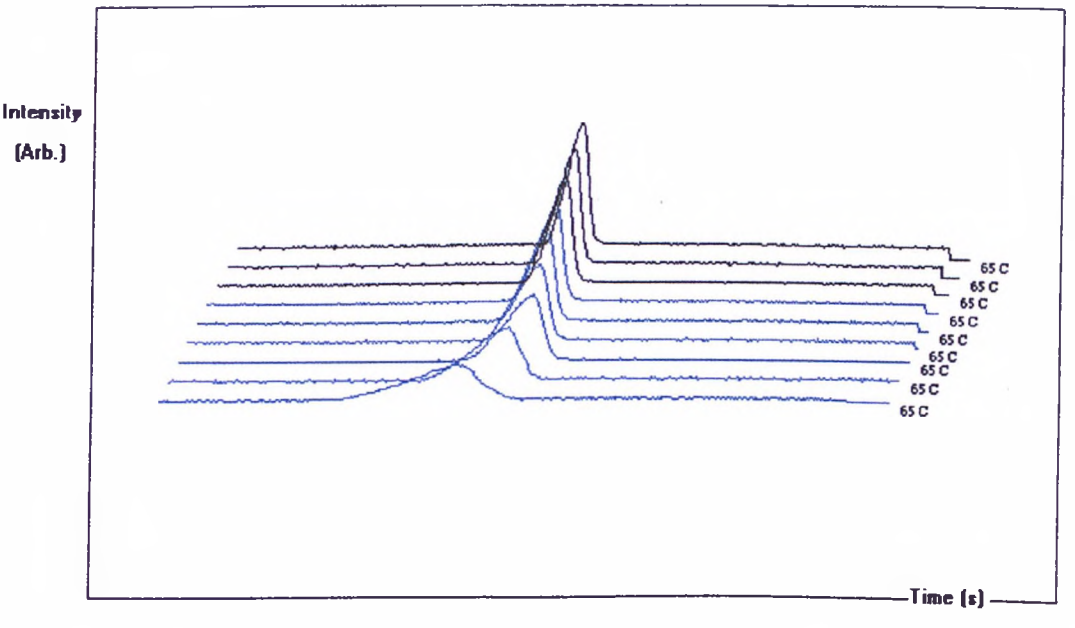

measured at 65 °C

(b)

V/μm	Ps ($nCcm^{-2}$)	V/μm	Ps ($nCcm^{-2}$)
1.18	31.6	7.08	40.4
2.36	33.2	8.26	43.6
3.54	36.3	9.44	42.4
4.72	36.3	10.6	42.4
5.90	39.1		

measured at 68 °C

(c)

V/μm	Ps ($nCcm^{-2}$)	V/μm	Ps ($nCcm^{-2}$)
1.18	63.2	7.08	64.4
2.36	64.4	8.26	65.2
3.54	63.2	9.44	67.2
4.72	63.2	10.6	66.8
5.90	64.0		

measured at 65 °C

Fig. 4.7.10 (b) and (c) Switching current curves and Ps values of compound **100*** (14, CH_3, C_5H_{11})

Fig. 4.7.11 (a) shows the overall trend in the Ps for compound **102*** (14, CH_3, C_6H_{13}) at a fixed applied voltage of 5.9 V/m at 20 Hz and over a temperature range 72-66 °C. Switching current curves show only single peaks.

Fig. 4.7.11 (b) shows the field dependence of the Ps of compound **102*** (14, CH_3, C_6H_{13}), using an applied voltage of 1.18-9.44 V/μm with 1.18 V/μm steps at 20 Hz and a temperature of 67 °C. The switching current peaks confirmed that compound **102*** (14, CH_3, C_6H_{13}) exhibited only ferroelectric switching, because the peaks in the SmC* phase are independent of the applied field strength.

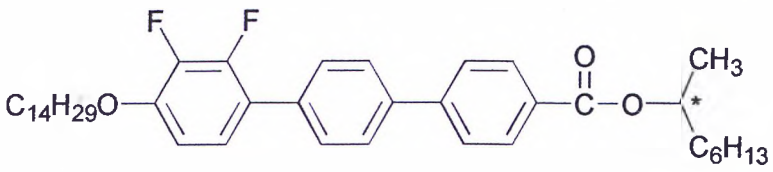

(a)

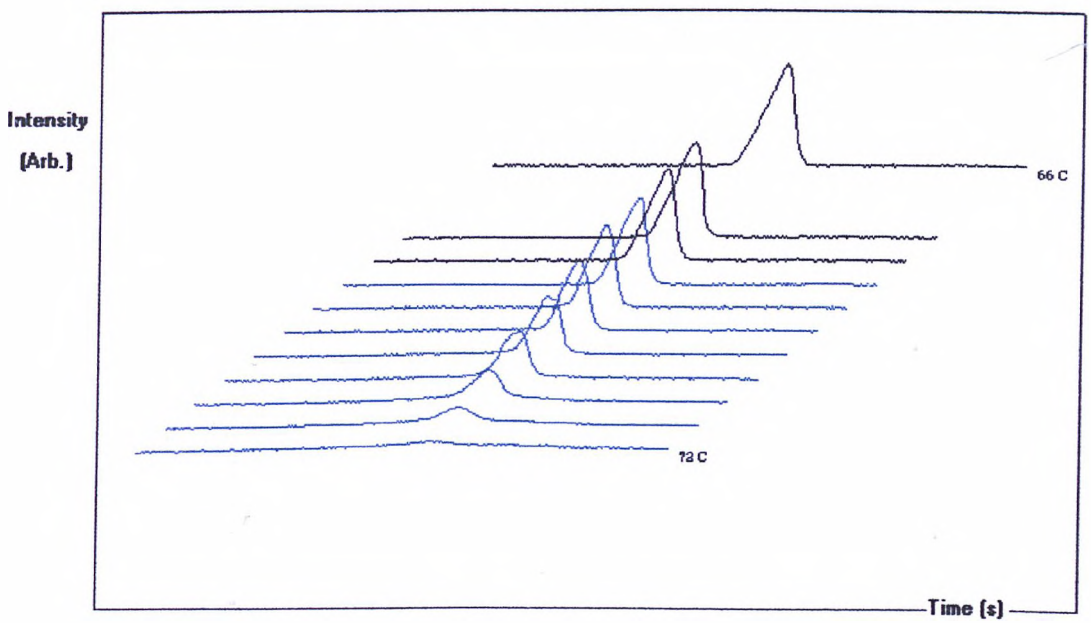

(a)

Temp. (°C)	Ps ($nCcm^{-2}$)	Temp. (°C)	Ps ($nCcm^{-2}$)
72.0	4.8	69.0	50.0
71.5	9.0	68.5	54.4
71.0	18.3	68.0	56.8
70.5	29.6	67.5	61.6
70.0	36.9	66.0	68.4
69.5	43.6		

measured at 5.9 V/ μm, 20 Hz

Fig. 4.7.11 (a) Switching current curves and Ps values of compound **102*** (14, CH_3, C_6H_{13})

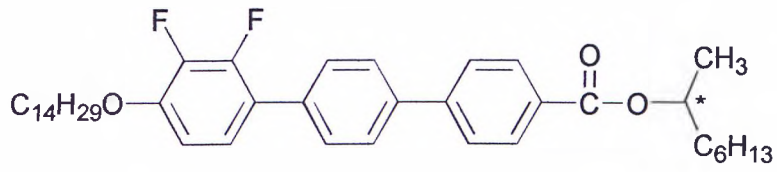

(b)

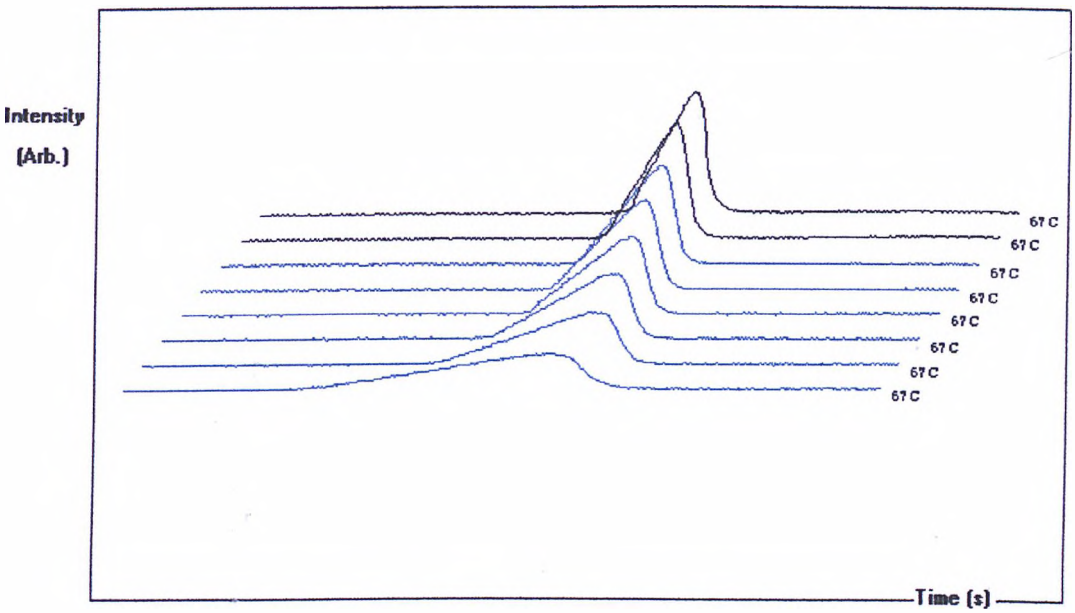

(b)

V/μm	Ps (nCcm^{-2})	V/μm	Ps (nCcm^{-2})
1.18	62.8	5.90	66.4
2.36	63.6	7.08	66.0
3.54	63.6	8.26	67.2
4.72	64.0	9.44	66.4

measured at 67 °C

Fig. 4.7.11 (b) Switching current curves and Ps values of compound **102*** (14, CH_3, C_6H_{13})

A comparison of the temperature dependent values for the Ps of compound **100*** (14, CH_3, C_5H_{11}) and **102*** (14, CH_3, C_6H_{13}) is shown in Fig. 4.7.12.

A comparison of the apparent tilt angles for compounds **100*** (10, CH_3, C_5H_{11}) and **102*** (14, CH_3, C_6H_{13}) versus temperature under an applied electric field of 10 V/μm using square wave of frequency 10 mHz) is shown in Fig. 4.7.13.

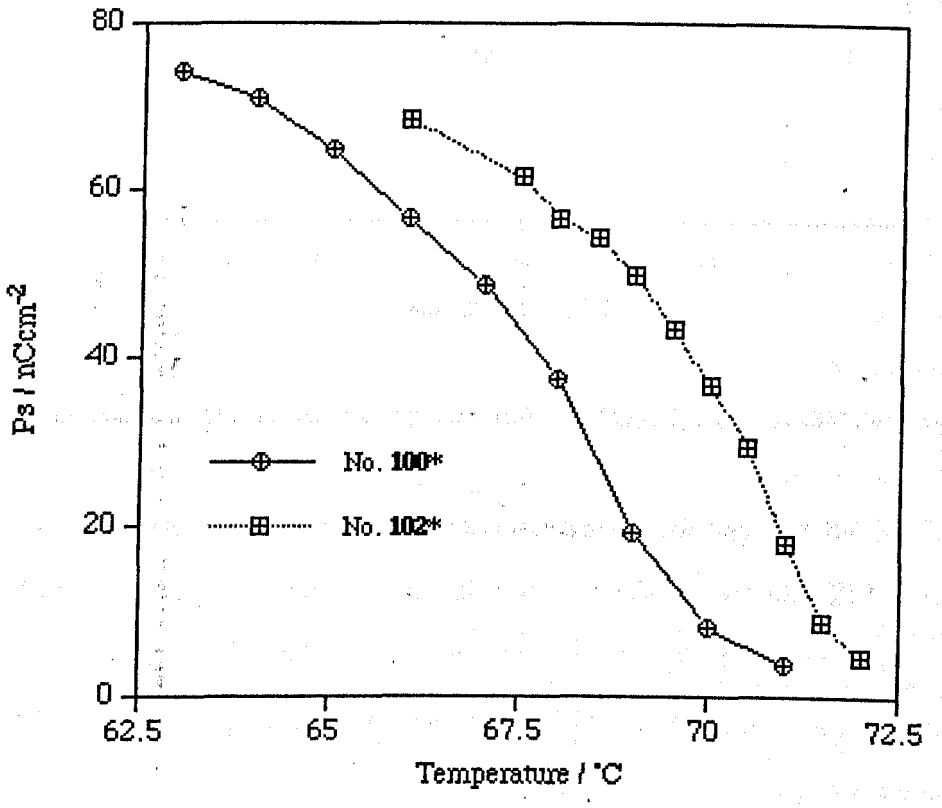

Fig. 4.7.12 Comparison of Ps values in compounds **100*** (14, CH_3, C_5H_{11}) and **102*** (14, CH_3, C_6H_{13})

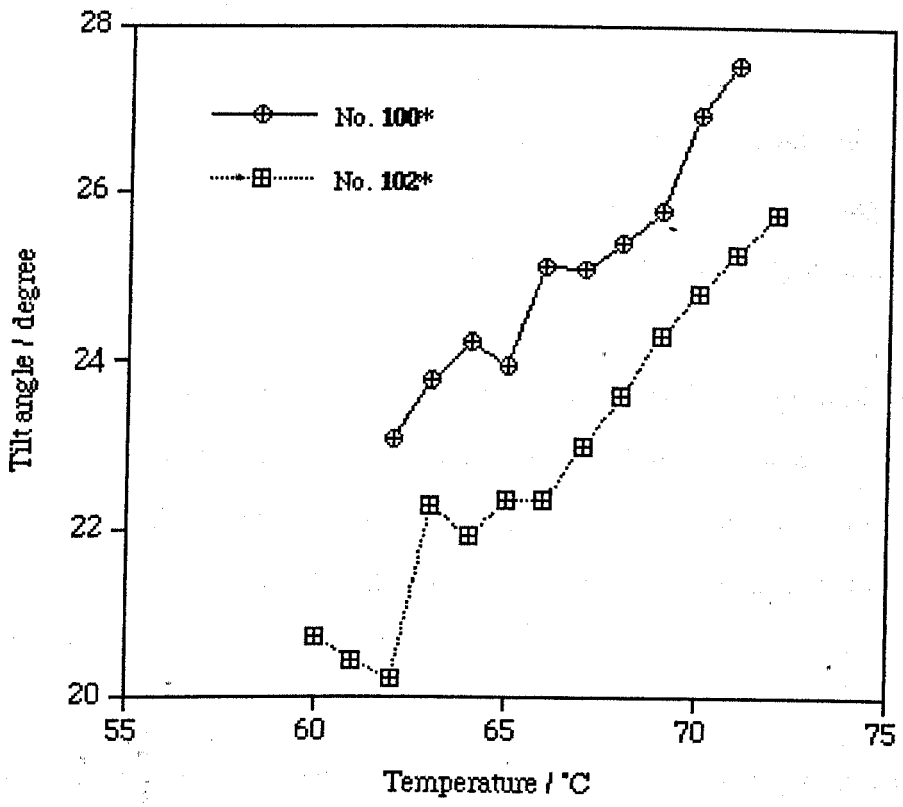

Fig. 4.7.13 Comparison of tilt angles for compounds **100*** (14, CH_3, C_5H_{11}) and **102*** (14, CH_3, C_6H_{13})

In Fig. 4.7.13, possible explanations for the decreasing tilt angle of the SmC* phases are; 1) Increasing viscosity causes molecules not to be fully switched. 2) The relaxation time of the antiferro to ferroelectric phase is too slow to detect in the triangular method (see Fig. 4.7.11) though compound **102*** (14, CH_3, C_6H_{13}) has an antiferroelectric phase.

4.8 Mixture Studies

In a typical application of liquid crystals, racemic compounds are mixed with a chiral compound/dopant in order to obtain a broad temperature range for the ferroelectric or antiferroelectric phase and to achieve a low viscosity material.

In this project, compound **60*** (8, CF_3, C_6H_{13}), which exhibited two well-separated peaks was selected as a dopant for mixture studies. Thus when it was mixed with non chiral compounds, it was expected to be possible to control the phase sequence and phase properties by mixing different amounts of the host and dopant (see Method 1, 2 and 3).

The polarization reversal currents of mixtures were measured using cells with 0.81 cm^2 electrode area (Linkam) and plate separation of 5.0 μm, at an applied voltage of 8.85 V/μm at 20 Hz and on cooling.

(Method1)

Fig. 4.8.1 shows the overall trend of the Ps for mixtures of the non chiral compound **63** (10, CH_3, C_5H_{11}) with the chiral compound **60*** (8, CF_3, C_6H_{13}) using different mixing ratios. Their values for the Ps as a function of temperature are plotted in Fig 4.8.2.

Compounds **63** (10, CH_3, C_5H_{11}) and **60*** (8, CF_3, C_6H_{13}) were mixed as following mixing ratio.

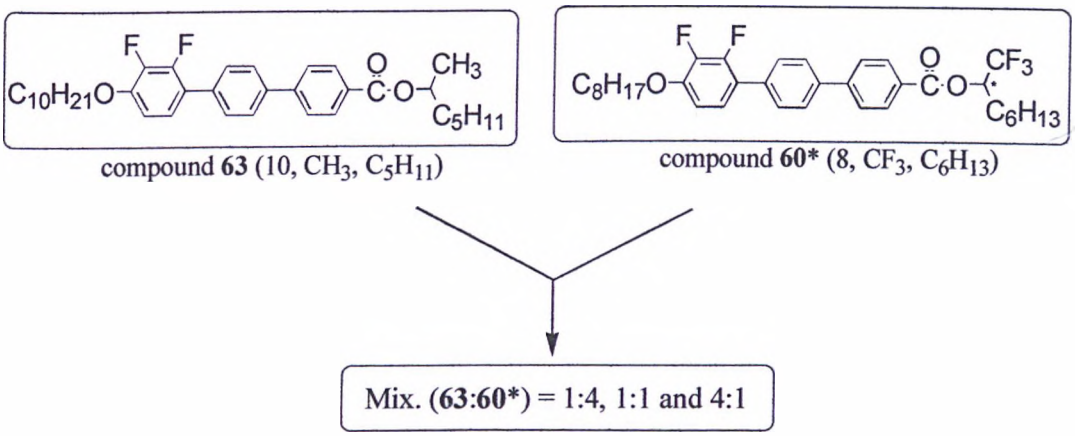

(a) Mix. (**63**:**60***) = 1:4

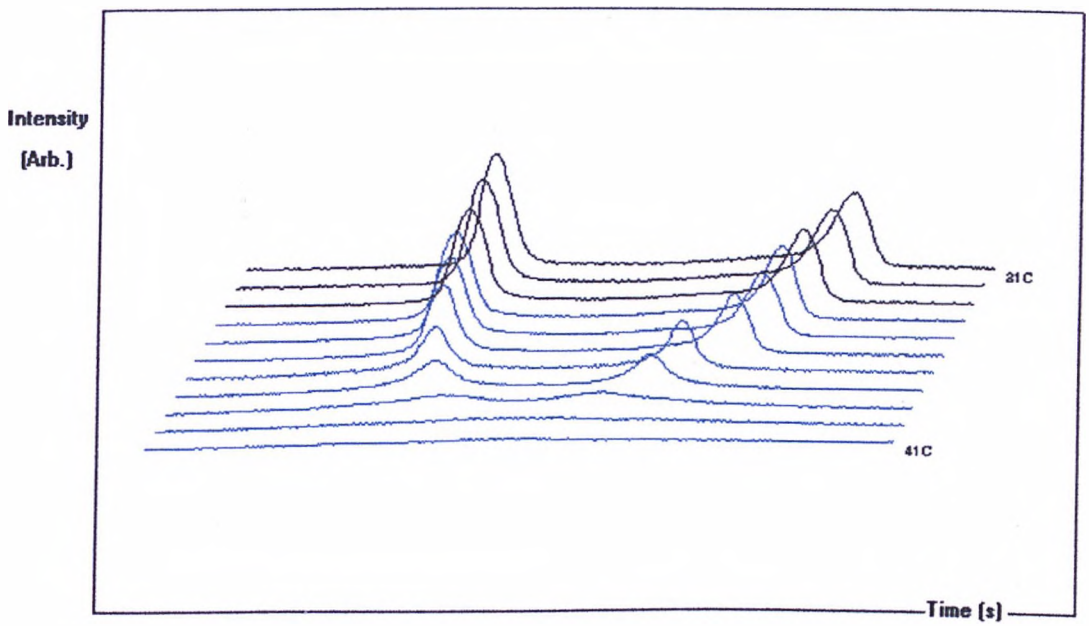

(b) Mix. (**63**:**60***) = 1:1

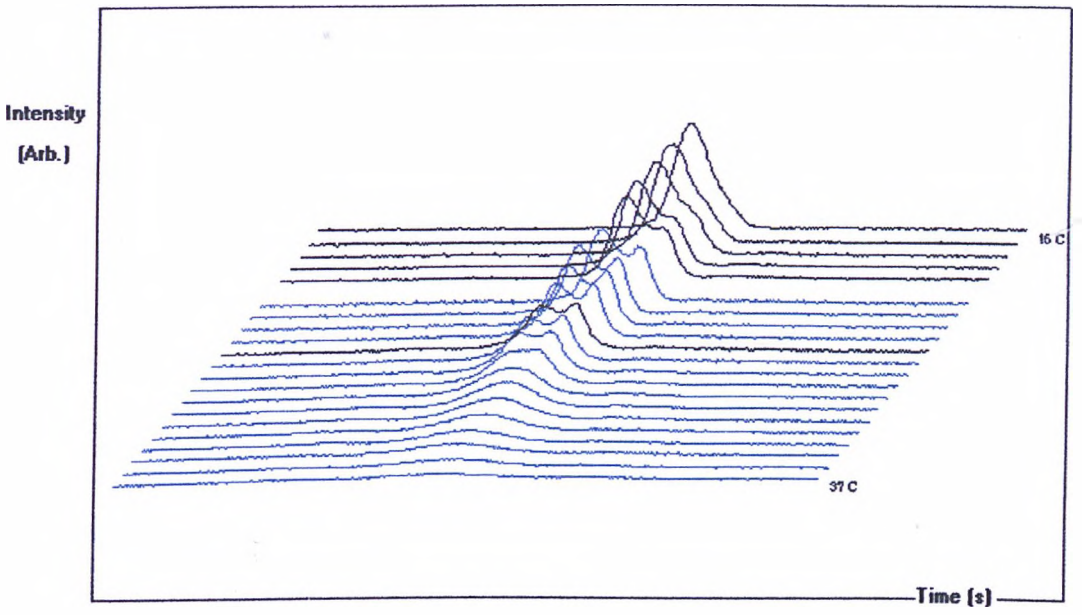

(c) Mix. (**63**:**60***) = 4:1

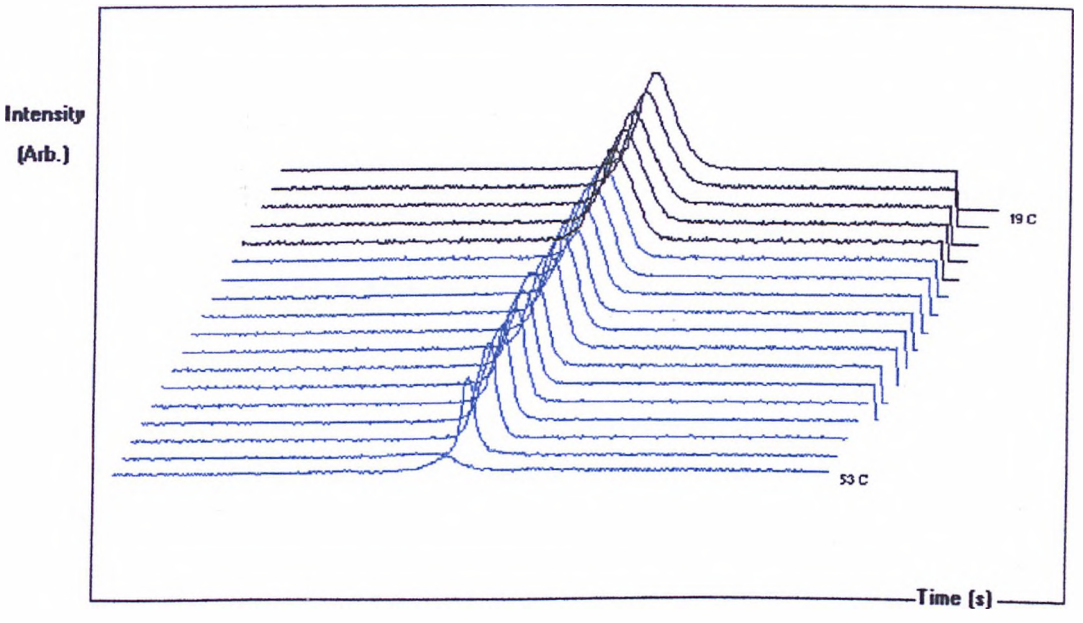

Fig. 4.8.1 (a), (b) and (c) Switching current curves of mixture **63** (10, CH_3, C_5H_{11}) and **60*** (8, CF_3, C_6H_{13}) with different mixing ratio

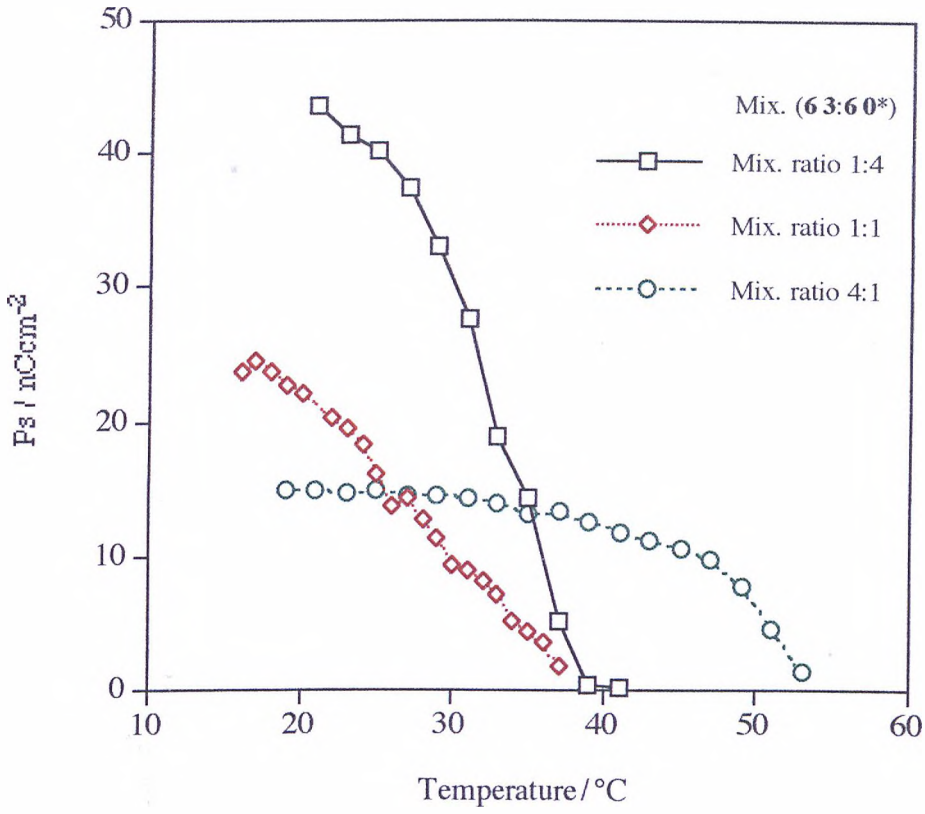

Fig. 4.8.2 Comparisons of Ps values of mixture **63** (10, CH_3, C_5H_{11}) and **60*** (8, CF_3, C_6H_{13})

As the amount of achiral compound **63** (10, CH_3, C_5H_{11}) increases, the mixture (**63**:**60***) has a SmC* phase which shows only single peaks. However, the temperature range for the SmC* phase is increased to over 30 °C.

(Method 2) Odd-even effect I

Compounds **63**, **65**, **66** and **67** were mixed with compound **60*** (8, CF_3, C_6H_{13}) using a 1:1 mixing ratio.

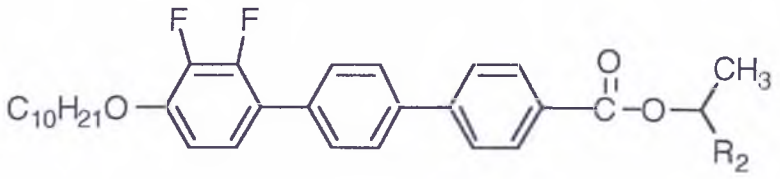

Compounds	R_2
63	C_5H_{11}
65	C_6H_{13}
66	C_7H_{15}
67	C_8H_{17}

Fig. 4.8.3 showed the overall trend for the switching current peaks for the various mixtures. Mixture (**63**+**60***) (Fig. 4.8.3 (a)) and mixture (**66**+**60***) (Fig. 4.8.3 (c)), where R_2 has an odd number of carbons, showed split peaks in the switching current curves. Mixture (**65**+**60***) (Fig. 4.8.3 (b)) and mixture (**67**+**60***) (Fig. 4.8.3.(d)), where R_2 has an even number of carbons, showed two well-separated polarization curves. Comparisons of the values of the Ps as a function of temperature are plotted in Fig. 4.8.4.

(a)

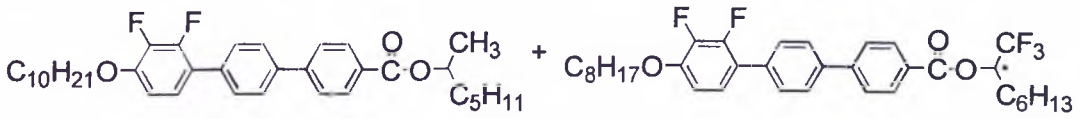
F
F
O
CH3
C10H21O
C
O
C5H11
+
C8H17O
CF3
C6H13

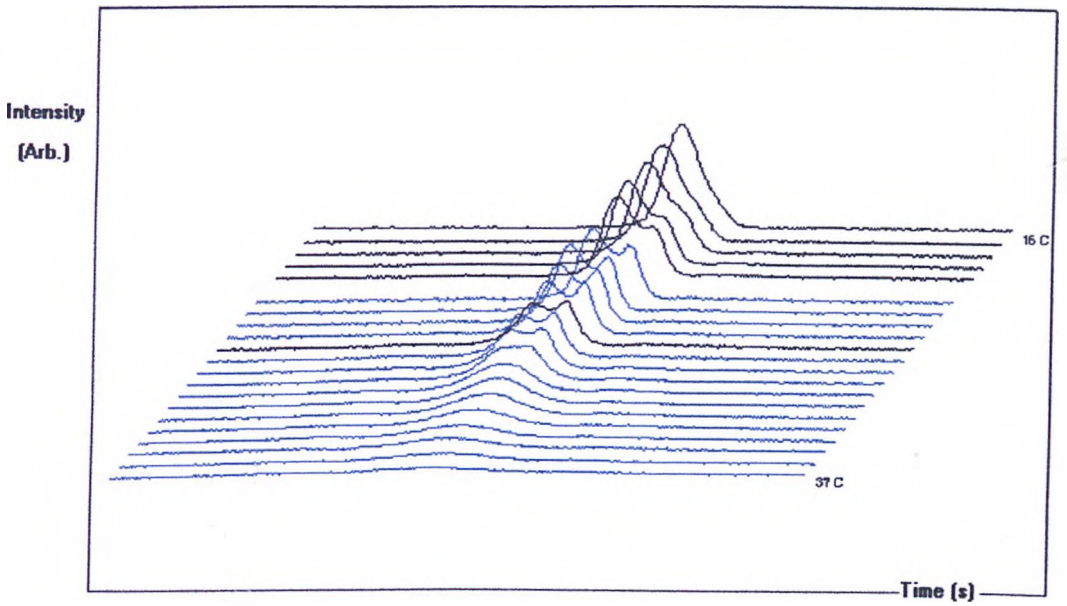
Intensity
(Arb.)
15 C
37 C
Time (s)

(b)

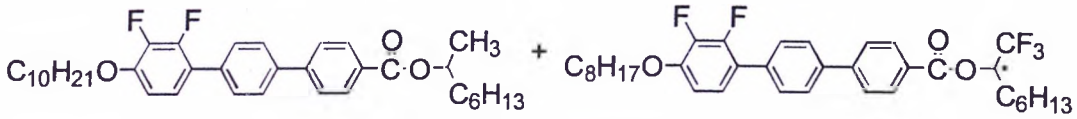
F
F
O
CH3
C10H21O
C
O
C6H13
+
C8H17O
CF3
C6H13

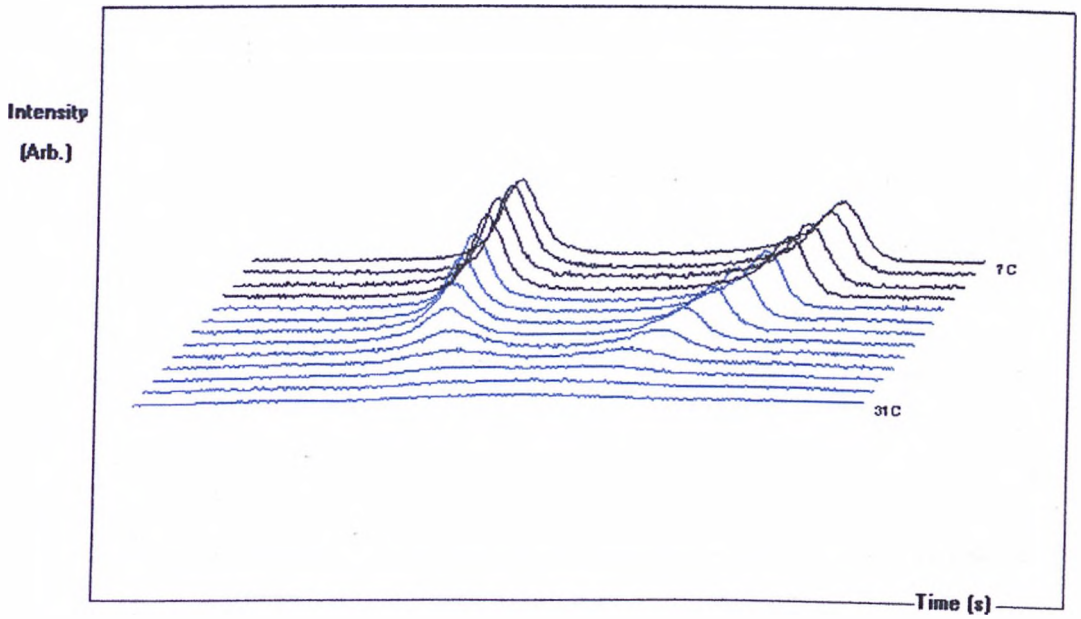
Intensity
(Arb.)
7 C
31 C
Time (s)

(c)

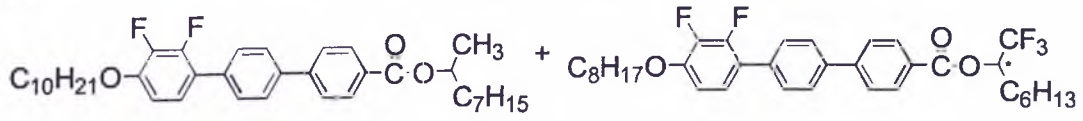

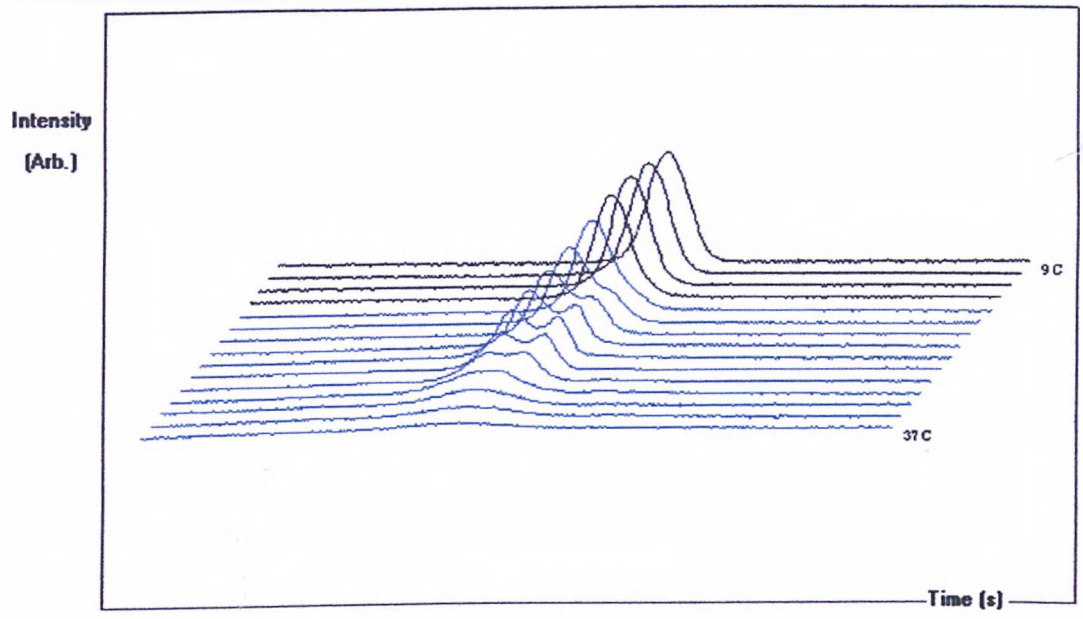

(d)

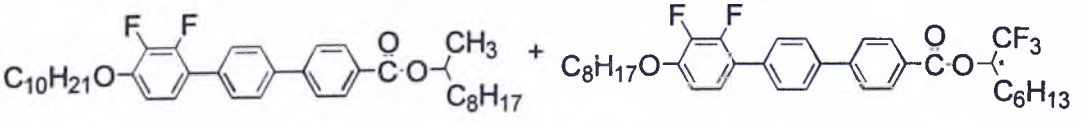

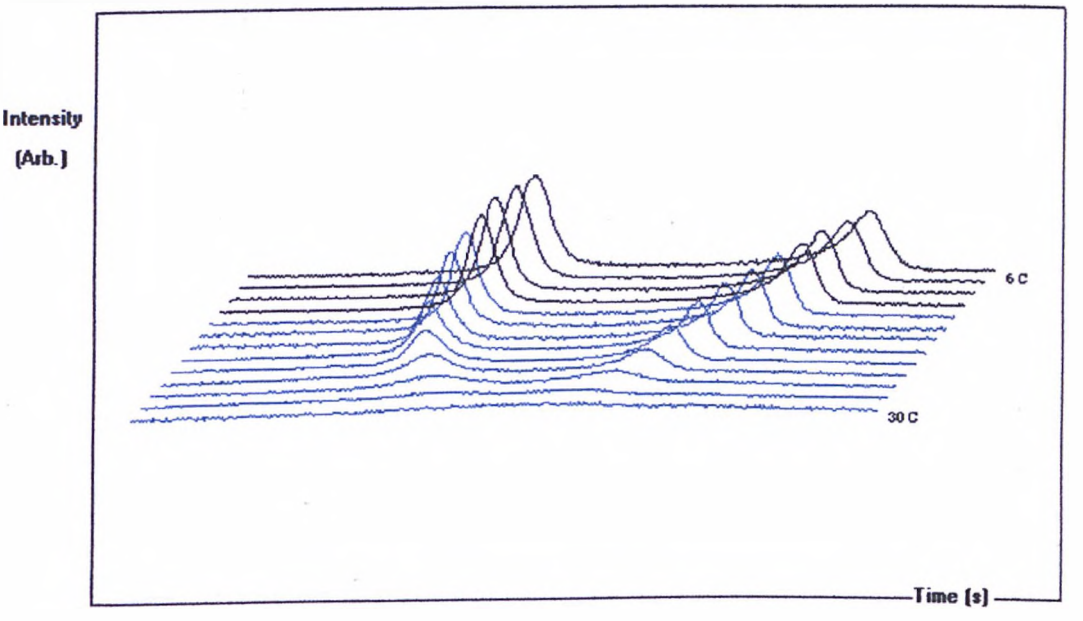

Fig. 4.8.3 (a), (b), (c) and (d) Odd-even effect (I)

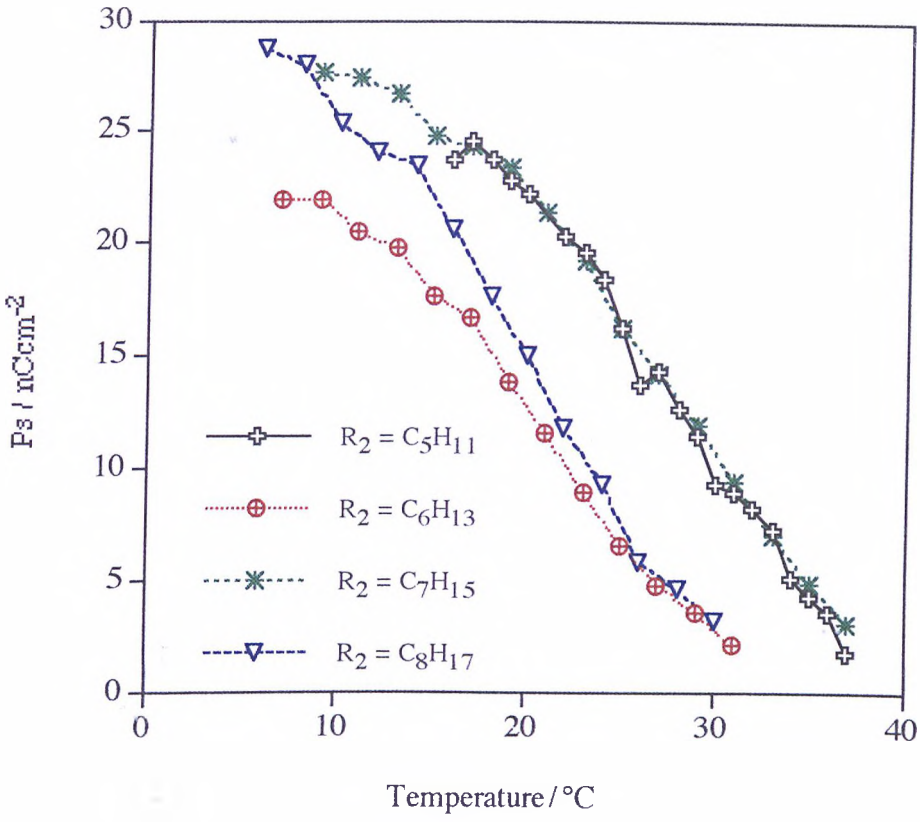

Fig. 4.8.4 Comparisons of Ps values from mixture **63** (10, CH_3, C_5H_{11}), **65** (10, CH_3, C_6H_{13}), **66** (10, CH_3, C_7H_{15}) and **67** (10, CH_3, C_8H_{16}) with **60*** (8, CF_3, C_6H_{13})

(Method 3) Odd-even effect II

This odd-even effect with respect to ferroelectric versus antiferroelectric switching also occurred for the homologous series as shown below;

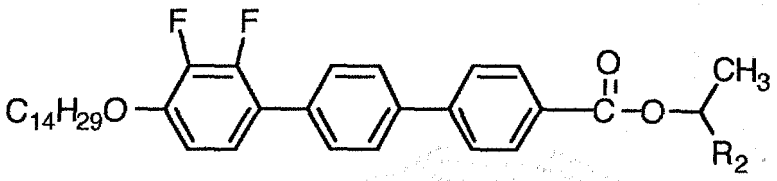

Compounds	R_2
101	C_5H_{11}
103	C_6H_{13}
104	C_7H_{15}
105	C_8H_{17}

Fig. 4.8.5 shows the overall trend in switching current peaks for the mixtures. Mixture (**101**+**60***) (Fig. 4.8.5 (a)) and mixture (**104**+**60***) (Fig. 4.8.5 (c)), where R_2 has an odd number of carbons, exhibited split peaks in the switching current curves. Mixture (**103**+**60***) (Fig. 4.8.5 (b)) and mixture (**105**+**60***) (Fig. 4.8.5.(d)), where R_2 has an even number of carbons, showed two well-separated curves for the Ps. Comparisons of the values of the Ps as a function of temperature are plotted in Fig. 4.8.6.

(a)

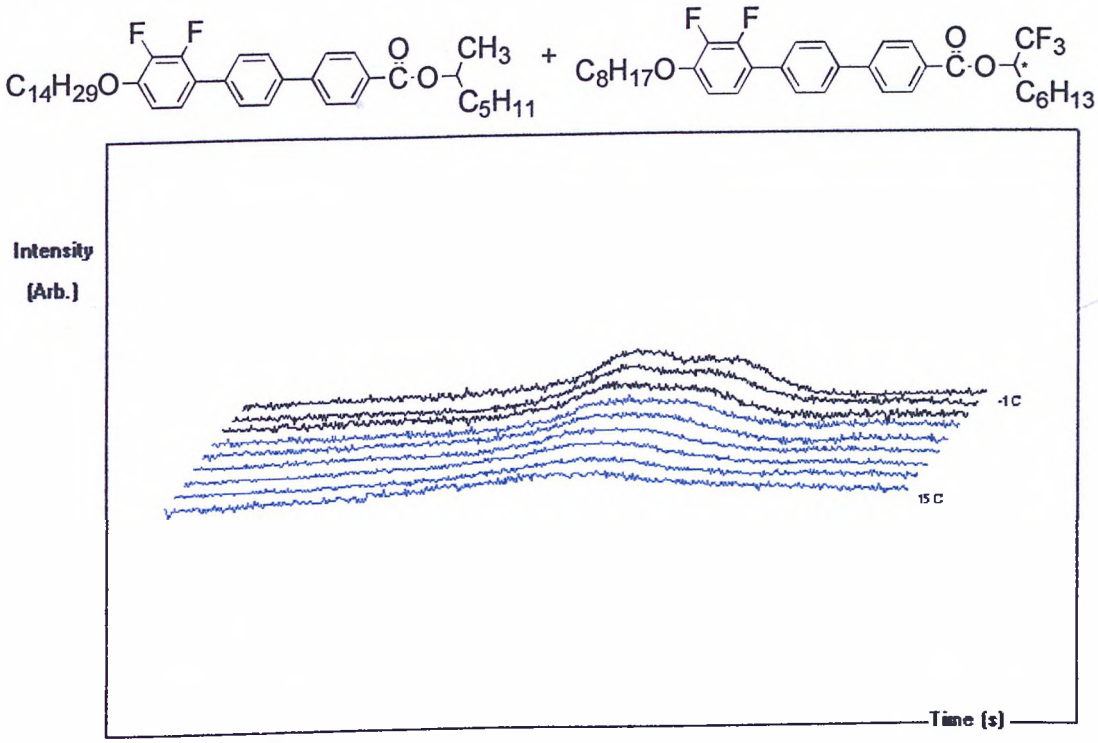
F
F
O
CH3
C14H29O
C·O
C5H11
+
C8H17O
CF3
C6H13
Intensity
(Arb.)
-1 C
15 C
Time (s)

(b)

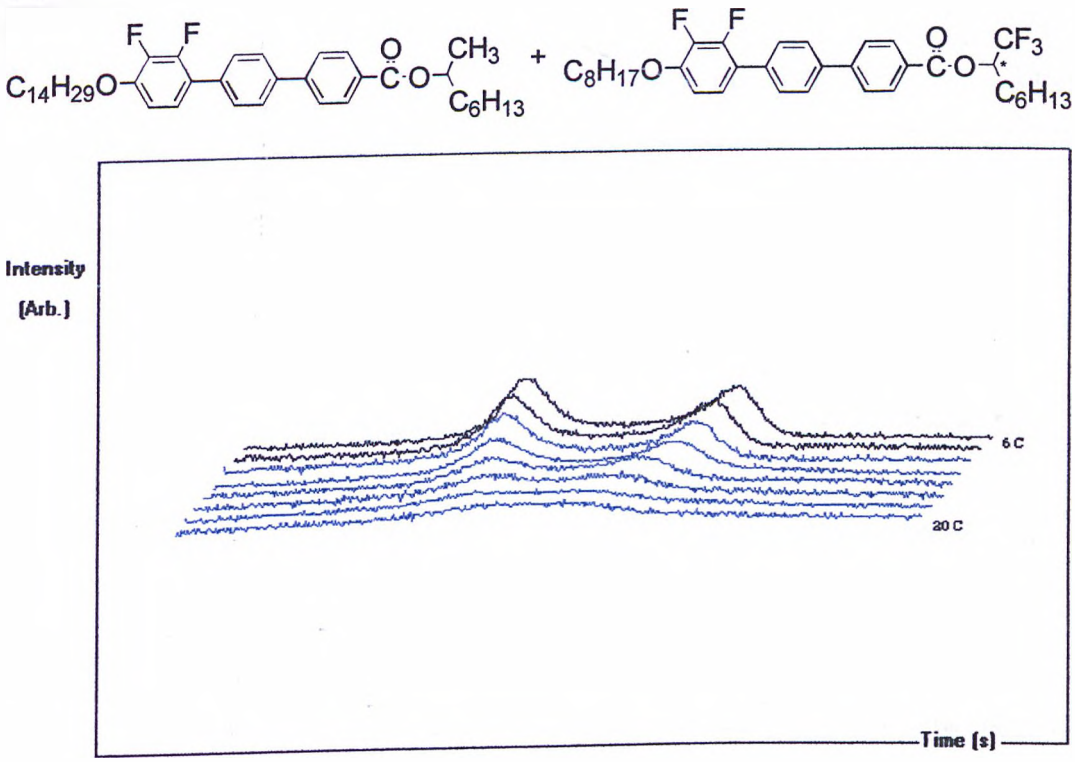
F
F
O
CH3
C14H29O
C·O
C6H13
+
C8H17O
CF3
Intensity
(Arb.)
6 C
20 C
Time (s)

(c)

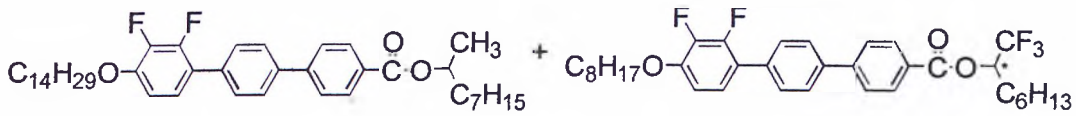

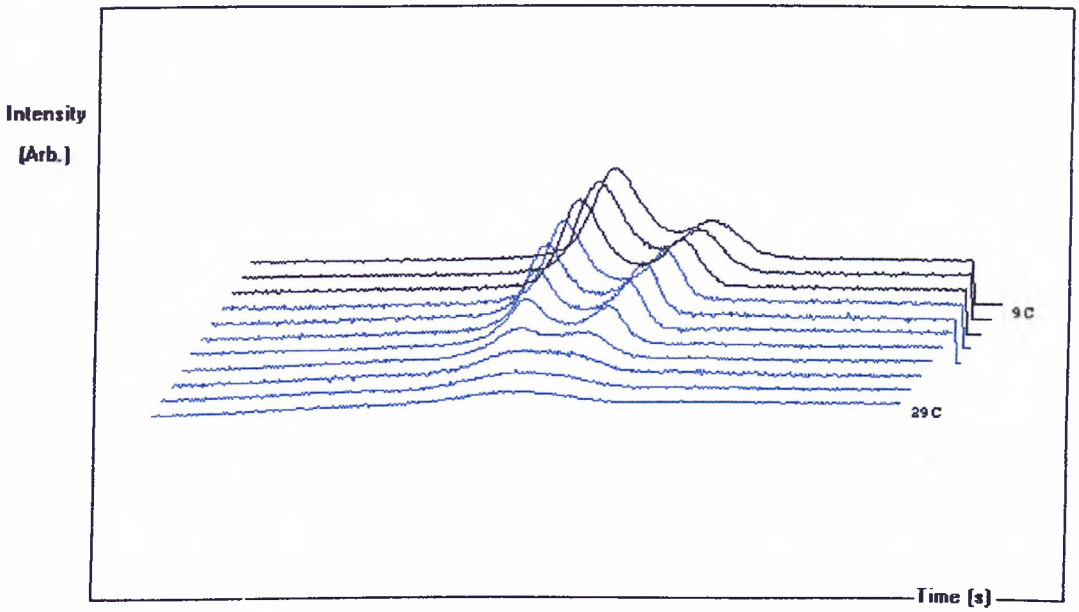

(d)

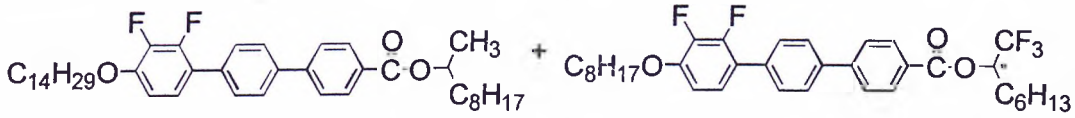

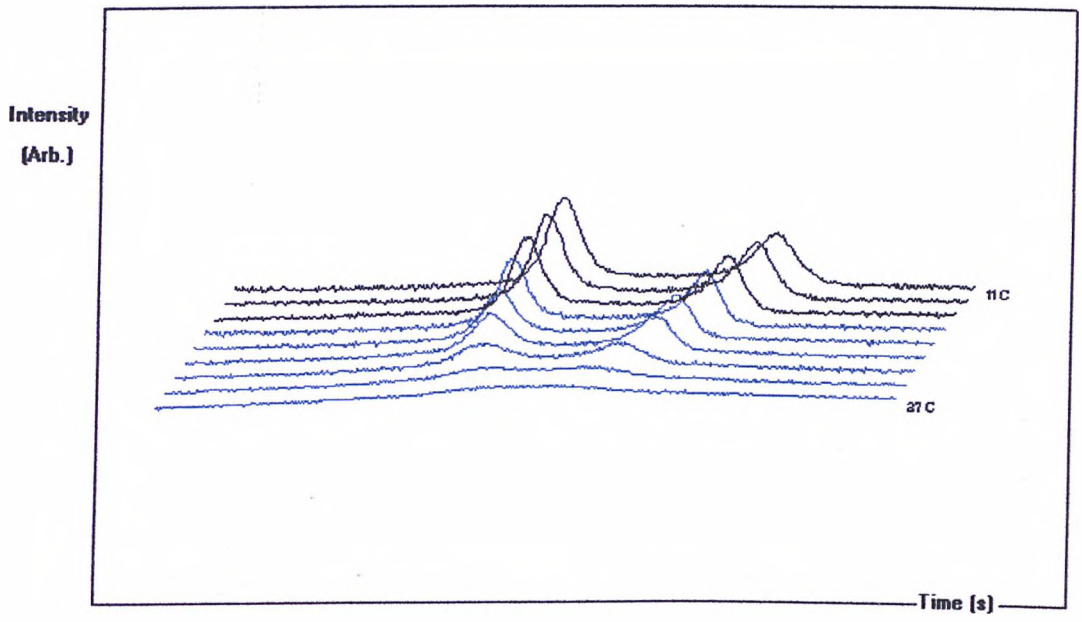

Fig. 4.8.5 (a), (b), (c) and (d) Odd-even effect (II)

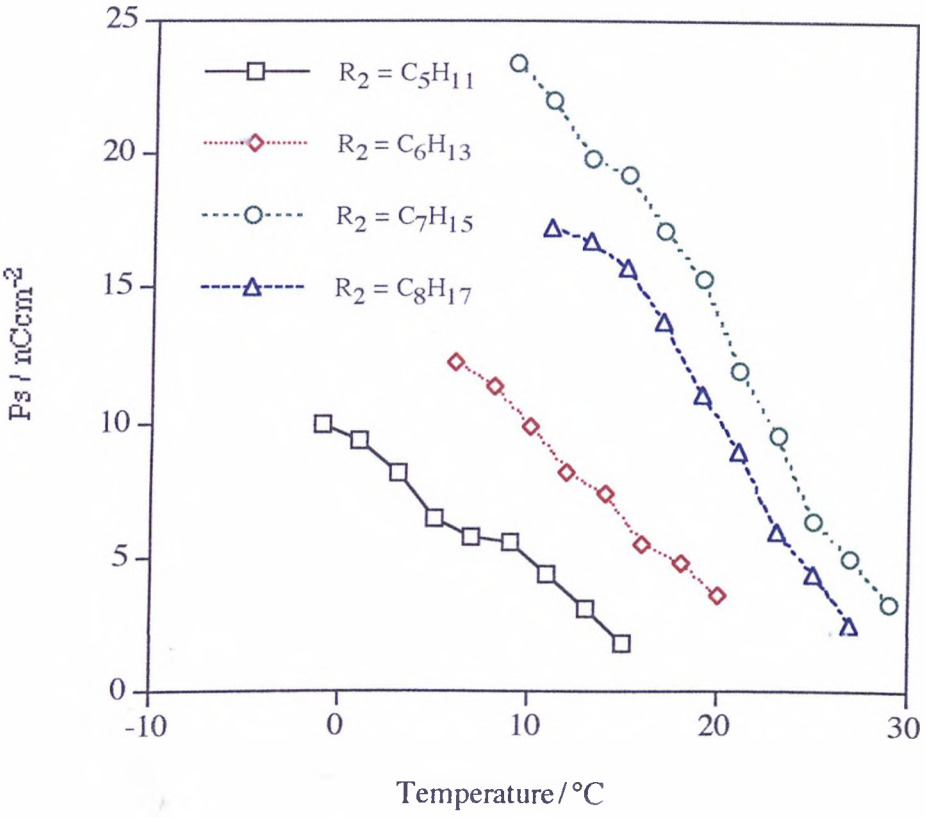

Fig. 4.8.4 Comparisons of Ps values from mixture **101** (14, CH_3, C_5H_{11}), **103** (14, CH_3, C_6H_{13}), **104** (14, CH_3, C_7H_{15}) and **105** (14, CH_3, C_8H_{16}) with **60*** (8, CF_3, C_6H_{13})

4.9 Direction of the Spontaneous Polarization (Ps)

Table 4.9.1 lists a number of chiral compounds that were synthesized with known absolute spatial configuration. Their optical rotations, $[\alpha]_D^{22°C}$, helical sense and the observed spontaneous polarization directions using a DC voltage (75.0 V) of know polarity are given.

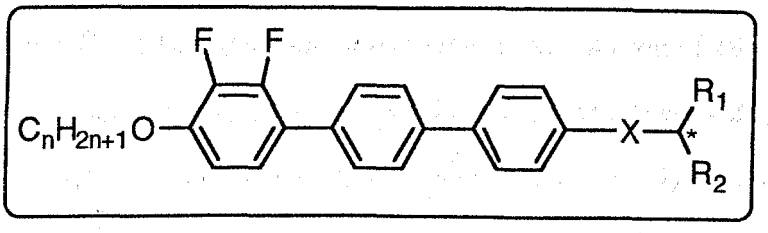

Compounds					Absolute Config.	$[\alpha]_D^{22°C}$	Helix Sense	Ps Direction
No.	n	X	R1	R2				
22*	8	O	CH_3	C_6H_{13}	(*S*)-	-2.22	RH	Ps (+)
48*	8	COO	CH_3	C_5H_{11}	(*S*)-	+20.5	LH	Ps (+)
50*	8	COO	CH_3	C_6H_{13}	(*R*)-	-24.0	RH	-
60*	8	COO	CF_3	C_6H_{13}	(*R*)-	-39.3	RH	Ps (+)
62*	10	COO	CH_3	C_5H_{11}	(*S*)-	+23.2	LH	Ps (+)
64*	10	COO	CH_3	C_6H_{13}	(*R*)-	-21.9	RH	Ps (-)
100*	14	COO	CH_3	C_5H_{11}	(*S*)-	+18.8	LH	Ps (+)
102*	14	COO	CH_3	C_6H_{13}	(*R*)-	-19.9	RH	Ps (-)

Table 4.9.1 Summary of optical properties

4.10 Molecular Modelling

Molecular modellings of compound **20** (8, CH_3, C_5H_{11}) and **60*** (8, CF_3, C_6H_{13}) were performed using the Dreiding force field on a Silicon graphic workstation. Two compounds were chosen because compound **20** (8, CH_3, C_5H_{11}) exhibited the ferroelectric structure whereas **60*** (8, CF_3, C_6H_{13}) had a stable antiferroelectric ordering.

Fig. 4.10.1 and Fig. 4.10.11 show the head to tail interdigitation of 10 molecules of compounds **20** (8, CH_3, C_5H_{11}) and **60*** (8, CF_3, C_6H_{13}) respectively. Compound **20** (8, CH_3, C_5H_{11}), an ether linked system shows the linearity of the molecules whereas in compound **60*** (8, CF_3, C_6H_{13}) which has the ester linked system, the molecules have a zigzag shape and the terminal aliphatic chain carrying the branching point is bent away from the aromatic core. However because of the sp^2 nature of the chemical bonds associated with the ester linkage the terminal aliphatic chain carrying the branching point is not bent away from the aromatic core as much as it is for the ether linked system. Therefore interdigitation of end chains may be stronger, which is suitable for the formation of zigzag shaped dimers.

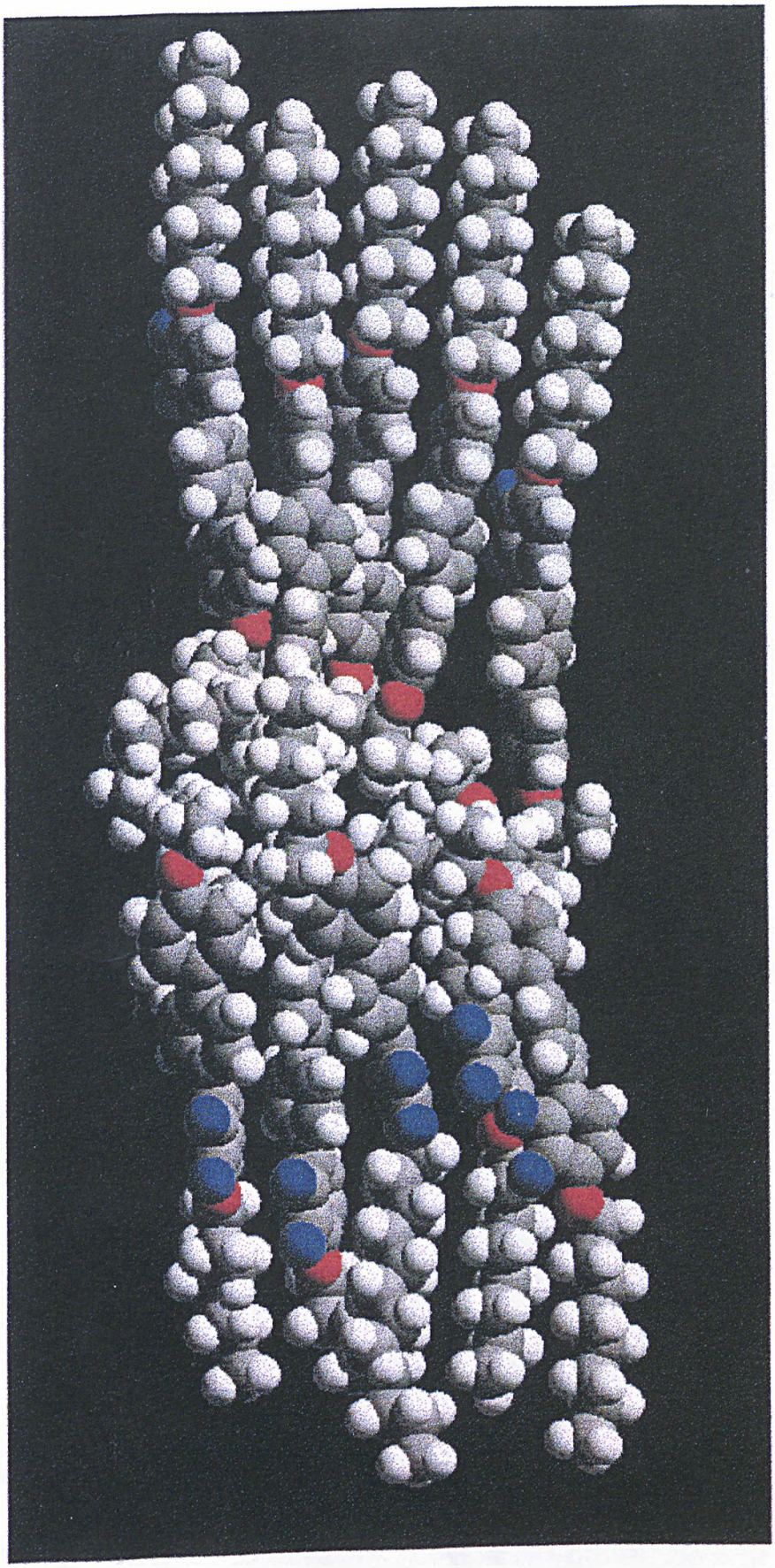

Fig. 4.10.1 10 molecule ensemble of compound **20** (8, CH_3, C_5H_{11}) created by molecular modelling

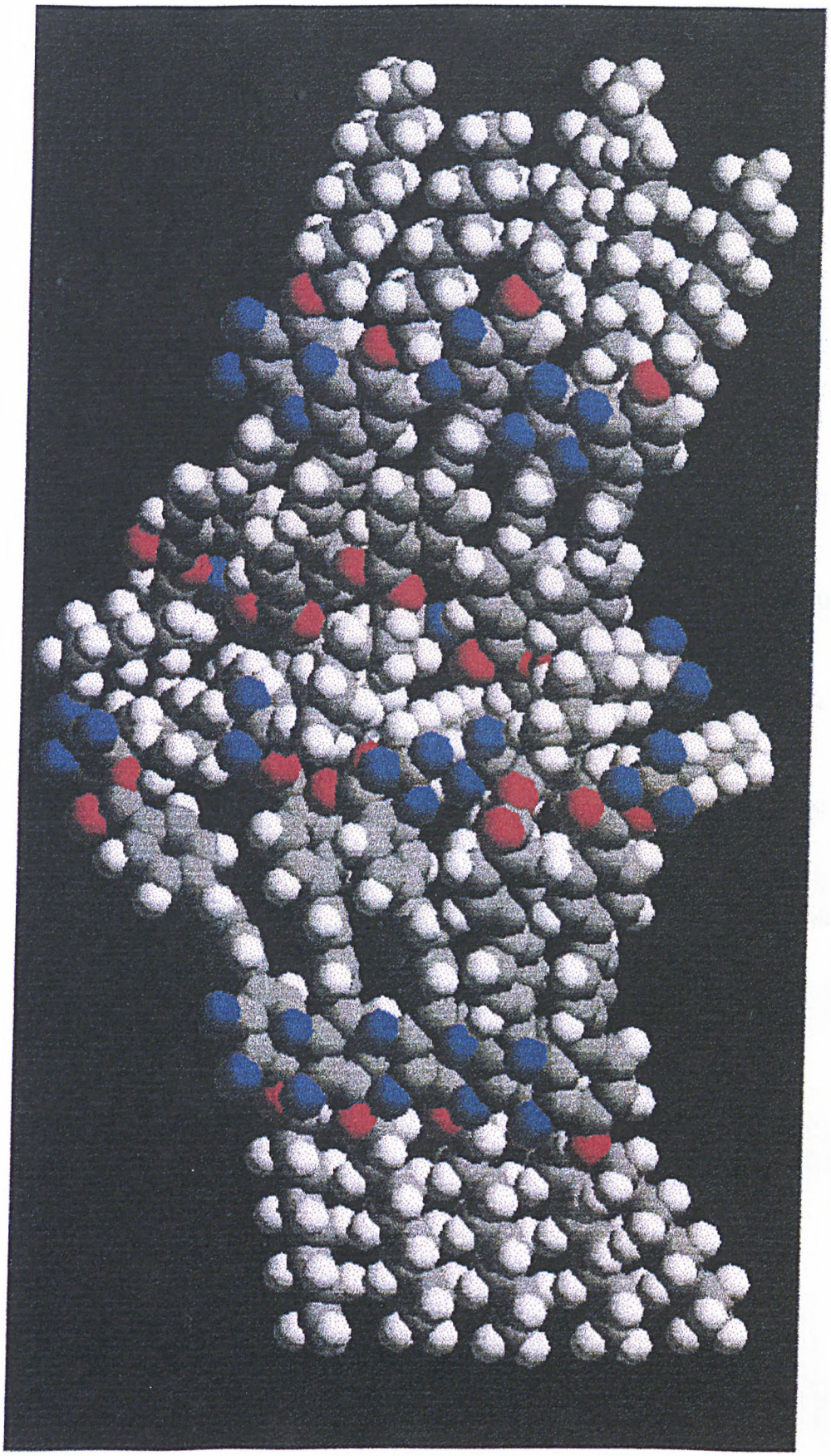

Fig. 4.10.2 10 molecule ensemble of compound **60*** (8, CF_3, C_6H_{13}) created by molecular modelling

4.11 References

1. O. Mitsunobu, *Synthesis*, 1981, **1**
2. J. March, *Advanced Organic Chemistry*, 3rd Edition, 1985, Wiley-Interscience, New York
3. A. Hassner and V. Alexanian, *Tetrahedron Lett.*, 1978, **46**, 4475
4. W. J. Scott and J. K. Stille, *J. Am. Chem. Soc.*, 1986, **108**, 3033
5. T. Watanabe, N. Miyaura and A. Suzuki, *Synlett.*, March, 1992, 207-210
6. Y. Takanishi, K. Hiraoka, V. K. Agrawal, H. Takezoe, A. Fukuda and M. Matsushita, *Jpn. J. Appl. Phys.*, 1991, **30**, No. 9A, 2023
7. N. Okabe, Y. Suzuki, I. Kawamura, T. Isozaki, H. Takezoe and A. Fukuda, *Jpn. J. Appl. Phys.*, 1992, **31**, L242R
8. A. Fukuda, Y. Takanishi, T. Isozaki, K. Ishikawa and H. Takezoe, *J. Mater. Chem.*, 1994, 4 (**7**), 997
9. J. Hou, J. Schacht, F. Giesselmann and P. Zugenmaier, *Liq. Cryst.*, 1997, **22**, No. 4, 401
10. J. Hou, J. Schacht, F. Giesselmann and P. Zugenmaier, *Liq. Cryst.*, 1997, **22**, No. 4, 409
11. S. Asahina, M. Sorai, A. Fukuda, H. Takezoe, K. Furukawa, K. Terashima, Y. Suzuki and I. Kawamura, *Liq. Cryst.*, 1997, **23**, No. 3, 339

5 Conclusions

It is a capital mistake to theorize before one has data. Insensibly one begins to twist facts to suit theories, instead of theories to suit fact.

Sir *Arthur Conan Doyle*

It is also a good rule not to put too much confidence in experimental results until they have been confirmed by theory.

Sir *Arthur Eddington*

First get your facts, then you can distort them at your leisure.

Mark Twain

5. Conclusions

1. System (I)

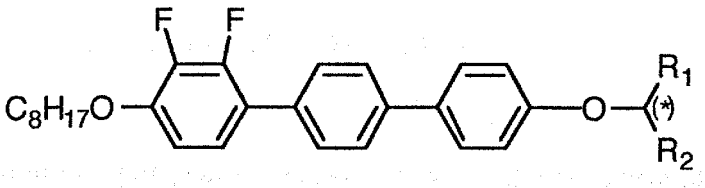

The terminal ether linkage system (I) exhibits an N/N* and SmC/SmC* phase sequence and does not have SmA or antiferroelectric ordering whereas system (II) which has cores containing an ester linkage exhibits SmA/SmA* and SmC/SmC* or SmC_{Alt}/SmC_A* phases.

2. System (II)

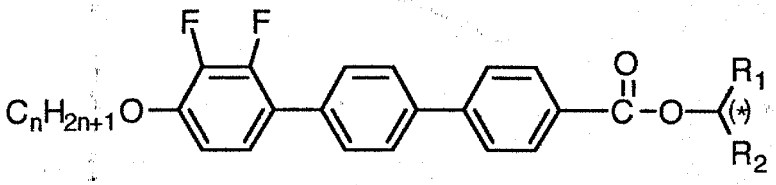

Compound **No.** (n, R_1, R_2)

In the homologous series, (8, R_1, R_2), asymmetrically branched swallow tailed compounds ($R_1 \neq R_2$) show a stronger tendency to form SmC_{Alt} and SmC_A* phases than symmetrically substituted swallow tailed compounds (R_1=R_2). When the compound is chiral, the peak associated with transition from SmA* to SmC_A* is detected with an extremely small enthalpy in DSC. In the case of the corresponding achiral compounds, the peak vanishes, therefore the SmA to SmC_{Alt} transition cannot be detected by DSC. When R_1 is substituted by CF_3, the compound tends to show more stable antiferroelectric behaviour.

In the homologous series, (10, R_1, R_2), SmC/SmC* phases are dominant and antiferroelectric ordering is suppressed. As a consequence, asymmetrically branched chiral compounds show an intermediary state, SmC_α*. In case of the homologous series, (14, R_1, R_2), SmC/SmC* phases are more pronounced, leading to the eclipse of the SmC_α* state in compound (14, CH_3, C_6H_{13}).

In switching studies, split peaks observed in the antiferroelectric phase are unique and imply possible uses in fast switching devices.

The odd-even effects found in mixtures of achiral and chiral compounds suggest that this is a new technique which might be able to control not only phase sequences but also phase properties.